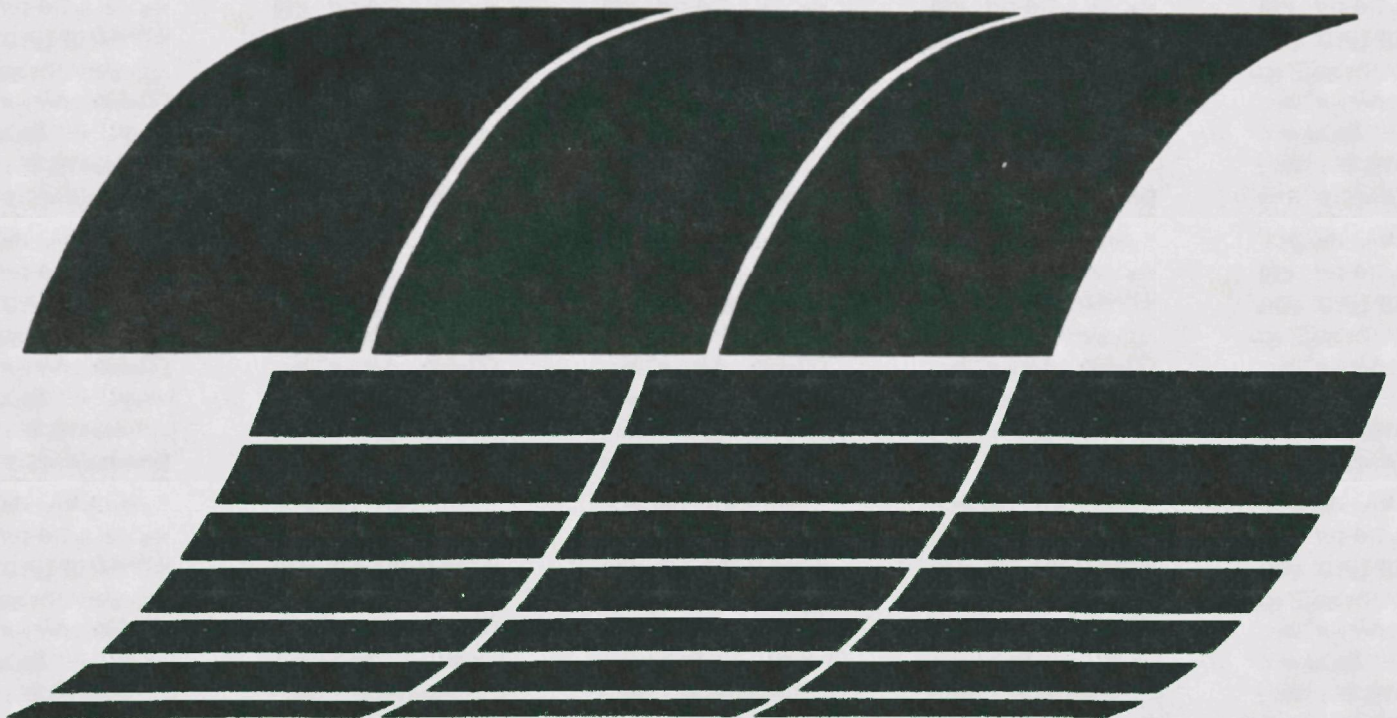




Experimental/ Engineering Support for EPA's FBC Program: Final Report Volume I. Sulfur Oxide Control

**Interagency
Energy/Environment
R&D Program Report**



RESEARCH REPORTING SERIES

Research reports of the Office of Research and Development, U.S. Environmental Protection Agency, have been grouped into nine series. These nine broad categories were established to facilitate further development and application of environmental technology. Elimination of traditional grouping was consciously planned to foster technology transfer and a maximum interface in related fields. The nine series are:

1. Environmental Health Effects Research
2. Environmental Protection Technology
3. Ecological Research
4. Environmental Monitoring
5. Socioeconomic Environmental Studies
6. Scientific and Technical Assessment Reports (STAR)
7. Interagency Energy-Environment Research and Development
8. "Special" Reports
9. Miscellaneous Reports

This report has been assigned to the INTERAGENCY ENERGY-ENVIRONMENT RESEARCH AND DEVELOPMENT series. Reports in this series result from the effort funded under the 17-agency Federal Energy/Environment Research and Development Program. These studies relate to EPA's mission to protect the public health and welfare from adverse effects of pollutants associated with energy systems. The goal of the Program is to assure the rapid development of domestic energy supplies in an environmentally-compatible manner by providing the necessary environmental data and control technology. Investigations include analyses of the transport of energy-related pollutants and their health and ecological effects; assessments of, and development of, control technologies for energy systems; and integrated assessments of a wide range of energy-related environmental issues.

EPA REVIEW NOTICE

This report has been reviewed by the participating Federal Agencies, and approved for publication. Approval does not signify that the contents necessarily reflect the views and policies of the Government, nor does mention of trade names or commercial products constitute endorsement or recommendation for use.

This document is available to the public through the National Technical Information Service, Springfield, Virginia 22161.

January 1980

**Experimental/Engineering Support
for EPA's FBC Program:
Final Report
Volume I. Sulfur Oxide Control**

by

**N.H. Ulerich, W.G. Vaux, R.A. Newby,
and D.L. Keairns**

**Westinghouse Research and Development Center
1310 Beulah Road
Pittsburgh, Pennsylvania 15235**

**Contract No. 68-02-2132
Program Element No. INE825**

EPA Project Officer: D. Bruce Henschel

**Industrial Environmental Research Laboratory
Office of Environmental Engineering and Technology
Research Triangle Park, NC 27711**

Prepared for

**U.S. ENVIRONMENTAL PROTECTION AGENCY
Office of Research and Development
Washington, DC 20460**

PREFACE

The Westinghouse R&D Center is carrying out a program to provide experimental and engineering support for the development of fluidized-bed combustion systems under contract to the Industrial Environmental Research Laboratory (IERL), U. S. Environmental Protection Agency (EPA), at Research Triangle Park, NC. The contract scope includes atmospheric and pressurized fluidized-bed combustion processes as they may be applied for steam generation, electric power generation, or process heat. Specific tasks include work on calcium-based sulfur removal systems (e.g., sorption kinetics, regeneration, attrition, modeling), alternative sulfur sorbents, nitrogen oxide emissions, particulate emissions and control, trace element emissions and control, spent sorbent and ash disposal, and systems evaluation (e.g., impact of new source performance standards on fluidized-bed combustion system design and cost).

This report contains the results of work defined and completed under the sulfur oxide control task of the contract. Work performed on this task was performed from January 1976 to January 1979 and is documented in the:

- Present report which presents results on desulfurization performance of limestones and dolomites, prediction of desulfurization performance for FBC plants, and sorbent attrition behavior
- Report on the "Effect of SO₂ Emission Requirements on Fluidized-Bed Combustion Systems: Preliminary Technical/Economic Assessment," issued in August 1978 (EPA-600/7-78-163)
- Report on "Regeneration of Calcium-Based SO₂ Sorbents for Fluidized-Bed Combustion: Engineering Evaluation," issued in March 1978 (EPA-600/7-78-039)
- Report on "Alternatives to Calcium-Based SO₂ Sorbents for Fluidized-Bed Combustion: Conceptual Evaluation," issued in January 1978 (EPA-600/7-78-005).

ABSTRACT

The desulfurization performance and attrition behavior of limestones and dolomites are investigated for atmospheric and pressurized fluidized-bed combustion (FBC) systems. Results from these experimental and analytical studies are important in providing information for the design of FBC processes to achieve energy cost objectives and environmental requirements. Results are presented on the impact of selected FBC operating conditions on desulfurization performance, further comparisons of the ability of the Westinghouse desulfurization model to predict desulfurization performance, and the development of an understanding of sorbent attrition. The studies show that:

- PFBC systems can be operated at high temperatures (e.g., 1000°C) or high excess air (e.g., 300%) and achieve sulfur control without increasing sorbent requirements; this allows for higher operating efficiency and greater flexibility in turndown without sacrificing sulfur removal efficiency.
- The agreement between fluidized-bed data and the Westinghouse kinetic model utilizing thermogravimetric (TG) data has been further demonstrated using data collected at atmospheric and pressurized operation; this permits a practical, economical method for determining sulfur sorbent requirement, given a plant design and a specific sorbent, or for selecting the optimal sorbent to achieve the desired sulfur removal performance.
- Sorbent attrition screening tests indicate that sorbent type and operating parameters will effect particle attrition. An attrition model is presented for sorbent attrition in

the bubbling bed region of the FBC, and the model is supported by experimental data. The understanding of attrition permits a basis for selecting sulfur sorbents and design and operating conditions to minimize attrition and for improving fine particle carry-over and sulfur control predictions.

These investigations provide further information for the development of an integrated fluidized-bed combustion model incorporating sulfur control and particulate profile models

NOMENCLATURE

AFBC	= atmospheric-pressure fluidized-bed combustion
ANL	= Argonne National Laboratories
ECAS	= Energy Conversion Alternatives Study
EPA	= Environmental Protection Agency
FBC	= fluidized-bed combustion
PFBC	= pressurized fluidized-bed combustion
STP	= standard temperature and pressure
TG	= thermogravimetric
TGA	= thermogravimetric apparatus
TVA	= Tennessee Valley Authority

DESULFURIZATION

A	= cross-sectional area of bed, cm^2
a	= stoichiometric reaction coefficient for the solid = 1
b	= stoichiometric reaction coefficient for the gas = 1
C	= SO_2 concentration, mole/cc
C_o	= SO_2 concentration fed to batch fluidized bed, mole/cc
D	= diffusion coefficient
D_p	= pore diffusion coefficient
Ea	= activation energy, kcal/mole
F	= total superficial volumetric gas flow rate, cc/s
f	= mole fraction of SO_2 in effluent gas
F_o	= total gas flow rate, mole/s
h_s	= static bed height, cm
K	= rate constant for sulfur sorption by limestone
K_s	= surface rate constant, cm/s
M_{Ca}	= moles of calcium in batch fluidized bed, mole
m	= molecular weight
N	= moles of Ca reacted per particle of limestone
n	= order of reaction
P	= pressure, kPa
P_{CO_2}	= partial pressure of CO_2 , kPa

$P_{CO_2 \text{ equil}}$ = equilibrium partial pressure of CO_2
 R = gas constant
 R_a = $(d\alpha/dt)_P / (d\alpha/dt)_{P=1}$
 r = particle radius
 \bar{r} = average pore radius
 S = surface area of particles in bed, cm^2
 T = temperature, K
 t = time, s
 w_b = bed weight, g
 X = particle porosity
 α = mole fraction of sorbent calcium sulfated
 δ = volume fraction of bubble phase
 ϵ = bed voidage in emulsion fraction
 ρ = particle density, mole Ca/cc
 θ = $\frac{a p r^2}{6 b D_p C}$
 θ_A = absolute temperature
 τ = tortuosity (2-6)

PARTICLE ATTRITION

A = extent of particle attrition
 c = constant in Gonzales and Otero equation
 C = extent of calcination
 D_p = particle diameter defined by sieve analysis
 D_{vs} = volume-surface particle diameter
 F = mass fraction in cumulative size distribution
 $F(t)$ = decreasing function
 f = fraction of mass smaller than $710 \mu m$
 g = gravity acceleration
 g_c = Newton's Law conversion factor
 K = unspecified constant
 k = regrouping of K

L	= rate of loss of coarses, mass loss per unit time
M	= mass of large particles in a fluidized-bed
M_o	= mass of large particles before an interval of attrition
M_l	= mass of large particles after an interval of attrition
P	= pressure; ΔP = pressure drop
R	= attrition rate, % loss per unit time
R_θ	= rate of heating
t	= time
t_o	= reference time interval
S	= percent of possible sulfation
T	= temperature
U	= superficial gas velocity
U_{mf}	= minimum fluidization velocity
X	= fraction of calcium in bed solids
Y	= mass fraction loss of CO_2 on ignition
Z	= depth into the bed, measured from the surface
ρ	= gas velocity
ρ_s	= particle density
σ	= particle strength
μ	= gas viscosity

Subscripts

l	= stone after attrition
o	= original stone
f	= filter

ACKNOWLEDGEMENT

We want to express our high regard for and acknowledge the contribution of Mr. D. B. Henschel who served as the EPA project officer. Mr. P. P. Turner and Mr. R. P. Hangebrauck, Industrial Environmental Research Laboratory, EPA, are acknowledged for their continuing contributions through discussions and support of the program.

We thank Mr. R. E. Brinza, Mr. J. Capozzi, Ms. L. J. Cwynar, Ms. C. A. Hill, and Mr. W. F. Kittle for performing sample analyses and carrying out the thermogravimetric and batch fluidized-bed experiments on desulfurization. We thank Mr. A. W. Fellers for his work on the sorbent attrition test program.

TABLE OF CONTENTS

	<u>Page</u>
1 INTRODUCTION	1
2 SUMMARY AND CONCLUSIONS	3
3 RECOMMENDATIONS	9
4 SULFUR OXIDE CONTROL - CALCIUM-BASED SORBENTS	11
Desulfurization	11
Particle Attrition	56
Sorbent Regeneration	115
5 SULFUR OXIDE CONTROL - ALTERNATIVE SORBENTS	118
6 REFERENCES	120
APPENDICES	
A SULFUR OXIDE REMOVAL DATA BASE AND MODEL	125
B SORBENT INFORMATION AND TG RATE DATA	145
C FLUIDIZED-BED DATA	179
D A MODEL FOR PARTICLE ATTRITION BY ABRASION IN THE UPPER ZONE OF A FLUIDIZED BED	187
E 3.5-in FLUIDIZED-BED TEST SYSTEM	225

LIST OF TABLES

	<u>Page</u>
1 TG Experimental Program Outline: Operating Range Impact on Desulfurization Performance	13
2 The Effect of Temperature on Sorbent Utilization at 1013 kPa (10 atm)	20
3 Relative Effectiveness of Large-Grained Dolomite in Sulfation	41
4 Batch Fluidized-Bed Experiments	45
5 Summary of Models Used to Analyze Fluidized-Bed Data	47
6 Range of Values of Test Variables in Several Test Systems	62
7 Percent of Solids Attrited in Four Hours	65
8 Summary of Attrition Test Data Statistics	65
9 Description of Test Conditions	68
10 Attrition Test Data	69
11 Percentages of Fines Formed during Attrition Testing and Percentages Attributable to Fluidization Only	73
12 Relation between Extent of Attrition and Degree of Roundness as Judged by Six Observers	88
13 Comparison of Mean Sizes of Grove Limestone Particles Calcined and Untreated	91
14 Effect of Resieving a Single Size Fraction of Tymochtee Dolomite	93
15 High and Low Levels of the Independent Variables	100
16 The Results of High-Temperature Attrition Testing of Grove 1359	106
17 Factorial Model Coefficients Describing Attrition of Grove 1351	107
18 Dependence of Solids Specific Surface on Time of Fluidization	115
19 Distribution of Particle Surface Area for Various Particle Sizes after 15 Minutes of Fluidization of Grove Limestone at 25°C	116

LIST OF FIGURES

	<u>Page</u>
1 The Pressurized TG Apparatus	16
2 Schematic Diagram of the Pressurized TG System	17
3 The Effect of Temperature on the Pressurized Sulfation of Limestone and Dolomite	21
4 The Effect of High Temperature on the Pressurized Sulfation of Small and Large Limestone Particles	21
5 The Effect of Temperature on the Pressurized Sulfation of Greer Limestone (74-149 μm particles)	22
6 The Effect of Temperature on the Pressurized Sulfation of Greer Limestone (420-500 μm particles)	22
7 The Effect of Temperature on the Pressurized Sulfation of Greer Limestone (2380-3360 μm particles)	22
8 The Effect of CO_2 Pressure during Calcination on SO_2 Emissions from a Fluidized Bed	25
9 The Influence of Oxygen Partial Pressure on the Rate of Dolomite Sulfation (101.3 kPa/1 atm)	29
10 The Influence of Oxygen Partial Pressure on the Rate of Dolomite Sulfation (1013 kPa/10 atm)	29
11 The Influence of Excess Air Level on the Pressurized Sulfation of Uncalcined Limestone	30
12 The Influence of Sorbent Residence Time on the Sulfation of Greer Limestone (1013 kPa/10 atm)	30
13 The Influence of Sorbent Residence Time on the Sulfation of Limestone 1359 (1013 kPa/10 atm)	33
14 The Influence of Sorbent Residence Time on the Sulfation of Greer Limestone (101.3 kPa/1 atm)	34
15 The Influence of Sorbent Residence Time on the Sulfation of Limestone 1359 (101.3 kPa/1 atm)	34
16 Comparison of Sulfation Rates at 101.3 and 1013 kPa (1 and 10 atm) Pressure (Greer Limestone)	36

LIST OF FIGURES (Continued)

	<u>Page</u>
17 Comparison of Sulfation Rates at 101.3 and 1013 kPa (1 and 10 atm) Pressure (Tymochtee Dolomite)	36
18 The Effect of Pressure on the Sulfation Rate of Tymochtee Dolomite	37
19 TG Sulfation of Canaan Dolomite (420-500 μm particles)	39
20 Sulfur Penetration at Periphery and Grain Boundaries of 500 μm Particle of Canaan Dolomite (~ 300 μm grains)	40
21 TG Sulfation of Canaan Dolomite (74-149 μm particles)	41
22 Schematic of Batch Fluidized-Bed Reactor	43
23 Comparison of Fluidized-Bed Models (Bellefonte limestone)	49
24 Comparison of Fluidized-Bed Models (Carbon limestone)	49
25 Comparison of Rate Constants Derived from Fluidized-Bed Data (Model 1) and TG Data: Limestone 1359	51
26 Comparison of Rate Constants Derived from Fluidized-Bed Data (Model 1) and TG Data: Carbon Limestone	51
27 Comparison of Rate Constants Derived from Fluidized-Bed Data (Model 1) and TG Data: Brownwood Limestone	52
28 Comparison of Rate Constants Derived from Fluidized-Bed Data (Model 1) and TG Data: Ames Limestone	52
29 Comparison of Rate Constants Derived from Fluidized-Bed Data (Model 1) and TG Data: Bellefonte Limestone	53
30 Comparison of Rate Constants Derived from Fluidized-Bed Data (Model 1) and TG Data: Mississippi Limestone	53
31 Comparison of Rate Constants Derived from Cambridge Fluidized-Bed Data (Model 1) and Westinghouse TG Data	54
32 Attrition Rate Dependence upon Stone Type and Atmosphere	67
33 Gas Velocity and Temperature Patterns in the Attrition versus Time Tests	71
34 Effect of Duration of Fluidization on Extent of Attrition in Fluidization of Grove Limestone at 815°C	72
35 Temperature History When Cold Grove Limestone Is Added to 815°C 3.5 cm Attrition Cell (Runs A1, A1 Repeated, A2)	75
36 Measurement of Perpendicular Dimensions for Measurement of Particle Shape	78
37 Grove Limestone Particles before and after Fluidization at $U - U_{mf} = 30$ cm/s for 329 Hours	80

LIST OF FIGURES (Continued)

	<u>Page</u>
38 Sorbent Micrographs - Grove Limestone	82
39 Particle Size Distributions before and after Hot Fluidization of Grove Limestone, Run A-9	87
40 Mean Rankings of Particle Angularity	89
41 Mean Rankings of Particle Angularity for the Effect-of-Duration Tests	89
42 Apparent Swelling of Sausage-Shaped Particles	90
43 Micrographs of Grove Limestone before and after Calcination	92
44 Size Distributions of Tymochtee Dolomite after Hot Fluidization at 100 and 1000 kPa	96
45 Attrition Test Cell	98
46 Test Procedure for Attrition Testing of Grove Limestone for Effects of Grain Size, Temperature, and Sulfation	99
47 Determination of U_{mf} from the ΔP -U Curve	101
48 Flow Diagram of Sorbent Attrition Test System	102
49 Attrition Test Cell	103
50 Leak in 10.3-cm Fluidized Bed	108
51 Size Frequency Plots for Grove Limestone	110
52 Cumulative Distributions for Grove Limestone	110
53 Flow Diagram for Room-Temperature Fluidized Bed	113
54 Photomicrograph of Elutriated Grove Limestone Recovered from the Balston Filter	113

1. INTRODUCTION

The design of fluidized-bed combustion (FBC) systems for electric power generation, industrial steam or process heat, or cogeneration applications depends on an understanding of desulfurization in order to achieve energy cost and environmental objectives and requirements. Fluidized-bed combustion systems can offer energy cost and environmental advantages when compared with alternative process choices if the system design incorporates an understanding of the component/subsystem performance, limitations, and available trade-offs as a function of operating and design parameters. Limestone and dolomite desulfurization performance and attrition behavior represent two areas that must be understood when selecting design and operating parameters to achieve the process objectives and environmental requirements at the lowest energy cost. The results reported in this document extend our previous understanding of these phenomena to provide a basis for FBC design and performance evaluation.

A data base of over 700 atmospheric-pressure and 100 pressurized thermogravimetric (TG) tests is now available, based on experiments performed at Westinghouse. These results and the results from other investigators have been used to develop an understanding of desulfurization phenomena. The quantitative prediction of sorbent desulfurization performance was shown in our earlier work under contract to EPA utilizing reaction rate constants derived from TG data and the Westinghouse FBC desulfurization model. The selection of the work reported here is based on an analysis of the available laboratory and plant data and systems

evaluation studies which identified research and development needs. The results of work in five areas are presented: The impact of selected FBC operating conditions on desulfurization in atmospheric (AFBC) and pressurized fluidized-bed combustion (PFBC) systems, the comparison of reaction rate constants derived from TG data and batch fluid-bed data, further testing of the Westinghouse desulfurization model against available bench-scale and pilot plant data, screening tests to assess the effect of sorbent type and operating conditions on sorbent attrition in the fluidized bed, and the development and experimental confirmation of an attrition model for attrition in the "bubbling bed."

2. SUMMARY AND CONCLUSIONS

Experimental and analytical studies were carried out to investigate desulfurization performance of limestones and dolomites for AFBC and PFBC systems to extend our capability for predicting desulfurization performance and to initiate a program to understand particle attrition in fluidized-bed combustion systems.

DESULFURIZATION PERFORMANCE

Westinghouse has conducted an extensive program, under sponsorship of EPA and other organizations, to study limestone and sulfur sorption utilizing thermogravimetric analysis test facilities. Previous results have indicated areas where additional data and analyses were needed to evaluate performance. The areas selected for this study included the impact of selected operating conditions on desulfurization:

- The effect of high temperature (e.g., 1000°C) PFBC operation, which is of interest for achieving high plant efficiency through increased turbine inlet temperatures and for providing turndown flexibility.
- The effect of oxygen concentration, which is of interest for assessing the desulfurization performance for adiabatic FBC process concepts utilizing high excess air (e.g., 300%).
- The performance of uncalcined, impure limestones for PFBC operation, which is of interest for increasing the potential sorbents available for commercial applications.
- The effect of sorbent residence time, which is of interest for assessing the impact of long (e.g., 10-20 hours) exposures at operating temperature in commercial plants and for interpreting TG or batch fluid-bed data taken at short residence times.

- The use of large-grained dolomites, which is of interest for increasing the potential sorbents available for application.

Conclusions from the experimental test program are that:

- Desulfurization performance for PFBC operation at 1013 kPa (10 atm) pressure will be maintained or improved at high temperature (900–1000°C) operation. Sulfur removal of 85 and 90 percent can be achieved at temperatures as high as 900 to 1000°C without increased sorbent feed requirements (over 800–850°C operation) for most sorbents.
- Desulfurization performance will be maintained at high excess air operation. Dolomite sulfation is zero order in oxygen concentration throughout the range of FBC operation (0.75–16% oxygen) at pressures of 101.3 and 1013 kPa. Sulfur removal of 85 and 90 percent can be achieved at high excess air levels without increasing sorbent feed requirements over low excess air operation.
- Impure limestones, such as Greer, can be effective sorbents in the uncalcined form, provided that the carbon dioxide (CO_2) partial pressure is not much greater than the equilibrium for calcination. This result increases the sorbents available for FBC systems where operating temperature and pressure ranges result in operation with calcium carbonate (CaCO_3).
- The residence time of a sorbent at the operating temperature may change the sulfation kinetics for some sorbents from the first-order relationship observed at initial reaction periods. The effect of sorbent residence time on desulfurization performance should be tested when TG data are used to project calcium feed requirements.

- Large-grained dolomites tested at elevated pressure show that low calcium-to-sulfur ratios can be achieved only if fine particles (e.g., 74 to 149 μm) are utilized. Results are consistent with plant test data.

DESULFURIZATION PERFORMANCE PREDICTIONS

The desulfurization performance of fluidized-bed combustion systems can be predicted by utilizing a kinetic model for sulfur dioxide (SO_2) capture previously developed by Westinghouse.¹ This model - using rate constants derived from TG data - is capable of projecting sorbent requirements as a function of FBC operating and design parameters. The importance of selecting proper fluid-bed combustor operating conditions (e.g., gas velocity, bed depth, sorbent particle size) was shown in a previous Westinghouse study.² Further confirmation of the accuracy of model projections was an objective under this contract. Comparison of the models' predictions with available bench-scale and pilot plant FBC data were previously reported,² with additional comparisons presented in this report, with specific focus on the 90 percent desulfurization obtained in the pressurized Exxon miniplant. The use of batch fluidized-bed tests as an alternative to TG tests to obtain rate constant data was also investigated.

The conclusions from the experimental and analytical work on predicting desulfurization performance are that:

- The agreement between fluidized-bed data and the kinetic model utilizing TG data has been further demonstrated with data collected at 1013 kPa (10 atm) pressure as well as at atmospheric pressure, and at sulfur removal efficiencies of up to 90 percent.
- The ability to compare predictions with plant performance is limited by the availability of complete pilot plant data (e.g., particle size distribution, fraction of inert particles in the bed, bed expansion, etc.) and the accuracy of pilot plant data

- Batch fluidized-bed data can also be utilized to obtain reaction rate constants for predicting performance. The calculation of the rate constant requires the use of a fluid-bed model that represents the test unit. Rate constants from batch fluidized-bed tests performed by Westinghouse with six sorbents and by Cambridge University with one sorbent compare favorably with rate constants from TG data.

SORBENT ATTRITION

The attrition of sorbent particles will effect the selection of sulfur sorbents, the desulfurization performance given a sulfur sorbent, and the design of the particulate control system for fine particles to achieve process (e.g., turbine tolerance) and environmental requirements. An understanding of particle attrition in FBC systems is important for the design and operation using limestones or dolomites and is critical for regenerative sulfur control processes utilizing alternative sorbents.³ An approach to understanding particle attrition in FBC systems was developed as part of the present effort. The objective was to develop a unified attrition model that would incorporate the separate attrition mechanisms occurring in a FBC system. This model will be integrated into the sulfur removal system and particle profile models being developed under this contract and under contract 68-02-3110.

The initial effort was to review the available literature, to perform screening tests to gain perspective on the effect of sorbent type and operating conditions on attrition in the fluidized bed, and to develop and confirm an attrition model for the attrition phenomena due to the "bubbling bed" behavior.

The conclusions from the review of available information, our experimental test programs, and our modeling work are that:

- The understanding of particle attrition in fluidized-bed processes is fragmented and incomplete - comprehensive understanding or models for the attrition mechanisms are not available.

- Screening tests on the effect of sorbent type and operating conditions on attrition show that sorbent type, particle atmosphere and temperature, particle composition (degree of calcination and degree of sulfation), duration of fluidization, residence time at temperature, rate of heating, and gas jets will effect the extent of particle attrition.
- A model was developed to relate the rate of attrition in the bubbling zone of the FBC above the influence of any grid jets. The relationship is

$$\left[\frac{RZ}{U - U_{mf}} \right] = [F(t) + 1] \left[\frac{g}{g_c} \frac{\rho_s}{\sigma_s} Z^2 \right]^m; m \approx 1$$

where

- | | |
|--|--|
| g = gravity acceleration | ρ_s = particle density |
| g_c = Newton's Law conversion factor | σ_s = particle strength |
| R = attrition rate | U = superficial gas velocity |
| Z = depth into the bed,
measured from the surface | U_{mf} = minimum fluidization
velocity. |
- $F(t)$ = a transient function describing the variation of attrition rate with time. $F(t) \rightarrow 0$ as $t \rightarrow \infty$,
 $dF(t)/dt \leq$ for $t > 0$

- Experimental results from our test program and available literature data support the model. Attrition by the bubbling bed results in the formation of fines but does not alter the basic particle shape.
- The attrition rate in the bubbling zone of a fluidized-bed combustor can be controlled by choosing a weak or strong sorbent and by specifying bed depth, gas velocity, and particle diameter as it affects U_{mf} .
- Attrition from jets, thermal shock, cyclones, and impact devices that may be incorporated in the system design are expected to result in the greatest extent of attrition; these and other sources, such as the bubbling bed, may all

be important in the production of fines ($<3\text{ }\mu\text{m}$), which are important for process considerations and environmental impact.

3. RECOMMENDATIONS

The following recommendations are made for further work on desulfurization and sorbent attrition:

- Continue the work to compare model predictions with available bench-scale, pilot plant, and commercial plant performance for confirmation and identification of suggested areas for improvement. The projection of high sulfur removal efficiencies (≥ 90 percent) should be emphasized.
- Extend the desulfurization model to particle size distribution and particle size residence times, incorporating particle attrition and carry-over models.
- Comprehensive reporting of pilot plant and commercial plant data is required in order to extend the capability for desulfurization performance of the present predictive model, to develop comparisons of attrition performance with model predictions, and to permit accurate interpretation of plant results.
- Extend the development of fundamental gas-solid modeling. Development of a reaction model of the sulfation of limestones and dolomites could result in innovative methods for improving sorbent utilization through an understanding of the reaction mechanisms; improved tests to determine reaction performance; or, as an ultimate objective, the prediction of sorbent utilization based on physical and chemical properties of the sorbent.
- Investigate techniques to improve sorbent performance based on experimental and modeling work.

- Review and extend the test procedures developed for sorbent selection in FBC applications. Principal considerations would be the sorbent reactivity for high sulfur removal requirements and attrition characterization.
- Develop an understanding of attrition phenomena in FBC systems. Priority areas for study are sorbent and fuel attrition resulting from jets (e.g., grid), thermal shock, solids transport, and cyclones.
- Develop an integrated attrition model that incorporates the important attrition mechanisms in FBC systems. The model will permit extension of the desulfurization performance model and the particle profile model for estimating particle size distributions and loadings through the FBC system.

Recommendations for work on sorbent regeneration using calcium-based and alternative sorbents and for further systems analyses are presented in companion reports previously issued.²⁻⁴

4. SULFUR OXIDE CONTROL - CALCIUM-BASED SORBENTS

DESULFURIZATION

The impact of sulfur removal on the operation of a fluidized-bed power generation unit depends on the sorbent calcium utilization in desulfurization. The reaction kinetics of limestone with SO_2 must be understood in order to develop a rational basis for sorbent selection and to maximize calcium (Ca) utilization in fluidized-bed combustion. The evaluation of sorption kinetics was achieved by mathematically modeling the fluid-bed combustor and performing TG laboratory experiments simulating fluidized-bed operating conditions to define the kinetic rate constants for the model, investigate data gaps, and study the effect of sorbent type on desulfurization.

Westinghouse has conducted a substantial TG program studying limestone and dolomite sulfur sorption under the sponsorship of EPA and other organizations.^{1,2,5-10} Previous results have indicated areas in which additional data and analysis were needed to evaluate the sulfur removal performance of sorbents. These specific areas, addressing the impact of FBC operating conditions on desulfurization in AFBC and PFBC, were investigated.

The desulfurization performance expected in fluidized-bed units can be projected by using rate constants derived from TG data. The fluidized-bed model used and the method of making the projections are summarized in Appendix A. The models' projections were compared to data obtained from bench-scale and pilot-plant fluidized-bed units. In particular, we modeled the achievement of more than 90 percent desulfurization in high-pressure work at the Exxon miniplant.

Previous Work Perspective and Approach

FBC Operating Range Impact on Desulfurization Performance

Previous TG work has identified the following subjects, where little information is available, as important in understanding the impact of various operating conditions on desulfurization. The specific data sets collected, and their scope and operating conditions, are outlined in Table 1.

High Temperature Operation. The range of fluidized-bed combustion conditions has been generally considered to lie in the temperature range of 730 to 950°C. The Energy Conversion Alternatives Study (ECAS),¹¹ however, showed the desirability of extending the operating range to 1010°C for pressurized operation. Almost no data are available to project sulfur removal efficiency at these temperatures. Work at Exxon¹² showed that desulfurization adequate for achieving EPA sulfur oxide (SO_x) emission limits could be achieved at operating temperatures above 980°C in PFBC.

Previous pressurized TG studies at Westinghouse, using Tymochee dolomite, showed only a slight decrease in the reaction rate for sulfation in the range of 843 to 954°C. Pressurized studies with Limestone 1359 gave ambiguous results, but the data showed only a slight decline in calcium utilization, from 40 to 35 percent in the range of 900 to 950°C.

Limestone usage in PFBC may be practical at temperatures above 950°C, since calcination would occur. The stable form of dolomite at high temperatures would also be in the fully calcined ($\text{CaO} \cdot \text{MgO}$) rather than in the half-calcined ($\text{CaCO}_3 \cdot \text{MgO}$) form. The effect of temperature on the pressurized sulfation of limestone and dolomite, therefore, was studied in data sets 1 and 2. Since there is also little data available on large ($>2000 \mu\text{m}$) and small ($<100 \mu\text{m}$) sorbent particles, the temperature effect was examined using various particle sizes of limestones.

Table 1

TG EXPERIMENTAL PROGRAM OUTLINE:
OPERATING RANGE IMPACT ON DESULFURIZATION PERFORMANCE

Data Set	Scope	Sorbent(s)	Pressure, kPa	Particle Size, μm	% Excess Air	Temperature, $^{\circ}\text{C}$
1	Effect of Temperature on Pressurized Limestone Sulfation	Greer limestone	1013	420-500 74-149 149-420 2380-3360	300	840-1010
2	Effect of Temperature on Pressurized Dolomite Sulfation	Dolomite 1337	1013	420-500	300	840-1010
3	Effect of O_2 Concentration on Atmospheric Pressure Desulfurization of Dolomite	Tymochtee dolomite	101	1000-1190	15.2 kPa CO_2 (2-16% O_2)	815
4	Effect of O_2 Concentration on Pressurized Desulfurization of Dolomite	Tymochtee dolomite	1013	1000-1190	15.2 kPa CO_2 (0.7-16% O_2)	815
5	Effect of Excess Air on Uncalcined Limestone Sulfation	Greer limestone	1013	1000-1190	15-200	815
6	Effect of Sorbent Residence Time on Desulfurization	Greer limestone Limestone 1359	101 1013	1000-1410	20	815
7	Large-Grained Dolomite Performance	Kaiser dolomite Canaan dolomite	101 1013	420-500 74-149	20	815

High and Low-Oxygen Concentrations. Previous tests⁵ showed no increase in the sulfation rate of dolomites at high partial pressures of oxygen (O_2) (4-11%). Since stoichiometric utilization of the calcium in dolomites has been achieved, however, the influence of oxygen concentration on dolomite sulfation through high levels of calcium conversion is of interest. The effect of oxygen concentration over a wide range (0.75-16%) was studied in data sets 3 and 4.

The Effect of Excess Air on Uncalcined Limestone Sulfation. Results from one limestone¹ in the uncalcined form showed that the sorbent absorbed very little SO_2 . The limestone tested, however, was a very pure stone with small, interlocking grains. Since the sulfation of half-calcined dolomite proceeds readily, and since most pressurized operating conditions do not permit complete calcination of the sorbents, the use of an impure limestone in the uncalcined form was investigated (data set 5).

Sorbent Residence Time. The influence of prolonged exposure of sorbents to FBC temperatures has not been studied on the TGA. TG sulfations have been carried out in 0.5% SO_2 . At this SO_2 concentration the sorbent sulfation time is convenient for laboratory study, about two hours. In order to simulate the longer residence times of sorbents in fluidized beds, TG sulfations were carried out in lower SO_2 concentrations (data set 6).

Large-Grained Dolomites. The worst sorbents tested on the TGA have been large-grained dolomites. The possible use of these sorbents in powderized, fine-particle form was tested in data set 7.

Prediction of Desulfurization Performance

The qualitative information gained from TG studies has been greatly enhanced by the development of models that permit the quantitative prediction of sorbent performance in fluidized-bed units. We had previously developed a model¹ to project fluidized-bed desulfurization performance using reaction rate constants derived from TG data. The model was tested

here against bench-scale and pilot-plant data. In addition, rate constants derived from TG data were compared to those derived from batch fluidized-bed tests we had carried out, using several models for gas/solid dynamics in the batch unit.

FBC Operating Range Impact on Desulfurization Performance

TG Experimental Facility

The fractional utilization of a sorbent (fraction of the calcium oxide [CaO] sulfated) was determined as a function of time by sulfating sorbents suspended from a Du Pont 951 thermogravimetric balance. This system has been described previously.^{5,8} The gas flow path and the reaction tube geometry have been modified to improve the temperature measurement. Linear mass flow controllers have replaced rotameters for flow-rate measurement and control. Schematics of the apparatus are given in Figures 1 and 2.

TG experiments were run according to the following procedure:

- Size limestone by sieving.
- Suspend a 20 mg sample in a platinum mesh basket from the balance arm. Place the thermocouple into the basket, about 1 mm from the sample.
- Pressurize the system.
- Heat the sample at a rate of 10°C/min to reaction temperature in the reactant gas, minus SO₂, flowing at a rate of 2 l/min at standard temperature and pressure (STP).
- After complete calcination or half-calcination as indicated by a stable sample weight, introduce SO₂ into the reactant gas mixture.
- Monitor the sample weight gain as a function of reaction time.

TG Experimental Program

Twelve sorbents were used throughout the TG experimental program. Sorbent quarry and supplier information and a summary of sorbent analyses are given in Appendix B. TG rate data referenced in the report are also appended.

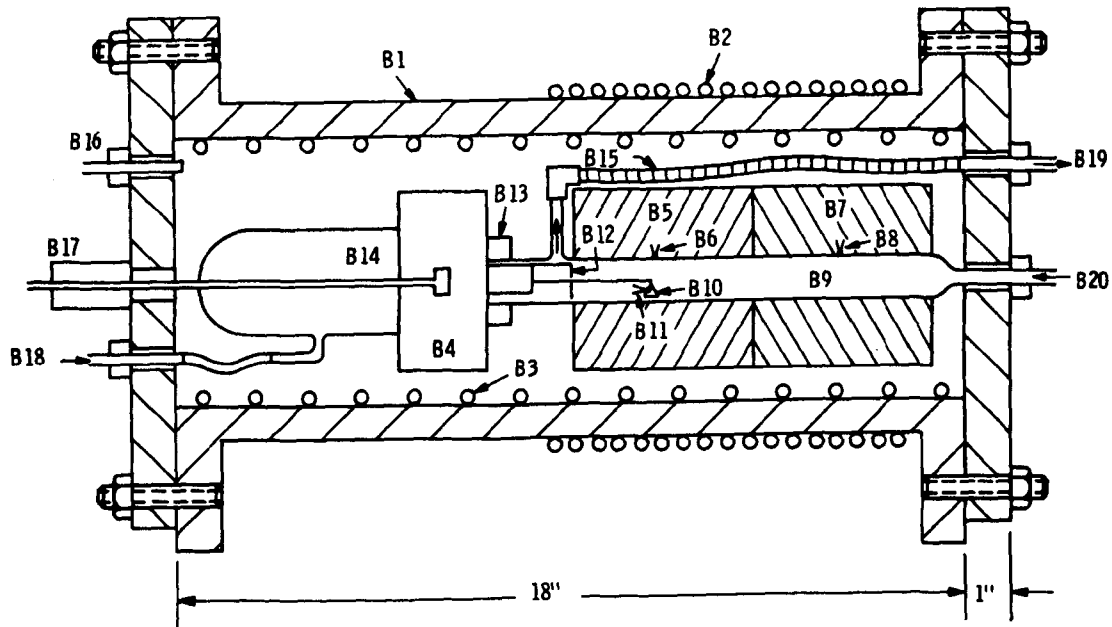


Figure 1 - The Pressurized TG Apparatus

KEY

B1	Stainless Steel Pressure Vessel	B11	Sample Thermocouple
B2	External Cooling Coil	B12	Baffle Assembly
B3	Internal Cooling Coil	B13	Reaction Tube Retaining Ring
B4	TG Balance Housing	B14	TG Bell Jar
B5	Reaction Zone Furnace	B15	Flexible Metal Exhaust Hose
B6	Reaction Zone Thermocouple	B16	Atmospheric-Pressure Vent
B7	Preheat Zone Furnace	B17	TG Balance Electrical Feed-through
B8	Preheat Zone Thermocouple	B18	Inert Purge Gas Inlet
B9	Quartz Reaction Tube	B19	Exhaust Gas Outlet
B10	Sample Basket	B20	Reaction Gas Inlet

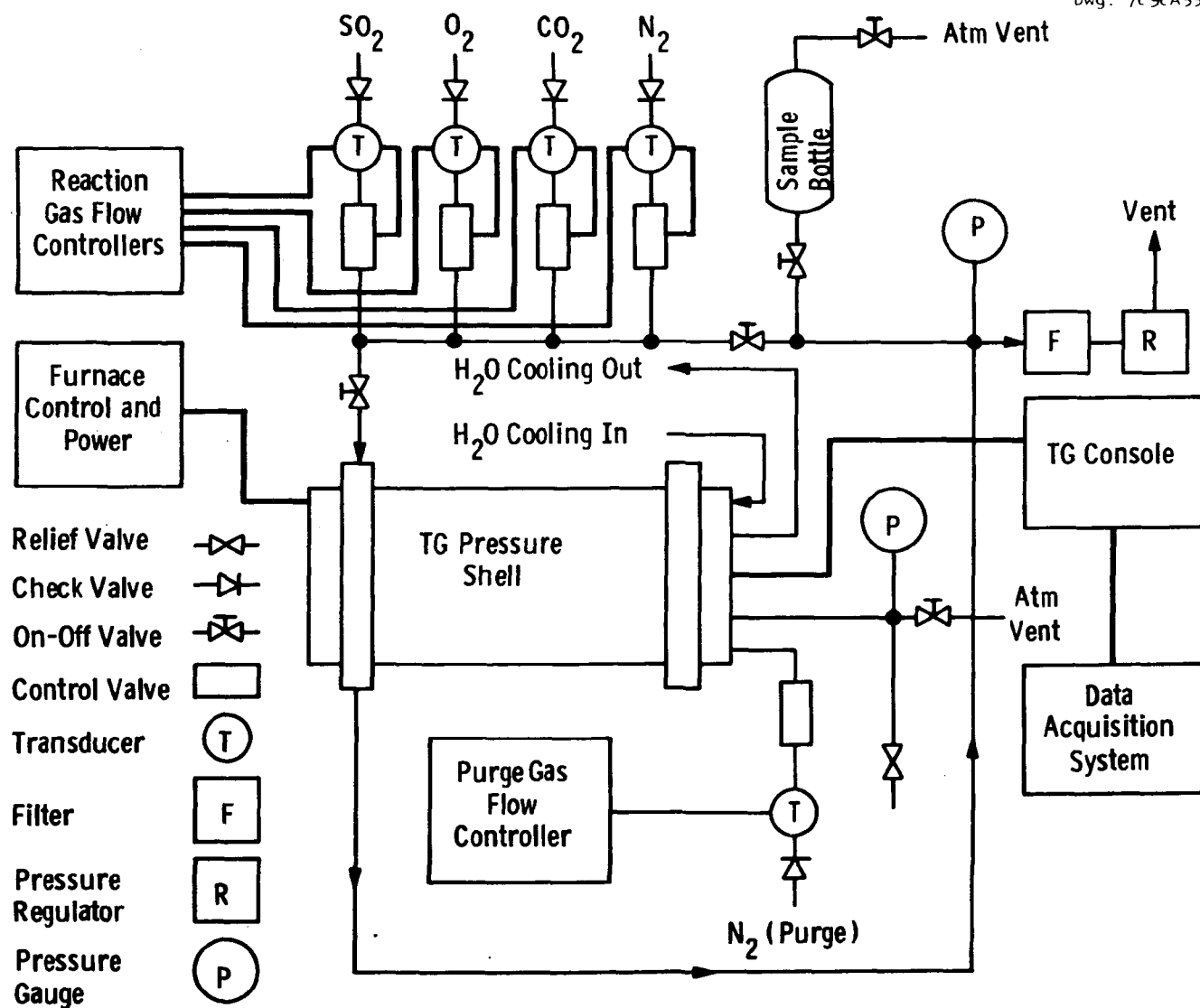


Figure 2 - Schematic Diagram of the Pressurized TG System

Temperature. Previous work¹ with Limestone 1359 calcines has shown that the initial sulfation rates at 101.3 kPa (1 atm) pressure at temperatures from 750 to 950°C are nearly identical. After 20 percent utilization of the calcium, however, the reaction rate varied. The utilization of the stone after one hour of reaction time improved with increasing temperature, up to 860°C. Further increasing the temperature caused sorbent utilization to decrease. Others^{13,14} have also found this phenomenon of an optimum temperature for limestone utilization at atmospheric pressure in laboratory- and bench-scale studies. Westinghouse TG results at 1013 kPa (10 atm) pressure,¹ however, showed that the extent of limestone sulfation increased with increased temperatures up to 900°C; further increasing the temperature to 950°C gave inconclusive results.

Operating fluidized-bed combustors at high temperatures is desirable, since at high pressures higher temperatures are required to calcine CaCO_3 . (Increased turbine inlet temperature will also improve turbine efficiency.) The use of limestone in high-pressure (1013 kPa/10 atm) FBC, therefore, is dependent on its performance at higher temperatures (>900°C). We, therefore, assessed the effect of temperature on the pressurized sulfation of limestone and dolomite.

Thermogravimetric experiments studying the influence of temperature on the pressurized sulfation of limestone and dolomite were carried out at 1013 kPa (10 atm) pressure. Greer limestone and Dolomite 1337 were the sorbents tested. Particles of 420 to 500 μm diameter were precalcined by heating them at a rate of 10°C/min up to the sulfation temperature in 4.3% CO_2 and 15.8% O_2 in nitrogen (N_2). The oxygen and CO_2 concentrations are representative of a 300 percent excess air level in combustion. This condition was chosen so that sorbents would be in the fully calcined state throughout the range of temperatures tested. The sorbents were then sulfated in the same atmosphere, plus 0.38% SO_2 .

Improved sorbent utilization was observed for both limestone and dolomite with increased temperature, up to 1000°C. Only a few runs were

done at temperatures greater than 1000°C because of furnace limitations. These runs, however, indicate that maximum sorbent utilization occurs at around 1000°C at 1013 kPa (10 atm) pressure. Table 2 summarizes the results. Figure 3 illustrates the temperature effect. The extent of sulfation was compared at the point at which the reaction rate was 0.1% calcium sulfating per minute. Although the sorbent is not saturated at this point, its rate of reaction is too slow for additional effective sulfur capture.

We suspect that the scatter in the data from Dolomite 1337 runs is the result of gas leakages in the TG system. Inlet and outlet seals were readjusted after this TG run series was completed.

The increased utilization of limestone with temperature (up to 1000°C) in pressurized TG sulfation was tested with particles of Greer limestone in three additional size ranges, 74 to 149 μm , 149 to 420 μm , and 2380 to 3360 μm . In agreement with the results obtained with 500 μm particles, the sorbent did not lose reactivity at high temperatures (see Figure 4). Tests on the large particles of Greer limestone, however, showed some scatter in the results. The larger particles of Greer limestone reached 25 to 50 percent of the utilization obtained by the 500 μm particles. No improvement in extent of sulfation occurred when the particle size was reduced to 149 to 420 μm . Little improvement in sorbent utilization would be expected, however, if the actual size of the sample was near 420 μm . The 74-to-149- μm particles were utilized 25 to 35 percent more than the 500 μm particles.

The TG rate data used to generate the plots are shown in Figures 5 through 7. The initial rates of reaction are fairly insensitive to temperature variation. Only after about 30 percent sulfation does the variation in sulfation rates with temperature become evident. At this extent of reaction, diffusion of SO_2 through the sorbent's pores would have an effect on the reaction rates.

Table 2

THE EFFECT OF TEMPERATURE ON SORBENT UTILIZATION AT 1013 kPa (10 atm)

Particle Size - 420-500 μm Sulfation Atmosphere - 0.38% SO_2 , 4.3% CO_2 , 15.8% O_2 , balance N_2 Precalcination - Heated at $10^\circ\text{C}/\text{min.}$ up to sulfation temperature in 4.3% CO_2 , 15.8%, balance N_2

Pressure - 1013 kPa (10 atm)

Greer Limestone			Dolomite 1337		
Run No.	Temperature, $^\circ\text{C}$	% Sulfation*	Run No.	Temperature, $^\circ\text{C}$	% Sulfation*
76-122	842 ± 8	43	P-7	840	60
76-123	896 ± 4	55	P-10	868.8 ± 0.4	65
76-124	866 ± 8	55	P-16	901 ± 1	58
76-125	955 ± 2	67	P-8	924 ± 2	> 67
76-126	928 ± 2	60	P-17	929 ± 3	67
76-127	978 ± 3	68	P-15	951 ± 3	77
76-128	980.3 ± 0.4	65	P-11	972 ± 1	> 75
P-23	1011 ± 1	55.5	P-13	976 ± 1	88
			P-14	979	83
			P-18	1005 ± 2	85

*% conversion of CaO to CaSO_4 when the sulfation rate falls below 0.1% $\text{Ca}/\text{min.}$

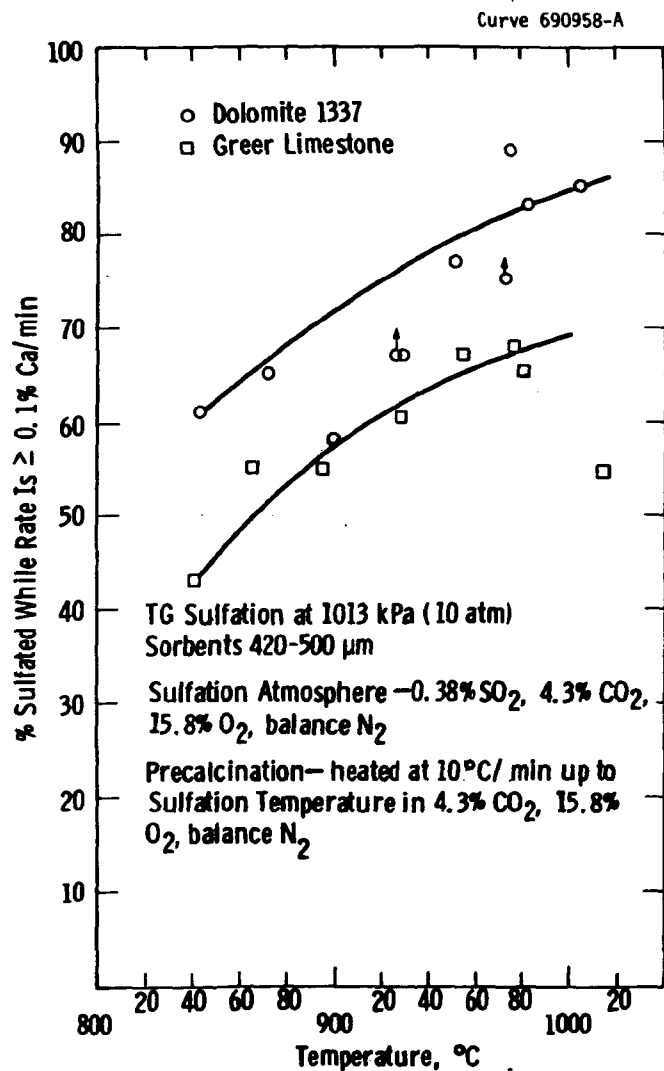


Figure 3 - The Effect of Temperature on the Pressurized Sulfation of Limestone and Dolomite

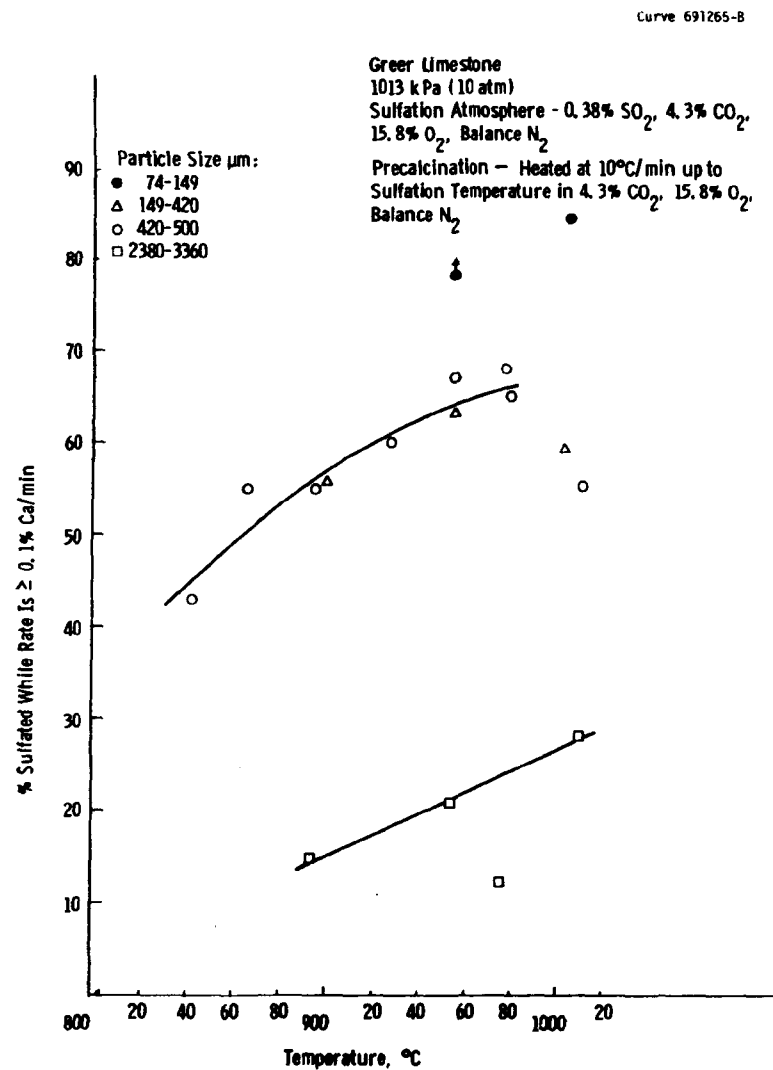


Figure 4 - The Effect of High Temperature on the Pressurized Sulfation of Small and Large Limestone Particles

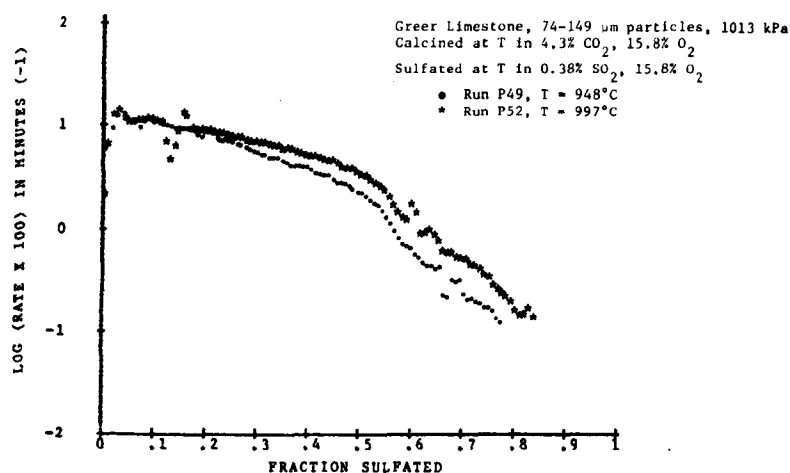


Figure 5 - The Effect of Temperature on the Pressurized Sulfation of Greer Limestone (74-149 μm particles)

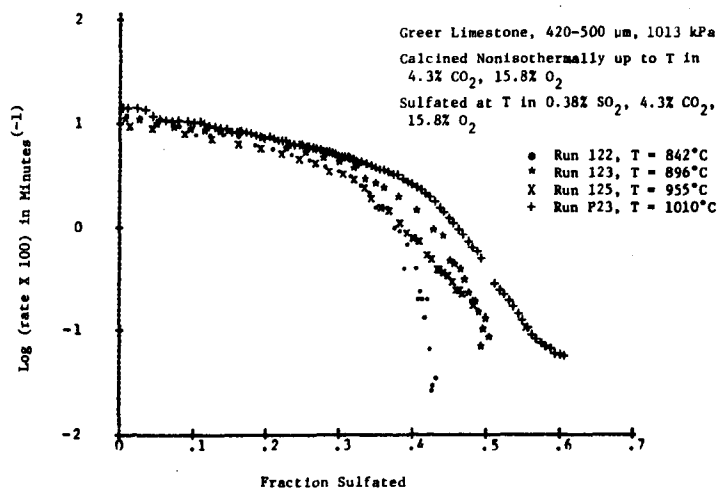


Figure 6 - The Effect of Temperature on the Pressurized Sulfation of Greer Limestone (420-500 μm particles)

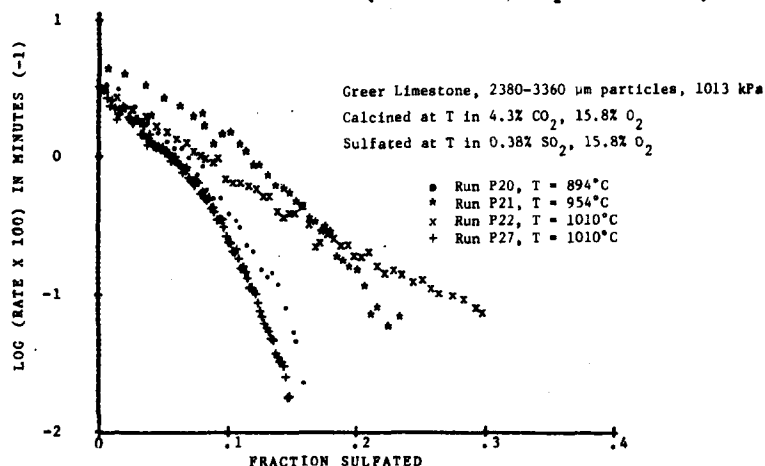
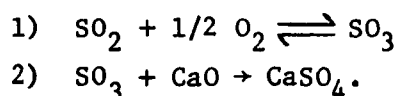


Figure 7 - The Effect of Temperature on the Pressurized Sulfation of Greer Limestone (2380-3360 μm particles)

Several mechanisms have been postulated to explain the occurrence of an optimum sulfation temperature at atmospheric pressure and the absence of such a temperature (up to 980°C) under pressure.

1) The Sulfite Mechanism

Moss¹³ has proposed a mechanism of sulfation based on the formation of sulfite (SO_3).



Using the Arrhenius equation and the observation that the rate is proportional to the gas concentration, we have for reaction 2

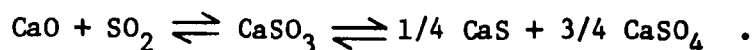
$$\text{rate} = K[\text{SO}_3]^n e^{-\frac{E_a}{RT}}.$$

The exponential term has the rate increasing with temperature, but the equilibrium concentration of SO_3 from reaction 1 decreases with temperature. Thus, an optimum temperature for sulfation should be observed, as it has been in the atmospheric case. The mechanism predicts a shift to higher optimum temperatures in pressurized sulfation because of increasing partial pressures of SO_3 as pressure is increased. Thus, one would expect that an optimum temperature would be observed in pressurized testing as well, when the testing is extended to higher temperatures.

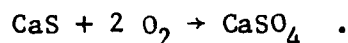
More recent work by Burdett,¹⁵ however, argues that the SO_3 concentration in fluid beds is far from the equilibrium level. It is likely that raising the temperature in the bed increases the oxidation rate and thus raises the local SO_3 concentration. As the temperature rises, therefore, the sulfation tends to occur at the outer edge of the stones, halting diffusion, lowering sorbent utilization, and producing a maximum in the sulfur retention/temperature curve.

2) The Sulfide/Sulfate Mechanism

An alternative explanation is that unstable calcium sulfite (CaSO_3) is formed first, and disproportionation to sulfate and sulfide occurs:⁶



This reaction is readily reversible, and the equilibrium SO_2 increases with temperature. Opposing the tendency to reject SO_2 , however, is the reaction in which the sulfide is air oxidized to the sulfate:



This oxidation reaction is extremely rapid, particularly at low sulfur contents (but, in the case of limestone, it is greatly impeded by formation of an impervious sulfate shell). A competition between SO_2 rejection and sulfide oxidation then controls the rate of reaction. At increased pressures the rate of SO_2 rejection would decrease, but the rate of SO_2 reaction with CaO and the sulfide oxidation would both increase. The balance point between the competing reactions would shift to higher temperatures, and the temperature maximum would shift to a higher temperature.

3) The Pore Structure Mechanism

The pore structure mechanism postulates that the rate of sulfation becomes too slow to be useful when the pores in CaO are filled with product calcium sulfate (CaSO_4). The pore structure is formed during calcination: when calcination is slow, i.e., retarded by a high local partial pressure of CO_2 , fine pores consolidate into wider pores, thus increasing the capacity of the sorbent. When calcination is rapid, CO_2 is expelled, reducing the local CO_2 partial pressure and forming fine pores. The reaction front moves rapidly away from the fine pores, freezing in place the fine pore structure initially formed.

When limestone is calcined in a fluidized-bed combustor at temperatures of around 820°C or lower, the partial pressure of CO_2 present is high relative to the equilibrium partial pressure over CaCO_3 (because of coal combustion), and the calcination reaction is slow, permitting consolidation of the pore volume among pores with larger radii and eventually greater sulfate capacity. If the temperature is raised to 900°C , the retarding action of the local CO_2 pressure is relatively trivial, since it is now only a small fraction of the equilibrium partial pressure. Calcination is rapid and mainly fine pores are created in the solid. This effect is illustrated in Figure 8 by plotting sulfur removal

Curve 718607-A

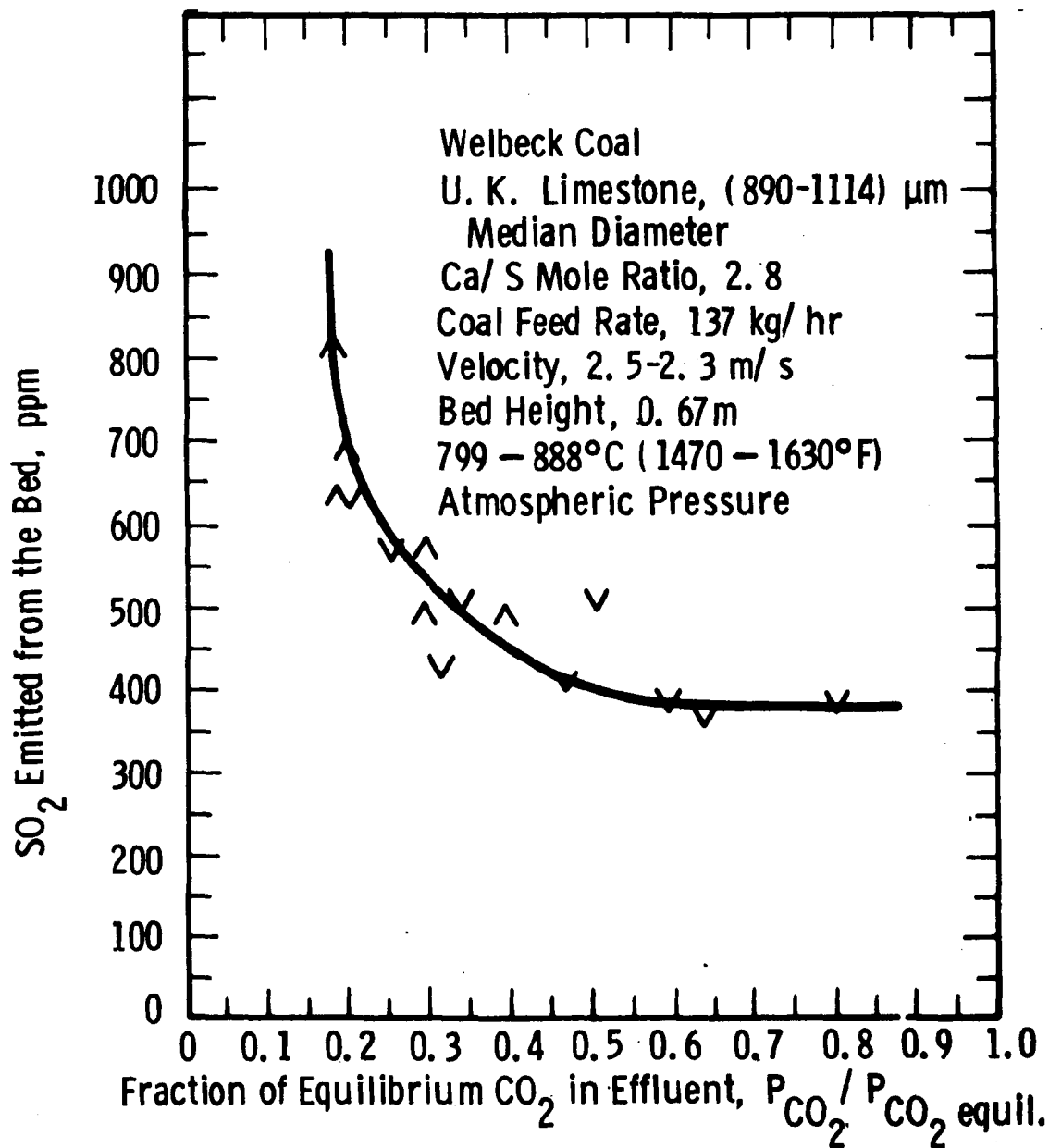


Figure 8 - The Effect of CO_2 Pressure during Calcination on SO_2 Emissions from a Fluidized Bed (calculated by Westinghouse using data from Reference 12, page A1.95)

results obtained by the National Coal Board (NCB),¹⁴ not as a function of temperature (the controlled variable) but as a function of partial pressure of CO₂ (P_{CO_2}) relative to the equilibrium value ($P_{CO_2 \text{ equil}}$). $P_{CO_2}/P_{CO_2 \text{ equil}}$ is a measure of the thermodynamic potential for slowing down calcination.

At atmospheric pressure calcination will not proceed to completion at low temperatures. As the temperature is increased, calcination occurs slowly to produce an optimum calcine. Further increasing the temperature increases the rate of calcination to the point where an inactive pore structure is formed and sorbent activity drops. If the system is operated at pressure, the partial pressure of CO₂ generated from combustion is greater than that generated at atmospheric pressure. Calcination, therefore, is slow, producing porous, active calcines at temperatures greater than those at atmospheric pressure. Active calcines are produced at those partial pressures of CO₂ that correspond to a $P_{CO_2}/P_{CO_2 \text{ equil}}$ ratio of 0.6.⁷ A combustor operating at 1013 kPa (10 atm) with 10 percent excess air would be operating at a $P_{CO_2}/P_{CO_2 \text{ equil}}$ of 0.6 at 980°C.

Two other mechanisms that have been postulated to explain the temperature effects, the silica deactivating mechanism¹⁶ and the oxidizing/reducing cycle mechanism, do not account for the fact that the phenomena are observed in the TGA where these mechanisms are not operative.

All of the proposed explanations for the temperature effects are incomplete in that they oversimplify a complex gas/solid reaction. The SO₃ and the sulfate/sulfide mechanisms are based on a chemically controlled reaction rate. They do not consider the influence of pore diffusion on the reaction rate. The pore structure mechanism does not explain why an optimum temperature for sulfation is observed when identical calcines, prepared at the same temperature, are sulfated at varied temperatures.¹⁰

Temperature influences the performance of the sulfur sorbent in two ways. It directly affects sulfation kinetics and indirectly affects the sorbent's performance by dictating the speed at which calcination occurs

(if at all) and, therefore, determines the pore structure of the calcine. Westinghouse TG, porosity, and electron microprobe data have shown that the pore-size distribution developed during calcination has a profound influence on the temperature response of different sorbents.^{8,10} The model for sulfation of porous limestone, developed by Hartman and Coughlin, which considers the chemical rate of sulfation at the individual grains of CaO, as well as the rate of diffusion of SO₂ through the sorbent's pores and through the product sulfate shell,¹⁷ was used to explain the TG results obtained.

In conclusion, high-temperature operation will not hinder the reactivity of limestones and dolomites at 1013 kPa (10 atm) pressure. Sorbent utilization, in fact, improves with increased temperatures up to 1000°C. The optimum temperature for desulfurization will depend on the sorbent type and its calcination process or pore structure. Thermogravimetric data can, experimentally, be used to determine the specific optimum temperature for any specified sorbent and operating conditions. To determine the optimum temperature theoretically, however, requires a much better understanding of the mechanism of sulfation than is currently possible.

Excess Air (O₂ and CO₂ Concentration) Effects. Fluidized-bed combustors are being designed to operate at excess air levels of 10 to 300 percent. Increasing the amount of excess air used to burn the coal changes the gas composition in which the sulfur sorbent reacts. The partial pressure of oxygen is increased, and the partial pressure of CO₂ is reduced. Typical concentrations of oxygen and CO₂ found in the bed are tabulated below as a function of excess air level.

% excess air	% O ₂	% CO ₂
10	1.9	15.7
20	3.5	14.4
100	10.5	8.7
200	14.0	5.8
300	15.8	4.3

The effects of oxygen and CO_2 concentrations on calcium-based sorbent sulfation were studied independently by varying the gas composition in TG experiments.

Previous work at Westinghouse⁵ has shown no effect of oxygen on the sulfation of dolomite with gas concentrations of 2 to 11 percent oxygen. In this work the range of oxygen concentrations tested was expanded to include all FBC operating conditions.

The effect of oxygen concentration on Tymochtee dolomite sulfation was studied at 101.3 and 1013 kPa (1 and 10 atm) pressure (Figures 9 and 10). The dolomite was sieved to 16 to 18 mesh and fully calcined on the TGA at 815°C in 15.2 kPa (0.15 atm) of CO_2 before the sulfations. The entire reaction was zero order in oxygen concentration at levels from 0.75 to 16% O_2 (0.075-1.6 atm O_2 for pressurized sulfation). The variations observed in the sulfation rates were independent of oxygen concentration and, therefore, attributable to sorbent inhomogeneity.

The sulfation rate curves for Tymochtee dolomite indicate greater than 100 percent sulfation of the sorbent. Since the fraction sulfated is calculated from the original calcium content of the sorbent, an inconsistency between the calcium in the analyzed sorbent and the sample sulfated might account for the excess sulfation. Sulfation of the magnesium fraction, however, or formation of the double salt found by Hubble et al.,¹⁸ $\text{Mg}_3\text{Ca}(\text{SO}_4)_4$, may be occurring.

The CO_2 level in the combustor directly determines the form of the sorbent, oxide or carbonate that will be absorbing SO_2 . The partial pressure of CO_2 in the combustor also has important secondary effects on sulfur sorption kinetics. In AFBC the calcined sorbent's pore structure and, hence, its reactivity depends on the partial pressure of CO_2 under which the sorbent is calcined. This phenomenon is a topic of another report⁷ and, therefore, was not investigated here. During PFBC, the CO_2 partial pressures generated are often greater than the equilibrium CO_2 partial pressure for CaCO_3 decomposition. The CaCO_3

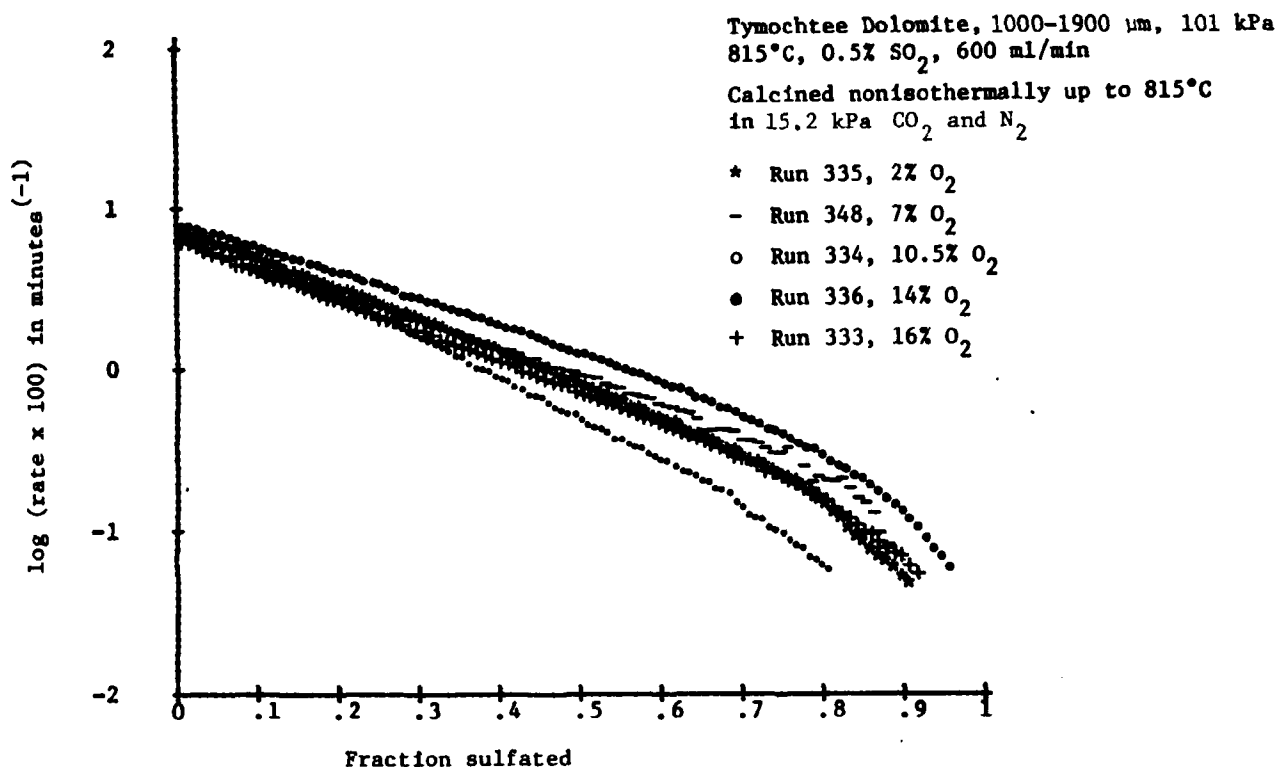


Figure 9 - The Influence of Oxygen Partial Pressure on the Rate of Dolomite Sulfation (101.3 kPa/ 1 atm)

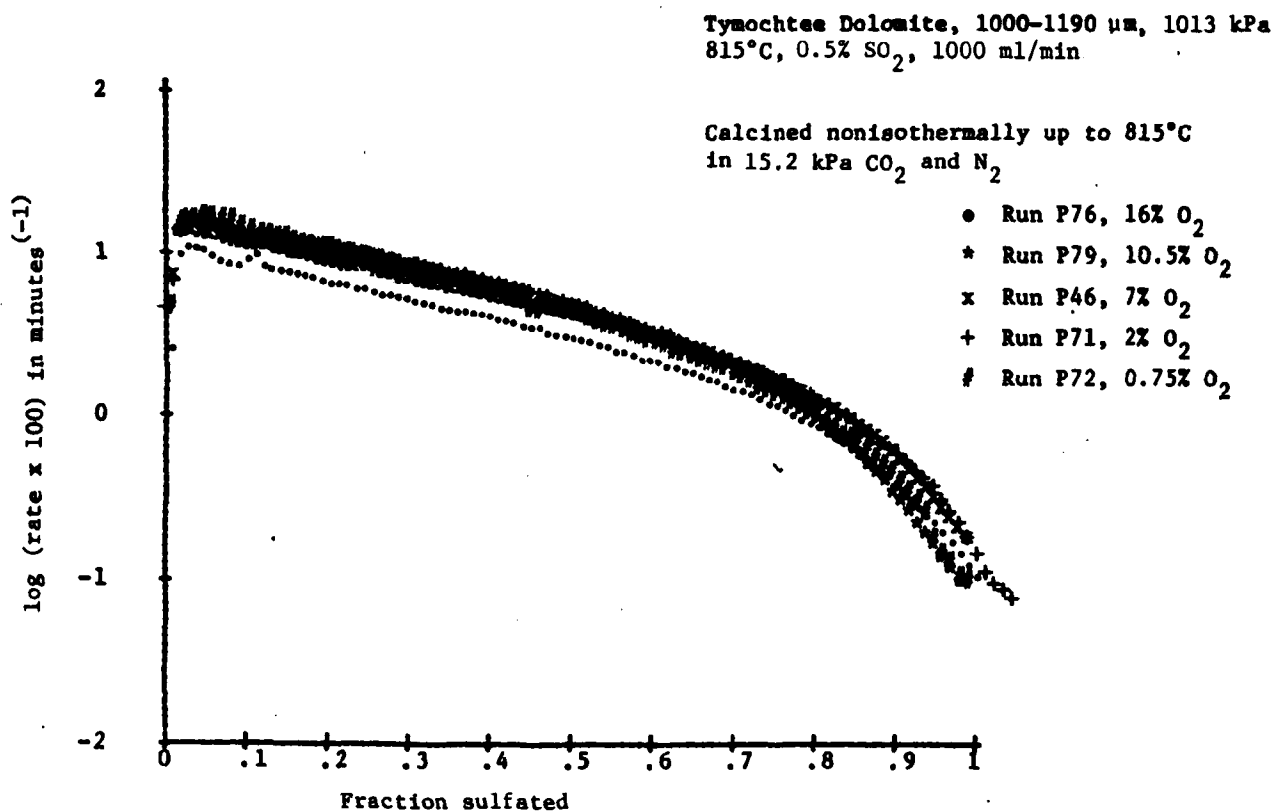


Figure 10 - The Influence of Oxygen Partial Pressure on the Rate of Dolomite Sulfation (1013 kPa/10 atm)

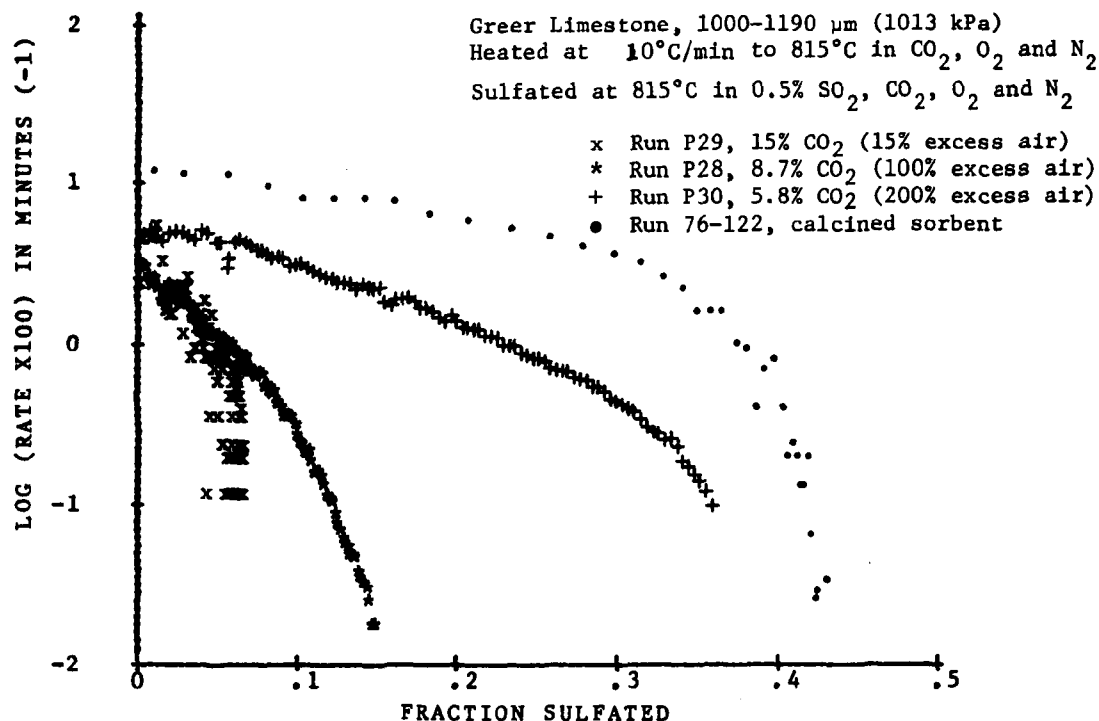


Figure 11 - The Influence of Excess Air Level on the Pressurized Sulfation of Uncalcined Limestone

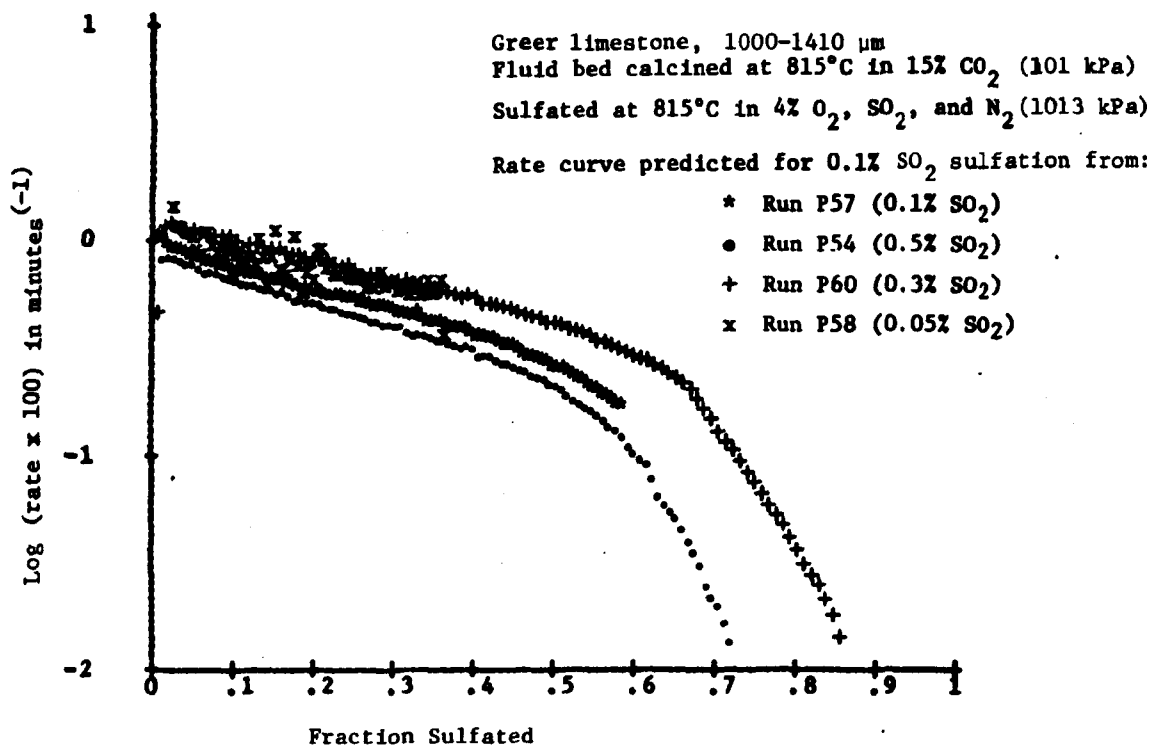


Figure 12 - The Influence of Sorbent Residence Time on the Sulfation of Greer Limestone (1013 kPa/10 atm)

fraction of limestone and dolomite, therefore, is often not calcined. Previous work² on carbonated sorbents has indicated that

- Most half-calcined dolomites ($\text{CaCO}_3 \cdot \text{MgO}$) are very active sulfur sorbents.
- Uncalcined limestone is a very poor sulfur sorbent.

Since it may be desirable to use limestone in high-pressure operation, the possibility of using uncalcined limestones was investigated further.

The sulfation of limestone in the presence of CO_2 at pressures greater than the equilibrium for the reaction $\text{CaCO}_3 \rightarrow \text{CaO} + \text{CO}_2$ is kinetically limited but thermodynamically favorable. The equilibrium concentration of SO_2 is less than 1 ppb at 871°C in 10% CO_2 , 4% oxygen, at 1013 kPa; yet, TG experiments using 500 μm particles of Limestone 1359 have shown only 3.4 percent sulfation at 850°C in 0.18% SO_2 , 4% oxygen, and 60% CO_2 in nitrogen (101 kPa). Limestone 1359, however, is a very pure calcitic stone, with small, interlocking grains. Diffusion of SO_2 through its carbonated structure is slow. Since the sulfation of half-calcined dolomite proceeds readily, an impure limestone, Greer, was tested for reactivity with SO_2 in the carbonated state. Although the magnesium (Mg) content of Greer limestone is low, 0.67 percent, the stone loses weight when heated in CO_2 because of the reactions of the impurities, aluminum (Al) (2.6%), silicon (Si) (7.2%), and iron (Fe) (1.3%). The structure of the Greer limestone was expected to be open to SO_2 diffusion.

Greer limestone particles of 1000 μm sulfated up to 36 percent in the carbonated state of 1013 kPa. The effect of excess air on the reaction was studied by using varied amounts of oxygen and CO_2 in the reactant gas. The sorbent was preheated at $10^\circ\text{C}/\text{min}$ at 815°C in CO_2 , oxygen, and nitrogen. The sulfation atmosphere was 0.5% SO_2 and 15% (2.7% O_2 and 15% CO_2), 100% (10.5% O_2 and 8.7% CO_2), and 200% (14% O_2 and 5.8% CO_2) excess air. As the excess air level increased (% O_2 increased and % CO_2 decreased), the utilization of the sorbent improved (see Figure 11). Argonne National Laboratories (ANL)¹⁹ have observed increased rates of

sulfation of half-calcined Dolomite 1337 when the CO_2 concentration was decreased from 100 to 40 percent at 101 kPa, 640 to 800°C. In high concentrations of CO_2 , it is likely that retarded diffusion of CO_2 away from the product CaSO_4 decreases the rate of sulfation in the carbonated material.

Impure limestones, such as Greer, should be useful sulfur sorbents in low-temperature combustion where the carbonated form of the sorbent is stable. TG results indicate that the reactivity of the carbonated sorbent will improve as the amount of excess air used in combustion is increased.

Sorbent Residence Time. Various investigators^{5,20,21} have reported that the sulfation of limestone is first order with respect to SO_2 concentration. The application of a first-order reaction model at high sulfate loadings, however, must be questioned.

The Tennessee Valley Authority (TVA)²¹ used the rate of sulfation after one minute of reaction to justify a first-order reaction in SO_2 . Borgwardt's²⁰ data were taken at a 10.5 percent conversion level of Dolomite 1337 at 870°C. This is also early in the reaction, since Dolomite 1337 has been shown to sulfate 100 percent at 815°C. Data from Battelle's dispersed phase reactor²² have indicated that the apparent order of sulfation increases with sulfate loading.

Thermogravimetric sulfation has typically been carried out in 0.5% SO_2 . Using 0.5 percent SO_2 provides sulfations that occur in about 2 hours and, therefore, are convenient to study in the laboratory. Sorbent residence times in fluidized beds, however, may be 12 hours. In burning a coal that contains 4 percent sulfur (S), the resulting SO_2 level is in the range of 0.09 to 0.34 percent, depending on the amount of excess air used.

The longer residence times and lower SO_2 concentrations in the fluid bed could cause sintering of the sorbent, changing its pore structure and, thus, its reactivity toward SO_2 . The effect of residence time at temperature on the sulfation kinetics of limestones at 101.3 and 1013 kPa (1 and 10 atm) was studied by sulfating sorbents on the TGA in gases of varied SO_2 concentrations.

The rate of sulfation at 1013 kPa (10 atm) in 0.1 percent SO_2 was predicted for Greer limestone using TG data from runs with 0.05 to 0.5 percent SO_2 in the gas and assuming first-order kinetics (Figure 12). The predicted curve is fairly consistent, indicating a first-order reaction is followed and the sorbent is unaffected by the time held at temperature (the time required for 37% utilization varied from 15 to 89 minutes). The same analysis using Grove limestone, however, indicates sintering of the stone decreases its reaction rate with temperature exposure (Figure 13). (The time of exposure when sulfated 8% varied from 4 to 66 minutes.) Similar results were obtained for Grove and Greer limestone at 101.3 kPa (atmospheric) pressure (Figures 14 and 15).

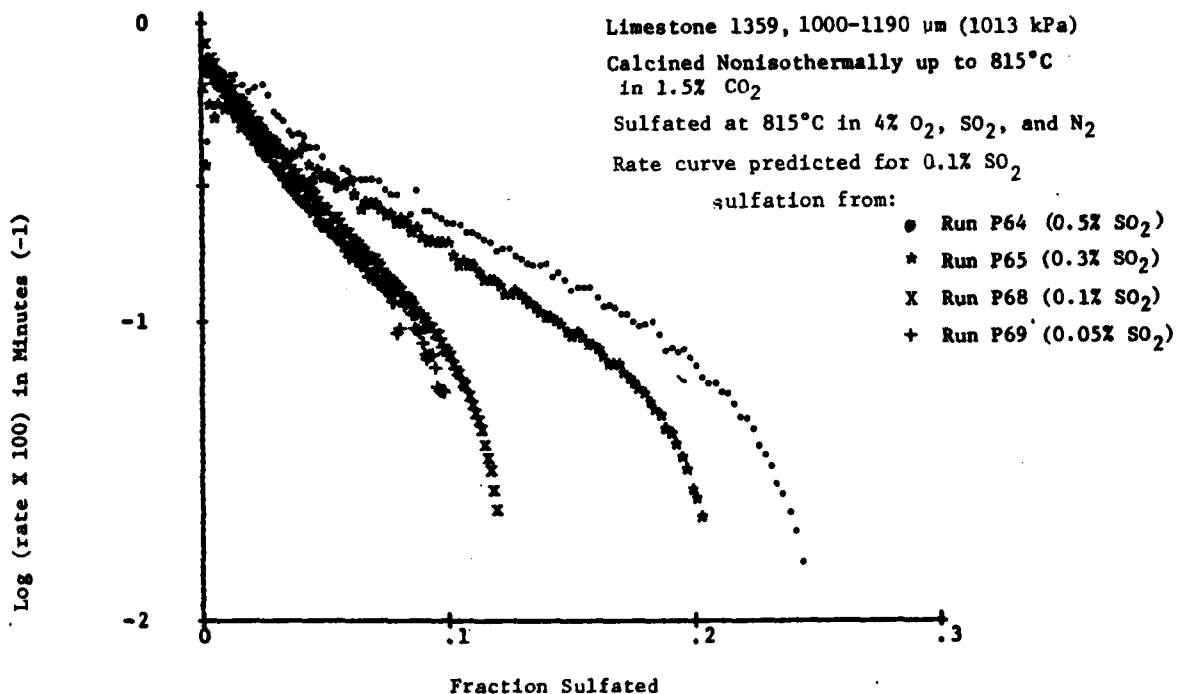


Figure 13 - The Influence of Sorbent Residence Time on the Sulfation of Limestone 1359 (1013 kPa/10 atm)

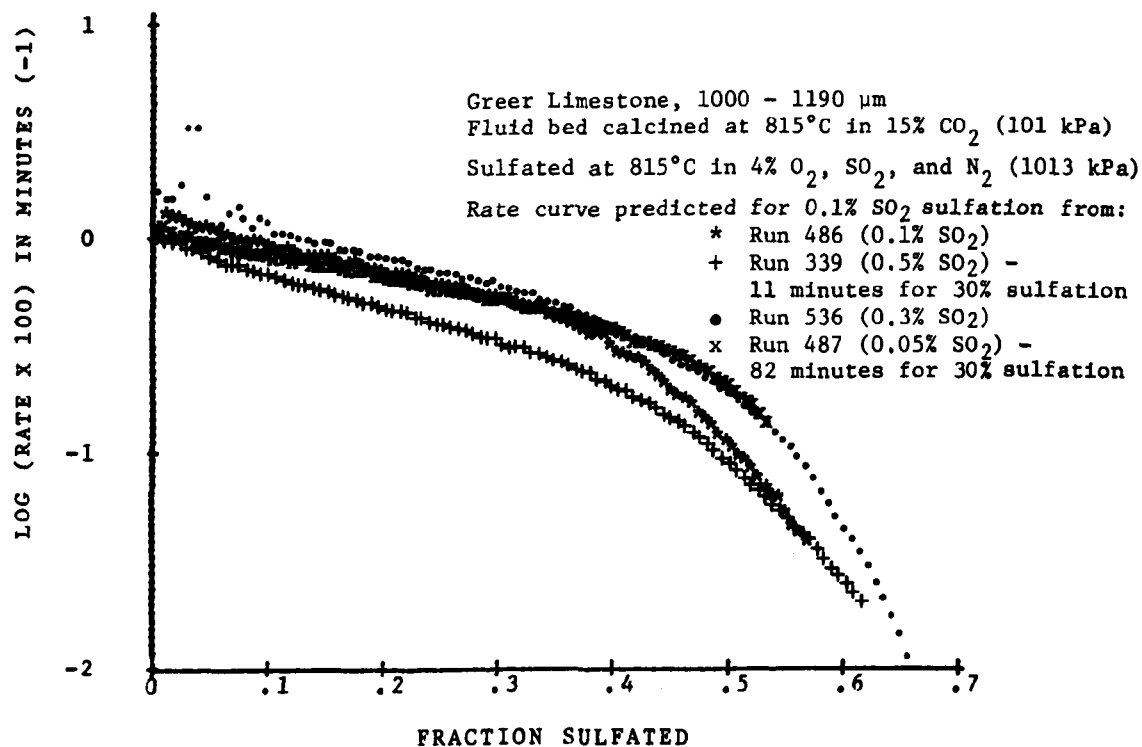


Figure 14 - The Influence of Sorbent Residence Time on the Sulfation of Greer Limestone (101.3 kPa/1 atm)

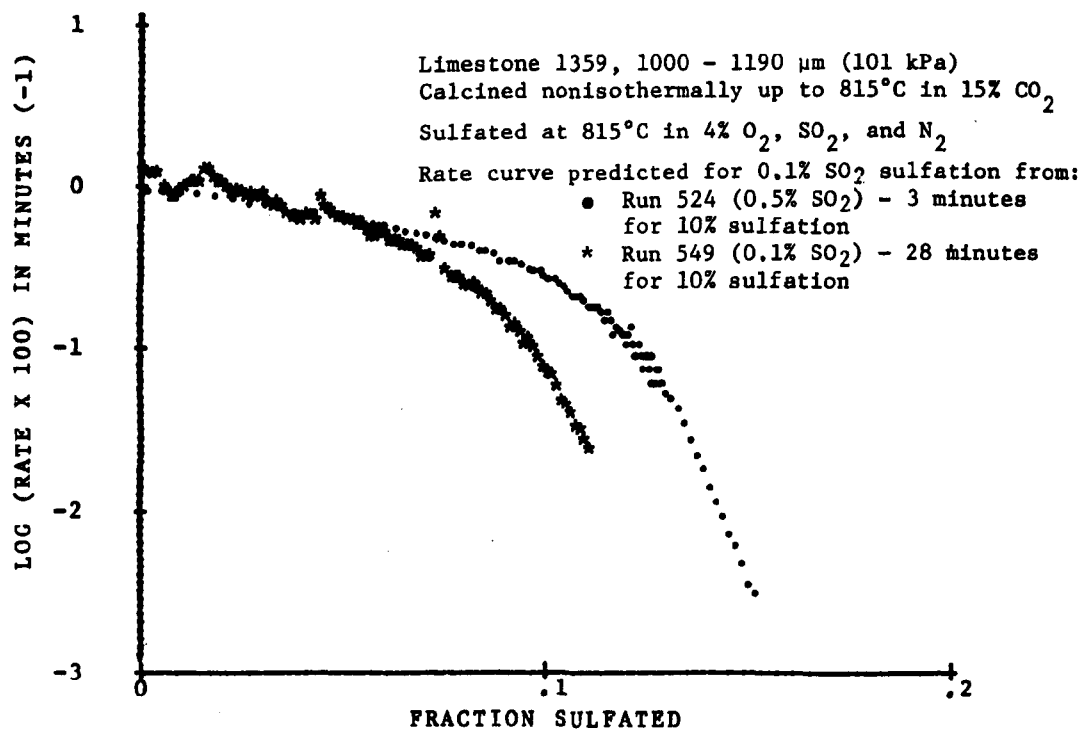


Figure 15 - The Influence of Sorbent Residence Time on the Sulfation of Limestone 1359 (101.3 kPa/1 atm)

We conclude that the residence time of a sorbent at temperature may change the sulfation kinetics by varying the sorbents' pore structure, from the first-order relationship observed at initial reaction periods. Depending on the type of sorbent, this effect could lead to errors in rate constants projected from TG data. Unfortunately, the types of sorbent that will show varied kinetics with residence time have not yet been identified. It is possible that the higher sodium content in the Greer Limestone, 0.2 percent sodium (Na), prevented shrinkage of the calcine's structure during the high-temperature exposure.

Pressure. Early Westinghouse studies⁵ at 1013 kPa (10 atm) pressure found that the sulfation rates at such high pressures were not significantly greater than those at atmospheric pressure. The variation in the sulfation rates of Greer Limestone and Tymochtee dolomite with pressure, when calcined under corresponding conditions, that was found during this test series is illustrated in Figures 16 and 17. The rate of sulfation increases with pressure; the increase, however, is not of the magnitude predicted by a first-order reaction in SO₂.

The ratio of the rate of sulfation at 1013 kPa (10 atm) to the rate at 101.3 kPa (1 atm) is shown in Figure 18 for Tymochtee dolomite sulfation. The dolomite was sieved to 16 to 18 mesh and calcined at 815°C in 0.15 atmosphere of CO₂ before sulfation. Increasing the pressure from 101.3 to 1013 kPa (1 to 10 atm) has increased the reaction rate by a factor of 2 to 3 over most of the sulfation. This relation can be rationalized by considering the rate of pore diffusion in a shrinking core model,

$$\frac{d\alpha}{dt} = \frac{1}{2\theta[(1 - \alpha)^{-1/3} - 1]} \quad *$$

where

$$\theta = \frac{a_p r^2}{6b D_p C}$$

The gas concentration, C, is proportional to P, and the pore diffusion coefficient, D_p, is the sum of two terms, one representing Knudsen

*See Nomenclature.

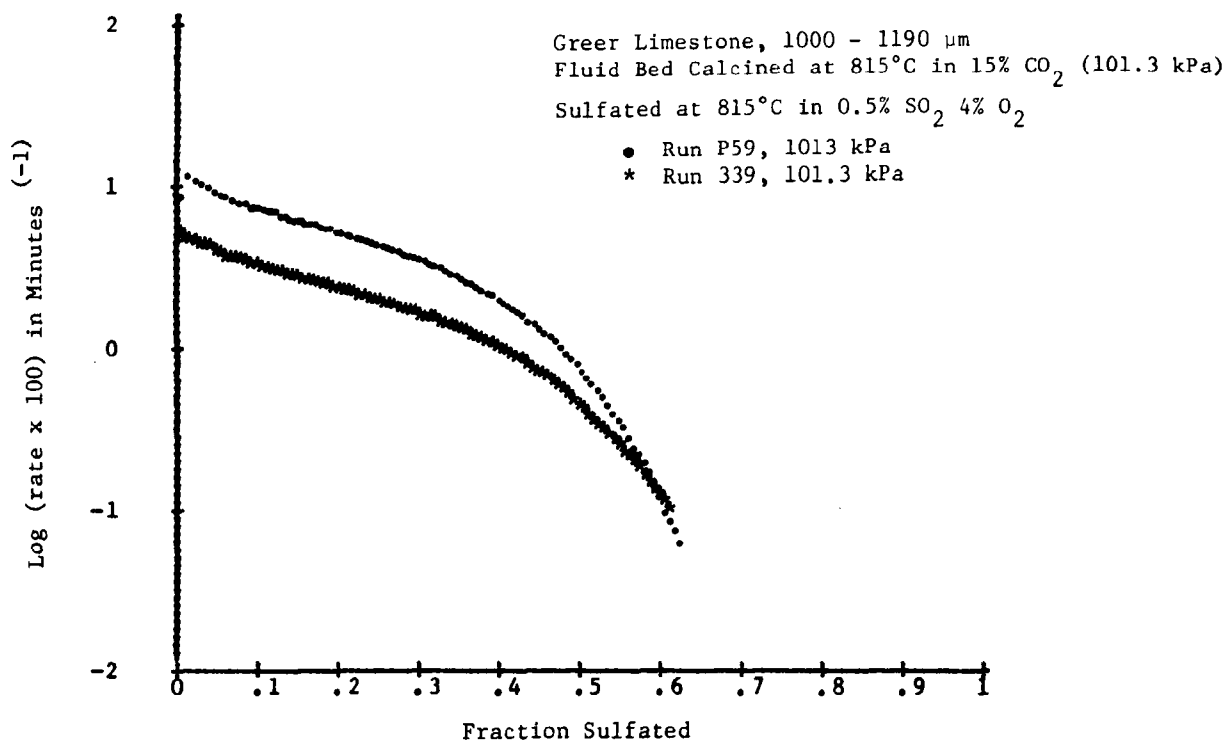


Figure 16 - Comparison of Sulfation Rates at 101.3 and 1013 kPa (1 and 10 atm) Pressure (Greer Limestone)

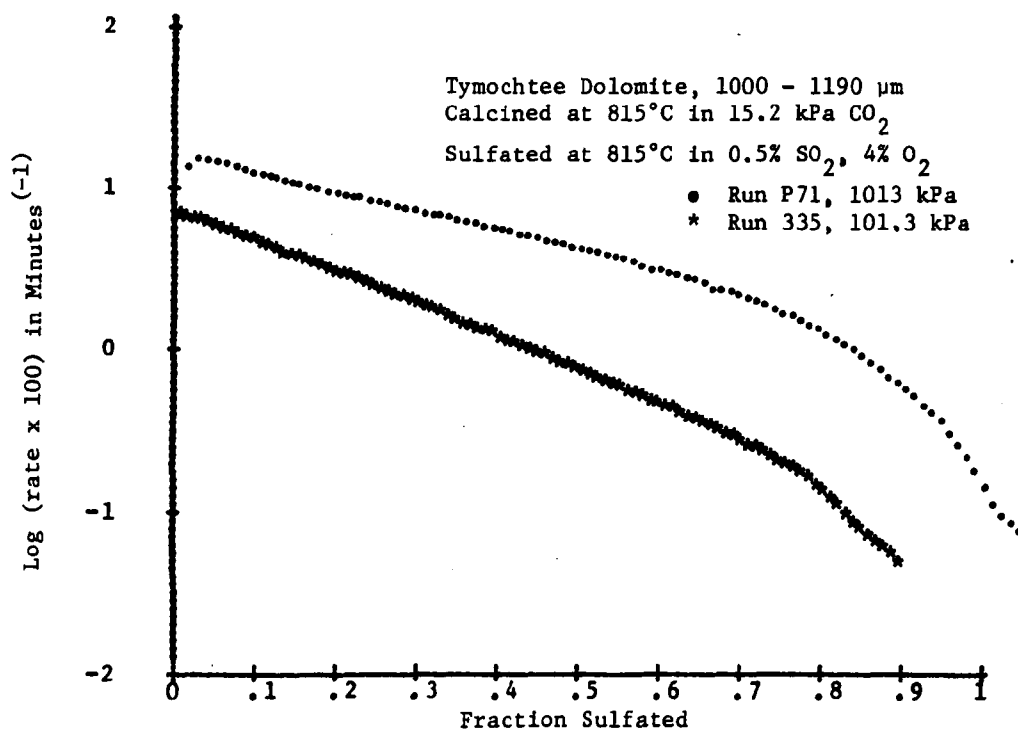


Figure 17 - Comparison of Sulfation Rates at 101.3 and 1013 kPa (1 and 10 atm) Pressure (Tymochtee Dolomite)

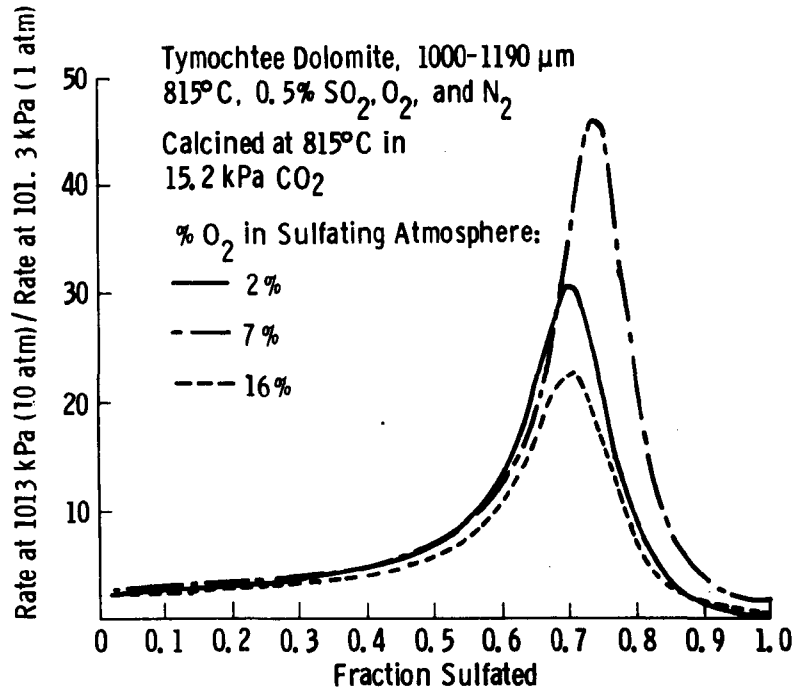


Figure 18 - The Effect of Pressure on the Sulfation Rate of Tymochee Dolomite

diffusion in small pores where collisions between gas molecules and the pore walls are more frequent than collisions between gas molecules:

$$D_p = \frac{X}{\tau} \left[\frac{3}{4\bar{r}} \left(\frac{\pi m}{2R\theta_A} \right)^{1/2} + \frac{1}{D} \right]^{-1}$$

Now the ratio of the rate at pressures to that at atmospheric, R_a , is

$$R_a = \frac{\left(\frac{d\alpha}{dt} \right)_P}{\left(\frac{d\alpha}{dt} \right)_{P=1}} = \frac{\theta(P=1)}{\theta(P)} = \frac{D_p C_{\text{SO}_2} (\text{at } P)}{D_p C_{\text{SO}_2} (\text{at } P=1)}$$

$$= \frac{P \left[\frac{3}{4\bar{r}} \left(\frac{\pi m}{2R\theta_A} \right)^{1/2} + \frac{1}{D(P=1)} \right]}{\left[\frac{3}{4\bar{r}} \left(\frac{\pi m}{2R\theta_A} \right)^{1/2} + \frac{1}{D(P)} \right]}$$

If no small pores are present, Knudsen diffusion is unimportant and

$$R_a = \frac{P \cdot D(P)}{D(P = 1)} = 1 \quad .$$

Since $D \propto \frac{1}{P}$, the rate is not affected by pressurization. If only Knudsen diffusion were important, however, the rate would be proportional to the pressure. In reality, limestone particles have a broad distribution of pore sizes, so D_p is a function of the fractional conversion, and this function could vary with pressure. The ratio of the diffusion controlled rates, therefore, could exceed 10. As the stones reach 100 percent conversion, the rates as well as the ratio approach zero.

The reaction, however, does not proceed by a simple shrinking core mechanism, and the combined effects of pore diffusion with chemical reaction must be considered to accurately project the effect of pressure on the sulfation reaction.

Sulfation of Large-Grained Dolomites. Two dolomites, Canaan from Connecticut and Kaiser from California, were chosen to study the sulfation of large-grained sorbents. We observed poor TG sulfation of 420 to 500 μm particles of Canaan dolomite in run P5 at 1013 kPa (10 atm) pressure, 843°C (see Figure 19). Electron microprobe scans of the sulfated product from Run P5 to show sulfur is concentrated almost solely at the grain boundaries of the sorbent (Figure 20). The low utilization is consistent with the finding by Combustion Power Company that sulfur penetration into large particles of massive-grained dolomites is not very deep and that fine particles are needed to achieve low calcium-to-sulfur (Ca/S) feed ratios and good desulfurization.

To determine if the large-grained dolomite could be utilized in a fine particle form, 74 to 149 μm particles of the sorbent were tested at 815°C at atmospheric pressure. The fine particles were precalcined to activate the sorbent. Greater than 50 percent utilization was achieved (see Figure 21). On a weight basis, however, the fine, precalcined sorbents were still less useful than 1000 μm particles of other

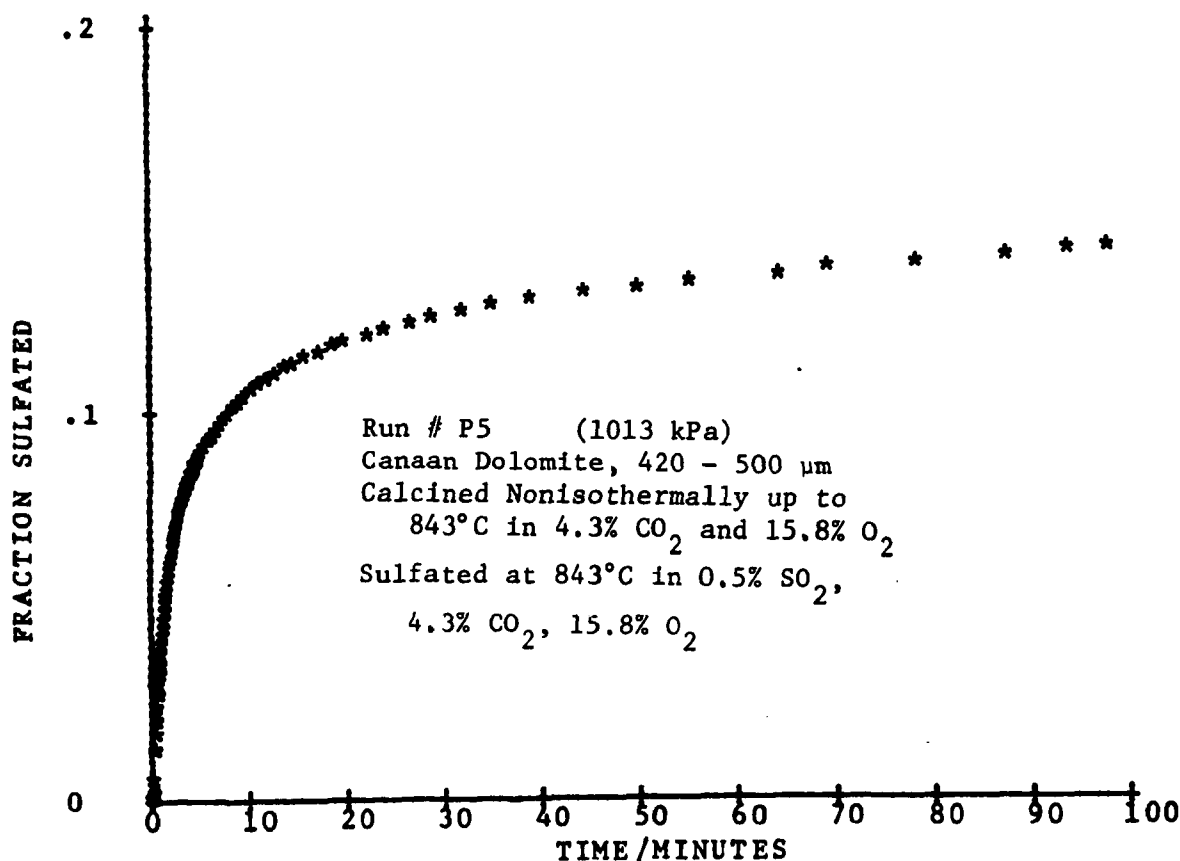


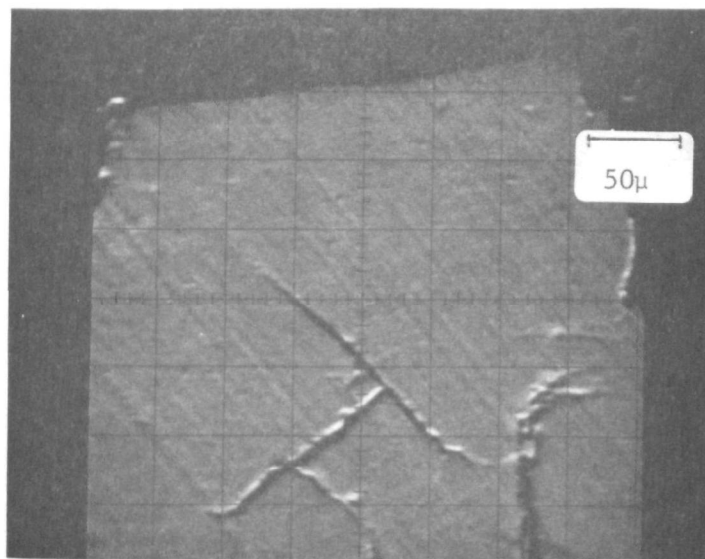
Figure 19 - TG Sulfation of Canaan Dolomite
 (420 - 500 μm particles)

smaller-grained, precalcined sorbents (Table 3). Although this extent of sulfation would require a Ca/S molar feed ratio of only 1.6 for 80 percent sulfur removal with Canaan dolomite, other limestones, or Dolomite 1337, would require a smaller feed on a weight basis, and the additional pulverizing would be unnecessary.

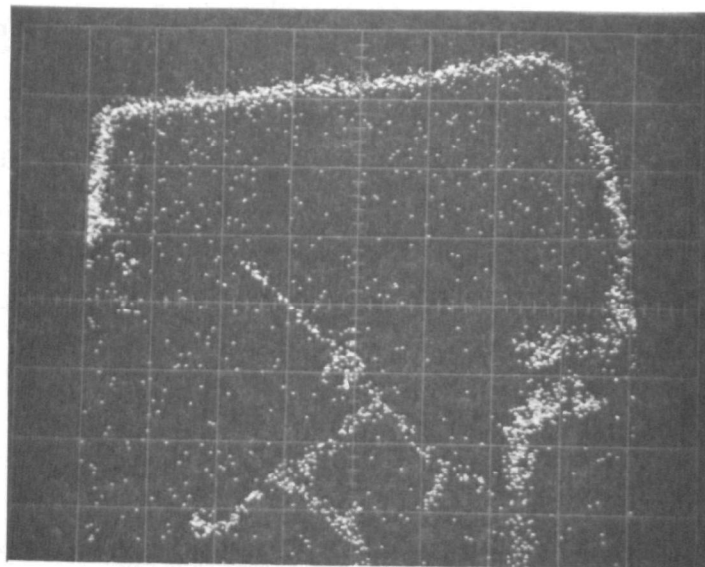
Prediction of Desulfurization Performance

Analysis of Pilot Plant Fluidized-Bed Data

We derived the projections of Ca/S molar feed ratio required to achieve any selected degree of desulfurization in a fluidized-bed combustor by using a simplified model for fluidized-bed desulfurization, with kinetic rate constants developed using laboratory TG data. For confirmation, where possible, we have compared the TG-supported model with available data from fluidized-bed combustors. The TG data base,



Photomicrograph of Scanned Area



Sulfur Scan

Figure 20 - Sulfur Penetration at Periphery and Grain Boundaries
of 500 μm Particle of Canaan Dolomite (~300 μm grains)

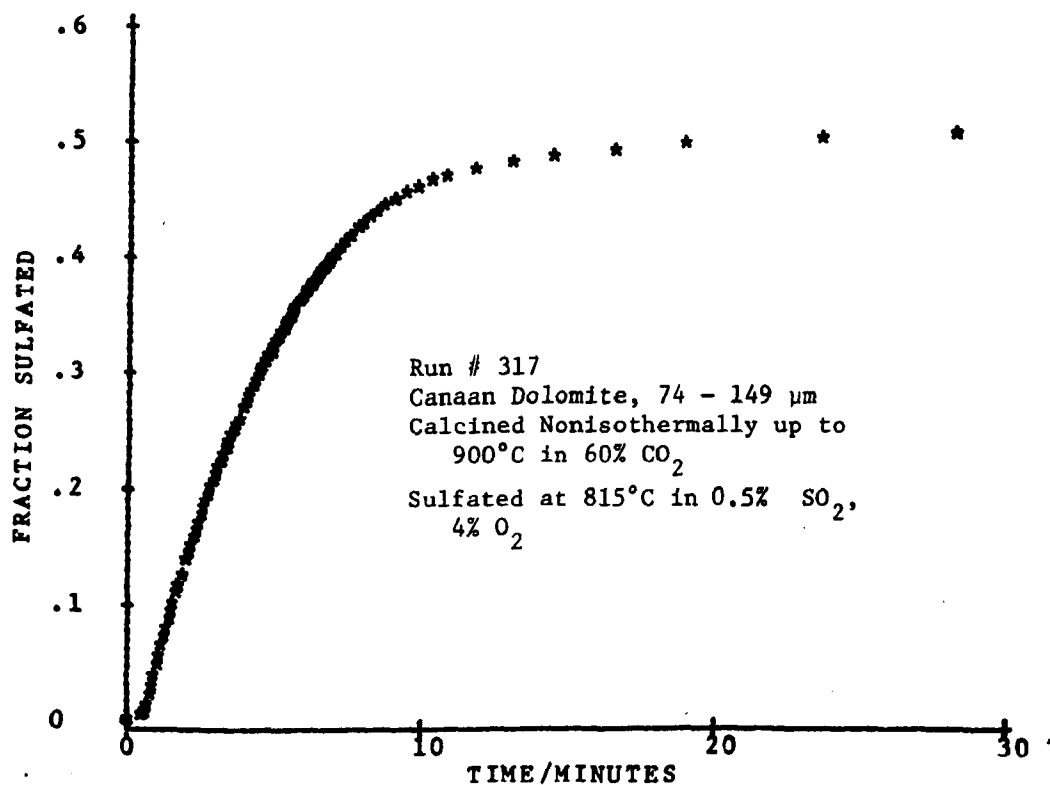


Figure 21 - TG Sulfation of Canaan Dolomite
(74-149 μm particles)

Table 3

RELATIVE EFFECTIVENESS OF LARGE-GRAINED
DOLOMITES IN SULFATION

Sorbent ^a	Grain Size, μm	SO_3 Pickup, ^b mg SO_3 /mg Sorbent	Particle Size, μm
Dolomite 1337	27	0.36	1000-1190
Greer Limestone	6	0.31	1000-1190
Lowellville Limestone	40	0.29	1000-1190
Limestone 1359	6	0.28	1000-1190
Canaan Dolomite	300	0.22	74-149
Kaiser Dolomite	>400	0.25	74-149

^a Sorbents were precalcined at 900°C in 60% CO_2/N_2 .

^b SO_3 pickup during 815°C sulfation (0.5% SO_2 , 4% O_2) while rate is $\geq 0.1\%$ Ca/min.

the model, and its agreement with fluidized-bed data are discussed in Appendix A. Areas for improvement of the projection technique are also identified.

Westinghouse Batch Fluidized-Bed Data

Batch fluidized-bed experiments were performed under an Electric Power Research Institute (EPRI) contract¹⁰ to compare the attrition rates of six sorbents. During these runs the limestones were sulfated, and the concentration of SO_2 in the effluent line was monitored as a function of time. The data collected (Appendix C) were analyzed here to determine how well rate constants derived from TG data compare to those found in the fluidized-bed unit. TG data from a seventh sorbent, Penrith limestone, were used to compare the rate constants from TG data to batch fluidized-bed data obtained by Cambridge University.²³

Fluid Bed Experimental Facility. Batch fluidized-bed experiments were performed in a 3.5-cm-diameter Inconel 600 batch reactor (Figure 22). The reactor sits in a shell that may be pressurized to 1013 kPa (10 atm). For these experiments the shell was open to the atmosphere. The four electric heating coils that surround the furnace were controlled by a Trendtrak programmer. Bed temperature was recorded by a thermocouple extending through the flanged reactor lid and down into the solids region.

The reactant gas, metered through rotameters, was preheated as it passed between the reactor and the furnace before entering the base of the bed. The distributor plate was made of an Inconel 600 disk through which 37 holes 0.012 cm in diameter were drilled. Pressure gauges were located on the manifold and effluent lines. The effluent gas passed through a continuously monitoring Dynasciences SO_2 meter.

The minimum fluidization velocity for the raw stone, 1000 to 1410 μm , was about 67 cm/s. Two run procedures were used. Some sorbents were sulfated immediately after calcination (Procedure 1). Other sorbents were cooled to room temperature after calcination (Procedure 2). A

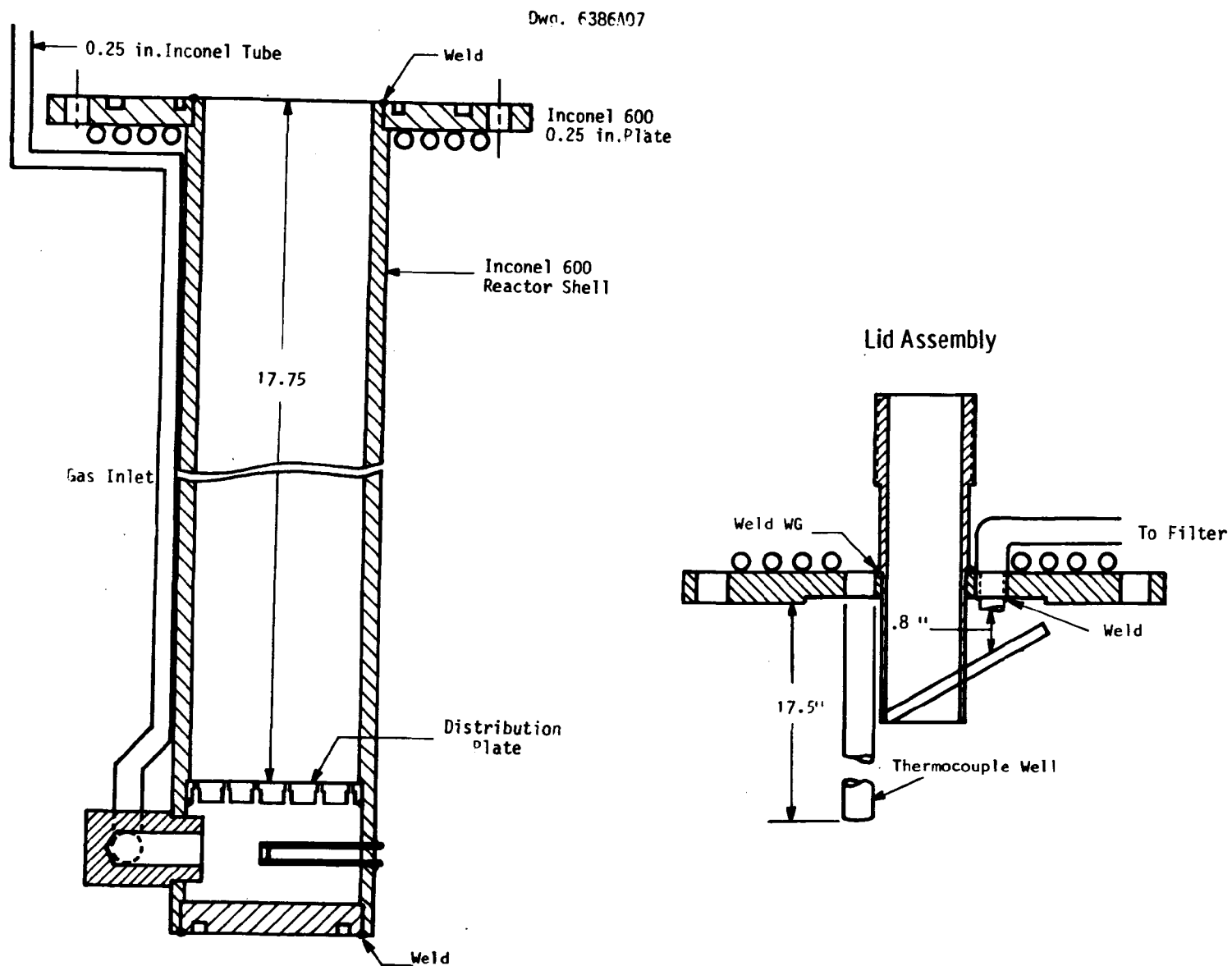


Figure 22 - Schematic of Batch Fluidized-Bed Reactor

sample of the fluidized-bed calcine was sulfated on the TG. The sorbent was later reheated and sulfated. The two procedures are outlined as follows:

- Procedure 1: Raw limestone, 100g, was heated at 10°C/min up to 815°C. The fluidizing gas was switched on (15% CO₂ in nitrogen). After four hours in the calcining atmosphere, the sulfating atmosphere was introduced (0.5 percent SO₂, 4 percent oxygen in nitrogen). When the monitor indicated a 20 or 80 percent breakthrough of SO₂ (0.1 or 0.4 volume percent SO₂ in the effluent), the fluidizing gas was turned off and the sample was cooled.
- Procedure 2: After four hours in the calcining atmosphere, the sorbent was cooled to room temperature and stored in a desiccator. A sample of calcine was TG sulfated. Before being sulfated in the fluidized bed, as outlined in Procedure 1, the sorbent was reheated at 10°C/min up to 815°C.

The operating conditions for the batch fluidized-bed runs are summarized in Table 4.

Estimation of Reaction Kinetics. The reaction rate of the sorbents can be defined in terms of an effective surface rate constant, K_s , based on the external surface area of the particles used,

$$\frac{dN}{dt} = K_s 4 \pi r^2 C ,$$

where

N = moles of solid reactant/particle

C = SO₂ concentration in emulsion gas, mole/cc

r = particle radius, cm.

Table 4

BATCH FLUIDIZED-BED EXPERIMENTS

Run	Limestone	Fluidizing Velocity, cm/s	Bed Height, cm ^a		Procedure Number	Surface Mean Particle Radius of Bed Material, cm	
			Static	Fluidized		After Calcination	After Sulfation
<u>W 3.5 cm Reactor</u>							
NU5	1359	95	-	7.6	2	0.056	0.055
NU6	Carbon	95	-	-	2	0.053	0.052
NU7	Brownwood	95	-	-	2	0.047	0.051
NU8	Ames	95	-	-	1	-	0.046
L6	Bellefonte	100	4.8	6.7	2	0.051	0.056
L11	Mississippi	100	5.4	-	2	0.043	-
<u>Cambridge 7.8 cm Reactor</u>							
Cambridge: Penrith		43.6	9.5	-	-	-	-

^aAs measured in open bed, prior to experiment.

The batch fluidized-bed data were analyzed with four models, as outlined in Table 5. All of the models assume perfect mixing of the solid phase. The particle surface area was calculated from the surface mean particle size of the bed material (Table 4); the particles are assumed to be spheres. The fraction of the bed calcium sulfated, α , was calculated from the effluent SO_2 concentrations, f = fraction of SO_2 in effluent line, by

$$\alpha = \frac{F_o \int_0^t (f_o - f) dt}{M_{\text{CA}}} ,$$

where M_{CA} is the number of moles of calcium in the bed and F_o is the total gas molar flow rate, mole/min.

The model that corresponded most closely to data from TG experiments (model 1) assumed plug flow of the gas phase, with sulfur generation occurring at the bed's base.

$$K_s = \frac{F}{S} \ln \frac{C_o}{C} ,$$

where

F = total gas flow rate, cc/s

S = surface area of particles in the bed.

If we assume spherical particles in the bed,

$$S = \frac{3 w_b}{\rho r}$$

(ρ = density of the limestone, g/cc; w_b = bed weight, g).

The effective surface rate constant was calculated from TG data as follows:

$$\frac{dN}{dt} = K_s 4 \pi r^2 C = \frac{d\alpha}{dt} \rho \left(\frac{4}{3} \pi r^3 \right)$$

Table 5

SUMMARY OF MODELS USED TO ANALYZE FLUIDIZED-BED DATA

Model	K_s from Fluid Bed Data	Comments
1 • Plug flow with S generation at base of bed • Quasi-steady-state	$K_s = F/S \ln C_o/C$	Best agreement with TG data
2 • Plug flow with uniform S generation • Quasi-steady-state	$C/C_o = \frac{F}{SK_s} (1 - e^{-\frac{SK_s}{F}})$	K_s in fluid-bed initially much higher than from TG data
3 • Perfect gas mixing • Quasi-steady-state	$K_s = \frac{F}{S} \left(\frac{C_o}{C} - 1 \right)$	K_s in fluid-bed initially much higher than from TG data
4 • Perfect gas mixing • Transient	$K_s = \frac{Ah_s}{St} \frac{\delta + (1-\delta)\epsilon}{1 + \delta} \ln \frac{C_o}{C}$	Valid only where t is on the order of gas residence time

Nomenclature:

K_s = surface rate constant, cm/s
 F = superficial volumetric gas flow rate, cc/s
 S = surface area of particles in bed, cm²
 C = SO₂ concentration in effluent line
 C_o = SO₂ concentration fed to bed
 h_s = static bed height, cm
 δ = volume fraction of bubble phase
 ϵ = void fraction of emulsion phase
 t = time, s
 A = cross-sectional area of bed, cm²

or

$$K_s = \frac{da}{dt} \frac{\rho r}{3C} \quad .$$

Modeling Results. Figures 23 and 24 compare the rate constant derived from the four fluidized-bed models. The surface rate constants calculated from the transient model are much smaller than the others. The transient model would be expected to apply at reaction times on the order of the gas residence time, which was only 0.05 to 0.08 s for the fluidized-bed runs. Sulfur dioxide evolution data were not measurable until one or two minutes of reaction. Steady-state models, therefore, would apply. At low values of the ratio of the SO_2 concentration leaving the bed to that fed, C/C_0 , the second and third models gave rate constants that were much greater than those predicted from model 1 and the rate constant measured in TG data. At higher levels of SO_2 emission, C/C_0 , however, the rate constants predicted using models 1 through 3 were very similar. The similarity is illustrated by comparing the ratio of the rate constant predicted from model 1 (plug flow of gas with below-bed sulfur generation) to the rate constant predicted from model 3 (perfect gas mixing) as a function of C/C_0 :

C/C_0	$K_s \text{ (Model 3)}/K_s \text{ (Model 1)}$
0.1	3.9
0.2	2.5
0.5	1.4
0.8	1.3

At low C/C_0 , where a large fraction of the sulfur fed is absorbed by the bed, perfect gas mixing is not likely. Since sulfur is fed at the bed's base, uniform generation of sulfur is an unlikely model when most of the sulfur is being absorbed by the sorbent (i.e., at low C/C_0). As might be expected, rate constants derived from model 1 (plug flow of gas with

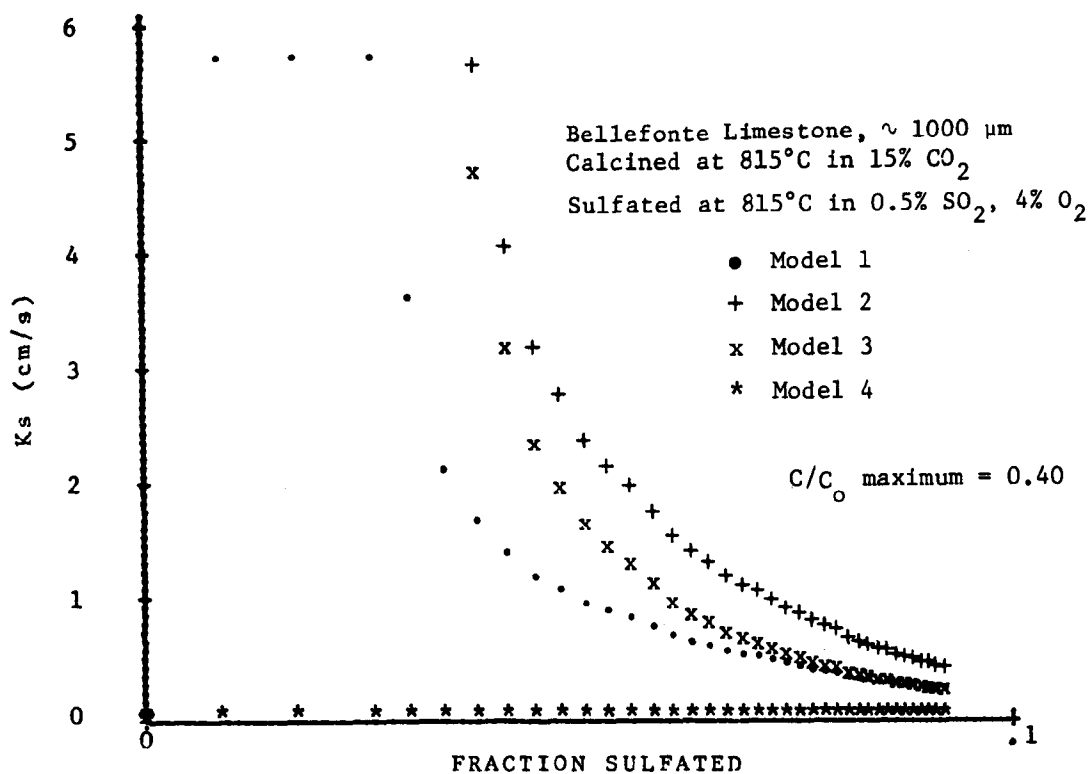


Figure 23 - Comparison of Fluidized-Bed Models (Bellefonte limestone)

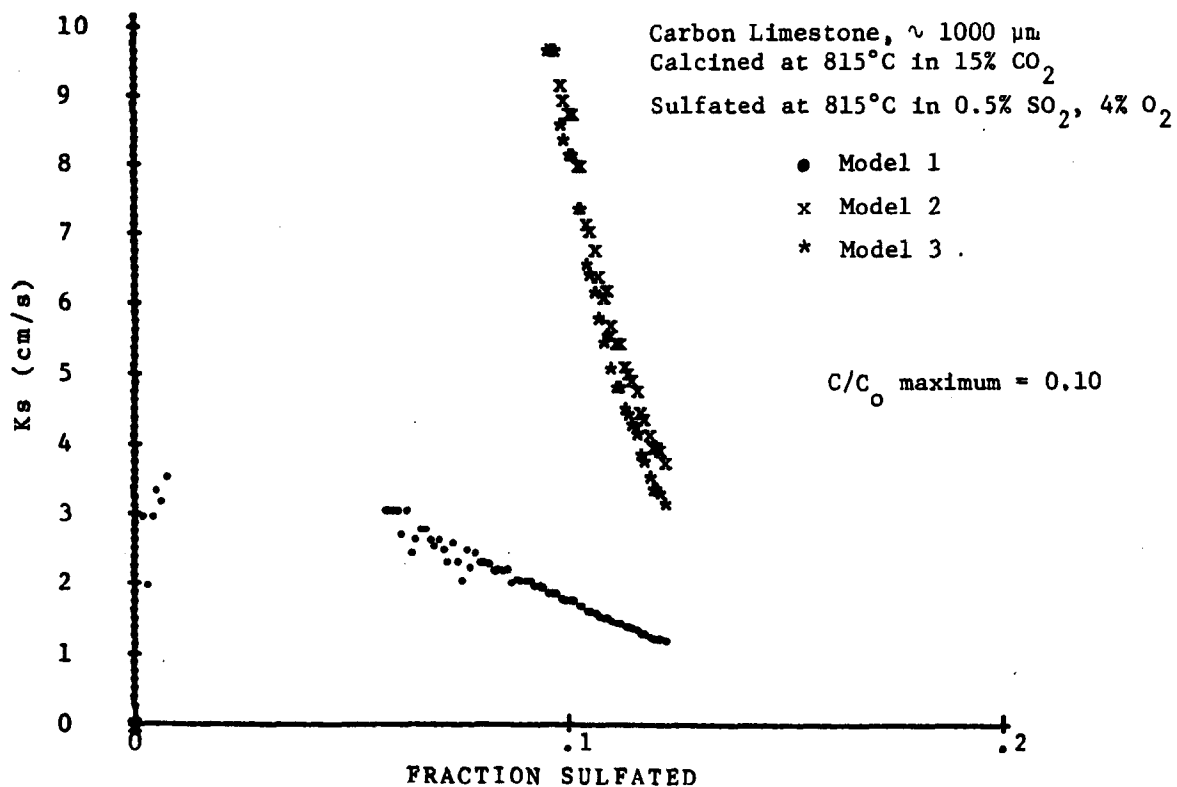


Figure 24 - Comparison of Fluidized-Bed Models (Carbon limestone)

sulfur generation at the bed's base) corresponded most closely to the rate constants measured on the TGA. At high C/C_0 , however, there was little difference in the quasi-steady-state models.

The comparison between rate constants derived from fluidized-bed data using model 1 and rate constants measured on the TGA is illustrated in Figures 25 through 30. The agreement is excellent for Carbon, Grove, and Brownwood limestones. The worst agreement was found for Ames limestone. During previous work,¹⁰ however, this stone was found to be inhomogeneous. In addition, the calcine used for the TG sulfation was prepared in the TGA. If any large deviation in calcination conditions (i.e., temperature, CO_2 partial pressure) existed between the fluidized-bed and the TGA, the sorbent's pore structure and, therefore, its sulfation rate would be varied. The rate constants of Mississippi and Bellefonte limestone, derived from fluidized-bed data, differed from those measured on the TGA by, at most, a factor of three. Sorbent utilization at any particular rate constant does not vary greatly since the sorbents were not highly utilized.

Some shortcomings of the fluidized-bed apparatus should be noted. The bed heights were very low, and, therefore, the fluidization produced may not be representative of larger units. The drilled distributor plate sometimes became partially plugged during operation. Dead regions in the bed near the plate, therefore, may have restricted the active section of the bed.

The comparison of TG rate constants for Penrith limestone to those obtained from a 28-cm batch fluidized-bed unit at Cambridge University using a bubbling bed model is shown in Figure 31. Rate constants obtained in the batch fluidized-bed were greater at low sulfate conversions than at those derived from TG data.

In conclusion, rate constants derived from batch fluidized-bed data are fairly insensitive to the bed model used to interpret the data, provided C/C_0 is >0.2 . Quasi-steady-state models tested include plug flow

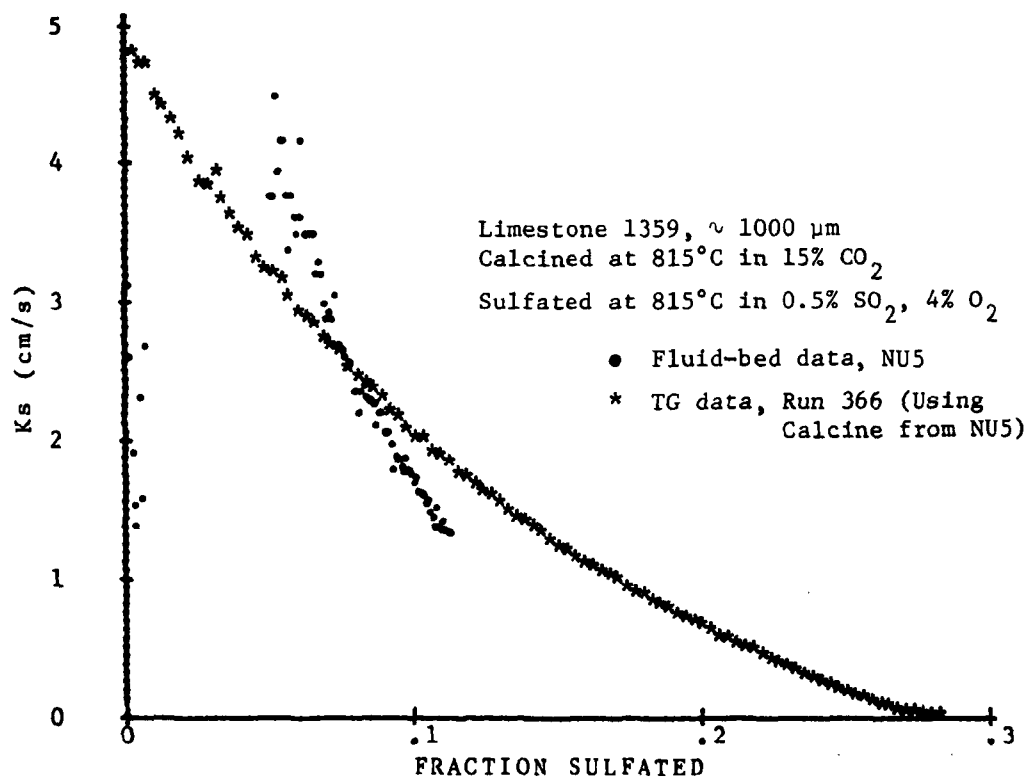


Figure 25 - Comparison of Rate Constants Derived from Fluidized-Bed Data (Model 1) and TG Data: Limestone 1359

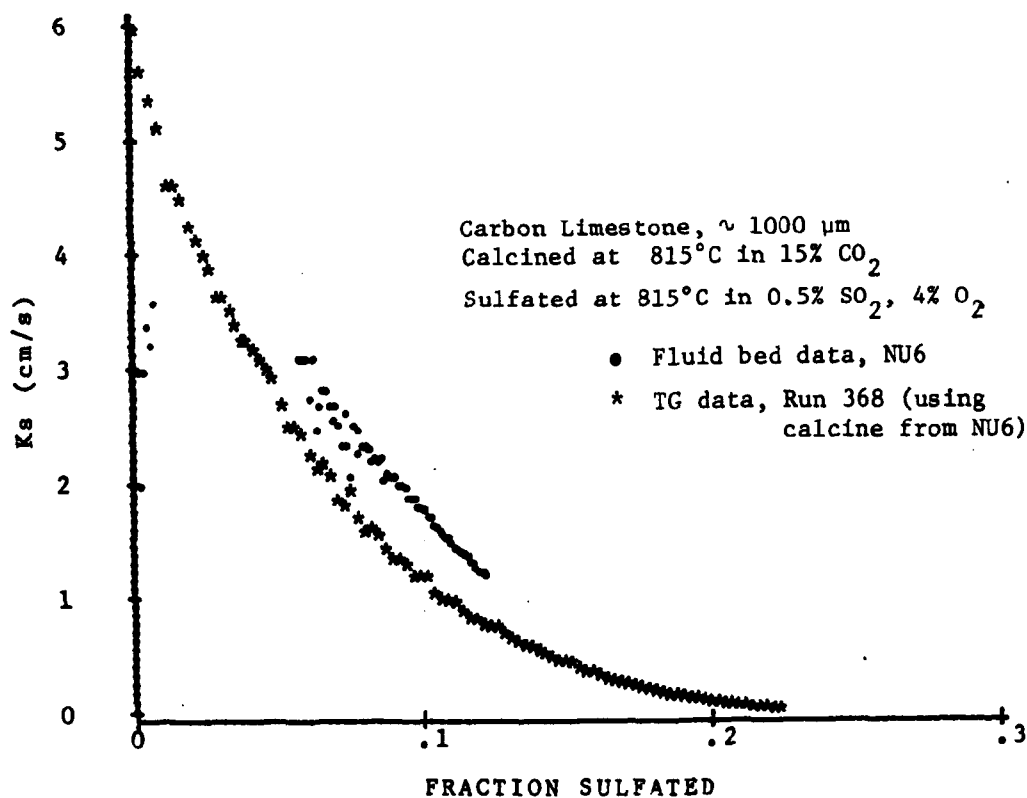


Figure 26 - Comparison of Rate Constants Derived from Fluidized-Bed Data (Model 1) and TG Data: Carbon Limestone

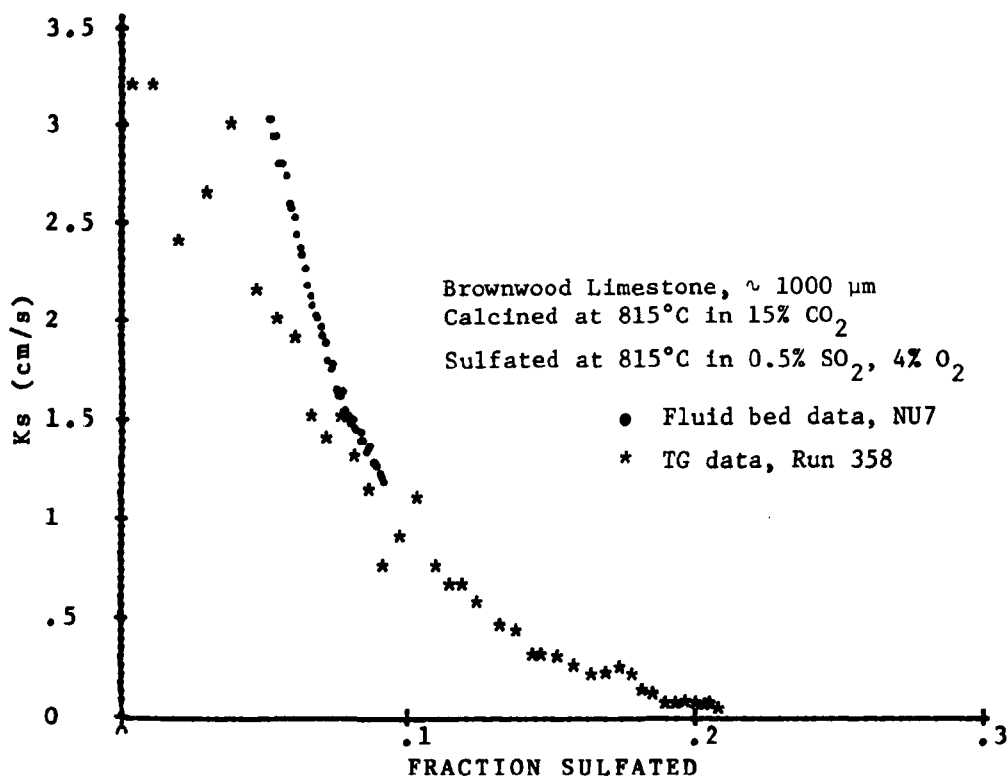


Figure 27 - Comparison of Rate Constants Derived from Fluidized-Bed Data (Model 1) and TG Data: Brownwood Limestone

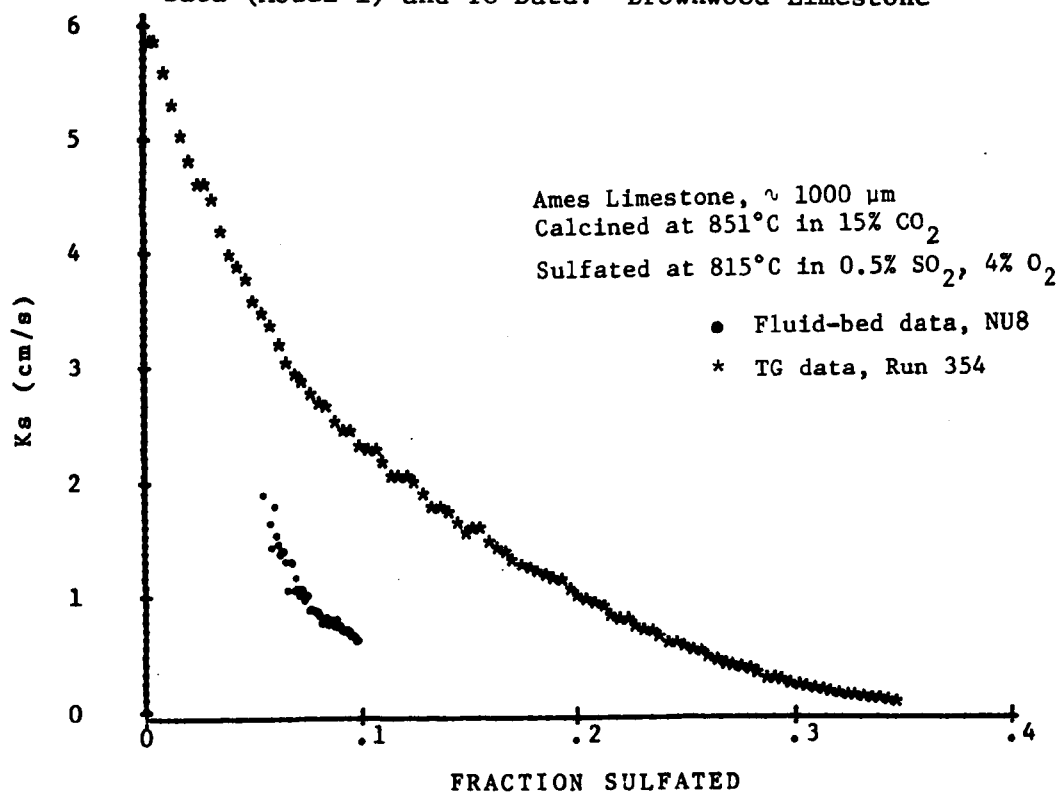


Figure 28 - Comparison of Rate Constants Derived from Fluidized-Bed Data (Model 1) and TG Data: Ames Limestone

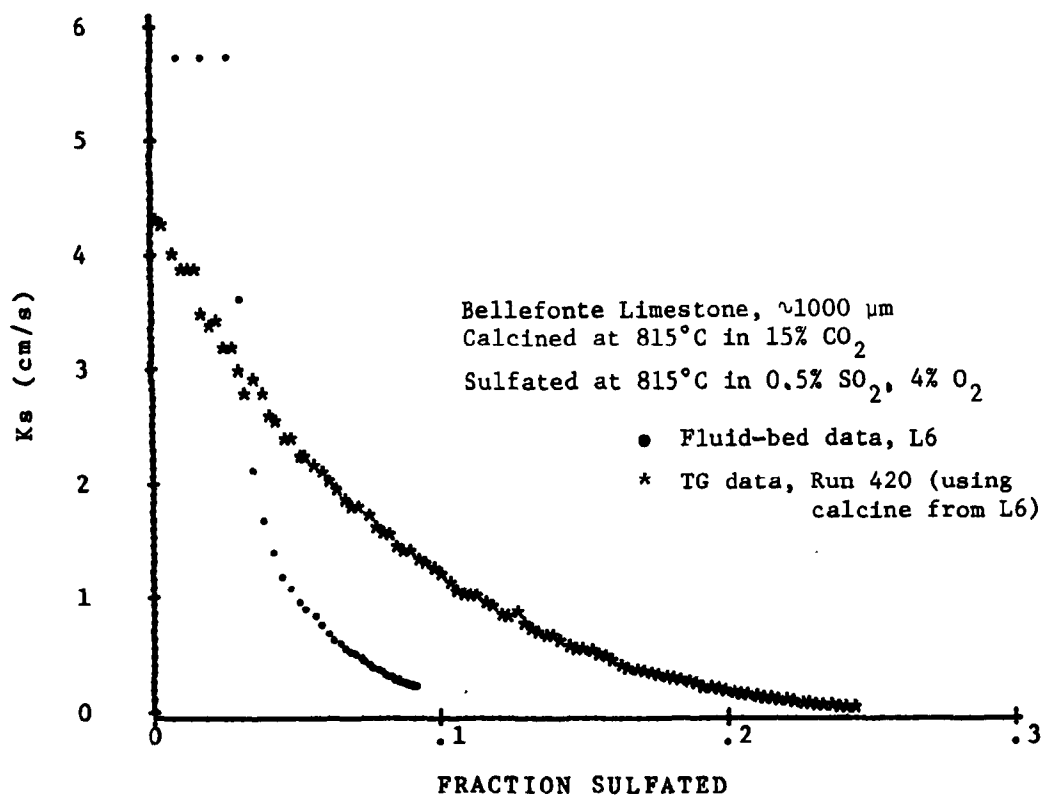


Figure 29 - Comparison of Rate Constants Derived from Fluidized-Bed Data (Model 1) and TG Data: Bellefonte Limestone

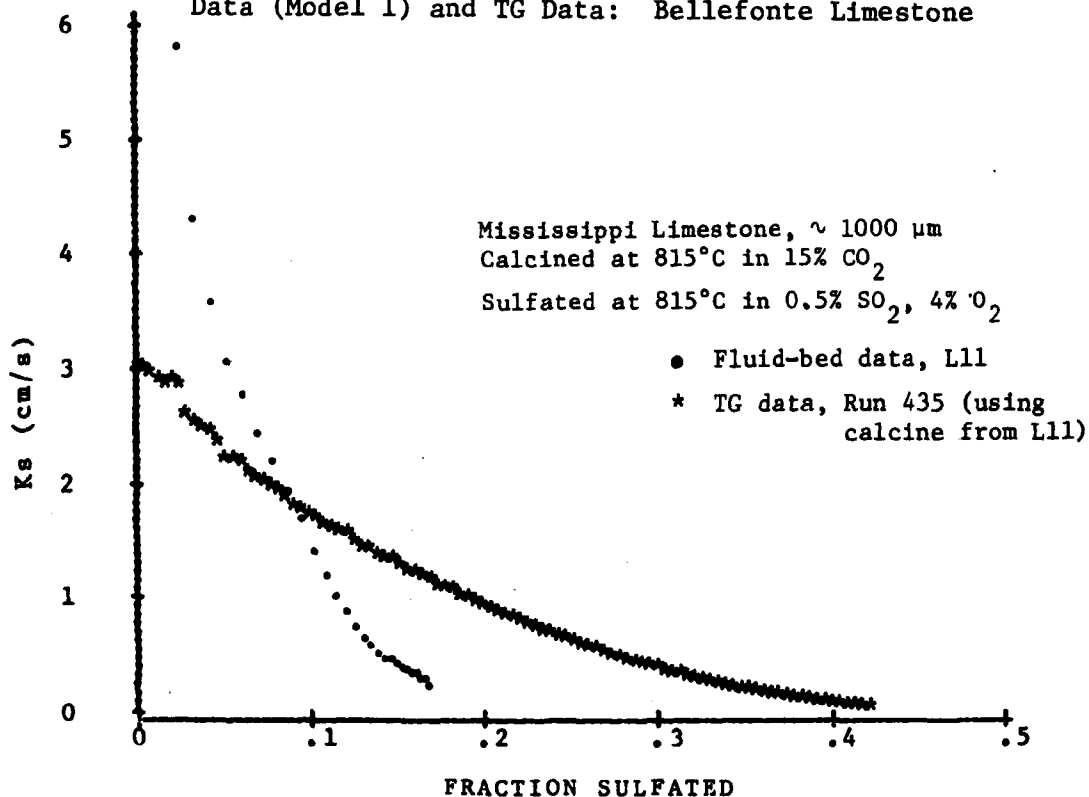


Figure 30 - Comparison of Rate Constants Derived from Fluidized-Bed Data (Model 1) and TG Data: Mississippi Limestone

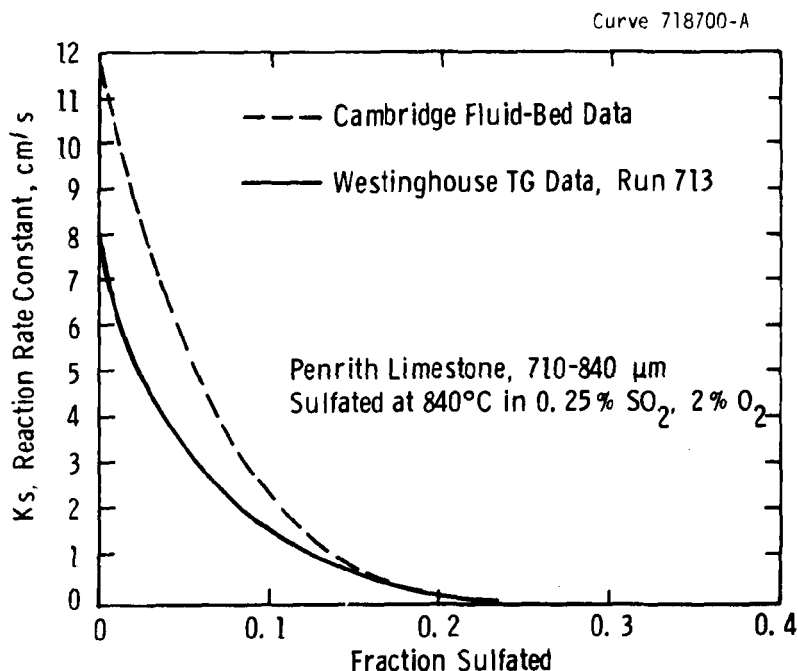


Figure 31 - Comparison of Rate Constants Derived from Cambridge Fluidized-Bed Data (Bubbling Bed Model) and Westinghouse TG Data

(with uniform sulfur generation and with below-bed sulfur generation) and perfect gas mixing. The same conclusion was reached at Cambridge²³ where a bubbling bed model was also tested. Since modeling assumptions must be made to analyze batch fluidized-bed data, the rate constants derived are subject to more uncertainty than those measured directly on the TGA. Care must be taken, however, to assure good gas/solid contacting on the TGA. A mass transfer correlation for the initial rates measured on the TGA would also be useful. Uncertainties in measurements and modeling techniques during initial reaction in the fluidized-bed make this technique unsuitable for deriving initial reaction rates.

Conclusions

FBC Operating Range Impact on Desulfurization Performance

High-temperature (900-1000°C) operation is recommended for pressurized fluidized-bed combustion. At higher temperatures limestones may

be used in the calcined form. Thermogravimetric tests indicate that sorbent (limestone or dolomite) utilization in PFBC will not decrease at temperatures of from 900 to 1000°C.

Dolomite sulfation is zero order in oxygen concentration throughout the range of typical FBC operation (0.75-16% O₂) at pressures of 101.3 kPa (1 atm) and 1013 kPa (10 atm).

Impure limestones, such as Greer, are useful sorbents in the uncalcined form, provided that the CO₂ partial pressure is not much greater than the equilibrium for calcination.

The residence time of a sorbent at high temperatures may alter its sulfation kinetics by varying the sorbent's pore structure. The effect of sorbent residence time on its performance should be tested when TG data are used to project calcium feed requirements.

Large-grained dolomites are not worth considering as sulfur sorbents for FBC. Even when pulverized (~100 µm) and precalcined they are not as active as 1000 µm particles of other sorbents.

Prediction of Desulfurization Performance

Thermogravimetric rate data can be successfully used to determine the rate constant of sulfation as a function of sorbent utilization for calcium-based sorbents. By judiciously selecting operating conditions that represent conditions in fluidized-bed combustion, the rate constant can be used to predict sulfur retention in fluidized-bed units. The agreement between fluidized-bed data and TG projections has been demonstrated using data collected at 1013 kPa (10 atm) pressure, as well as at atmospheric pressure.

The TG projections are limited by the availability of complete pilot plant data (particle size distribution in the bed, fraction of inert particles in the bed, bed expansion data), the accuracy of pilot plant data (including fluctuations in coal and sorbent properties and nonsteady-state operation), the representability of the 20 mg sample used in the TGA of the bulk limestone, as well as the basic assumptions applied in the projections.

Data obtained from batch fluidized-bed experiments may also be used to determine rate constants of sulfation as a function of sorbent utilization. The rate constants, however, are dependent on the model assumed for the fluidized bed. Rate constants derived by assuming perfect mixing of the solids and plug flow of the gas phase agree well with rate constants measured on the TGA. At low levels of sulfur retention, the type of model assumed has a minimal effect on the derived rate constants from quasi-steady-state models.

PARTICLE ATTRITION

Perspective on Need

Fluidized-bed combustors operate burning coal in a fluidized bed of granular, noncombustible particles. These bed particles may consist of limestone or dolomite, which acts as a sorbent for the sulfur released during coal combustion. The performance of an FBC system will depend upon the attrition resistance of these bed material particles.

An understanding of particle attrition in fluidized-bed combustion processing systems is important for:

- Selecting sulfur sorbents that have the desired attrition characteristics, so that operability of the FBC system can be maintained. (For example, sulfur sorbents resistant to attrition will be required for FBC processes in which the sorbent is regenerated for re-use^{3,4} and are generally desired for processes in which the sorbent is used on a once-through basis.²)
- Permitting the prediction of sorbent particle size history or, in turn, predicting sulfur removal for a given sorbent and process design
- Permitting the prediction of particle size history for estimating flue gas particulate loading and size distribution from the fluidized-bed combustor and other process components (e.g., carbon burnup cell, sorbent regenerator, sorbent pretreater, spent sorbent processing unit). Information on flue

gas particle loading and size distribution is necessary in order to assess environmental impact and particle control technology requirements.

- Aiding in the interpretation of other process phenomena (e.g., time element profiles, char or low-grade fuel combustion).

The objectives for the particle attrition work are to develop predictive models that describe sorbent (and fuel) attrition in fluidized-bed combustion systems. The models will relate attrition to particle properties, FBC system design parameters, and FBC system operating conditions. The models provide a basis for incorporating particle attrition characteristics into the assessment of sulfur sorbent selection, sulfur removal system evaluation, and particulate profile modeling through fluidized-bed combustion systems. These assessments will be utilized to achieve optimal plant design for given environmental emission requirements.

Approach

The approach selected to develop an understanding of particle attrition is to:

- Identify sources of attrition in fluidized-bed combustion systems.
- Select specific attrition mechanisms for study.
- Assimilate available data and propose a model.
- Carry out an experimental program and analysis to develop a predictive model for the respective mechanisms.
- Formulate a unified attrition model.
- Integrate the attrition model into the sulfur removal system and particulate control system models (inclusion in other system models to be performed as needed - e.g., trace element profiles).

The work reported includes three aspects:

- Screening tests to gain perspective on the effect of operating conditions (including interactions) and stone type on attrition, and to develop experimental techniques. These

tests include tests on the effect of stone type, atmosphere, temperature, pressure, particle size, particle composition (sulfation, calcination), rate of heating, and time on attrition; and tests on sampling, particle size measurements, and the effect of sieving attrition.

- Development of an attrition model for one attrition mechanism (abrasion or "bubbling-bed" attrition), and experimental confirmation of the model.
- Identification of future work to be carried out.

The study of attrition in fluidized beds is fragmented and incomplete. In other areas, such as ball milling and jet milling, there are unified theories of attrition. Fluidized-bed attrition is, at best, described only in part in a limited number of references. Nowhere is there a comprehensive model incorporating all of the attrition sources in a fluidized-bed system, nor reference to the mechanism of each source.

The wearing down of particles, called attrition, is variable and not well understood. If attrition rates are related to various properties of the particulate solids and fluidization gas and operating conditions, we should be able to develop an expression describing the rate of attrition in any given system. Several researchers have studied the effects of single variables under various conditions, but no general prediction equations have been formulated. This study is a beginning in defining a complete fluidized-bed model. The principal sources of attrition are identified and examined.

The specific objectives of this study were to:

- Identify the various causes or sources of attrition applicable to attrition in fluidized-bed combustion systems
- Develop expressions relating attrition rate to design and operating conditions, and to sorbent properties
- Test the proposed attrition formulas in controlled laboratory experiments.

Sources of Attrition

The frequently considered source of attrition in a fluidized bed is the obvious grinding and shattering collisions of particles. There are several causes of particle wear, which include the following.

Abrasion

In this process, defects, edges and corners are knocked from particles by low-energy collisions. Abrasion can occur during passage of a gas bubble through the bed of solids.

High-Energy Collisions

Particles may be accelerated to high velocity - for example, when entrained in a jet at the grid. The high-velocity particle can strike another particle or vessel wall and shatter into relatively large fragments.

Blinichev, Strel'tsov and Lebedeva²⁴ have distinguished two zones in a fluidized bed - the lower, which they call the nozzle effect zone, in which gas jets accelerate large particles to energies sufficient for shattering; and the upper zone, characterized by intensive mixing and low-energy impacts that abrade particle surfaces.

Thermal Shock

When cold sorbent particles are added suddenly to a bed of red-hot solids, there is severe thermal stress on the cold particles. One expects spalling at the particle surface and perhaps shattering of the entire particle into large fragments.²⁵

Chemical Stress

Sorbent particles calcine upon injection into the bed ($\text{CaCO}_3 \rightarrow \text{CaO} + \text{CO}_2$) and then may react with SO_2 to form CaSO_4 . These reactions cause subsequent changes in the lattice structure. This change in the structure of a particle at its surface hardens particles in some cases, or in other cases causes internal stresses leading to spalling or weakened particle surfaces.^{26,27}

Internal Gas Pressure

When cold limestone or dolomite makeup sorbent is added to a hot fluidized bed, the resulting calcination generates CO_2 within the particle. The internal gas pressure may cause the particle to fracture. Esso Research Centre in Abingdon, UK, found that a lower calcination rate of fresh limestone results in lower production of fines.²⁸ Similarly, water within particle cracks will flash when heated to bed temperatures. While CO_2 pressures are moderate (100.0 kPa equilibrium at 900°C), steam pressures are high and might explode particles.

Transfer Lines, Rotary Valves, and Cyclones

This is important auxiliary equipment in fluidized-bed combustion systems. Sorbent breakage rate is related to the circulation rate of solids and is controlled by equipment design effects on solids impact.

Screening Tests

Purpose

In selecting sorbents and in designing equipment there is a need for understanding the fundamental characteristics of attrition. Comparison of two or more candidate sorbents requires applying the attrition forces that will act in hot fluidization. The purpose of the current attrition test program is to:

- Identify areas of concern in screening sorbents for fluidized-bed combustion
- Measure the relative effects of the several sources of attrition to provide a basis for developing screening techniques
- Compare the attrition tendencies of candidate sorbents for fluidized-bed combustion
- Develop techniques for sorbent screening.

Scope

In this test program we have investigated a number of variables over their expected ranges in fluidized-bed combustion. Testing has included

several fluidized-bed systems available at the Westinghouse R&D Center. The scope of testing and equipment used are summarized in Table 6.

Terminology

Attrition Rate is an obscure term, defined in different ways by various researchers. Attrition rate is rigorously defined by both a description of the rate of breakage of each size particle and a description of the fractions of fragment sizes produced by breaking each size particle. Calculation of these rate and breakage functions is notably difficult, and extensive data collection is required. In this study we have defined attrition rate, R , as the rate of disappearance of particles larger than a stated size. The mass of large particles (coarses) in a fluidized bed, M , and the attrition rate R are related by

$$R = - \frac{1}{M} \frac{dM}{dt} .$$

The extent of particle attrition A is defined as

$$A = \int_0^t R dt = \int_{M_0}^{M_1} - \frac{dM}{M} = \ln \frac{M_0}{M_1}$$

in which M_0 and M_1 are the masses of coarses before and after an interval of attrition.

Attrition in this work is taken to be the process by which particulate solid is reduced in size by breaking.

Extent of Attrition is defined as the fraction of sorbent mass larger than a stated size that is reduced by attrition to fragments smaller than the stated size.

Effect of Sorbent Type and Atmosphere on Attrition

The purpose of this testing on the 3.5-cm test system was to determine the dependence of extent of attrition upon various combinations of sorbent types and reactor atmospheres (gas compositions) at 101.3 kPa (1 atm) pressure.

Table 6

Dwg. 1701865

RANGE OF VALUES OF TEST VARIABLES IN SEVERAL TEST SYSTEMS

Fluidized Bed Test System	Variable Tested		Test Date
	Description	Range	
3.5 -cm -diam Attrition Test System	Sorbent Type	3 sorbents	Nov. 1976
	Atmosphere	3 Gas compositions	
	Duration of fluidization,	0 to 9 hour	Jan. 1977
	Time held at 815°C	0 to 10	
	Heating Rate	10°C/min and 400°C/min	
	Decree of calcination	10% and 100%	
	Thermal shock	10°C/min and 400°C/min	Oct. 1976
	Character of wear in fluidized-bed attrition	(Photomicro - graph analysis)	Feb. 1977
10 -cm -diam Attrition Test System, Sintered Grid	Particle diameter	650 and 815°C -710 + 500 and -1410 + 1000 µm	Dec. 1977
	Degree of sulfation	0 and 10%	
	Grid jet	Present and absent	June 1977
7 -cm -diam Plexiglas Attrition Test System	Velocity ($U - U_{mf}$)	12.5 and 25°	Appendix
	Variation of attrition rate with time	0.25 to 647 h	Appendix
	Size of attrited fragments		Dec. 1977
	Change in limestone sorbent shape during fluidization		Oct. 1977

Our apparatus for these tests was the 3.5-cm-id attrition test cell system described in Appendix E.

Stones selected are those that have performed well in earlier work. They are Tymochtee dolomite; Greer, an impure limestone containing 11.3 percent silicon, aluminum, and iron; and Grove, a pure limestone that is 98 percent calcite. The atmospheres investigated are the two calcining compositions and a sulfating atmosphere:

Atmosphere 103 kPa, 815°C		Composition, %			
Symbol	Type	N ₂	CO ₂	SO ₂	O ₂
C1	Calcining (low CO ₂)	85	15	0	0
C2	Calcining (high CO ₂)	50	50	0	0
ST	Sulfating	96.8	0	0.2	3

The procedure was as follows:

1. Grind stone, separate it into sieve fractions, and measure the size distribution of the 1000 to 1400 μm (12 to 16 mesh) fraction with sieves.
2. Fluidize the 1000-1400- μm fraction of the stone in the attrition test cell with cold nitrogen and note the gas velocity, U_{mf} , at incipient fluidization. From this calculate the stone mass mean particle diameter as defined by Wen and Yu's equation²⁹

$$Re_o = (33.7^2 + 0.0408 Ar)^{1/2} - 33.7$$

where:

$$Re_o = d_p U_{mf} \rho(T) \mu^{-1}(T)$$

$$Ar = \rho(T) d_p^3 (\rho_p - \rho(T)) g \mu^{-2}(T).$$

Knowing only T and U_{mf} , we can calculate d .

3. Gradually heat (10°C/min) 70 g of stone in the attrition test cell to 815°C. Gradual heating avoids attrition from thermal stress.

4. Initiate gas flow at 1.2 times the minimum fluidization velocity* calculated for the stone diameter as calculated in step 2 above, gas species, and temperature. Maintain gas flow for four hours, then turn off the gas flow and allow the bed to cool slowly to room temperature.
5. Weigh the solids removed from the bed. Measure the size distribution of solids by sieve analysis. Weigh the solids on the exhaust filter. Assay samples of original and reacted stone for the fraction CO_2 (LOI) and the fraction of calcium for mass balance calculations.

Attrition is defined in different ways by different investigators. Various terms, including decrepitation, elutriation, and attrition, are used to define the breaking of fluidized-bed particles. In this test the extent of attrition denotes the rate at which particles smaller than $710 \mu\text{m}$ are formed. We chose $710 \mu\text{m}$ as the larger size limit of stone charged to the system. On a fully calcined solids basis, the extent of attrition is defined as

$$\begin{aligned} \text{extent of attrition} &= (\text{final bed fines} - \text{initial bed fines} + \\ &\quad \text{final filter fines}) \div \text{input mass} = \\ &= \frac{\left(\frac{\text{final bed}}{\text{mass}} \right) \left(\frac{\text{frac} <}{710 \mu\text{m}} \right) (1-y_b) - \left(\frac{\text{initial}}{\text{bed mass}} \right) \left(\frac{\text{frac} <}{710 \mu\text{m}} \right) (1-y_l) + \left(\frac{\text{final}}{\text{filter mass}} \right) \left(\frac{\text{frac} <}{710 \mu\text{m}} \right) (1-y_f)}{\text{mass of input stone}} \\ &= [M_b x F_b (1-y_b) - M_l x F_l (1-y_l) + M_f (1-y_f)] \div [M_l (1-y_l)] \end{aligned}$$

where:

M = mass

F = mass fraction in cumulative size distribution

Y = mass fraction loss of CO_2 on ignition

Subscripts

b = stone after attrition

l = original stone

f = filter.

*Later in this study we abandoned use of multiples of U_{mf} and set values of $U-U_{mf}$. This is discussed in Appendix D.

The results of these attrition measurements are listed in Table 7.

Table 7

PERCENT OF SOLIDS ATTRITED IN FOUR HOURS

Stone Type	Atmosphere		
	C1, Calcining	C2, Calcining	ST, Sulfating
Tymochtee	1.842	1.003	0.4680
	1.813	0.783	0.4500
	0.600	0.684	*
Grove	0.554	4.405	0.5460
	0.711	1.989	0.4360
	0.777	1.039	*
Greer	0.846	8.326	1.9450
	2.121	7.190	1.0160
	3.377	3.390	*

*Denotes no observation.

Table 8 summarizes statistical calculations on these data.

Table 8

SUMMARY OF ATTRITION TEST DATA STATISTICS

Source of Error	d.f.	Sum of Squares	Mean Square	F Ratio
Atmosphere (A)	2	9.298	4.650	2.89
Stone Type (S)	2	10.774	5.099	3.17
Interactions	4	7.253	1.821	1.13
Error	15	24.118	1.608	----

Compare the F ratios for the data with tabulated F ratios:

$$F_{2,15}(0.95) = 3.68$$

$$F_{2,15}(0.90) = 2.70 \quad .$$

These F values lead us to conclude that stone type for the two stones tested and atmosphere do not affect attrition. There is a chance of only about 5 percent that we will conclude significant effects when none exist.

Initially, we may say with some certainty that there are no interactions ($F = 1.13$) between stone type and atmosphere. With regard to how stone type and atmosphere affect attrition, the conclusion is unclear; there probably are effects on attrition caused by choice of stone type and atmosphere; these effects, however, are not shown decisively by these test data. The test data are plotted in Figure 32 with atmosphere and stone type plotted as parameters. Some individual data are included to show the variability of the data.

Accepting the hypothesis that atmosphere and stone type do affect attrition rate and that their effects are independent (do not interact), we conclude that:

1. Tymochtee and Grove sorbents attrite least in the three atmospheres tested. Greer limestone attrites notably faster than either Tymochtee or Grove stone under the atmospheres tested.
2. The sulfating atmosphere causes least attrition; this is consistent with Exxon's³⁰ finding that sulfation of dolomite creates a hard outer shell resulting in less attrition. The worst attrition occurs in the atmosphere of 50 percent CO_2 in 50 percent nitrogen.

A separate sample of Chemstone[®] limestone recommended by Engelhard Minerals and Chemicals Corporation was also tested. Its attrition rate in a C1 (15 percent CO_2 , 85 percent N_2) atmosphere was 0.425 percent/hr, intermediate between the other sorbents tested.

Curve 713774-A

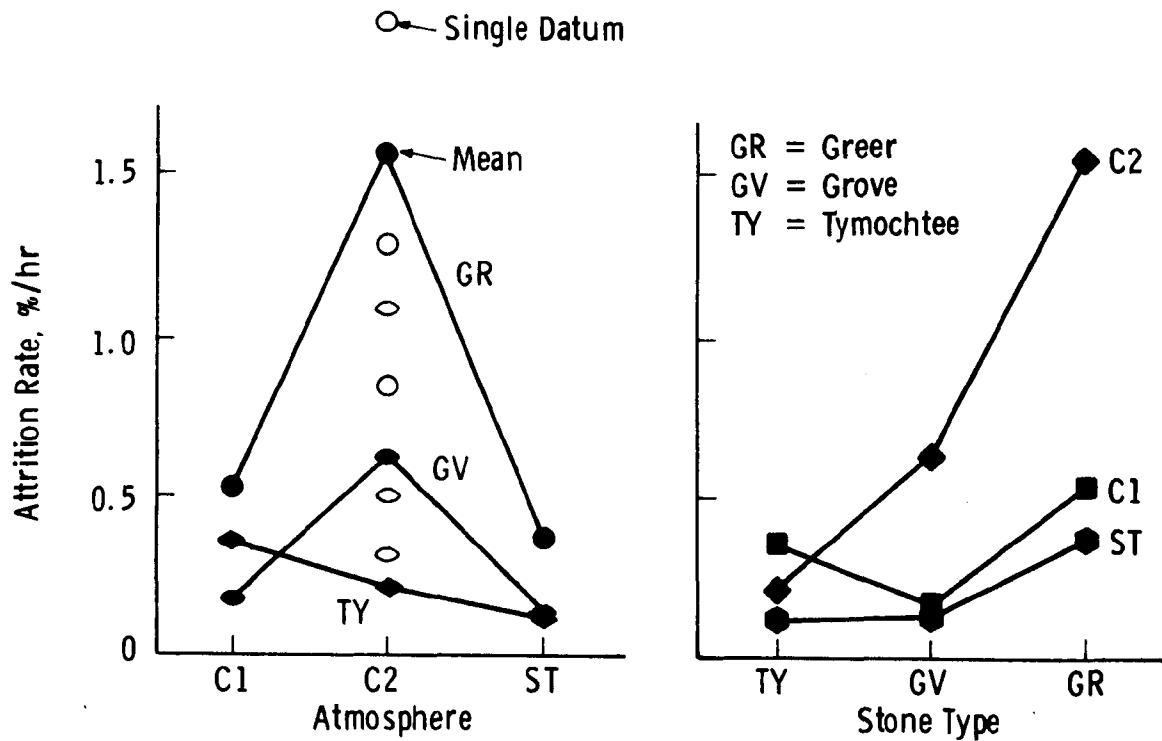


Figure 32 - Attrition Rate Dependence upon Stone Type and Atmosphere

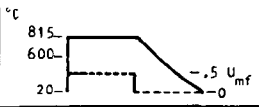
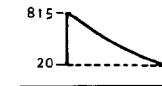
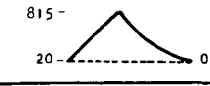
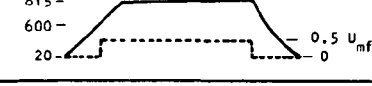

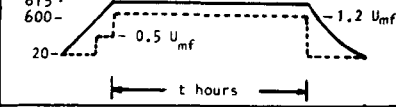
Effect of Duration of Fluidization, Time Held at 815°C, Heating Rate, and Degree of Calcination of Attrition

A short series of tests on the 3.5-cm system (Tests A1 through A10) was completed for study of the effects of the duration of fluidization, the time the stone is held at 815°C, the rate of heating, and the degree of calcination to see their influence on the extent of attrition.

Table 9

DESCRIPTION OF TEST CONDITIONS

Dwg. 1687B35

Test No.	Rate of Heating	Extent of * Calcination	Hours Fluidized	Hours at 815°C	Profiles of Temperature (—) and Gas Velocity (----)
A1	Rapid	100%	0	1	
A2	Rapid	~ 10%	0	0	
A3	10°/m	~ 10%	0	0	
A4	10°/m	100%	0	4	
A5	10°/m	100%	0	1	
A6	10°/m	100%	t = 0.16	1.16	
A7	10°/m	100%	t = 1	2	
A8	10°/m	100%	t = 2	3	
A9	10°/m	100%	t = 4	5	
A10	10°/m	100%	t = 9	10	

Tests compared to determine effects of time of fluidization: A6 through A10
 hours at 815°C: A4 & A5
 rate of heating: A1 & A5, A2 & A3
 ext. of calcination: A3 & A5, A1 & A2

* Calcination was complete except for runs A2 and A3, in which bed cooling was initiated as soon as the sample reached 815°C

Table 10

ATTRITION TEST DATA
(Grove Limestone)

Test Date	Test No.	Degree of Calcination	Rate of Heating	Hrs at 815°C	Hrs Fluidized	Bed Before/Bed After				Filter Solids, g M_f	Mass Balance		Fines Formed, %
						Y_o/Y_b	F_o/F_b	M_o/M_b	X_o/X_b		Stone	Calcium	
10-14	A-1	100%	Rapid	1	0	0.3723/ 0.0010	0.0004/ 0.00856	70 44.35	0.321 0.5296	0.0302	100.57	104.60	0.892
10-15	A-1 (Re-peat)	100%	Rapid	1	0	0.3723/ 0.0006	0.0004/ 0.00661	70 43.8296	0.321 0.5421	0.0111	99.82	105.77	0.645
10-8	A-2	~ 10%	Rapid	0	0	0.3723/ 0.3410	0.0004/ 0.01852	70 66.9612	0.321 0.3435	0	100.27	102.36	1.820
10-7	A-3	~ 10%	Gradual	0	0	0.3723/ 0.3640	0.0004/ 0.00369	70 67.7293	0.321 0.3263	0	98.77	98.35	0.322
10-18	A-4	100%	Gradual	4	0	0.3723/ 0.0012	0.0004/ 0.04571	70 43.6613	0.321 0.5475	0.0069 0.0069	99.54	106.40	4.513
10-19	A-5	100%	Gradual	1	0	0.3723/ 0	0.0004/ 0.00502	70 43.7421	0.321 0.5354	0.0170	99.74	104.27	0.499
10-22	A-6	100%	Gradual	1.16	0.16	0.3723/ 0.0018	0.0004/ 0.00821	70 43.8235	0.321 0.5276	0.0514	99.80	103.02	0.894
10-28	A-7	100%	Gradual	2	1	0.3723/ 0	0.0004/ 0.01289	70 43.4447	0.321 0.5662	0.1929	99.56	109.95	1.673
10-25	A-8	100%	Gradual	3	2	0.3723/ 0.0001	0.0004/ 0.01681	70 43.3879	0.321 0.5686	0.1023	99.35	110.05	1.852
10-20	A-9	100%	Gradual	5	4	0.3723/ 0.0002	0.0004/ 0.01518	70 43.4248	0.321 0.5686	0.1403	99.45	110.24	1.779
12-2	A-10	100%	Gradual	10	9	0.3723/ 0.0037	0.0004/ 0.01597	70 43.1842	0.321 0.5095	0.1650	98.93	98.29	1.898
1-7	A-10	100%	Gradual	10	9	0.3723/ 0	0.0004/ 0.02673	70 42.6621	0.321 0.5370	0.4674	98.84	103.07	3.619

In two of these tests, Grove limestone was heated as rapidly as possible by pouring cold stone directly into the preheated cell. In the remaining tests, the Grove limestone was heated in the attrition test cell at 10°C/min from room temperature to 815°C; this gradual heating avoided attrition from thermal stress. At 600°C nitrogen flow was turned to $1/2 U_{mf}$ to carry CO_2 from the bed and aid calcination. After holding the bed at 815°C for one hour under a gas flow of $1/2 U_{mf}$, we fluidized the bed by increasing the gas flow to $1.2 U_{mf}$. The patterns of controlling temperature and gas flow are shown in Figure 33; in tests A1 and A2, however, the stone was brought to 815°C within several seconds. A description of test conditions and which tests were compared to draw various conclusions is listed in Table 9.

Size distribution, masses of bed and filter solids, loss on ignition (a measure of CO_2 loss in calcining), and calcium fraction were measured before and after attrition testing.

Data from these tests are listed in Table 10. The mass balances are calculated from:

Fully Calcined Stone Mass Balance

$$\left\{ \left[\begin{array}{c} \text{Mass of} \\ \text{filter solids} \end{array} \right] + \left[\begin{array}{c} \text{Mass left} \\ \text{in bed} \end{array} \right] + \left[\begin{array}{c} \text{Liberated} \\ CO_2 \end{array} \right] \right\} \div \left[\begin{array}{c} \text{Initial} \\ \text{bed mass} \end{array} \right]$$

$$M_f (1-Y_f) + M_l (1-Y_l) + M_o Y_o \div M_o$$

Calcium Mass Balance

$$\frac{[\text{Calcium in Filter and Bed after the Test}]}{[\text{Calcium Charged to the Bed}]}$$

$$(M_f X_f + M_l X_l \div M_o X_o)$$

The extent of attrition is calculated from

$$\left\{ \left[\begin{array}{c} \text{Final Bed} \\ \text{Fines} \end{array} \right] + \left[\begin{array}{c} \text{Final Filter} \\ \text{Fines} \end{array} \right] - \left[\begin{array}{c} \text{Initial Bed} \\ \text{Fines} \end{array} \right] \right\} \div \left[\begin{array}{c} \text{Initial Bed} \\ \text{Mass} \end{array} \right]$$

based on the fully calcined stone:

$$[M_l (1-Y_l) f_l + M_f (1-Y_f) f_f - M_o (1-Y_o) f_o] \div [M_o (1-Y_o)]$$

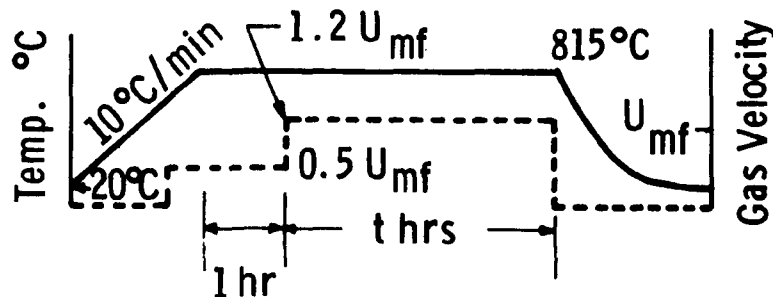


Figure 33 - Gas Velocity and Temperature Patterns in the Attrition Versus Time Tests

where:

- M_f = mass of filter solids
- M_1 = final mass of bed solids
- M_o = initial mass charged to the bed
- Y_f = fraction of CO_2 in filter solids as determined by LOI
- Y_1 = fraction of CO_2 in final bed solids as determined by LOI
- Y_o = fraction of CO_2 in original stone as determined by LOI
- X_f = fraction of calcium in filter solids
- X_1 = fraction of calcium in final bed solids
- f_f = fraction of filter solids smaller than 710 μm
- f_1 = fraction of final bed solids smaller than 710 μm
- f_o = fraction of original bed smaller than 710 μm .

Dependence of the Extent of Attrition on Duration of Fluidization

The results of tests A5 through A10, inclusive, infer the dependence of the extent of attrition on duration of fluidization. The amount of fines generated in test A5, 0.499 percent, shows that fines are formed in the absence of fluidization; the processes of heating and calcination alone cause attrition. In order to show only the effect of fluidization

of Grove limestone on attrition, the concentration of fines caused by heating and calcination of Grove limestone has been subtracted from the total fines formed. The percentages of fines caused by fluidization alone are listed in Table 11 and plotted in Figure 34.

The attrition theory proposed by Kuttyavina and Baskakov³¹ models attrition as a rapid initial rate from the fracture of projections and defects that decreases as particles become rounded and free from defects. Finally, the rate of attrition reaches a constant value after six to eight hours in their tests. Our earlier tests, which extended over a six-hour interval, indicated a constant attrition rate. The test data in Table 11 and Figure 34 agree with the Kuttyavina and Baskakov model

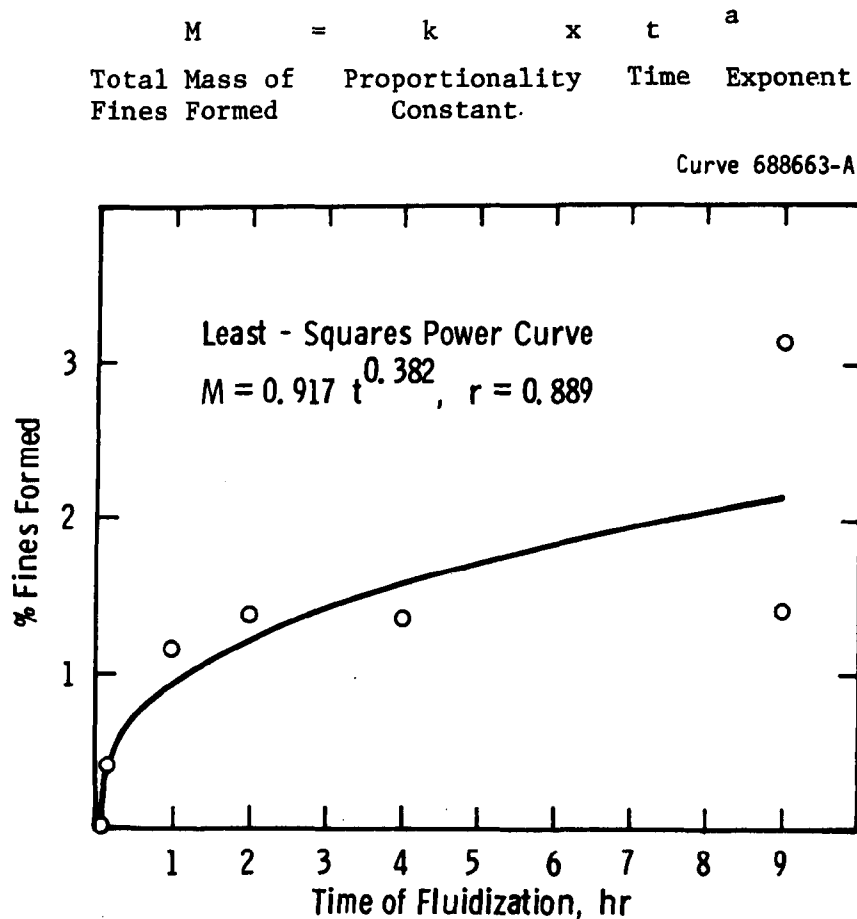


Figure 34 - Effect of Duration of Fluidization on Extent of Attrition in Fluidization of Grove Limestone at 815°C

Table 11

PERCENTAGES OF FINES FORMED DURING ATTRITION TESTING AND
PERCENTAGES ATTRIBUTABLE TO FLUIDIZATION ONLY
(Grove Limestone)

Time of Fluidization	Percent of Fines	
	Total	Less Fines at t=0
0	0.4988	0.0000
0.16	0.8939	0.3951
1	1.6730	1.1742
2	1.8520	1.3532
4	1.7794	1.2806
9	1.8978	1.3990
9	3.619	3.120

The data from our tests, in least squares analysis, are represented by

$$M(\%) = 0.917 t^{0.382}$$

with a correlation coefficient of $r = 0.89$. The average rate of attrition over the nine-hour interval was 0.23 percent/hr.

Dependence of the Rate of Attrition on the Hours the Stone Was Held
at 815°C

Tests A4 and A5 were designed to indicate the effect on particle attrition of holding the bed temperature at 815°C without fluidization. A gas flow of one-half the minimum fluidization velocity was maintained to assure complete calcination. The results from Table 10 are

Hours Stone Held 815°C	Percent Attrition	Degree of Calcination
1	0.499	100.0
4	4.513	99.8

This difference appears to be significant and indicates that holding Grove limestone at 815°C without fluidization causes attrition. The degree of calcination is virtually the same in both tests and does not confound the conclusion.

Dependence of the Rate of Attrition on the Rate of Heating and the Degree of Calcination

A literature survey of attrition mechanisms has suggested that thermal shock or (thermal stress) may aggravate attrition. Two mechanisms are possible:

- Stone may shatter immediately upon thermal shocking
- Stone may be catastrophically weakened by thermal shock.

After fluidization begins the new defects formed through the second mechanism may fail, increasing the attrition rate. Only the first mechanism has been tested in these experiments.

In the earlier of these studies (Runs A2 and A3), identical masses of Grove limestone were heated in the attrition test cell. The first test involved heating 70 g of stone at 10°C/min to 815°C, then allowing the mass to cool slowly. In the second test cold stone was suddenly charged to the hot cell and was cooled in the same manner. No fluidizing air was fed in these tests.

Mass balances over both tests gave excellent accounting for products and reactants. Gradual heating at 10°C/min caused reduction of 0.32 percent of the stone to smaller than 710 μm . Shock heating at approximately 400°C/min caused 1.82 percent reduction to smaller than 710 μm .

In the later study (Runs A1 and A5) the two rates of heating were a gradual warming of $10 \pm 0.1^\circ\text{C}/\text{min}$ and a sudden shock heating in which the stone was poured into the hot cell and came to a temperature of 400°C within one minute and 800°C in about eight minutes.

Figure 35 shows the temperature history for runs A1, A1 repeated, and A2. The conditions were nearly identical in all three tests and the temperature curves are similar. Figure 35 actually shows the thermocouple

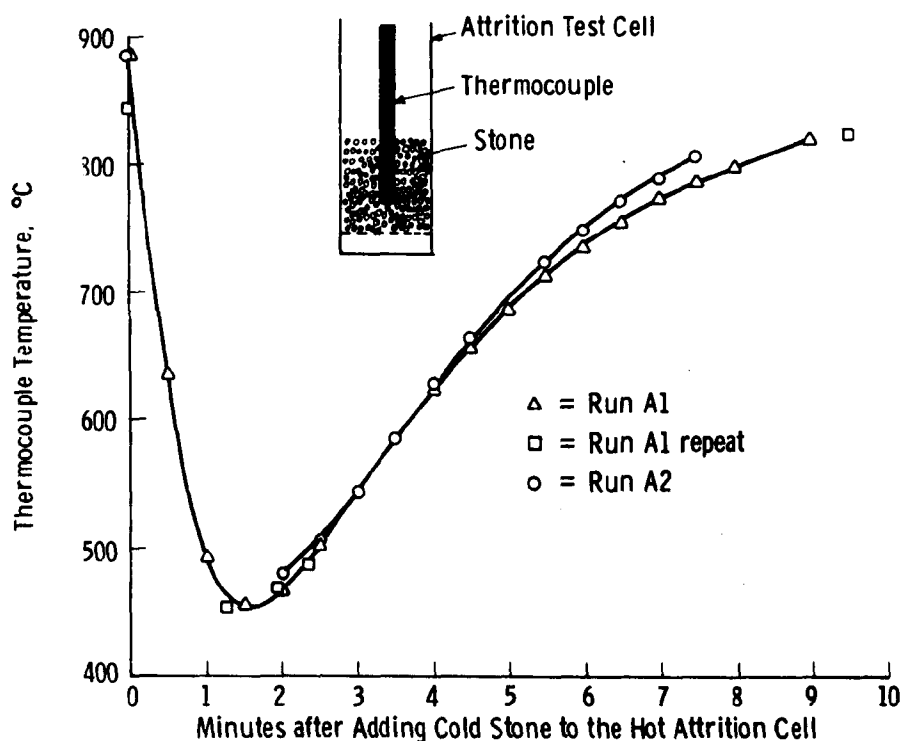


Figure 35 - Temperature History when Cold Grove Limestone is Added to 815°C 3.5 cm Attrition Cell (Runs A1, A1 Repeated, A2)

temperature, not the stone temperature. The thermocouple temperature was lowered rapidly by the cold stone dumped on it. As the stone temperature rose, the thermocouple temperature also began to climb, after about 90 seconds.

The degree of calcination was controlled by allowing time for calcination to go to completion (~100 percent) or by cooling the stone immediately after the heating to achieve approximately 10 percent calcination. Achieving a 10 percent calcination was the goal, and the levels of 12.4 percent and 5.4 percent, respectively, actually obtained are considered close enough to the 10 percent goal for our purposes.

The results pertaining to the thermal shock effects, as extracted from Table 10, are listed below.

100% Calcined (nominal) 0 hr Fluidized 1 hr at 815°C				10% Calcined (nominal) 0 hr Fluidized 0 hr at 815°C			
Test No.	Rate of Heating, °/min	% Attrit.	% of CaCO ₃ Actually Calcined	Test No.	Rate of Heating °/min	% Attrit.	% of CaCO ₃ Actually Calcined
A1	Rapid (400)	0.892	99.9	A2	Rapid (400)	1.820	12.4
A1 (repeated)	Rapid (400)	0.645	99.9				
A5	Gradual (10)	0.4990	100.0	A3	Gradual (10)	0.322	5.4

^aAverage = 0.768

These results indicate an interaction between R_θ the rate of heating (°C/min) and C the extent of calcination (%) influence the extent of attrition A . If K is defined as an unspecified constant, the model for extent of attrition A is of the form

$$\begin{aligned}
 A &= (K_1 R_\theta + K_2) (K_3 C + K_4) \\
 &= K_1 K_3 R_\theta C + K_1 K_4 R_\theta + K_2 K_3 C + K_2 K_4 \\
 &= k_1 R_\theta C + k_2 R_\theta + k_3 C + k_4
 \end{aligned}$$

Here k is merely a regrouping of K . The data in the above table when applied to this model give four equations for the four observations.

$$k_1 (400) (0.999) + k_2 (400) + k_3 (0.999) + k_4 = 0.768$$

$$k_1 (10) (1) + k_2 (10) + k_3 (1) + k_4 = 0.499$$

$$k_1 (400) (0.124) + k_2 (400) + k_3 (0.124) + k_4 = 1.820$$

$$k_1 (10) (0.054) + k_2 (10) + k_3 (0.054) + k_4 = 0.322 .$$

We have transformed the variables R_θ and C so that they range from -1 to +1 and rewrite the equations as

$$1.0 \quad k_1 + 1.0 \quad k_2 + 0.996 \quad k_3 + k_4 = 0.768$$

$$-0.952 \quad k_1 - 1.0 \quad k_2 + 1.0 \quad k_3 + k_4 = 0.499$$

$$-0.754 \quad k_1 + 1.0 \quad k_2 + 0.850 \quad k_3 + k_4 = 1.820$$

$$-1.0 \quad k_1 - 1.0 \quad k_2 - 1.0 \quad k_3 + k_4 = 0.322$$

with solution

$$k_1 = -0.71 \text{ coefficient on the interaction } R_\theta C$$

$$k_2 = +0.83 \text{ coefficient on the heating rate effect } R_c$$

$$k_3 = +0.11 \text{ coefficient on the degree of calcination effect } C$$

$$k_4 = +0.55 \text{ equation constant.}$$

These normalized coefficients are comparable and tell the relative effects of each variable in the absence of fluidization. The positive coefficients on the rate of heating R (thermal shock) and the degree of calcination C are expected; the negative interaction is unexpected.

The results of these tests suggest avoiding the thermal shock to sorbent in a fluidized-bed combustor. Thermal shock and its attendant attrition can be minimized by controlled heating of the sorbent with the exhaust gases from the combustor.

Change in Limestone Sorbent Shape during Fluidization

After fluidizing Grove 1359 limestone at room temperature in the 7-cm Plexiglas column for 329 hours, we observed that the particles

seemed to be about as angular as before. The fluidizing velocity was 46 cm/s, 30 cm/s above the U_{mf} of 16 cm/s, and fluidization was vigorous. The only apparent difference was that the evident dustiness of particles before fluidization disappeared during fluidization. There was no evident change in the incidence of points or sharp edges.

We had expected that corners or edges would be knocked off particles during fluidization. Although 9.5 weight percent of the largest mesh size (350 to 500 μm ; 32 to 42 mesh) was lost in fluidization, it apparently was not lost from edges or vertices. To test the hypothesis that particle shape remained unchanged in fluidization we measured the shapes of 55 particles before and 55 particles after fluidization.

The procedure was to measure first the longest dimension of a particle, then measure the largest perpendicular dimension (Figure 36). The particle shape was calculated as the ratio of the largest dimension to the greatest perpendicular dimension. All measurements were taken from 14X magnification photographs of representative fractions of the particle population.

Dwg. 7681A33

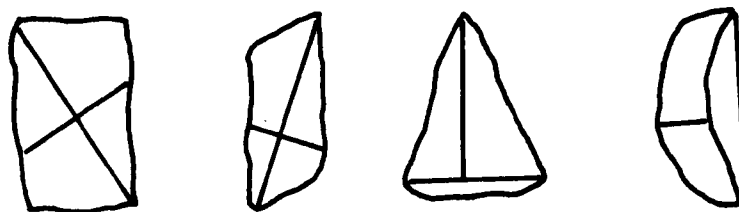


Figure 36 - Measurement of Perpendicular Dimensions
for Measurement of Particle Shape

Figure 37 shows the photos from which we measured the particle dimensions.

The results of analyzing the shape measuremental data are:

	Before	After
Mean Ratio	1.6573	1.6077
Standard Deviation	0.335	0.354
n	55	55
$t_{\text{calculated}} = 0.443$ with 108 d.f; $t_{\text{tabled}} = 1.98$		

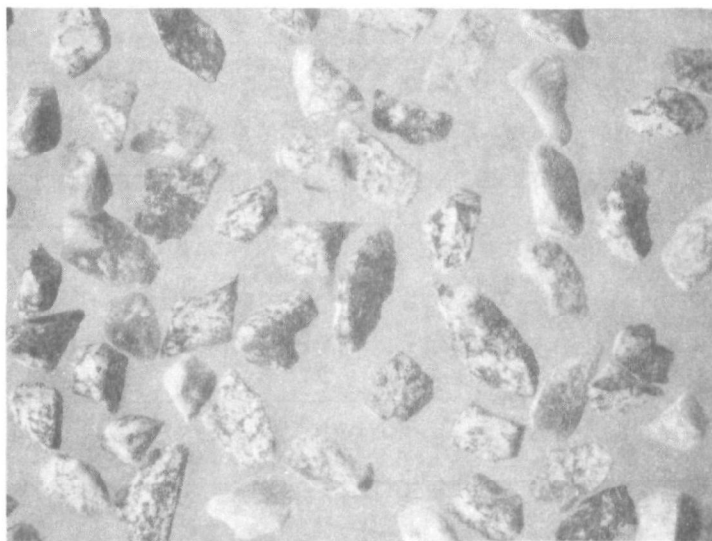
The shape ratio change from 1.66 to 1.61 is not statistically significant as inferred from the statistical t-test of the data.

Reference to Appendix D (Figure D7) shows a rapid initial rate of attrition, presumably from weak projections and defects being knocked from particles. For fluidization of uncalcined limestone in a cold system, however, the reduction in size mentioned previously apparently results from loss from flat particle surfaces, not from the sharp edges. The sharp-cornered, knife-edged particle shape is maintained. This is comparable to the process of flaking stone as in making arrowheads: sharp edges and corners are preserved and chips are from flat surfaces of uniform thickness as postulated in the attrition theory (Appendix D).

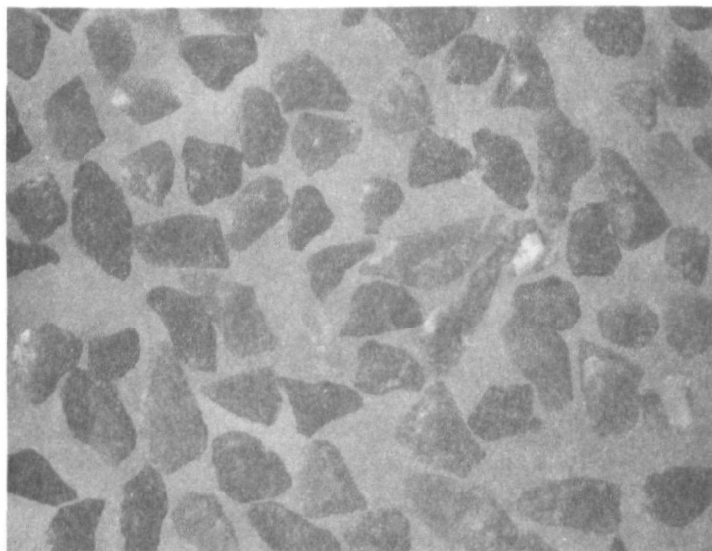
These results showed the need for hot testing to see if fluidization at calcination temperatures ($\sim 800^{\circ}\text{C}$) preserves particle shape. Such hot testing was completed in Runs A1 through A10, discussed previously, and is discussed further below.

Character of Wear in Fluidized-Bed Attrition

Following the tests of attrition dependence on time of fluidization, shock heating, and calcination (Runs A1 through A10), the Grove limestone



As Crushed - Before Fluidization 14X



After 329 hr of Fluidization 14X

Figure 37 - Grove Limestone Particles before and after Fluidization
at $U - U_{mf} = 30 \text{ cm/s}$ for 329 Hours

sorbent was photographed. The purpose of this close examination was to investigate the character of attrition - do particles attrite by splitting or by spalling tiny chips from the particle surface? - and to inspect the extent of particle rounding after attrition. The micrographs are shown in Figure 38. With each picture is a description of test conditions.

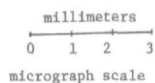
Initial inspection of the pictures suggests that particles do not calcine uniformly. While all of the original stone is a uniform gray, the reacted stone, particularly after test A5, varies from the dead white of fully calcined stone, to a gray like the original stone.

Initial inspection of the pictures also indicates that particles do not split off large pieces (or split in half), but chip away bit-by-bit from edges, corners, and defects. Compare photos of the original stone and that from test A10; the rounding of particles from nine hours of fluidization at 815°C is evident. ANL³² reported that the "mechanism for attrition is abrasion (the wearing away of surface material) in contrast to the breakup or splitting of particles due to particle-particle or particle-wall collisions." Kut'yavina and Baskakov³¹ begin their paper, "With fluidization, particles are ground by abrasion and splitting. Abrasion is evidently predominant even for brittle and insufficiently strong materials." They continue to explain, "Experiments ... showed that the rate of abrasion decreases over the course of time, with rubbing off of the uneven parts and a decrease in the number of defects of the particles." The results of the Westinghouse test described on pages 72 and 73 tend to support this conclusion that the attrition rate is highest in the beginning of the test when abrasion of projections and defects would be the greatest. The rate of fines (<710 μm) production R (%/hr) observed in the Westinghouse study reported here varied with time t (hours) as:

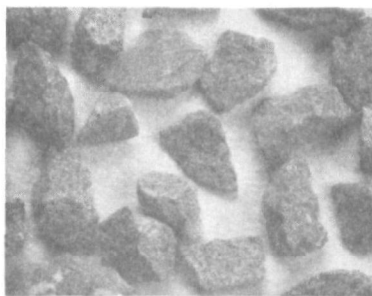
$$\begin{aligned} R &= dA/dt = d(0.917 t^{0.382})/dt \\ &= 0.350 t^{-0.618} \quad , \end{aligned}$$

Test & Description

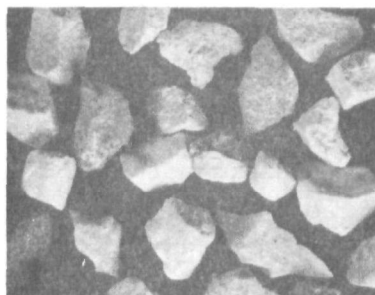
Original Stone



Micrograph, 10X



Micrograph, 10X



Test & Description

A1 10% Calcined
Rapid Heatup Rate
0 hrs Fluidization
0 hrs at 815 °C
0.892% Fines Production

Micrograph, 10X



Test & Description

A1' 100% Calcined
Rapid Heatup Rate
0 hrs Fluidization
1 hr at 815 °C
0.644% Fines Production

Micrograph, 10X



Test & Description

A2 10% Calcined
Rapid Heatup Rate
0 hrs Fluidization
0 hrs at 815 °C
1.820% Fines Production

Figure 38 - Sorbent Micrographs - Grove Limestone

Micrograph, 10X

Test & Description
A3 10% Calcined
Rapid Heatup Rate
0 hrs Fluidization
0 hrs at 815°C
0.322 Fines Production



Micrograph, 10X

Test & Description
A4 100% Calcined
10° C/min Heatup Rate
0 hr Fluidization
4 hr at 815°C
4.513% Fines Production



millimeters
0 1 2 3
micrograph scale

Micrograph, 10X

Test & Description
A5 100% Calcined
10° C/min Heatup Rate
0 hr Fluidization
1 hr at 815°C
0.499% Fines Production



Micrograph, 10X

Test & Description
A6 100% Calcined
10° C/min Heatup Rate
0.16 hr Fluidization
1.16 hr at 815°C
0.894% Fines Production



Figure 38 (Continued)

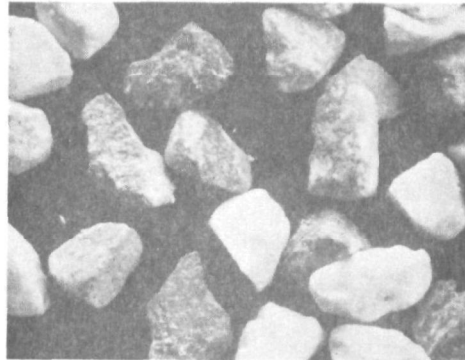
Micrograph, 10X

Test & Description		
A7	100%	Calcined
	10°C/min	Heatup Rate
	1 hr	Fluidization
	2 hr	at 815°C
	1.673%	Fines Production



Micrograph, 10X

Test & Description		
A8	100%	Calcined
	10°C/min	Heatup Rate
	2 hr	Fluidization
	3 hr	at 815°C
	1.852%	Fines Production



Micrograph, 10X

Test & Description		
A9	100%	Calcined
	10°C/min	Heatup Rate
	4 hr	Fluidization
	5 hr	at 815°C
	1.779%	Fines Production



millimeters
0 1 2 3
micrograph scale

Figure 38 (Continued)

Micrograph, 10X

Test & Description		
A 10	100%	Calcined
	10° c/mm	Heatup Rate
	9 hr	Fluidization
	10 hr	at 815°C
	1.898	Fines Production



Micrograph, 10X

Test & Description		
A 10'	100%	Calcined
	10° C/min	Heatup Rate
	9 hr	Fluidization
	10 hr	at 815°C
	3.619%	Fines Production

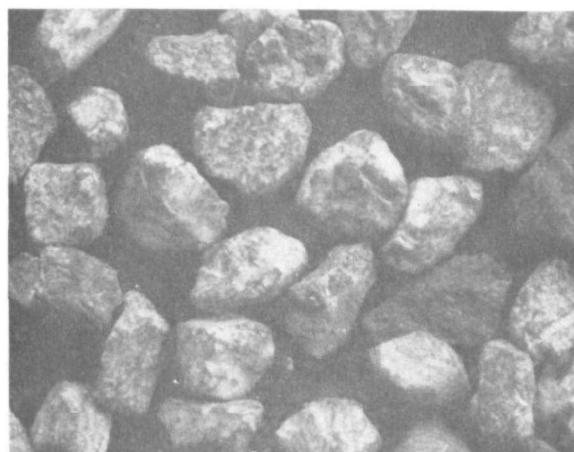


Figure 38 (Continued)

millimeters
0 1 2 3
micrograph scale

for which the attrition rate of 0.35%/hr at $t = 1$ hr falls to half (0.175%/hr) at $t = 3.07$ hours. The decreasing rate of attrition is referenced by Stanley et al.³³ in their expression for the rate of loss of coarse material to fine L:

$$L = L_{\text{ultimate}} \left(1 - e^{-\beta (t-t_o)} \right)$$

and by Mathur and Epstein³⁴ in their comment, "The grinding rate tended to drop off with spouting time, as would be expected in any batch grinding operation," and by Gonzales and Otero³⁵ in their empirical equation $d/dt D_{vs} = -CD_{vs}^{2.6}$ in which D_{vs} is volume/surface diameter and C is a constant accounting for system conditions and particle strength. This rate equation can be solved to give:

$$D_{vs} = \left(D_o^{-1.6} + 1.6 Ct \right)^{-1/1.6},$$

which implies a decreasing attrition rate with time, or rearranged to yield:

$$\frac{dM_B}{dt} = -3c \left(\frac{N\pi\rho}{6} \right) \frac{1-m'}{3} \left[M_B^{\frac{1-m'}{3}} - C (1-m') \left(\frac{N\pi\rho}{6} \right)^{\frac{1-m'}{3}} t \right]^{\frac{2+m'}{1-m'}}$$

where M_B is the bed mass, N is the number of particles in the bed, ρ is particle density, and m' is a constant ≈ 2.6 .

Further evidence that attrition is a result of surface abrasion, not splitting, is seen in the size distributions of particles before and after fluidization. Figure 39 shows differential size distribution curves of material before and after test A-9. Note that there is little difference in the fractions of particles larger than 710 μm ; the change in distribution occurs in the fines smaller than 710 μm . This result suggests that tiny chips are being broken off of the larger particles, not substantially changing the size of the larger particles but greatly increasing the quantity of fines.

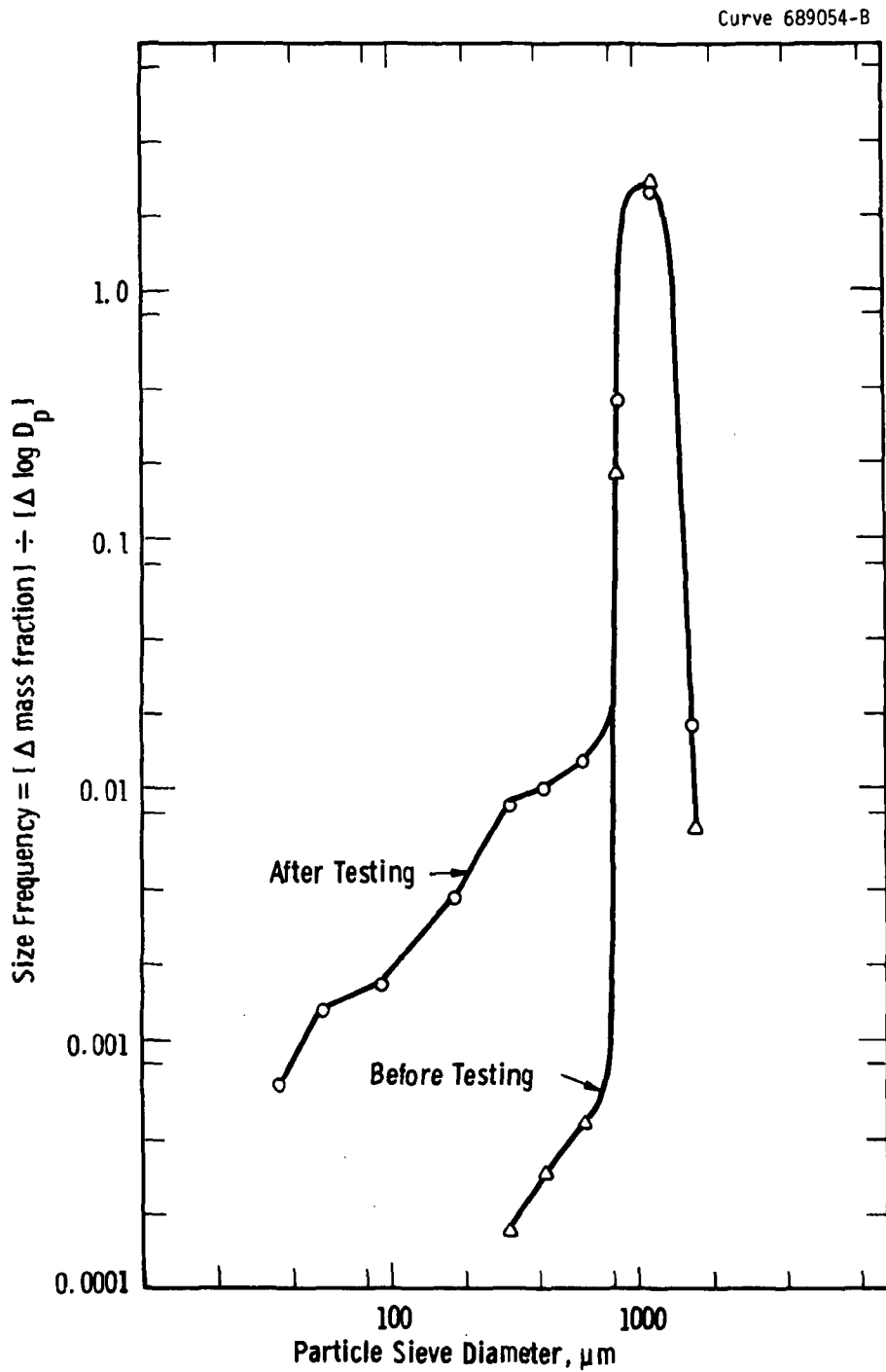


Figure 39 - Particle Size Distributions before and after Hot Fluidization of Grove Limestone, Run A-9

The pictures shown in Figure 38 were ranked from "most angular" to "most rounded" by six observers. Averaged rankings are shown in Figure 40. As might be expected, the as-received stone was judged to be angular, the stone fluidized for nine hours (A-1) was judged most rounded. Aside from these extremes in treatment, however, there was generally poor discrimination of attrition effects, judging by the photographs. Figure 41 shows little perceived difference in angularity between particles fluidized for 0.16, 1, 2, 4 and 9 hours. The extent of attrition test A-1 through A-10 (see Table 10) correlated well with time of fluidization (see Table 11) but agreed poorly with average rankings from inspecting the pictures (see Table 12). These rankings and extents of attrition correlated with $r = 0.028$, which is virtually no relation.

Table 12

RELATION BETWEEN EXTENT OF ATTRITION AND DEGREE
OF ROUNDNESS AS JUDGED BY SIX OBSERVERS

Test Number	A1	A2	A3	A4	A5	A6	A7	A8	A9	A10
Ranking, Roundness	1.83	5.67	6.17	4.00	3.00	8.83	8.17	7.33	8.83	10.00
Attrition, %	0.77	1.82	0.32	4.51	0.50	0.89	1.67	1.85	1.78	1.90

It seems that particle rounding is not apparent because the particles are indeed relatively unchanged in shape. With less than 5 percent of particle mass attrited, particle appearance is not changed appreciably.

This study suggests that limestone particles subjected to graded heating, shock heating,* calcination, and fluidization attrite by abrasion of surface defects, not by splitting; and visual inspection of particles subjected to less than 5 weight percent attrition cannot discriminate the extent of attrition very closely.

*Tests conducted after completion of this contract demonstrated that severe thermal shock causes splitting of particles into large fragments.

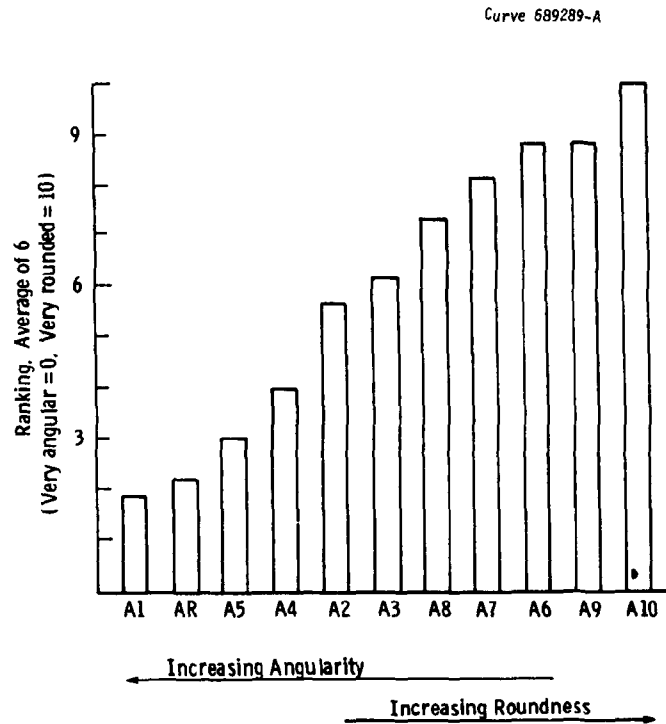


Figure 40 - Mean Rankings of Particle Angularity

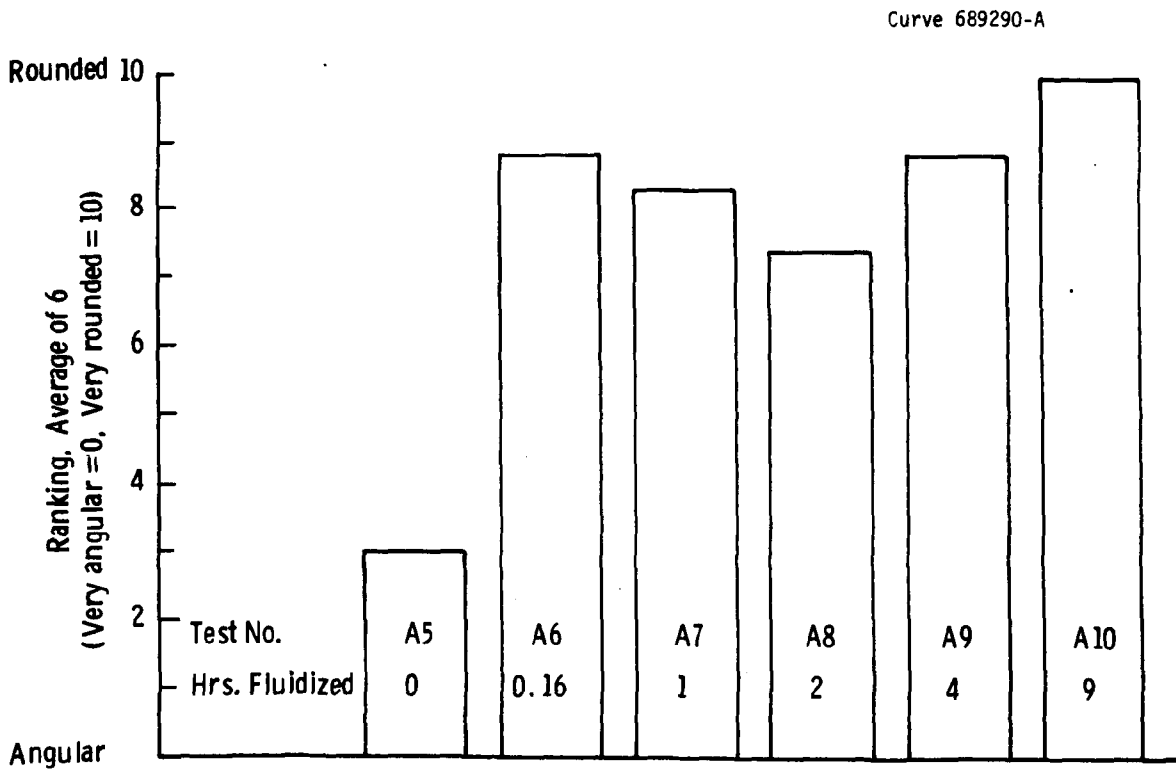


Figure 41 - Mean Rankings of Particle Angularity for the Effect-of-Duration Tests

Tests for Particle Swelling

In most attrition tests performed there appears to be an increase in the fraction of particles on the largest sieve mesh (as exemplified in Figure 39). One expects a decrease in frequency of the largest particles because of attrition. If the number of larger particle increases, it is because smaller particles swelled during treatment, or it is only an apparent increase in the fraction of large particles because of particle nonsphericity, as illustrated in Figure 42.

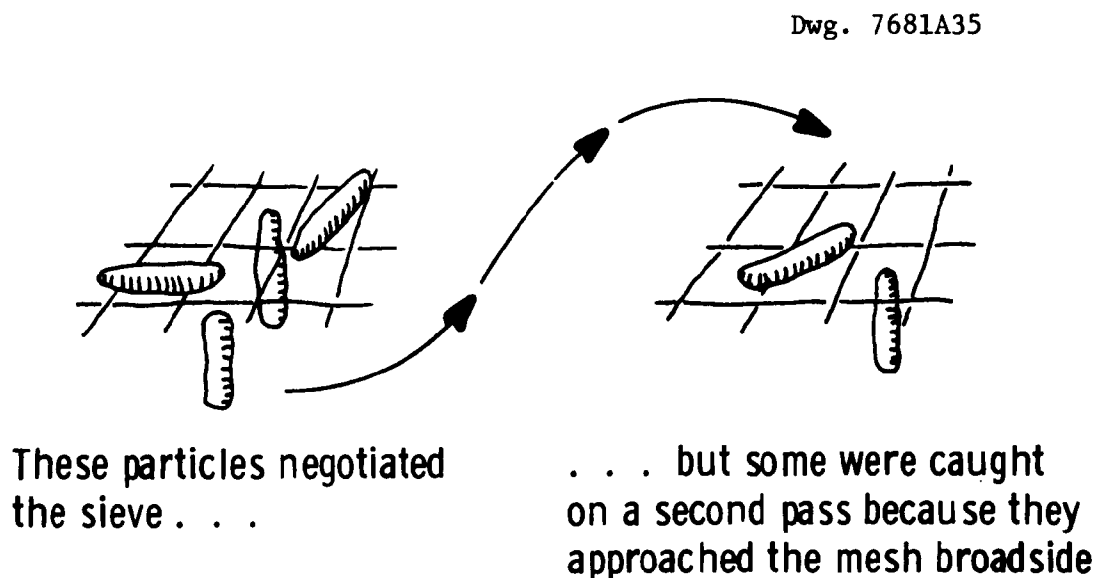


Figure 42 - Apparent Swelling of Sausage-Shaped Particles

Particle Swelling during Calcination

Comparison of screen analyses before and after calcination of sorbent has suggested that coarse particles swell when calcined. Microscopic examination of the particles does not show any evident changes such as with popcorn or puffed cereals, yet the screen analyses consistently indicate an increase in the number of larger particles.

In continued testing of particle swelling, 140 g of 710 to 1000 μm (16 by 24 mesh) Grove limestone was divided into equal halves. One-half was fluidized for four hours at 815°C with a gas flow of 1.2 times the minimum fluidizing velocity. Then both the treated half and the untreated half were screened to remove particles smaller than 710 μm (24 mesh).

Particles were photographed at 10X (Figure 43) and analyzed by the Zeiss (manual) and Leitz (automatic) methods. Results of the photograph measurement and statistical analysis are listed in Table 13.

Table 13
COMPARISON OF MEAN SIZES OF GROVE LIMESTONE
PARTICLES CALCINED AND UNTREATED

Method	Zeiss		Leitz	
Sample	Untreated	Treated	Untreated	Treated
Total Particles	340	262	62	65
Mean Diameter, mm	0.83	0.94	0.88	0.96
Standard Deviation, mm	0.2	0.2	0.21	0.22
Pooled Std. Dev., mm	0.2		0.215	
Statistic t & d.f.	6.69, 600		2.25, 125	
Tabulated t, 5% level	1.96		0.98	
Difference Significant ?	Yes		Yes	

While not conclusive with regard to all sorbents, these results for Grove limestone do support the hypothesis that stone particles do indeed swell upon calcination.



10X Before



10X After

Figure 43 - Micrographs of Grove Limestone before and after Calcination

Some nonspherical particles that pass a sieve on a first screening may not pass the sieve on a rescreening because elongated particles approach the screen sideways and do not pass. This appearance of particle swelling was tested using uncalcined Tymochtee dolomite. We sieved the sorbent, keeping that fraction that passed a 12 mesh (1410 μm) screen and was retained on a 16 mesh (1000 μm) screen after 10 minutes shaking on a mechanical sieve shaker. This fraction was resieved with a further 10 minutes of mechanical shaking. This experiment was replicated using two Tymochtee samples. One would expect that all particles would again pass the 12 mesh (1410 μm) screen and not pass the 16 mesh (1000 μm) screen.

Table 14 lists results of this experiment. There is good replication of the tests.

Table 14

EFFECT OF RESIEVING A SINGLE SIZE FRACTION OF TYMOCHTEE DOLOMITE

		After First Sieving			After Second Sieving		
Tyler Mesh	Opening μm D_p	Grams on Sieve	Percent on Sieve	% D_p	Grams on Sieve	Percent on Sieve	% D_p
1st Replicate							100.000
12	1410			100.000	0.26	0.372	99.628
16	1000	70.000	100.000	0.000	68.14	97.384	2.244
24	710				1.57	2.244	0
2nd Replicate							100.000
12	1410			100.000	0.20	0.286	99.714
16	1000	70.000	100.000	0.000	68.07	97.285	2.429
24	710				1.70	2.429	0

We conclude from this test that size distribution from identical successive sievings are not the same and that:

1. There appears to be an increase of larger sizes.
2. There appears to be an increase in smaller sizes, either by attrition or by particles passing that did not pass the first time.

These two tests indicate that there are separate, noninteracting processes that contribute to the observance of sorbent particle swelling. Calcination results in an increase in particle size, independent of sieve measurement; the very process of sieving measurement gives the appearance of particle size increase with uncalcined sorbent. These real and apparent increases need to be accounted for in precise measurement of particle size measurement in sorbent reaction processes.

Effect of Bed Pressure on Attrition Rate

It is difficult to state a priori whether varying pressure directly influences attrition rate, all other variables including $(U-U_{mf})/U_{mf}$ being equal. The increased density of fluidizing gas may accelerate particles faster and increase the extent of collisions. An indirect effect of pressure may be its influence on degree of calcination:

increased pressure	→	increased CO ₂ partial pressure	→	decreased rate (or extent) of calcination	→	change in particle strength	→	change in attrition rate
-----------------------	---	--	---	---	---	-----------------------------------	---	--------------------------------

Of course, this secondary effect will vanish with CO₂-free fluidizing gas and calcined stone.

The purpose of this experiment was to measure the influence of pressure on the extent of attrition, with other variables held constant.

Test conditions, apparatus, and procedure in this test were as follows:

Sorbent	Tymochtee dolomite
Particle diameter	1000 to 1410 μ m (12 to 16 mesh)

Temperature history	heat at 10°C/m to 815°C, hold for 4 hr, cool
Gas pressure	100 and 1000 kPaa (1 and 10 atm absolute)
Gas composition	15 vol % CO ₂ in N ₂
Gas velocity	U = 1.2 U _{mf}
Bed diameter	3.5 cm
Bed depth	~3 cm (initial charge of uncalcined stone = 70g)
Time of fluidization	4 hours

Figure 44 shows the size distribution curves for two replicate tests at 100 kPaa (○, ◐) and two replicate tests at 1000 kPaa (Δ, ◻). There are slight differences between the mean curves in Figure 44, but the curves are interpreted to be essentially the same. Those size fractions, comprising over half of the mass of fines (500-700, 350-500, 245-350, 43-61 μm) (24-32, 32-42, 42-60, 250-325 mesh), are statistically the same for both pressures.

The cumulative results from this test program are:

Pressure, kPaa	Percent of Sample Reduced to Smaller than 710 μm	
	1st Replicate	2nd Replicate
100	0.666	0.381
1000	0.534	0.516

A t-test of these data at the 10 percent level gives a calculated t of 0.01 compared with the tabulated t of 2.92, indicating that there is no significant effect of pressure.

The expression describing attrition rate in the bubbling zone of a fluidized bed

$$\frac{Rz}{U-U_{mf}} = k \left[\frac{g}{g_c} \frac{\rho_s}{\sigma_s} z^2 \right]^m$$

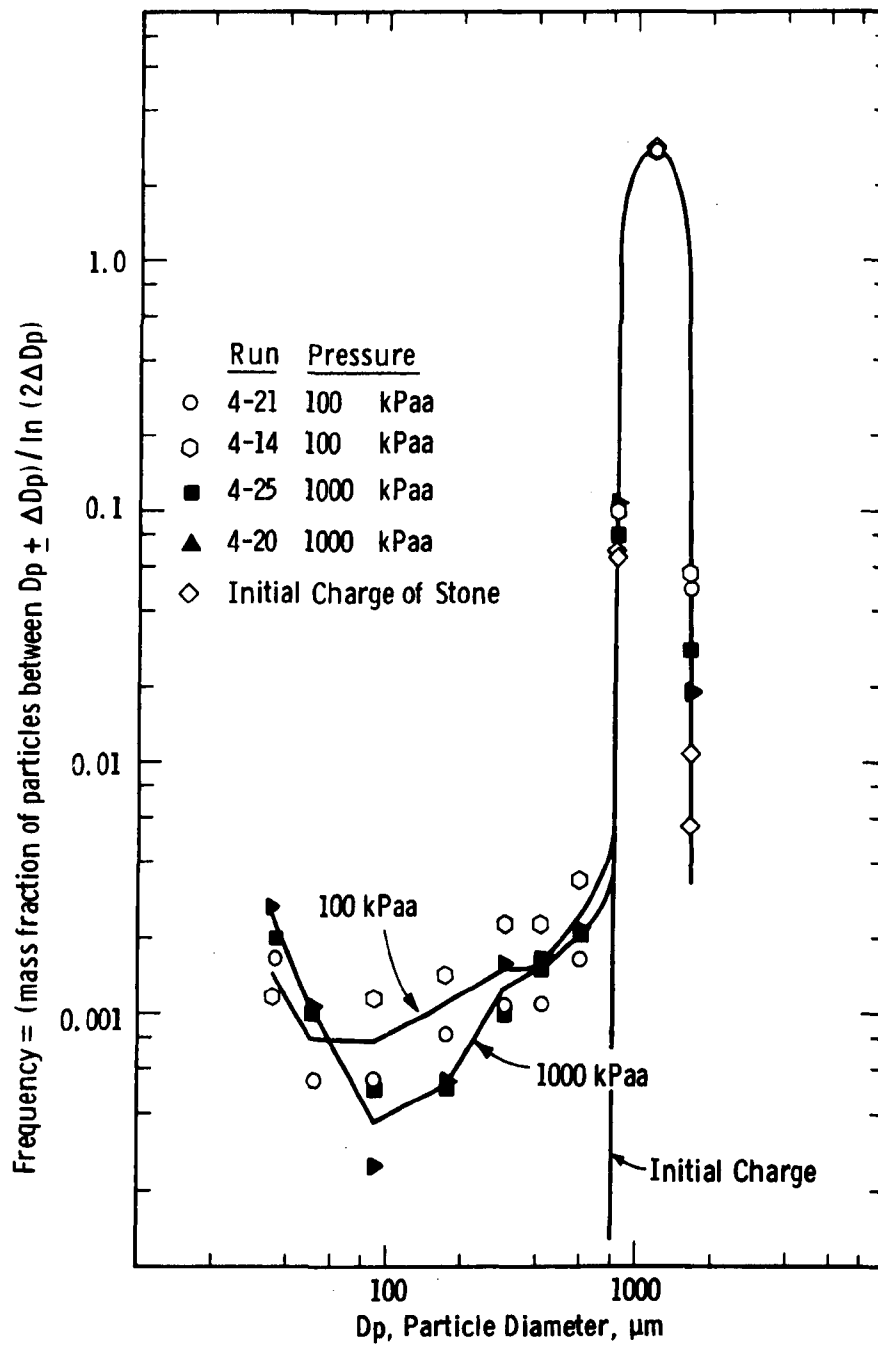


Figure 44 - Size Distributions of Tymochtee Dolomite after Hot Fluidization at 100 and 1000 kPa

is independent of gas pressure. Any pressure effects are accounted for in the dependence of U_{mf} on gas density; by relating attrition rate R to the excess gas velocity $U - U_{mf}$, the effects of pressure vanish. The experimental results reported here confirm that independence of pressure.

Effects of Bed Temperature, Particle Diameter, and Degree of Sulfation on Extent of Attrition

The theoretical study described in Appendix D concludes that attrition rate in the bubbling zone of a fluidized bed varies inversely with particle strength and is independent of particle diameter.

As part of our comprehensive study of attrition we chose to study the effects of three additional variables on the extent of attrition:

1. Fluidized-bed temperature because it affects particle strength and because it is an important controlled variable in any fluidized-bed combustion process.
2. Particle diameter because of uncertainty in the literature as to the effect of particle size on attrition rate
3. Degree of sulfation, as there is reason to believe that sulfating stone sorbents makes them harder and more resistant to attrition.

Craig and others²⁸ and Curran and others³⁶ have reported that sulfating sorbent grains increases particle strength and reduces attrition.

Description of the Apparatus and Test Plan

We fluidized Grove 1359 limestone in an attrition test cell 8.7 cm in diameter. A three-zone furnace heated the cell and bed to the test temperature. Figure 45 shows the apparatus and Figure 46 outlines the procedure. All stone was precalcined, carefully sized, and charged to the attrition test cell to a depth-to-diameter ratio of 1.0 to avoid slugging. Attrition measurements were based upon the mass of material that was reduced to a particle size smaller than the mesh size of the initial charge. Percent attrition is defined as $100 \times \ln (M_0/M_1)$ where M_0 = mass of the original charge and solids in the bed and M_1 = mass of

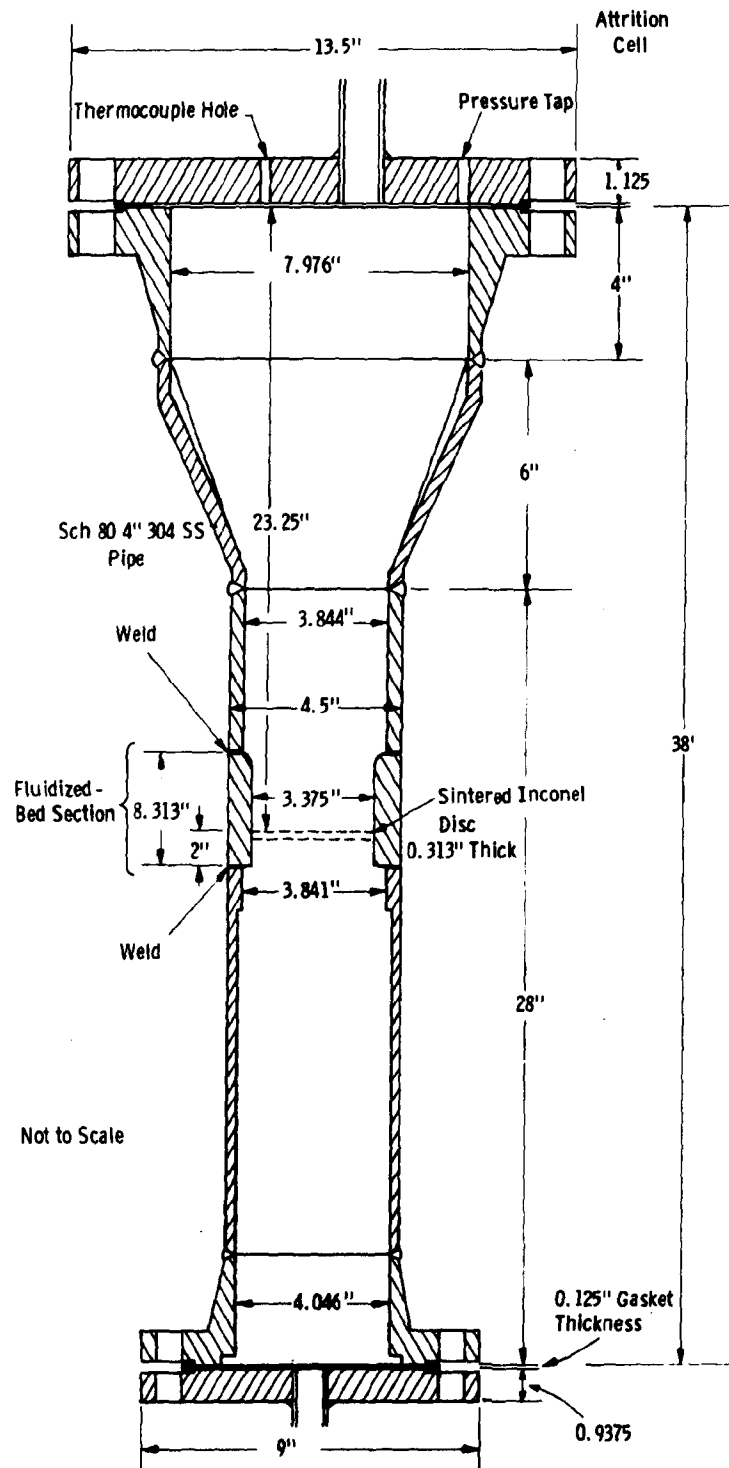


Figure 45 - Attrition Test Cell

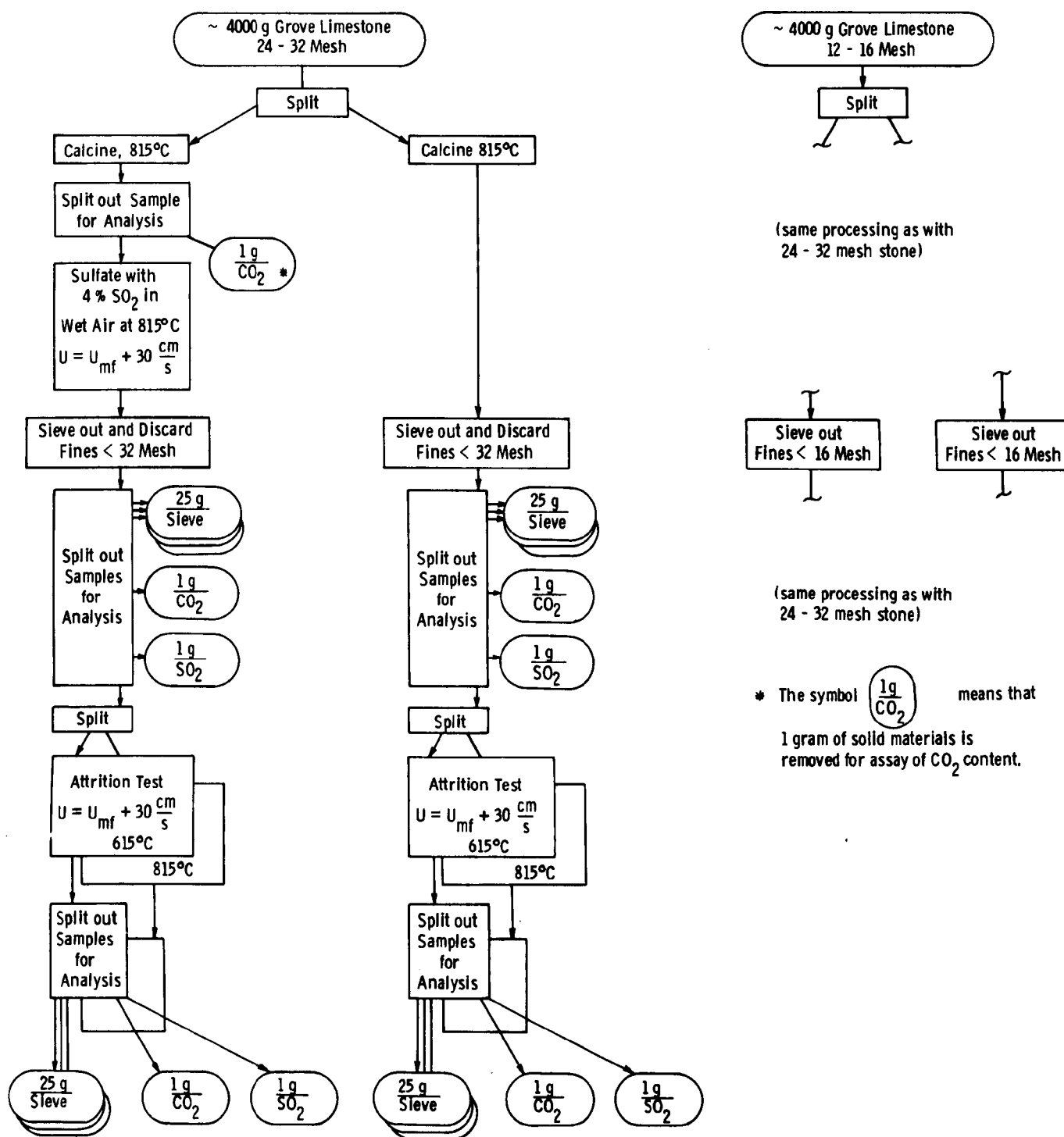


Figure 46 - Test Procedure for Attrition Testing of Grove Limestone for Effects of Grain Size, Temperature, and Sulfation

solids remaining in the bed after a time interval of fluidization. The mass of material smaller than the initial mesh size was determined by measuring the amount of fines in the bed and the fines carried out of the bed and captured in the off-gas filter.

Our theoretical studies (Appendix D) infer that the degree of attrition in freely bubbling fluidization is proportional to the pressure-volume power delivered to the bed in the form of bubbles. This is equivalent to saying that the attrition rate $R \propto (U - U_{mf})$, not a multiple of U or U/U_{mf} . From inspection of bubbling hot beds we chose $U - U_{mf} = 20$ cm/s as the excess velocity that gives vigorous bubbling without excessive splashing. In each test we measured the minimum fluidization velocity U_{mf} from a graph of ΔP across the bed versus the superficial velocity of hot gas flowing through the bed (Figure 47). The gas mixture used in these attrition tests was 85 percent nitrogen and 15 percent CO_2 .

We chose a full-factorial design that allows study of three variables each at two levels for main effects and interactions. The high and low levels of variables were as shown in Table 15.

Table 15
HIGH AND LOW LEVELS OF THE INDEPENDENT VARIABLES

Variable	Symbol	Low Level (coded as -1)	High Level (coded as +1)
Temperature	T	615°C	815°C
Particle Diameter	D	500 to 710 μm	1000 to 1410 μm
Percent of Possible Sulfation ^a	S	0%	10% ^b

^aBased on the amount of calcium in the stone sorbent

^bNominal

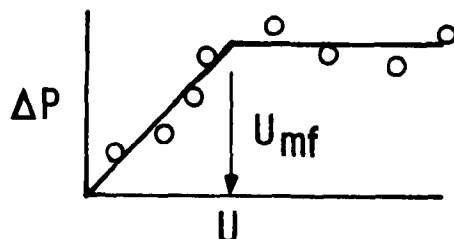


Figure 47 - Determination of U_{mf} from the ΔP - U Curve

Apparatus

The primary attrition test cell used in this work is pictured in Figures 48 and 49. The cell is 9.5 cm in diameter and can be fitted with a variety of perforated or sintered grids. Gas supplied from house lines or cylinders is metered through any of several flowmeters, preheated outside the cell, and flows through the cell, exiting through a sintered-metal filter. A three-zone furnace surrounds the cell, allowing fluidized-bed temperatures of up to 900°C. Thermocouples and pressure taps allow measurement of bed temperature, bed pressure, bed ΔP , and grid ΔP .

Results of the Tests

The procedure for calculating the fraction increase in surface area of the stone is shown in the following sample calculation:

Initial mass of stone (649.8 g stone measured) (1-0.0147 frac CO_2)
 on a CO_2 -free basis
 after calcination at 815°C = 640.26 g

Mass of stone after (637.55 g stone measured) (1-0.0109 frac CO_2)
 treatment, CO_2 -free
 basis = 630.60 g

Total loss of CO_2 - 640.26 - 630.60 = 9.66 g
 free stone by escape
 from the system or
 to the filter

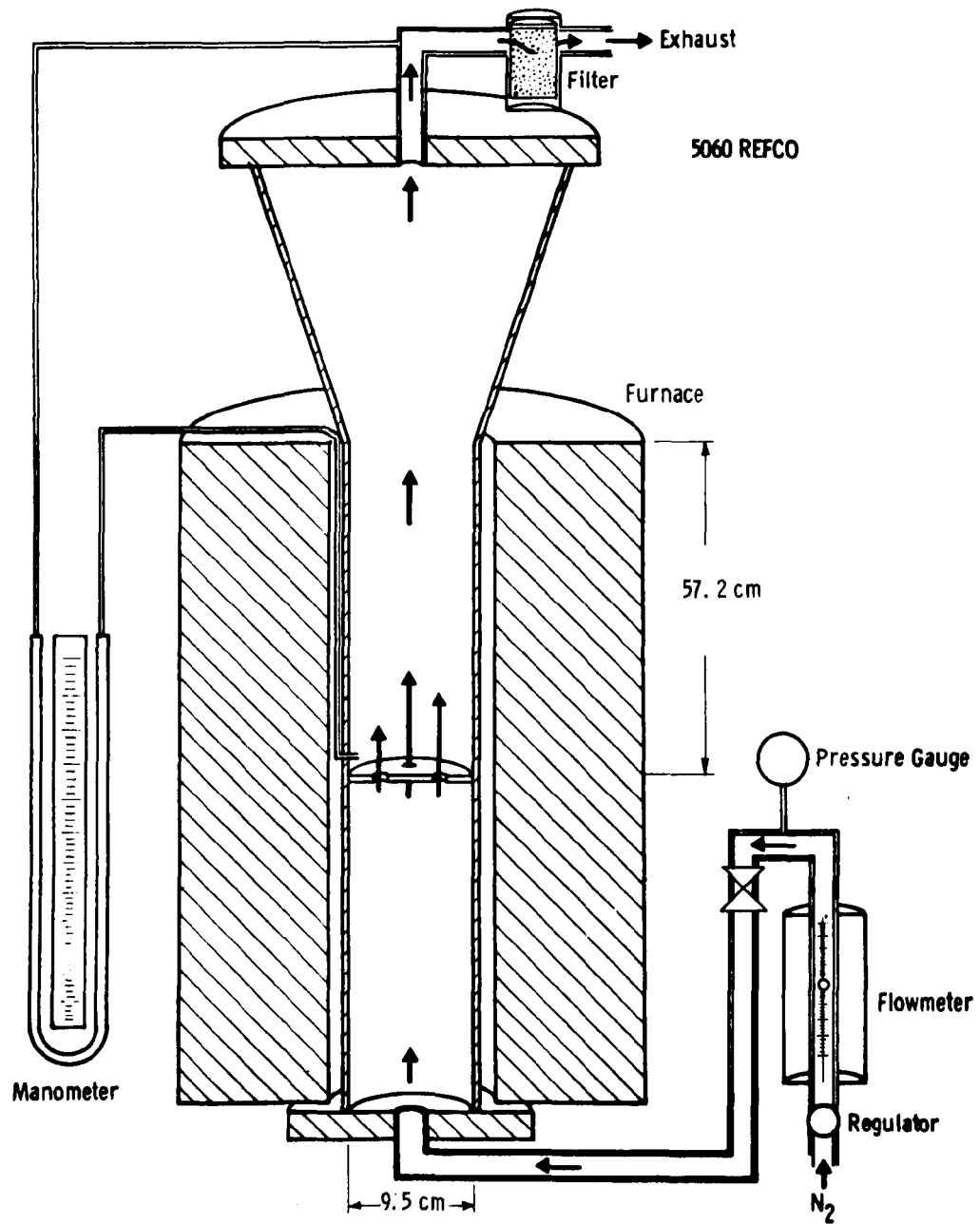


Figure 48 - Flow Diagram of Sorbent Attrition Test System,
Cell Diameter is 9.5 cm.

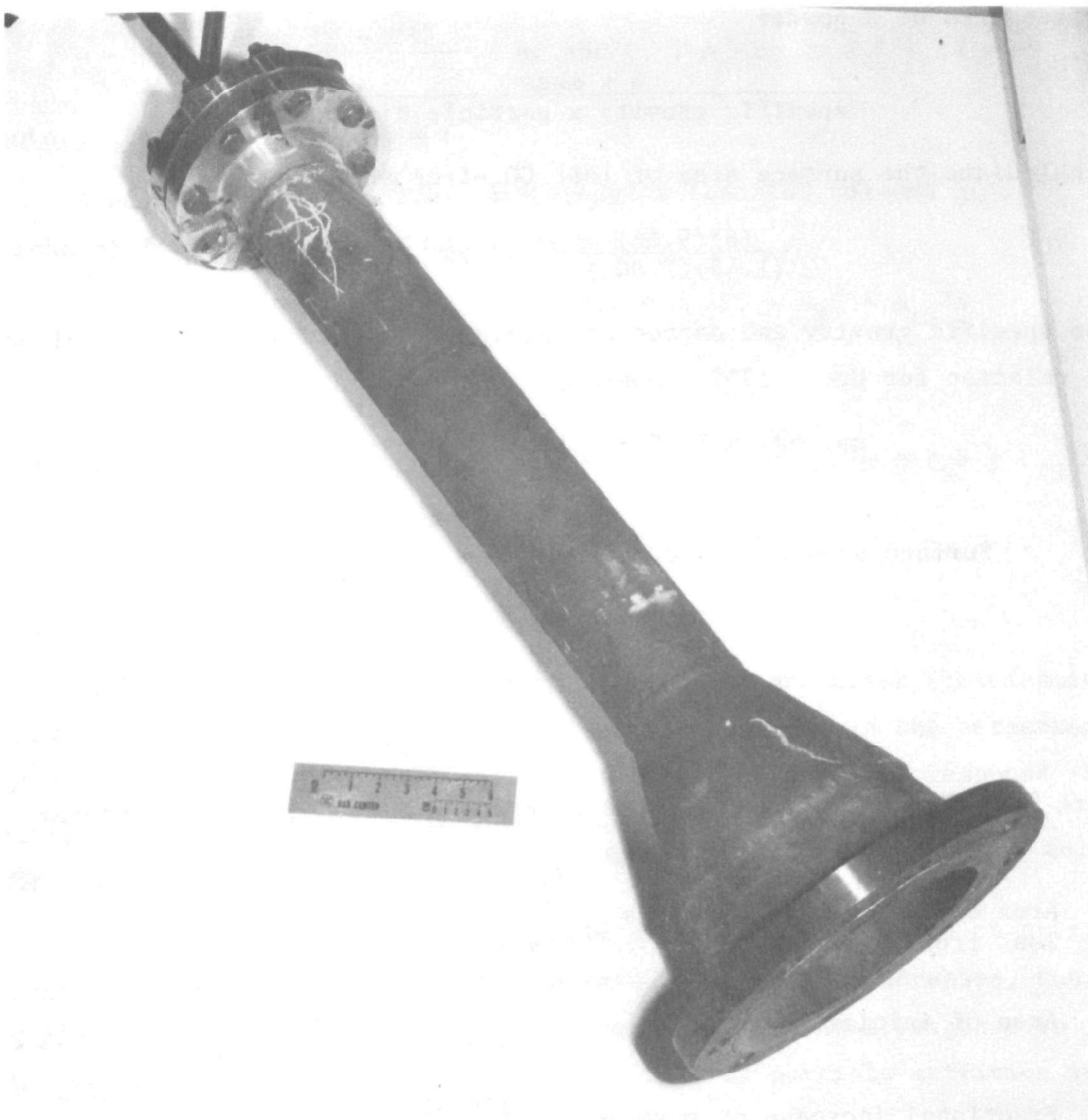


Figure 49 - Attrition Test Cell. The Grid is Welded into the Cylindrical Section near the Center. Cell Diameter is 9.5 cm id.

From measurements described in a later section we estimate the diameter of eliminated particles to range between 2.8 and 3.5 μm and here take the diameter of lost particles to be 3 μm . Using the formula for total surface area of a powder

$$\frac{6 \times \text{mass}}{\text{specific gravity} \times \text{particle diameter}} ,$$

we calculate the surface area of lost CO_2 -free stone to be

$$\frac{(6)(9.66)}{(1.45)(0.003)} = 133,241 \text{ cm}^2 .$$

From specific gravity and degree of calcination measurements we developed the relation for Grove 1359 limestone

$$\text{sp. gr.} = 1.45 + 2.51 (\text{wt fraction } \text{CO}_2)$$

$$\begin{aligned} \text{Surface area of stone in the bed} &= \frac{6 \times \text{mass} \times \Sigma(f_i/d_{pi})}{\text{specific gravity}} \\ &= \frac{6 \times 637.55 \times 8.9715}{1.45 + (2.51)(0.0109)} \\ &= 23,230 \text{ cm}^2 \end{aligned}$$

where $\Sigma(f_i/d_{pi})$ is the sum of mass fractions to mean-particle-diameter ratios for the several sieve sizes

$$\begin{array}{ll} \text{Area of stone in bed + fines} & \\ \text{lost from the bed} & = 133,241 + 23,230 = 156,471 \end{array}$$

$$\begin{array}{ll} \text{Area of initial charge} & = \frac{6 \times 649.81 \times 8.9451}{1.45 + (2.51)(0.0147)} = 23,455 \text{ cm}^2 \end{array}$$

$$\begin{array}{ll} \text{Fractional increase of surface} & \\ \text{area of solids} & = \frac{156,471 - 23,455}{23,455} = 5.67 \end{array}$$

The results of the hot attrition tests are listed in Table 16.

Coded values of T, D and S range from -1 to +1, corresponding to the upper and lower limits of the range of each variable; for example:

$$T = \frac{\text{Temperature, } ^\circ\text{C} - 732.5}{82.5} . \text{ At } 650^\circ\text{C, } T = -1; \text{ at } 815^\circ\text{C, } T = +1 .$$

Interpretation of the Results

Analysis of the attrition test results (the two columns at the right of Table 16) for the factorial model

$$\begin{aligned} \% \text{ Attrition, } A = & A_o + A_T T + A_D D + A_{TD} TD + A_S S + A_{TS} TS \\ & + A_{DS} DS + A_{TDS} TDS . \end{aligned}$$

$$\begin{aligned} \text{Increase in Powder Surface, } P = & P_o + P_T T + P_D D + P_{TD} TD + P_S S + P_{TS} TS \\ & + P_{DS} DS + P_{TDS} TDS \end{aligned}$$

gives these coefficients in Table 17.

The particle size distributions from before and after fluidization were interpreted in two ways. The first response (A) is the percentage of large particles lost to fines by attrition. The second response (P) is the fractional increase in surface area of the bed contents (including fines elutriated to the filter or lost from the system).

Both responses show an appreciable effect of temperature on attrition. As temperature increases, the rate of attrition increases, too. This effect is not surprising; one expects the sorbent strength σ to decrease at higher temperatures, and the rate of particle attrition is inversely proportional to sorbent strength σ .

Both responses show an effect of attrition rate decreasing as the degree of sorbent sulfation increases. This too is consistent with the findings of other workers.^{27,36}

Table 16

THE RESULTS OF HIGH-TEMPERATURE ATTRITION TESTING OF GROVE 1359

Dwg. 1693B08

Test Conditions					Before 4-Hour Fluidization					After 4-Hour Fluidization					% Attrition ^b	$\frac{S_f - S^o}{S^o}$ Increase in Surface Area
Date 1977	Temp °C	D _p Mesh (nominal)	% Sulfation	Coded Values For (T, D, S)	Frac. CO ₂ in Stone (after calcination)	Frac. > Smaller Mesh Size	Total Mass of Stone g	M°, Mass CO ₂ - Free Stone > Smaller Mesh Size ^a in the Bed	Total Surface Area of Stone in Bed, m ²	Frac. CO ₂ in Stone	Frac > Smaller Mesh Size in Bed	Total Mass of Stone g in Bed	M', Mass CO ₂ - Free Stone > Smaller Mesh Size ^a in Bed	Total Surface Area of Stone in Bed, m ²		
10/4	815	12-16	12.4	+++	0.0147	0.9647	649.81	617.66	2.35	0.0109	0.9576	637.55	603.86	15.65	2.26	5.67
10/6	815	24-32	0	+-	0.0241	0.9715	488.71	468.40	3.28	0.0182	0.9609	468.24	441.61	27.11	5.89	7.27
10/11	815	12-16	0	++-	0.0038	0.9534	478.87	454.82	1.67	0.0060	0.9601	472.21	449.47	13.99	1.18	7.40
10/13	650	24-32	9.4	--+	0.0171	0.9750	543.45	520.83	3.80	0.1612	0.9748	634.31	518.65	6.54	0.42	0.72
11/3	650	12-16	13.3	-++	0.0121	0.9643	556.97	530.59	2.02	0.0247	0.9690	551.59	522.52	18.9	1.53	8.36
11/10	815	24-32	14.7	+-+	0.0155	0.9750	532.10	510.76	3.73	0.0115	0.9614	523.50	497.51	12.49	2.63	2.35
11/15	650	12-16	0	-+-	0.0041	0.9534	454.00	431.48	1.58	0.0435	0.9461	463.90	419.80	13.15	2.74	7.31
11/17	650	24-32	0	---	0.0146	0.9787	386.00	372.26	2.62	0.3430	0.9816	580.30	374.26	1.34	-0.53	-.49

(a) Mass of CO₂- Free Stone > Smaller Mesh Size = (1 - Fraction CO₂ in Stone) × (Fraction > Smaller Mesh Size) × (Mass of Stone)(b) $100 \times \ln (M^o \div M')$

Table 17

FACTORIAL MODEL COEFFICIENTS DESCRIBING
ATTRITION OF GROVE 1351

1st Response, % attrition as loss of course particles	A	A _T	A _D	A _{TD}	A _S	A _{TS}	A _{DS}	A _{TDS}
	+2.1	+0.9	-0.2	-1.1	-0.4	-0.2	+0.3	0.8
2nd Response, fractional increase in surface area	P	P _T	P _D	P _{TD}	P _S	P _{TS}	P _{DS}	P _{TDS}
	+4.8	+0.9	+2.4	-1.5	-0.6	-1.1	+0.4	+0.4

The effect of particle diameter on attrition rate is not clear from these results. The analysis indicates that particle diameter has no significant effect on the rate of loss of large particles, but the analysis evidences a strong effect of particle size on the rate of creation of new surface. These results could be consistent (if big particles generate smaller fragments without significantly changing the size of the original particles). The conclusion of a significant effect between particle size and rate of surface formation, however, does not agree with our model (Appendix D). One is tempted to disregard this effect in support of a theory already formulated; but the magnitude of the effect is too great to ignore, and we recommend further study of the effect of particle size on attrition rate.

Among the interactions that of temperature and particle size is notable in both responses. We have no explanation for this interaction.

These results suggest the advantage of keeping the bed temperature down to reduce attrition. Similarly, this study confirms the avail of partially sulfating sorbent to increase its strength and lessen attrition losses.

Conclusions

- The rate of Grove limestone attrition increases with fluidized-bed temperature.
- The rate of Grove limestone attrition decreases with an increasing degree of stone sulfation.
- Results are uncertain as to the effect of particle size on limestone attrition rate during fluidization.

Severe Attrition Caused by a Jet at the Grid

This section describes severe attrition caused by an inadvertent jet on the grid of the 10.3-cm fluidized bed. In assembling the attrition test cell for testing on one day, we neglected to seal the grid at the cell wall. Inspection of the cell after testing showed a slit leak about 3 cm long (see Figure 50). Fluidizing the cell showed jetting from this leak and uneven gas distribution.

Dwg. 7681A32

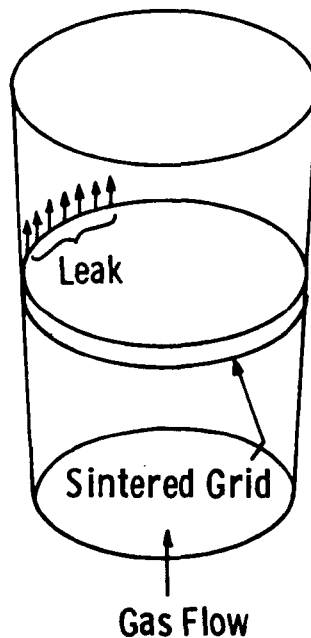


Figure 50 - Leak in 10.3-cm Fluidized Bed

Conditions in the test were:

Particle size range	95.1% < 1410 μm 0.2% < 710 μm
Temperature	815°C
Time of fluidization	4 hours
Minimum fluidization velocity	35.1 cm/s
Nominal gas flow velocity	45.8 cm/s
Gas composition	85% N ₂ , 15% CO ₂

These operating conditions are not irregular; only the presence of the jet along the wall was different from usual conditions.

Results of this test and an earlier test where no jet was detected are shown in Figure 51. This figure presents the same data on two sets of coordinates: the outside figure is plotted against an arithmetic ordinate (vertical axis) that emphasizes the differences in higher frequencies of particles. The inset curves are plotted against a logarithmic axis that details the lower frequencies. The Δ s are a plot of starting material for both attrition tests, the Os show the size distribution of limestone after attrition testing with the grid jet, the \bigcirc s represent material size after a test without the grid jet. The cumulative size distributions are shown in Figure 52.

The first and most obvious conclusion from these results is that the jet at the grid caused severe attrition. There was a decrease in the two largest classes of particles; these coarse particles were attrited. Conversely, there was an increase in all smaller sizes:

	Percent of mass smaller than:		
	710 μm	1000 μm	1410 μm
Original stone	0.212	5.37	95.1
Fluidized 4 hours, no grid jet	0.75	6.63	93.69
Fluidized 4 hours, grid jet	6.17	21.79	97.62

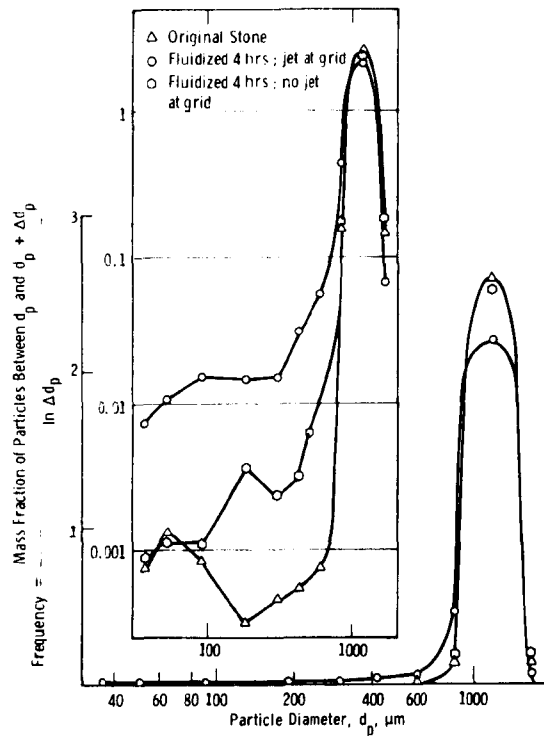


Figure 51 - Size Frequency Plots for Grove Limestone; Ordinate Shown in Both Arithmetic and Logarithmic Coordinates

Curve 590914-A

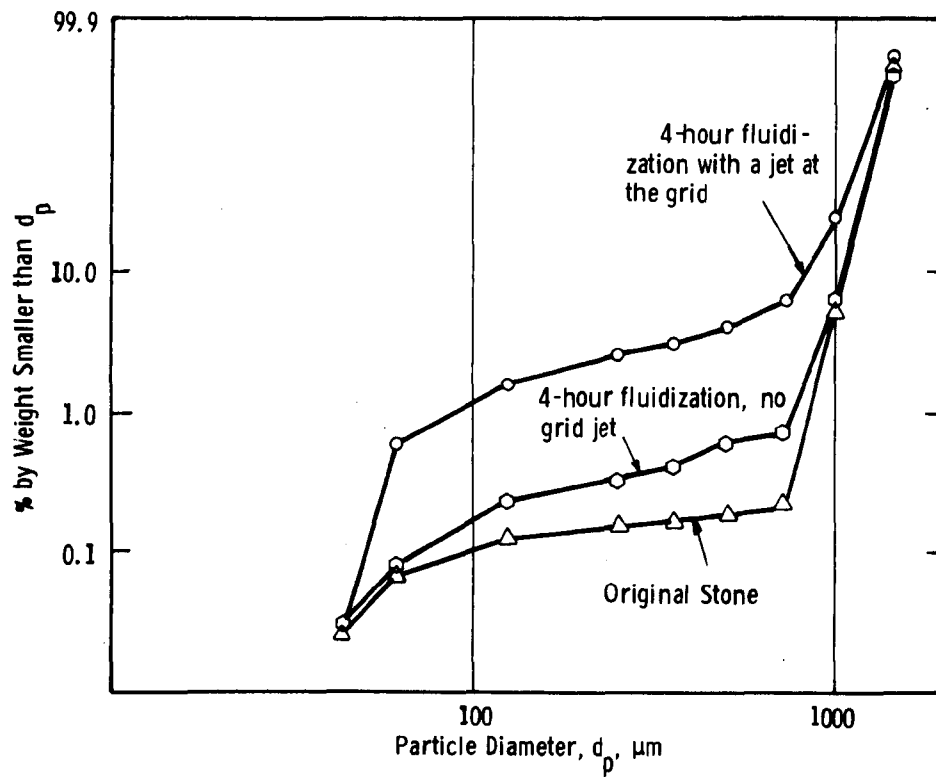


Figure 52 - Cumulative Distributions for Grove Limestone

A second observation is that the fraction of coarsest particles decreased under the severe grid jet conditions. In virtually all tests the fraction of coarsest particles increases, presumably from swelling. Under the conditions of acute attrition, any swelling effect was overcome by attrition of coarses, reducing their weight fraction from 4.9 to 2.3 percent. This suggests the influence of the grid design and the importance of controlling high-energy jets. Such effects have been eliminated in the bubbling-zone-attrition tests by use of sintered-metal grid.

Model of Attrition in the Bubbling Zone of a Fluidized Bed

A major part of the experimental attrition work in this study was development of a model describing the rate of attrition in the bubbling zone above the influence of grid jets. The results of this study are explained in detail in Appendix D.

The conclusions gained from this work are:

1. Attrition in the bubbling zone of a fluidized bed abrades particles, forming fine fragments. The attrition rate is defined as:

$$R \equiv \frac{\text{Mass of fines formed/second}}{\text{Mass of coarse bed solids}} .$$

2. In the bubbling zone the attrition rate, R , is proportional to the excess bubble velocity, $[U(\text{superficial gas velocity}) - U_{mf}(\text{minimum fluidization velocity})]$.
3. The attrition rate, R , in the bubbling zone is proportional to the bed depth, Z , at any point. The overall production rate of fines (g formed/s) is proportional to the square of the total bed depth.
4. The bubbling zone attrition rate, R , is proportional to particle density, ρ_s , inversely proportional to particle strength, σ_s .
5. The attrition rate in the bubbling zone is initially high; the rate decreases with time to a steady state.

6. The above conclusions are expressed symbolically as

$$\left[\frac{RZ}{U - U_{mf}} \right] \propto [F(t) + 1] \left[\frac{g}{g_c} \frac{\rho_s}{\sigma_s} Z^2 \right]^m; m \approx 1.$$

7. Research data published in the literature confirmed conclusion 3, above, and the implied conclusion that attrition rate is not affected by particle diameter.
8. Experimental results from our laboratory confirm conclusions 2 and 5, above.
9. Attrition rate in the bubbling zone of a fluidized bed can be controlled not only by choice of a weak or strong granular material, but by specification of bed depth, gas velocity, and particle diameter as it affects U_{mf} .

Size Distribution of Fragments Attrited from Particles in the Bubbling Zone of a Fluidized Bed

The purpose of this work was to measure the particle size of attrition fragments elutriated from a bed of fluidized sorbent and compare the measurements with the particle size distribution of fragments remaining in the bed.

In the bubbling zone of a fluidized bed we have observed formation of predominantly very fine fragments rather than large chips. Here we have investigated the extent of very fine particles formed by bubbling-zone attrition.

The apparatus we used was the 7-cm-id attrition test cell diagramed in Figure 53. The sintered grid eliminates grid jets and allows bubbling through the entire bed depth. The high freeboard permits splashing particles to fall back to the bed. Particles elutriated from the bed are trapped in the Balston filter.

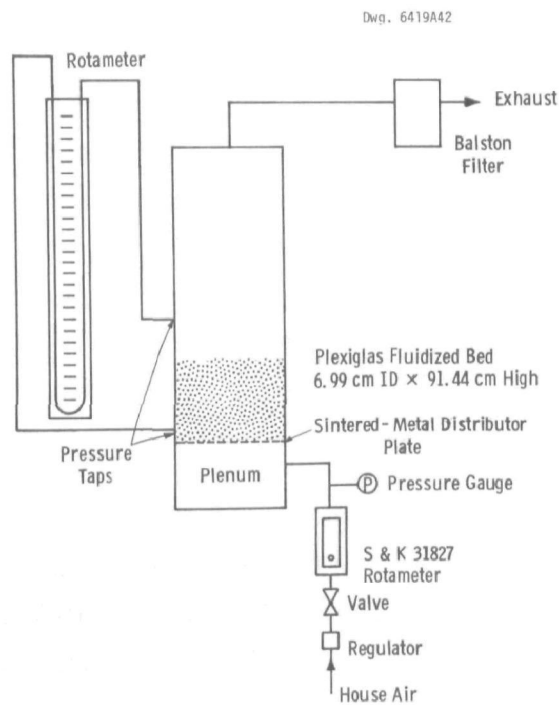


Figure 53 - Flow Diagram for Room-Temperature Fluidized Bed

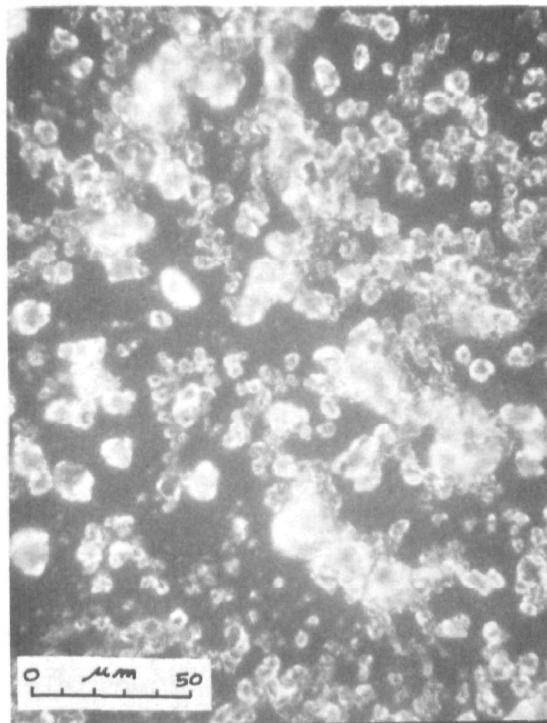


Figure 54 - Photomicrograph of Elutriated Grove Limestone Recovered from the Balston Filter, Magnification 500X

Our test procedure was to charge the attrition test cell with 300 g of uncalcined 32-x-42-mesh Grove 1359 limestone and measure the minimum fluidization velocity U_{mf} from a velocity- ΔP curve. We then fluidized the stone in air at $U_{mf} + 25$ cm/s. After 15 minutes of fluidization we disassembled the filter, measured the size of filter solids, and sieve-analyzed the bed contents. Another interpretation of this test is described in Appendix D following Equation 26.

The measurement of fine particle size was made from filter solids collected in a separate fluidization. After fluidizing Grove limestone in the same apparatus at $U_{mf} + 20$ cm/s for 23 hr, we photographed fines collected from the Balston filter. Figure 54 shows one such photograph at 500X magnification. Measurement of all grains intersected by a line drawn across the photograph yielded an estimate of the geometric mean particle diameter at $2.77 \mu\text{m}$. This seemed small, and we checked the measurement with Coulter Counter[®] analysis. The geometric mean diameter of filter solids by Coulter Counter measurements was $3.45 \mu\text{m}$, which compares well with the photographic measurements.

Results of the fluidization measurements for 15 minutes at $U_{mf} + 25$ cm/s are listed in Table 18. The specific surface contributions for the several sieve size ranges after fluidization are presented in Table 19. Inspection of the row of S_i values shows that 90 percent of the new specific surface formed is on particles elutriated from the bed. Of the mass fractions of particles lost or formed, 4.2 percent were lost in the largest size fraction, -32 + 42 mesh; 3.6 percent gained in the broad midrange from 42 mesh to the pan ($<43 \mu\text{m}$ in the bed); and 0.6 percent gained in the filter or were lost as $3 \mu\text{m}$ microfines. Thus, 14 percent of the attrition resulted in $3 \mu\text{m}$ microfines on a mass basis.

Very small particles generated in fluidization may present problems with downstream equipment or escape through particle control equipment (filters). Continued awareness and analysis for microfines is needed, as their presence can affect air quality or downstream system components.

Table 18

DEPENDENCE OF SOLIDS SPECIFIC SURFACE ON TIME OF FLUIDIZATION

Dwg. 1692853

U - U _{mf} = 25 cm/s								
Time Interval, hr		Start	1/4	1/4	1/2	1	2	4
Total Fluidization Time, hr		0	1/4	1/2	1	2	4	8
Sieve Mesh	D _p , Mean Diameter, cm	Mass of Solids on Sieve, g						
42	0.042	330	316.188	315.815	311.631	309.081	303.903	300.957
60	0.030	0	10.857	10.366	12.516	12.869	15.849	16.621
115	0.018	0	0.429	0.328	0.510	0.599	0.723	0.906
250	0.009	0	0.418	0.148	0.181	0.122	0.186	0.136
325	0.0052	0	0.048	0.010	0.013	0.012	0.025	0.019
Pan	0.0036	0	0.016	0.009	0.009	0.009	0.009	0.014
Filter	0.0003	0	1.336	2.487	3.984	5.691	7.643	9.002
Lost ^a	0.0003	0	0.709	0.837	1.156	1.617	1.662	2.345
Specific Surface, cm ² /g ^a		53.91	101.46	130.25	171.69	220.92	266.54	312.97
% Increase in Specific Surface		0	88.2	141.6	218.5	309.8	394.4	480.5

4.3 SORBENT REGENERATION

Westinghouse has performed an engineering evaluation of sorbent regeneration for both atmospheric and pressurized FBC. This evaluation has been reported in Regeneration of Calcium-Based SO₂ Sorbents for Fluidized-Bed Combustion: Engineering Evaluation, Report No. EPA-600/7-78-039 (March, 1978).⁴ No new work has been completed on sorbent regeneration since that report was published.

In the report the economics of FBC power plants operated with regeneration are projected on the basis of current estimates of regeneration process performance. Coal-feed reductive decomposition is the regeneration process considered for AFBC; three regeneration schemes (two reductive decomposition processes and a two-step process) are evaluated for PFBC. Estimated costs of FBC power plants with regeneration are compared with costs of FBC plants using once-through sorbent (no

Table 19

DISTRIBUTION OF PARTICLE SURFACE AREA FOR VARIOUS PARTICLE SIZES
AFTER 15 MINUTES FLUIDIZATION OF GROVE LIMESTONE AT 25°C

Sieve Mesh Range	-32 + 42	-42 + 60	-60 + 115	-115 + 250	-250 + 325	-325	Filter	Losses	Total
Mean Particle Size in Size Range, d_{pi} , cm	0.042	0.030	0.018	0.009	0.0052	0.0036	0.0003	0.0003	
Mass of Solids in Size Range, M_i	316.188	10.856	0.4287	0.4175	0.0475	0.0162	1.3359	0.7094 ^a	
Contribution to Specific Surface, S_b	51.65	2.48	0.16	0.32	0.06	0.03	30.55	16.21	101.46
Contribution to Specific Surface before Fluidization, cm^2/g	53.91	0	0	0	0	0	0	0	53.91
Increase in Specific Surface, ΔS_i	2.26	2.48	0.16	0.32	0.06	0.03	30.55	16.21	52.07

^aCalculated from mass balance.

^bSurface area at solids in size range ÷ total mass of solids; $\frac{6 (M_i/d_{pi})}{\rho \sum M_i} \quad \frac{6 (M_i/d_{pi})}{2.65 \times 330}$.

^cThis is calculated by assuming spherical particles; not rigorously measured.

regeneration). The economic feasibility of the regenerative system depends on several variables, including, in particular, the sulfur concentration achievable in the regenerator off-gas, the reduction in fresh sorbent feed rate possible through regeneration, and the cost of fresh sorbent and of solid residue disposal. The performance required for the regenerative FBC system to achieve economic feasibility is projected, and critical development needs are discussed. An integrated regeneration system for both AFBC and PFBC, capable of achieving the performance necessary, has yet to be demonstrated experimentally.

The sulfur recovery system is, in general, the dominant subsystem in the regeneration process. The economic and environmental potential, and the technical feasibility of regeneration are uncertain. The regenerative AFBC power plant shows more economic potential than does the regenerative PFBC plant, because of the higher levels of SO_2 achievable from the regenerator in the atmospheric pressure case. Major technical uncertainties are associated with the transport of high-temperature solids between the combustor and the regenerator. The reduced rate of sorbent consumption and solid residue disposal resulting from regenerative operation is accompanied by a reduction in power plant efficiency and an increase in the consumption of coal and other auxiliary fuels.

5. SULFUR OXIDE CONTROL - ALTERNATIVE SORBENTS

Westinghouse has performed an evaluation of alternative sulfur sorbents for FBC. This evaluation was reported in Alternatives to Calcium-Based SO₂ Sorbents for Fluidized-Bed Combustion: Conceptual Evaluation, Report No. EPA-600/7-78-005 (January, 1978).³ No new work has been performed on alternative sorbents since that report was published.

The report gives results of a conceptual engineering evaluation to screen supported metal oxides as alternatives to natural calcium-based sorbents (limestones and dolomites) for SO₂ control in atmospheric and pressurized FBC processes. We evaluated alternative sorbents, using three acceptance criteria.

- SO₂ removal capability in the combustor, predicted by thermodynamics
- SO₂ concentrations achievable in the regenerator off-gas, according to thermodynamics
- SO₂ concentrations of the regenerator, achievable on the basis of the material and energy balances.

The evaluation identified 14 potentially acceptable sorbents for AFBC and 11 for PFBC. We prepared cost estimates to project the maximum acceptable loss rates for the alternative sorbents because of attrition and/or deactivation. Loss rates must be less than 0.1 percent of bed inventory per hour in order to compete economically with natural calcium-based sorbents, even if maximum thermodynamic performance were obtained. U.S. resources of some minerals may be of extreme importance for many of the alternative metal oxide sorbents considered.

Unless the high levels (near maximum) of SO_2 or H_2S projected in this report can be achieved in the regeneration process, the alternative sorbents will be economically unfeasible. At present, too little is known about the cost of sorbent preparation. Feasible process technology for sorbent preparation should be proposed and the economic feasibility assessed. The availability of the sorbent materials and the support materials requires more modeling in order properly to assess all of the market factors. The area of industrial expansion into alternative sorbent preparation and distribution must also be explored.

The environmental impact (spent sorbent disposal, trace metals release, impact on NO_x , CO, particulates, etc.), of alternative sorbents may lead to the elimination of certain candidate materials. The complex sociological interactions of these materials must be explored before development is committed.

6. REFERENCES

1. Keairns, D. L., et al., Fluidized Bed Combustion Process Evaluation - Phase II - Pressurized Fluidized Bed Coal Combustion Development, Report to EPA, Westinghouse Research Laboratories, Pittsburgh, PA, EPA-650/2-75-027c, September 1975, NTIS PB 246-116.
2. Newby, R. A., N. H. Ulerich, D. F. Ciliberti, and D. L. Keairns, Effect of SO₂ Emission Requirements on Fluidized-Bed Combustion Systems, Preliminary Technical/Economic Assessment. Report to EPA, Westinghouse Research and Development Center, Pittsburgh, PA, August 1978, EPA-600/7-78-163.
3. Newby, R. A., and D. L. Keairns, Alternatives to Calcium-Based SO₂ Sorbents for Fluidized-Bed Combustion: Conceptual Evaluation. Report to EPA, Westinghouse Research and Development Center, Pittsburgh, PA, January 1978, EPA-600/7-78-005.
4. Newby, R. A., S. Katta, and D. L. Keairns, Regeneration of Calcium-Based Sorbent for Fluidized-Bed Combustion: Engineering Evaluation. Report to EPA, Westinghouse Research and Development Center, Pittsburgh, PA, March 1978, EPA-600/7-78-039.
5. Keairns, D. L., D. H. Archer, R. A. Newby, E. P. O'Neill, E. J. Vidt, Evaluation of the Fluidized Bed Combustion Process, Vol. I. Report to EPA, Westinghouse Research Laboratories, Pittsburgh, PA, December 1973, EPA-650/2-73-048a, NTIS PB 231-162.
6. O'Neill, E. P., D. L. Keairns, W. F. Kittle, A Thermogravimetric Study of Limestone and Dolomite - The Effect of Calcination Conditions, *Thermochimica Acta*, 14: 209; 1976.
7. Ulerich, N. H., E. P. O'Neill and D. L. Keairns, The Influence of Limestone Calcination on the Utilization of the Sulfur-Sorbent in

- Atmospheric Pressure Fluid-Bed Combustors. Final report to EPRI, Westinghouse Research and Development Center, Pittsburgh, PA, Contract RP720-1, February 1977, EPRI FP-426.
8. Ulerich, N. H., E. P. O'Neill, and D. L. Keairns, A Thermogravimetric Study of the Effect of Pore Volume - Pore Size Distribution on the Sulfation of Calcined Limestones, *Thermochimica Acta*, 26: 269-82; 1978.
 9. Ulerich, N. H., R. A. Newby, and D. L. Keairns, Sorbent Requirements for a Gulf Coast Lignite-Fixed Atmospheric Fluid Bed Combustion Power Plant. Final report to EPRI, Westinghouse Research and Development Center, Pittsburgh, PA, Contract RP1179-1, October 1978.
 10. O'Neill, E. P., N. H. Ulerich, R. A. Newby, and D. L. Keairns, Criteria for the Selection of SO₂ Solvents for Atmospheric Pressure Fluid Bed Combustors. Final report to EPRI, Westinghouse Research and Development Center, EPRI Contract RP721, January 1979.
 11. Beecher, D. T., et al., Energy Conversion Alternatives Study (ECAS) Vol. III. Report to NASA, Westinghouse Research Laboratories, Pittsburgh, PA, NASA (R-134942), Washington: National Science Foundation; 1976, NTIS PB 268558.
 12. Hoke, R. C., L. A. Ruth, and H. Shaw, Combustion and Desulfurization of Coal in a Fluidized Bed of Limestone, IEEE-ASME Joint Power Generation Conference, Miami Beach, FL, September 15-19, 1974.
 13. Moss, A., Chem. Eng. (Birmingham University), 23: 24; 1972.
 14. Reduction of Atmospheric Pollution, Final Report, Vol. 2. Office of Air Programs, National Coal Board, London, UK, September 1971, PB 210-674.
 15. Burdett, W. A., Sulphation of CaO by SO₂ and SO₃, Central Electricity Generating Board, London, UK, May 1979, Note R1M/N1052.

16. Yang, R. T., C. R. Krishna, and M. Steinberg, Fluidized-Bed Coal Combustion with Lime Additives. The Phenomenon of Peaking Sulfur Retention at a Certain Temperature, Ind. Eng. Chem., Fundam., 16 (4):465-467; 1977.
17. Hartman, M. and R. Coughlin, AIChE J., 22: 490; 1976.
18. Hubble, B. R., et al The Formation of $Mg_3Ca(SO_4)_4$ during the Sulfation Reaction of Dolomite, Journal of the Air Pollution Control Association, 27 (4): 343-346; 1977.
19. Hubble, B. R., S. Siegel, L. H. Fuchs, and P. T. Cunningham, Chemical, Structural, and Morphological Studies of Dolomite in Sulfation and Regeneration Reactions. Proceedings of the 4th International Conference on Fluidized-Bed Combustion McLean, VA, December 1975.
20. Borgwardt, R. H., Kinetics of the Reaction of SO_2 with Calcined Limestone, Env. Sci. & Tech., 4 (1): 59-63; 1970.
21. Hatfield, J. D., Y. K. Kim, R. C. Mullins, and G. H. McClellan, Investigation of the Reactivities of Limestone to Remove Sulfur Dioxide from Flue Gas. Report to Office of Air Pollution, Tennessee Valley Authority; 1971.
22. Coutant, R. W., et al., Investigation of the Reactivity of Limestone and Dolomite for Capturing SO_2 from Flue Gas. Report to NAPCA, Battelle Memorial Institute, Columbus, OH, November 20, 1970, NTIS PB 196 749.
23. Fields, R. B. and J. F. Davidson, Reaction of SO_2 with Limestone in a Fluidized Bed; Estimation of Kinetic Data from a Batch Experiment, Cambridge University, Cambridge, UK, paper presented at AIChE Meeting, Miami, November 1978.
24. Blinichev, V. N., V. V. Strel'tsov, E. S. Lebedeva, An Investigation into the Size Reduction of Granular Materials during their Processing in Fluidized Beds, Int'l Chemical Energy 8 (4): 615-18; October 1968.

25. Jonke, A. A. et al., Annual Report on a Development Program in Pressurized Fluidized-Bed Combustion, Argonne National Laboratories, Argonne, IL, July 1976, ANL/ES-CEN-1016.
26. Paige, J. I., J. W. Tron, J. H. Russell, and H. J. Kelly, Sorption of SO_2 and Regeneration of Alkalized Alumina in Fluidized-Bed Reactors. Report of Investigations 7414, U.S. Bureau of Mines, August 1970.
27. Chemically Active Fluidized Bed Process, Monthly Technical Narrative No. 20, Foster Wheeler Energy Corporation, Livingston, NJ, January 24 - February 20, 1977, prepared March 14, 1977.
28. Craig, J. W. T. et al., Chemically Active Fluidized Bed Process for Sulphur Removal during Gasification of Heavy Fuel Oil, Second Phase. Report to EPA, Esso Research Centre, Abingdon, UK, November 1973, EPA-650/2-73-039.
29. Wen, C. Y., and Yu, Y. A., Mechanics of Fluidization, Chem. Eng. Prog. Series, 62: 100-111; 1966.
30. Kinzler, D., Exxon Research and Engineering Co; Linden, NJ, personal communication, April 23, 1976.
31. Kut'yavina, T. A., and A. P. Baskakov, Grinding of Fine Granular Material with Fluidization, Chemistry and Technology Fuel Oils, 8 (3): 210-13; March - April 1972.
32. Jonke, A. A., A Development Program on Pressurized Fluidized-Bed Combustion, Monthly Progress Report, Argonne National Laboratories, Argonne, IL: 29-35; June 1976, ANL/ES-CEN-F092.
33. Stanley, D. A., L. Y. Sadler, III, D. R. Brooks, and M. A. Schwartz, Production of Submicron Silicon Carbide Powders by Attrition Milling, Fine Particles, Second International Conference, Boston, MA. Princeton, NJ: Electrochemical Society, Inc.; 1974: 331-36.
34. Mathur, K. B., and N. Epstein, Developments in Spouted Technology, Can. J. of Chem. Eng., 52 (2): 129-45.

35. Gonzales, V., and A. R. Otero, Powder Technology, 7 (3): 137-43.
36. Curran, G. P., et al., Formal report No. 5 to EPA, Project 550, Consolidation Coal Company, April 1977, EPA 600/7-77-031.
37. Encyclopedia of Chemical Technology, Second Edition, R. E. Kirk and D. F. Othmer, eds., New York: Intersciences Publishers; 1963.

APPENDIX A

SULFUR OXIDE REMOVAL DATA BASE AND MODEL

The feed ratio of calcium to sulfur required for desulfurization in fluidized-bed combustion depends on the system design, the operating conditions, the particular calcium-based sorbent, and the sorbent particle size used. In assessments of the overall FBC system it has been convenient in the past to select Ca/S feed ratios of about 3/1 for AFBC and about 2/1 for PFBC as base cases; and, over the years, these estimates have acquired a more permanent status, without reference to any particular sorbent, system design, or operating conditions. Desulfurization in the bed, however, is essentially a competition between two processes: once sulfur dioxide is released in the bed it may either remain in the gas and escape or react with calcium oxide (CaO) or carbonate (CaCO_3) in the bed to form calcium sulfate (CaSO_4). The balance between these processes can be drastically altered by enhancing the probability of escape (shallow bed, high gas velocity) or by changing the reaction rate of the sorbent (e.g., decreasing the sorbent particle size, raising the bed temperature at atmospheric pressure).

In order to predict the Ca/S molar rate required for a given level of desulfurization, a model of the desulfurization system that encompasses the effects of the relevant variables is required. Such a model must succeed in correctly projecting the effects of key variables on the system. In particular, since the following effects have been observed in experimental combustors, it should demonstrate

- That an optimum temperature for desulfurization exists at atmospheric pressure using sorbent particles 500 μm or larger in size

- That sorbent utilization improves at higher pressures (~1000 kPa)
- That there is no marked temperature effect at higher pressures (~1000 kPa).

Attempts to model fluidized-bed desulfurization to the extent of predicting Ca/S molar feed ratios may be: a) statistical correlations based on analysis of fluidized-bed combustion data (Babcock & Wilcox [B&W],^{A1} Battelle^{A2}); b) models that attempt to use sulfation rate data obtained in the Laboratory (Argonne National Laboratories [ANL],^{A3} Westinghouse,^{A4} National Coal Board [NCB];^{A5} or c) fundamental models in which the gas/solid reaction model is matched with the fluid dynamics of the bed (no successful model known).

The correlation models are generally untrustworthy outside the range of data correlated, and, since the objective is to project desulfurization under novel constraints, they are not useful here. Of the other models, the simplest and most direct is that developed at Westinghouse.

It may be noted that recent fundamental gas-solid modeling by Hartman and Coughlin^{A6} has yielded a sufficiently close prediction of effects observed in practice to be considered as a starting point for the development of a fundamental model: development and analysis of a reasonable body of self-consistent rate data has not yet been reported.

THE WESTINGHOUSE MODEL

The model used here has been described previously (Appendix E of Reference A4). The following assumptions are made in deriving the model;

1. Release of sulfur from coal as sulfur dioxide (SO_2) occurs with equal probability at any place in the bed.
2. Sulfur dioxide released at a distance, \bar{h} , below the upper bed surface passes in plug-flow through a homogeneous bed of sorbent of height h . If a mean reaction rate, K , can be assigned to the absorption of gas in the bed, the fraction of the sulfur

retained is $1 - e^{-Kt}$, where t is the gas residence time in the bed of height h . Integration for all points \bar{h} along the bed height yields an expression for the fractional sulfur removal, R , $R = 1 - \frac{1}{KZ} (1 - e^{-KZ})$, where Z is the residence time of gas entering the bed from below.

3. The mean rate constant for gas absorption in the bed, K , is obtained at any fixed mean utilization of the sorbent from thermogravimetric data reduced to unit gas concentration. The rate constant for any given sorbent type and chemical form will depend on the mean sorbent utilization, sorbent particle size, bed temperature, bed pressure, and gas composition in the bed.

The model of sulfur generation in the bed assumes that sulfur is released from coal with equal probability at all places in the bed. While this is a reasonable general assumption, it implies that, for example, 10 percent of the sulfur is released within the top 10 percent of bed height. Assume that all the sulfur generated in the bed below the top 10 percent is captured with 100 percent efficiency, and the overall desulfurization target is 97 percent. Then the top 10 percent of the bed must capture the sulfur liberated within it with at least 70 percent efficiency, despite the small remaining bed height and effective gas residence time.

As the emission standard becomes more stringent, the reaction constant term, KZ , required between SO_2 and CaO increases as the following table shows:

<u>Effective Sulfur Dioxide Removal Standard, %</u>	<u>Rate Constant/Rate Constant at 80% (at constant gas residence time)</u>
80	1
90	2
95	4
97.5	8
98.75	16

The rate constant for limestone sulfation required for varied sulfur removal efficiencies is projected in Figure A1 as a function of gas residence time. In practice, the rate constant could be varied by changing the sorbent particle size or bed temperature. Alternatively, bed residence time could be adjusted by varying gas velocity or bed depth.

If all of the sulfur is actually liberated in the lower two-thirds of the bed, then a different picture emerges. The top third of the bed behaves only as an absorber into which SO_2 is fed from the bottom. The reaction rates required for desulfurization with this kind of sulfur generation pattern are illustrated in Figure A2.

A generalized sulfur generation model has been published by ANL,^{A3} and this could be incorporated into the model discussed here, if desired. The choice of a particular sulfur generation pattern, however, in any case is speculative.

Operating conditions that would disturb the uniform sulfur generation pattern are: the location of coal feed points and their number, the coal particle size, and the extent of vertical mixing in the operating fluidizing mode. Thus, fine particles of coal fed near the base of a tall bed at low fluidization would probably cause disproportionate release of SO_2 near the base of the bed and improve sulfur removal relative to the prediction of a uniform sulfur generation model.

TG DATA

The use of TG data to model the fluidized-bed sulfation depends on several assumptions, which are listed below:

1. The rate-limiting process is governed by diffusion within the sorbent itself.
2. The residence time of the sorbent in the bed does not affect its reactivity (although the degree of sulfation does affect reactivity).

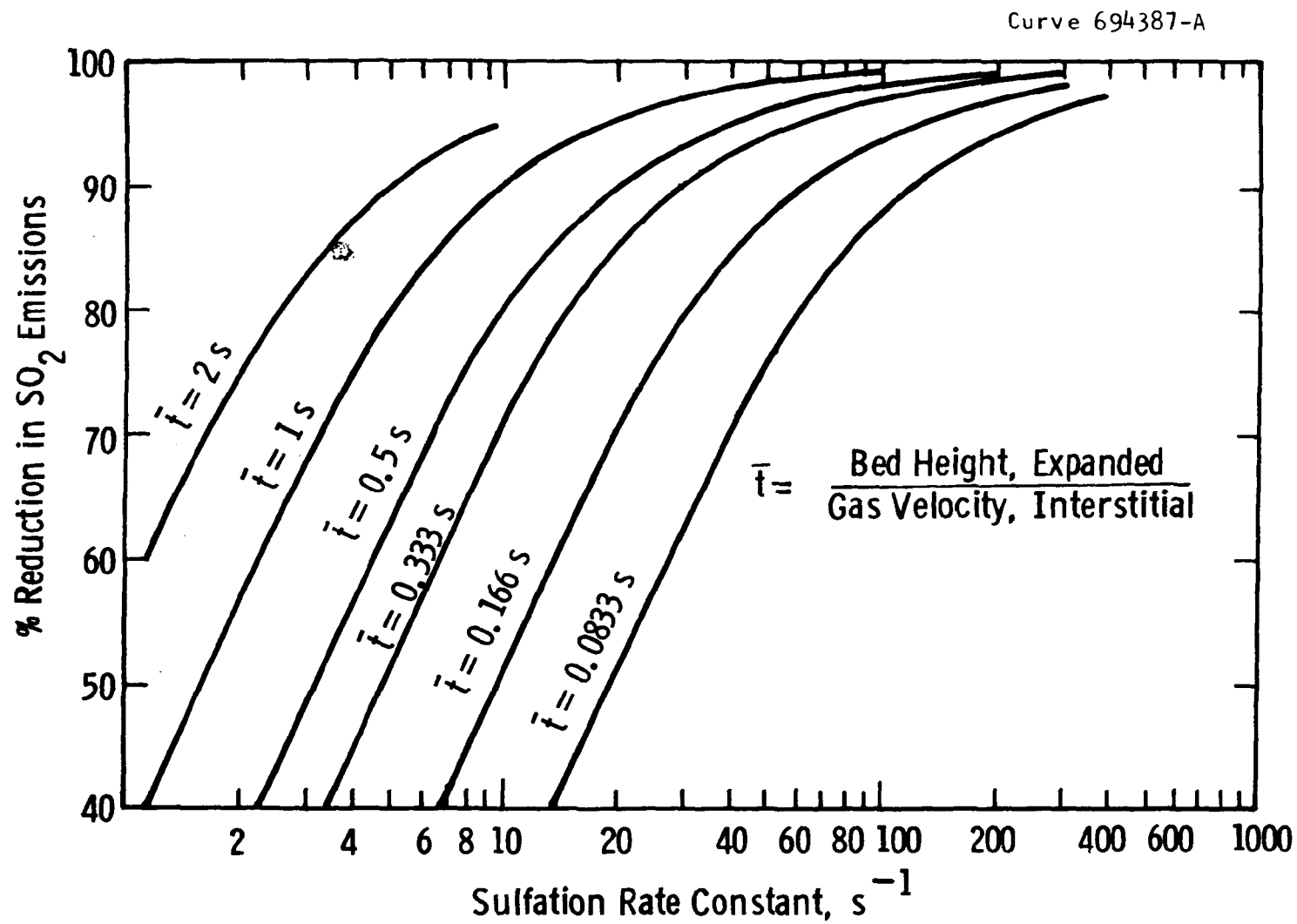


Figure A1 - Required Reaction Rate as a Function of Sulfur Removal Efficiency and Gas Residence Time (\bar{t})

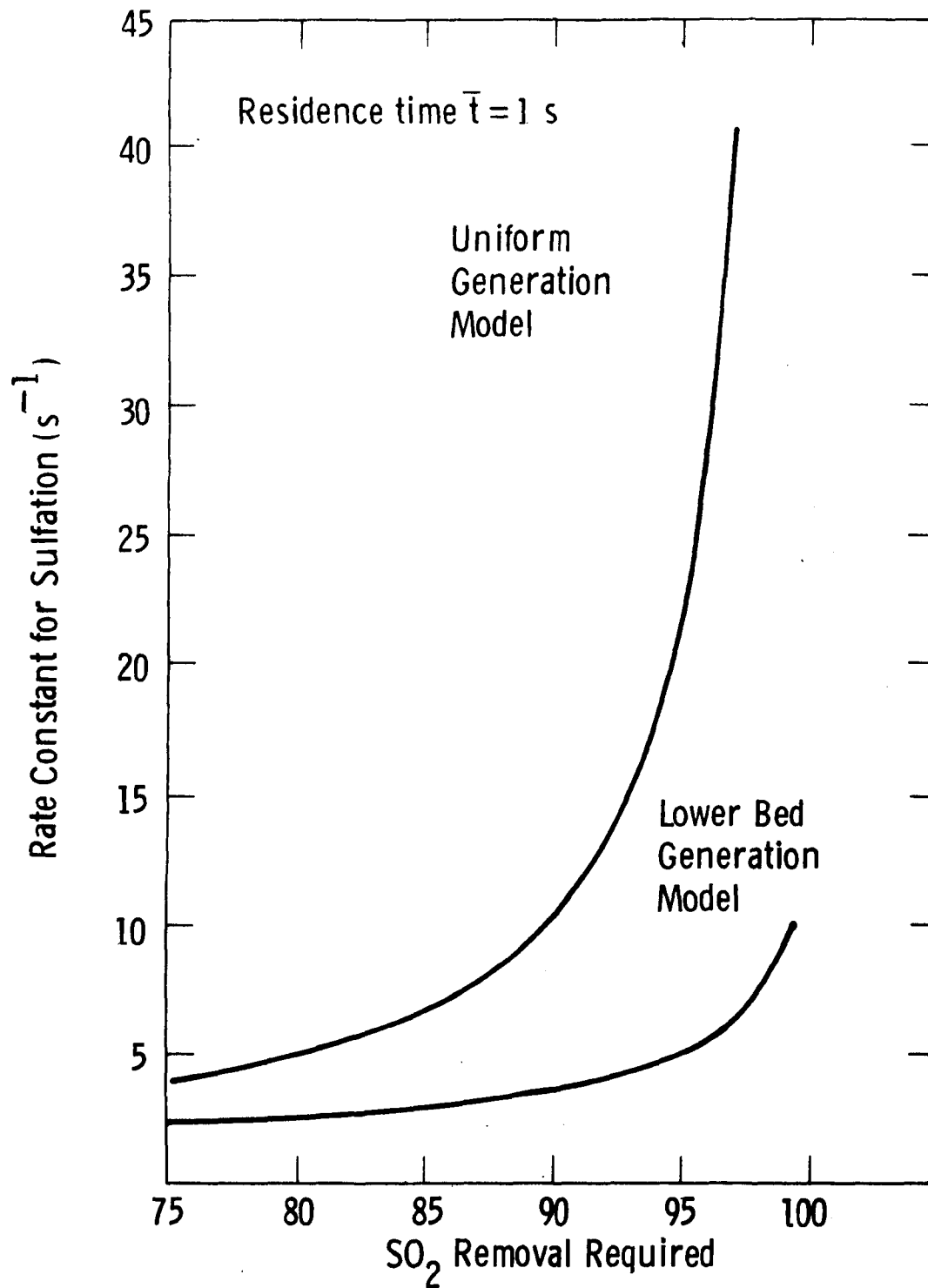


Figure A2 - The Impact of Sulfur Generation Pattern and Desulfurization Requirement on Required Reaction Rate

3. The fluidized-bed atmosphere surrounding the limestone particles is oxidizing with respect to the CaS/CaSO_4 transition.

The implication of the first assumption is that while mass transfer (e.g., of SO_2 from the gas phase to the sorbent particle) in the fluidized bed may be much greater than in the TG apparatus, mass transfer dominates the actual reaction rate over a small extent of reaction. Once the calcium utilization has reached about 10 percent, the rate is usually dominated instead by inter- and intragranular diffusion of the solid. (In some pressurized cases comparatively low mass transfer depresses the observed TG rate over a significant portion of the rate curve). The same internal pore structure must be provided in the sorbent during the TG test as would prevail during a fluidized-bed combustor operation. Thus, the calcination conditions under which the sorbent pore structure is generated must be carefully controlled before the TG sulfation experiment if the TG data are to provide a valid simulation of the effect of sorbent utilization on reaction rate.

Concerning the second assumption above, the mean residence time of the sorbent may be much longer in a fluidized bed (up to 24 hours) than in a TG experiment (~ 2 hours), unless the latter is carried out under conditions of low- SO_2 concentration (0.05%). The sorbent pore structure may be modified by this long exposure to temperature, and, unfortunately, this may either enhance or retard the sulfation rate, depending on the particular sorbent. This effect is not accounted for in the TG-based kinetic model.

It is often postulated that the existence of local reducing areas in the bed may cause sulfur capture as CaS , which is subsequently oxidized to sulfate. The assumption that this mechanism is unimportant in determining the overall rate of reaction is justified by the fact that oxidation of calcium sulfide (CaS) in limestone is limited in the same way that utilization of CaO is limited in sulfation. Oxidized sulfided limestone contains an inner layer of sulfided stone which has not been oxidized.

Since CaS is not found in the product stone from FBC, it is clear that there is no significant additional reaction rate component from sulfidation of the sorbent.

The TG data, which yield rate as a function of sulfur loading, or sorbent utilization, vary greatly according to the sorbent properties and combustor operating conditions. The variables that affect the reaction rate and can be studied on the TGA are

1. Type of sorbent
2. Form of sorbent (e.g., limestone, lime, hydrated lime)
3. Particle size of sorbent
4. Calcination conditions (in particular the temperature and partial pressure of CO_2 during calcination)
5. Residence time (time at temperature)
6. System pressure
7. System temperature
8. Percent excess air in the system
9. SO_2 partial pressure and other gas composition variables.

In making a projection of the effect of operating conditions on the Ca/S molar feed ratio, it is advisable to use TG data obtained under experimental conditions that correspond closely to those that will be encountered in the fluidized bed.

For any set of design input:

Bed height

Gas velocity

Bed voidage

Bed emulsion and bubble phase volume

Coal:

Ash content (heating value)

Sulfur content

the rate data can be used in the model to give Ca/S molar feed ratio projections. A data base of over 300 atmospheric-pressure and 70 pressurized TG runs exists at Westinghouse over the range of conditions listed in Tables A1 and A2.

Table A1
RANGE OF ATMOSPHERIC TG SULFATIONS

Stone(s)	Size, U.S. Mesh	% Excess Air	Temp., °C	Comment
Ames, Brownwood, 1359, Greer, Carbon 1337, Western, Mississippi Bellefonte	16/18 5-100/200	20	815	Varied calcination
Greer	16/18	20	780-950	Varied calcination
Ames	35/40	20	750-940	
Ames, Brownwood Greer, Carbon, 1359	35/40	20	900	Calcined at 900°C in 60% CO ₂
Ames, 1359, Greer, Carbon	5/6-35/40	20	850	Scattered particle sizes
1359 (2263)*	16/18	20	815	
Carbon	-325	20	800-950	
Tymochtee	16/18	2-16% O ₂	815	
Canaan, Kaiser	100/200	20	815	Calcined at 900°C in 60% CO ₂

*Residence time varied (0.1-0.5% SO₂ in sulfating atmosphere).

Table A2

RANGE OF PRESSURIZED TG SULFATIONS 1013 kPa (10 atm)

Stone	Size, U.S. Mesh	% Excess Air	Temp., °C	Comment
Canaan	35/40	300	843	
1337	35/40	300	843-1010	
1337	8/10	20	900	Half calcined
Greer	35/40	300	843-1010	
Greer	6/8	300	900-1010	
Greer	40/100	300	900-1010	
Greer	100/200	300	950-1000	
Greer	16/18	15-100	815	Carbonated
Greer*	14/18	20	815	FB Calcine 815, 15% CO ₂
Tymochtee	16/18	Calc. 815 (0.15 atm CO ₂) 0.75- 16% O ₂)	815	
1359 (2263)*	16/18	20	815	

*Residence time varied (0.05-0.5% SO₂ in sulfating atm).

PROJECTION METHOD

Sorbent feed projections are obtained using TG rate data. The rate data are fitted with polynomial equations for use in the computer-generated projections.

The average rate constant for SO₂ sorption in the bed, K, that is needed to maintain a given level of sulfur retention, R, is calculated at a defined gas residence time ($Z = \frac{\text{expanded bed height}}{\text{interstitial gas velocity}}$) using the equation

$$R = 1 - \frac{1}{KZ} (1 - e^{-KZ})$$

Note that K is related to the first-order rate constant for the reaction $\text{CaO} + \text{SO}_2 + 1/2 \text{O}_2 \rightarrow \text{CaSO}_4$, K^1 , by

$$K = K^1 \frac{(1 - \delta)\epsilon(1 - F)}{\delta + (1 - \delta)\epsilon}$$

where

$$K^1 = f(\alpha)$$

δ = volume fraction of bed bubbles

ϵ = bed voidage in emulsion phase

F = fraction of emulsion volume occupied by inerts.

The sorbent utilization, α , at which the reaction rate constant, K^1 , applies is determined from TG data. A mass balance on the TG system gives the molar rate of reaction, $\frac{d\alpha}{dt}$, in terms of the reaction rate constant as

$$\frac{d\alpha}{dt} = \frac{K^1 C \epsilon_{\text{TG}}}{\rho(1 - \epsilon_{\text{TG}})}$$

where

ρ = solids density, mole Ca/cc

C = mole SO_2 /cc in TG reaction gas.

The polynomial equations representing TG rate data $\alpha = f\left(\frac{d\alpha}{dt}\right)$ are then used to calculate the sorbent utilization. The required Ca/S molar feed ratio is then defined by

$$\text{Ca/S} = \frac{R}{\alpha}.$$

CONFIRMATION OF THE MODEL

The model has been used previously to show that TG data accurately demonstrate important features of desulfurization phenomena in fluidized beds. Desulfurization phenomena that have been observed in fluidized beds and demonstrated on the TG include:^{A4}

- The occurrence of an optimum temperature for desulfurization in AFBC with sorbent particle sizes of greater than 500 μm
- No marked temperature effect at higher pressures (~ 1000 kPa)

- Improved sorbent utilization at higher pressures (~ 1000 kPa)
- Improved sorbent utilization with precalcination.

The specific data that the TG has been used to model include data from the NCB, ANL, B&W, Pope, Evans and Robbins (PER), and Westinghouse.

Model projections of the Ca/S molar feed ratios required for various levels of desulfurization in AFBC, as a function of limestone type, are compared to the data collected from the ANL and British Coal Research (BCR) fluidized-bed units for limestone 1359^{A7} in Figure A3. Conditions for the fluidized-bed runs were:

101.3 kPa (1 atm), Limestone 1359
 490-630 μ m particles in the feed
 0.79-0.85 m/s (2.6-2.8 ft/sec) velocity
 788-798°C
 0.61 m (2 ft) bed height
 3% O₂, 15% CO₂ in the flue gas

To obtain the projections, TG rate data from sulfation at 815°C in 0.5% SO₂, 4% oxygen, and nitrogen were utilized. The sulfations were carried out with 420-to-500- μ m particles of limestone, calcined at 815°C in 15% CO₂ and nitrogen. The gas residence time (as determined by input bed height and velocity) was 0.66 s. ANL operated with a gas residence time of 0.74 s. This longer residence time may account for the slightly lower Ca/S molar ratio requirements in the ANL 1359 data.

An example of the TG projection of pressurized results obtained in the Exxon miniplant is shown in Figure A4. Projections of the desulfurization obtainable at varied Ca/S molar feed rates using Dolomite 1337 are compared to results obtained in Run 27^{A7} of the miniplant. More recent results from Runs 68-73^{A9} designed to investigate higher levels of sulfur removal could also be projected with accuracy (Figure A5).

AMENDMENTS TO THE MODEL

Future amendments to be made on the model include a) integration of sorbent particle size distribution, b) including the impact of attrition

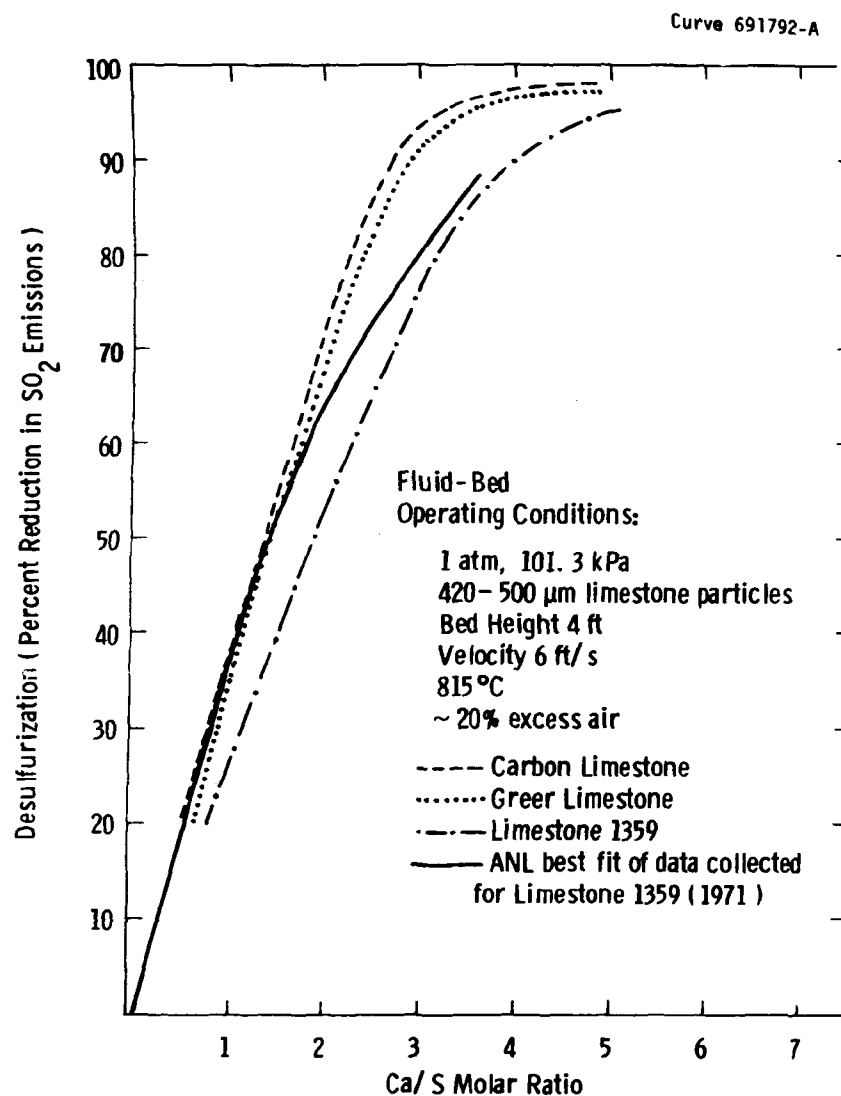


Figure A3 - Predictions of the Ca/S Feed Ratios Required for Desulfurization Using Westinghouse TG Data for Three Sorbents

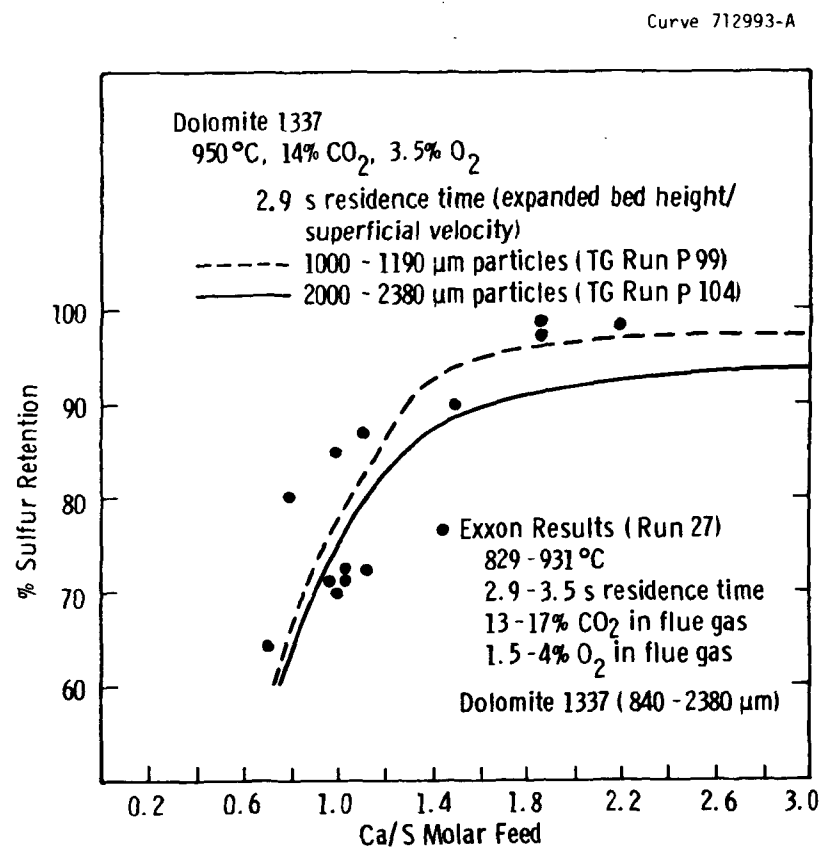


Figure A4 - Comparison of Pressurized TG Projections with Data from the Exxon Miniplant

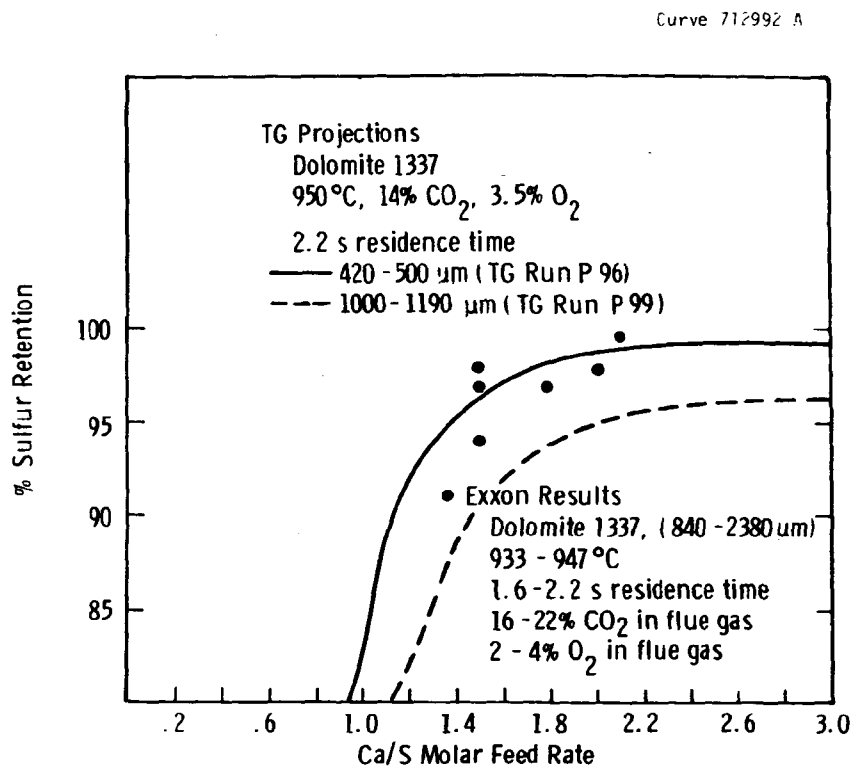


Figure A5 - Comparison of TG Projections for Greater than 90% Sulfur Removal with Exxon Data for Dolomite 1337

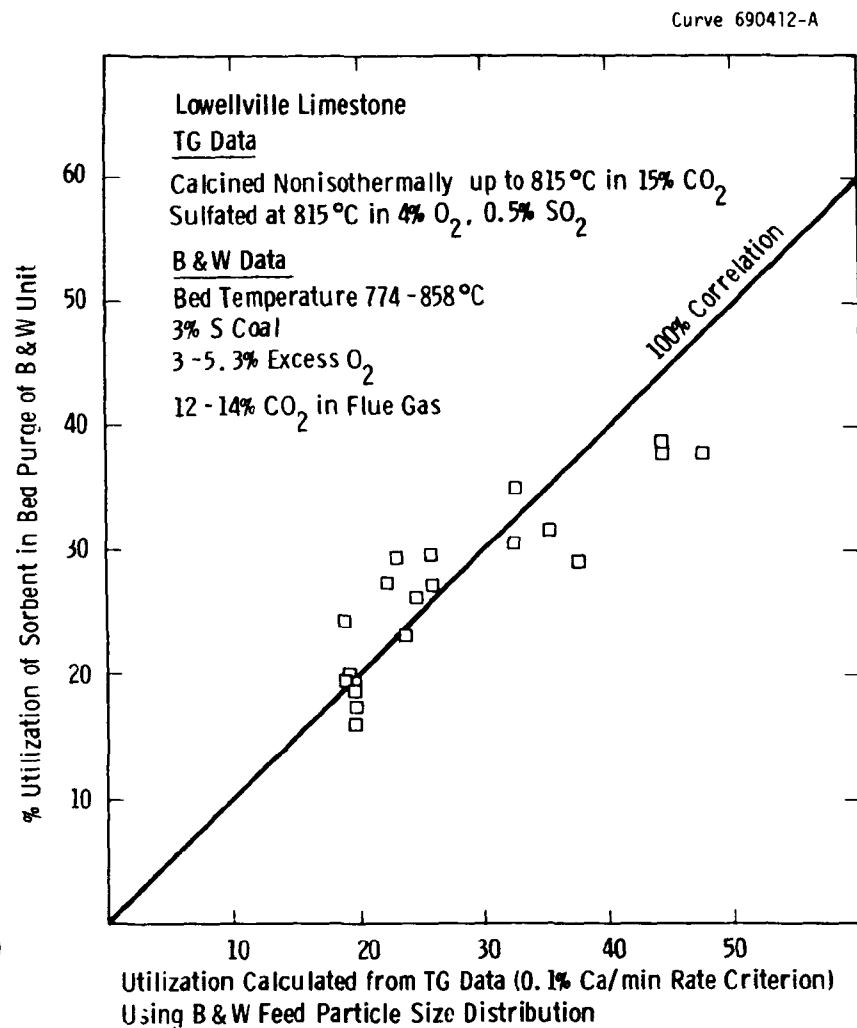


Figure A6 - Comparison of Sorbent Capacity Obtained from Westinghouse TG Data with B&W Fluid-Bed Results^{A10}

and elutriation on particle size distribution, and c) discerning the effect of different mass transfer rates on the TG and in fluidized beds.

Instead of using a TG curve based on one particle size representing the estimated average particle size in the bed, it would be preferable to use a composite TG curve representing the sorbent particle size distribution within the bed. Westinghouse has already calculated such a composite curve for one particular case - the atmospheric-pressure experiments of B&W,^{A10} with excellent results.

The Westinghouse TG data for different sizes of Carbon limestone were combined to derive a projected composite utilization for the size consistency in the bed of the Babcock and Wilcox 3 ft by 3 ft (0.9 m by 0.9 m) AFBC unit. The average operating parameters of 20 B&W runs (8 ft [2.4 m] bed, 1.5 ft [0.5 m]/s, 50% sulfur removal) using Carbon limestone were used to estimate a molar reaction rate on the TGA (0.1% Ca/min) that corresponds to the average bed rate constant. A weighted average, based on the B&W sorbent feed size distributions, of the sorbent utilization obtained on the TGA at 0.1 percent calcium reacting per minute was calculated for TG runs on finely divided size fractions of Carbon limestone at temperatures and gas compositions similar to those in the B&W combustor. The results of this comparison are shown in Figure A6. Westinghouse feels that the agreement is excellent. This technique to account for particle size distributions is time consuming, however, for many TG experiments are required to cover the full range of particle sizes. A fundamental model that would permit the construction of the TG curves for different particle size ranges from a base curve would be of inestimable value.

As another amendment, a more fundamental correction to the model would result from generation of a mean rate value for the bed given the residence time distribution of the sorbent in the bed. This mean rate would consider particle attrition within the bed and elutriation from the bed.

The third required amendment would adjust the initial rates of reaction to account for mass transfer effects in the fluidized bed. To

some extent this effect can be calculated from batch fluidized-bed results. Mass transfer should only be significant in cases for sorbent utilization of 10 percent or less, corresponding to Ca/S molar feed ratios of 10/1 or higher. Such high sorbent feed rates lie outside the range of practical interest, except for generative systems.

CONCLUSION

Thermogravimetric rate data can be successfully used to determine the rate constant of sulfation as a function of sorbent utilization for calcium-based sorbents. By judiciously selecting operating conditions that represent conditions in fluidized-bed combustion, the rate constant can be used to predict sulfur retention in fluidized-bed units. The agreement between fluidized-bed data and TG projections has been demonstrated using data collected at 1013 kPa (10 atm) pressure, as well as at atmospheric pressure.

The TG projections are limited by the availability of complete pilot plant data (particle size distribution in the bed, fraction of inert particles in the bed, bed expansion data), the accuracy of pilot plant data (including fluctuations in coal and sorbent properties and nonsteady-state operation), the representability of the 20 mg sample used in the TGA of the bulk limestone, as well as the basic assumptions applied in the projections. The modeling assumptions and the limitations implied by each are outlined in Table A3.

Table A3

LIMITATIONS OF TG PROJECTIONS

<u>Model Assumption</u>	<u>Limitation</u>	<u>Comment</u>
Diffusion Control	Mass transfer may influence initial reaction rate	
First-Order Reaction	No account for sorbent sintering	
Uniform Sulfur Generation	No variation in sulfur generation pattern is accounted for	
Generation and Sorption of Sulfur All Occur in Main Bed by Limestone	<ul style="list-style-type: none"> • Ash can absorb sulfur • Sulfur can be generated and absorbed outside of bed 	Has been included ^{A11} in the model

REFERENCES

- A1 Attig, R. C., et al., Additive Injection for Sulfur Dioxide Control, A Pilot Plant Study, APTP-1176, The Babcock and Wilcox Company, Alliance, OH, 1970, NTIS PB 226 761.
- A2 Liu, C Y., Personal Communication.
- A3 Jonke, A. A., et al., Reduction of Atmospheric Pollution by the Application of Fluidized-Bed Combustion, ANL ES-CEN-1002, Argonne National Laboratory, Argonne, IL, 1970.
- A4 Keairns, D. L., et al., Fluidized-Bed Combustion Process Evaluation - Phase II - Pressurized Fluidized-Bed Coal Combustion Development. Report to EPA, EPA-650/2-75-027c, Westinghouse Research Laboratories, Pittsburgh, PA, 1975, NTIS PB 246 116.
- A5 Bethell, F. U., D. W. Gill, and B. B. Morgan, Mathematical Modeling of the Limestone-Sulfur Dioxide Reaction in a Fluidized Bed Combustor, Fuel 52; 1973.
- A6 Hartmen, M., and R. W. Coughlin, Reaction of Sulfur Dioxide with Limestone and the Grain Model, AIChE J., 22(5); 1976.
- A7 Jonke, A. A., et al., Reduction of Atmospheric Pollution by the Application of Fluidized-Bed Combustion, ANL ES-CEN-1004, Argonne National Laboratory, Argonne, IL, 1971.
- A8 Hoke, R. C., et al, Studies of the Pressurized Fluidized-Bed Coal Combustion Process, Exxon Research and Engineering Co., Linden, NJ, September 1977, EPA-600/7-77-107.
- A9 Hoke, R. C., et al, A Regenerative Limestone Process for Fluidized Bed Coal Combustion and Desulfurization, Monthly Report Nos. 97-99 to EPA, Exxon Research and Engineering Co., Linden, NJ, March-May 1978.

- A10 Lange, H. B., and C. L. Chen., SO₂ Absorption in Fluidized Bed Combustion of Coal-Effect of Limestone Particle Size, EPRI FP-667, The Babcock & Wilcox Company, Alliance, OH, 1978.
- A11 Ulerich, N. H., R. A. Newby, and D. L. Keairns, Sorbent Requirements for a Gulf Coast Lignite-Fired Atmospheric Fluid Bed Combustion Power Plant. Final report to EPRI, Westinghouse Research and Development Center, Pittsburgh, PA, Contract RP1179-1, October 1978.

NOMENCLATURE

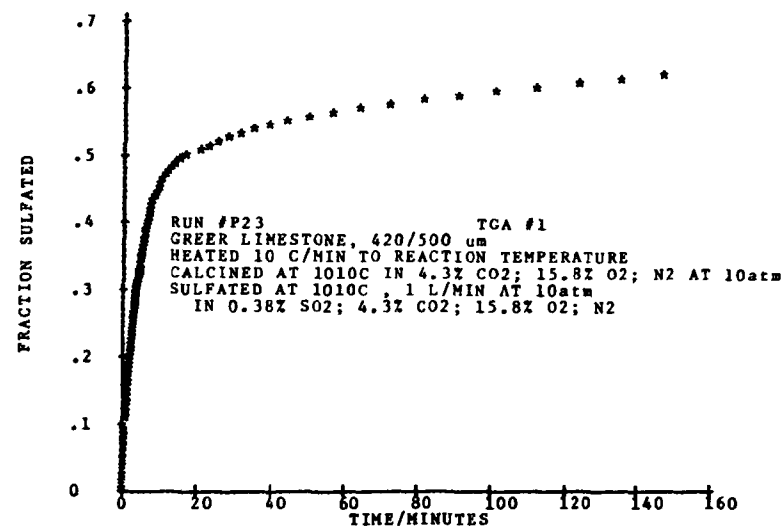
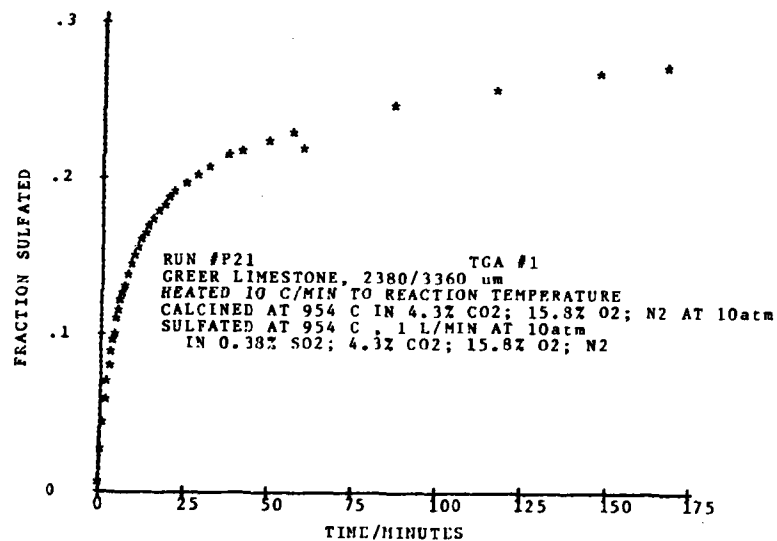
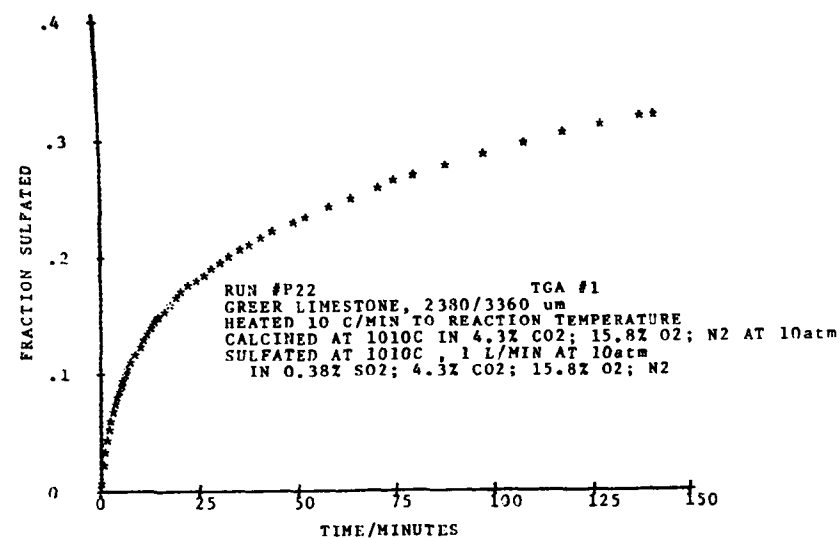
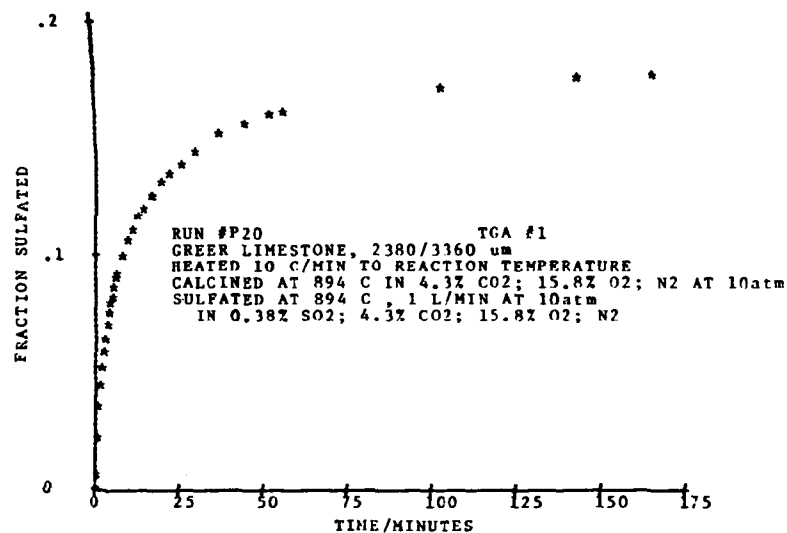
FBC	Fluid-bed combustion
AFBC	Atmospheric fluid-bed combustion
PFBC	Pressurized fluid-bed combustion
TGA	Thermogravimetric analysis
TG	Thermogravimetric
B&W	Babcock and Wilcox
ANL	Argonne National Laboratories
NCB	National Coal Board
PER	Pope, Evans and Robbins
h	bed height, expanded
R	Sulfur removal, fractional
Z	gas residence time, expanded bed height/interstitial gas velocity
K	average rate constant for SO ₂ sorption in the bed
K ¹	first-order rate constant for the reaction
	$\text{CaO} + \text{SO}_2 + 1/2 \text{O}_2 \rightarrow \text{CaSO}_4$
δ	volume fraction of bed bubbles
ε	bed voidage in emulsion phase
F	fraction of emulsion volume occupied by inerts
σ	sorbent utilization, fractional
C	mole SO ₂ /cc in TG reaction gas
ρ	solids density, mole Ca/cc
ε _{TG}	TG voidage
d	particle diameter

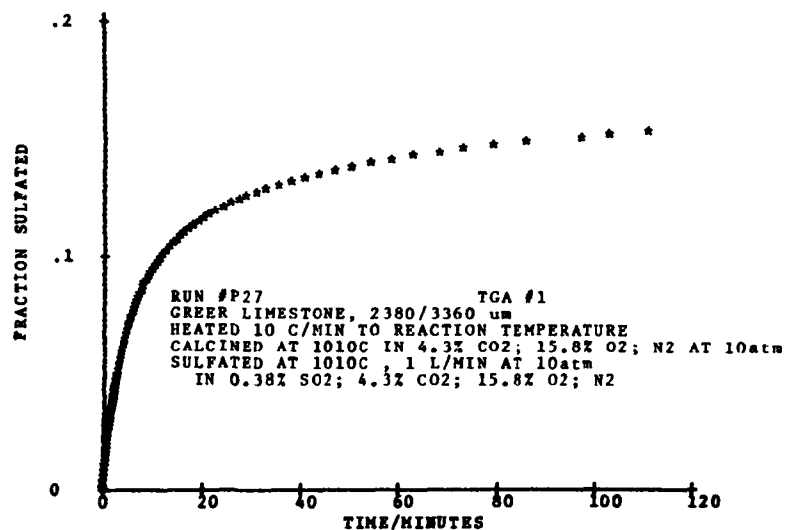
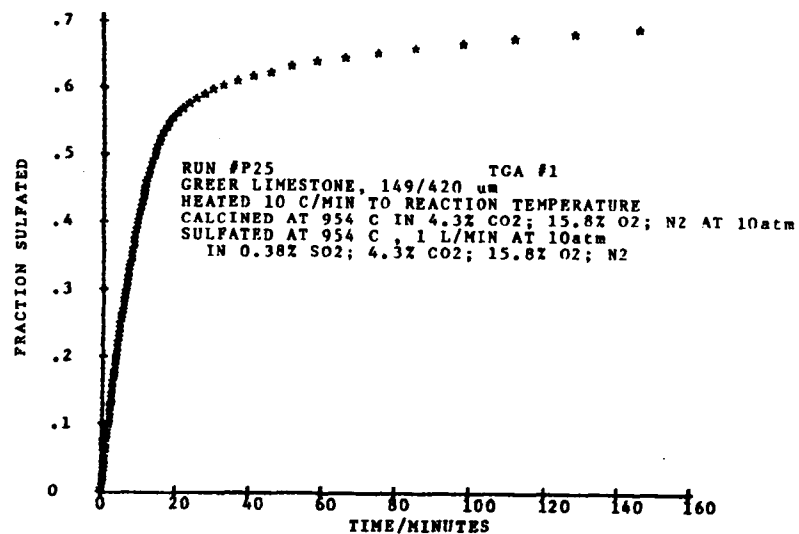
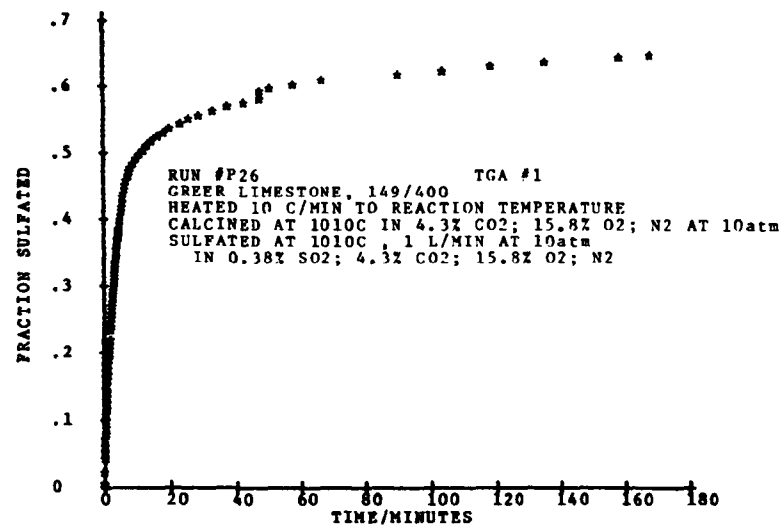
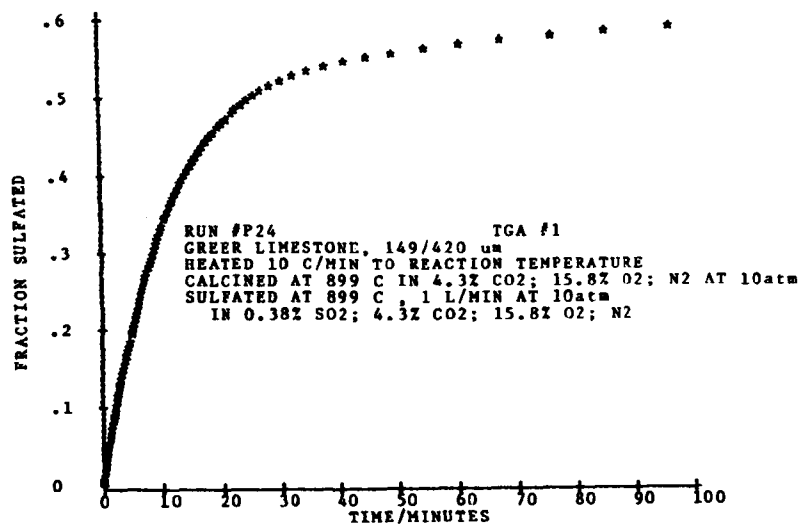
APPENDIX B

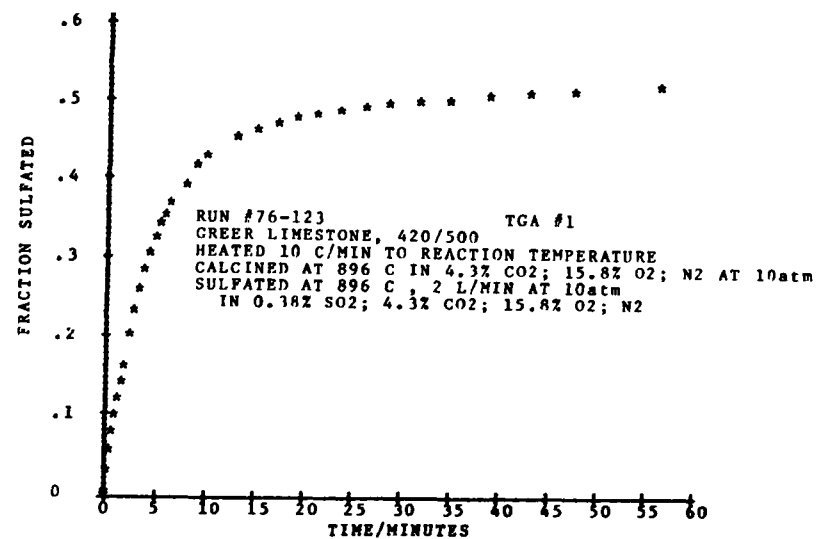
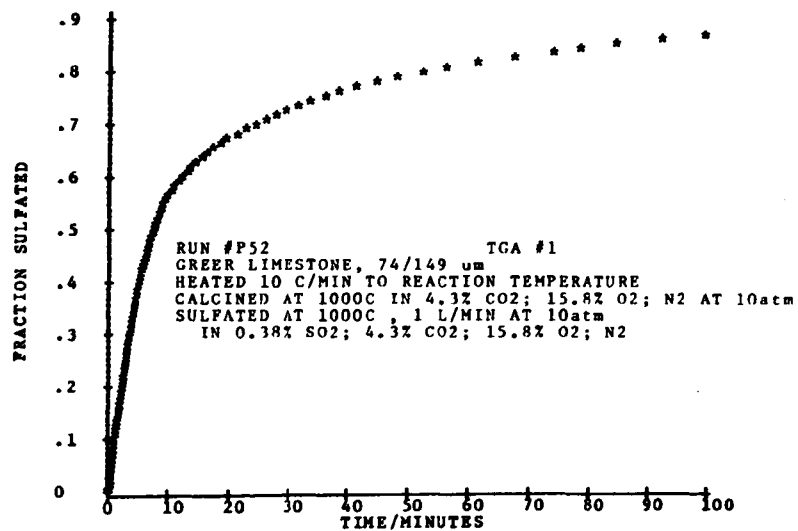
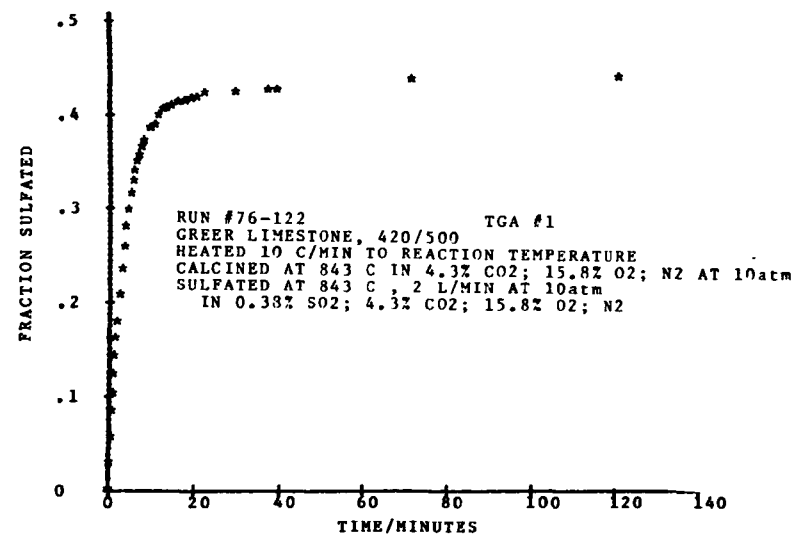
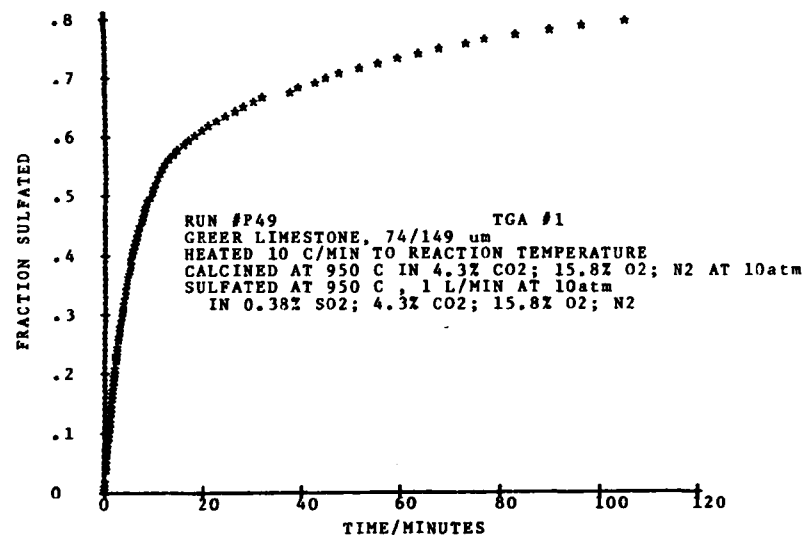
SORBENT INFORMATION AND TG RATE DATA

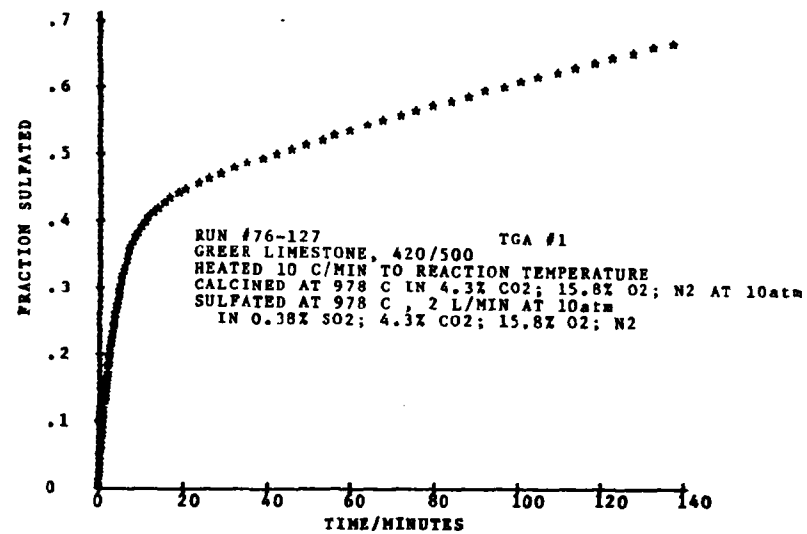
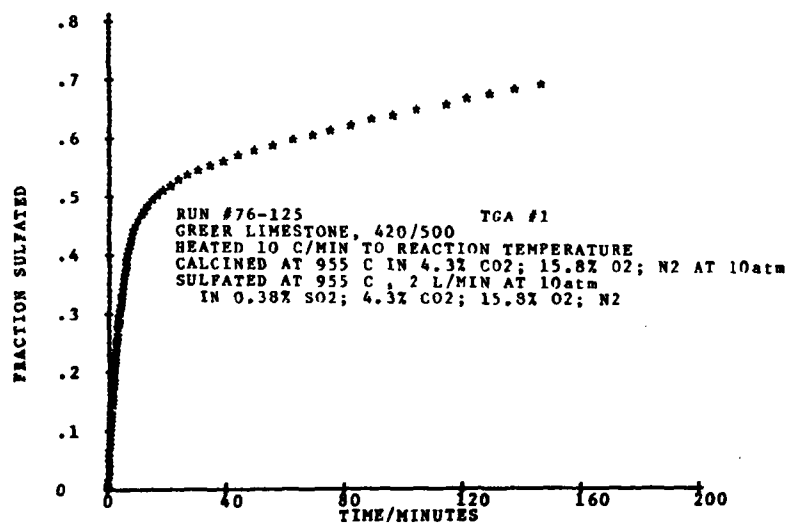
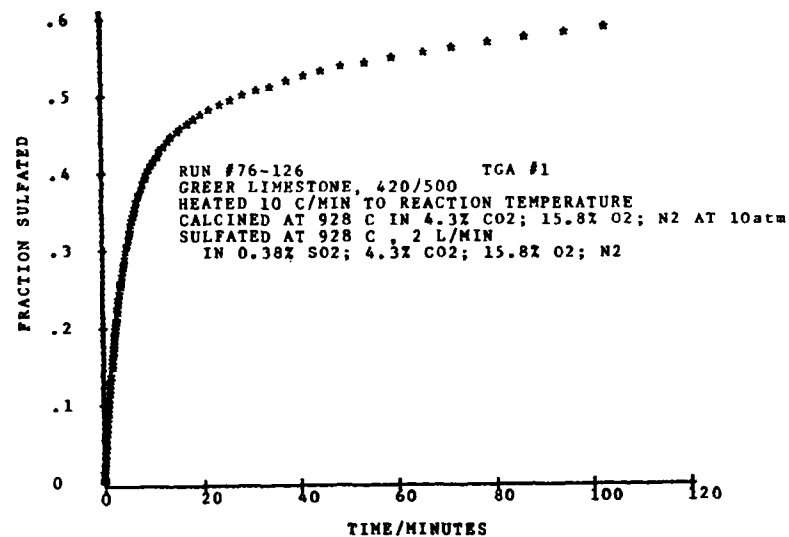
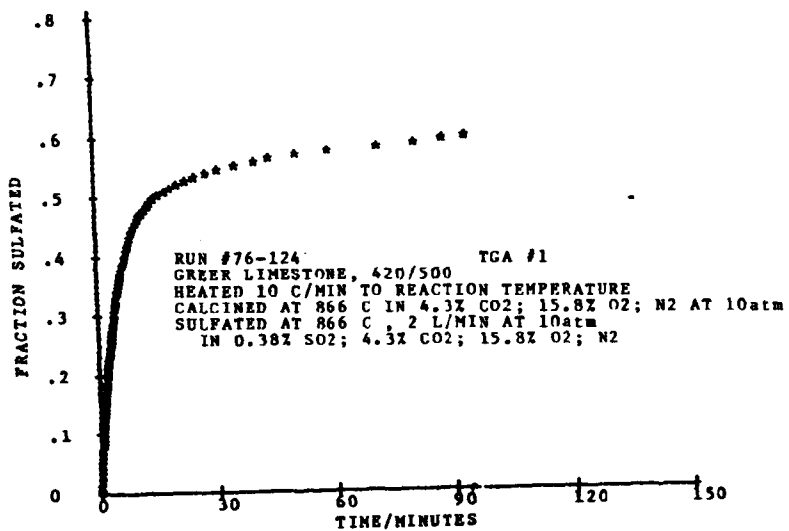
Set 1

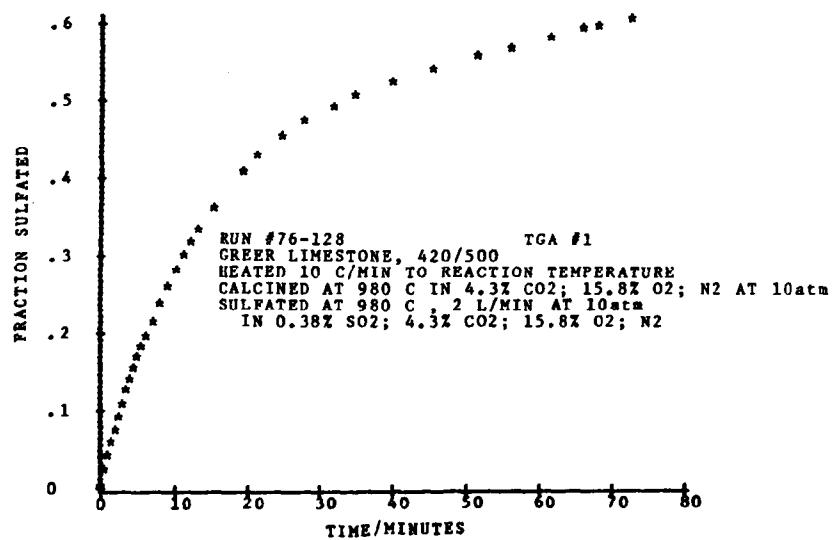
The Effect of Temperature on Pressurized
Limestone Sulfation





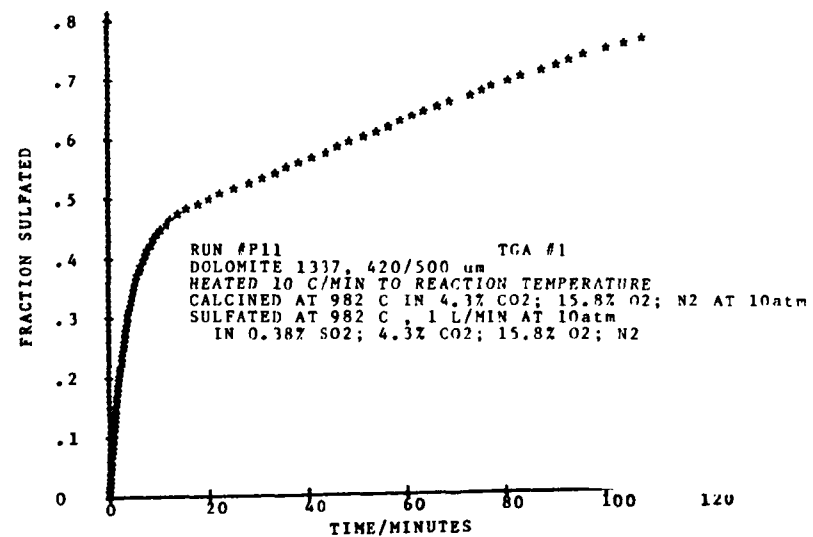
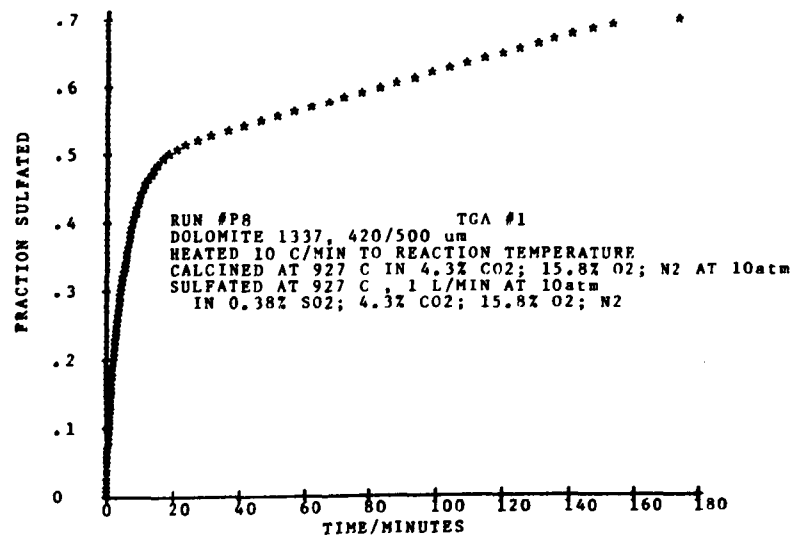
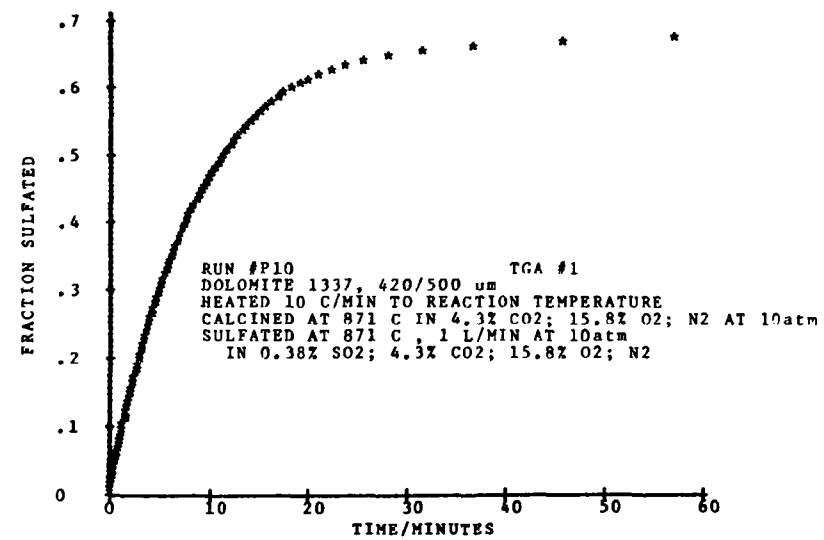
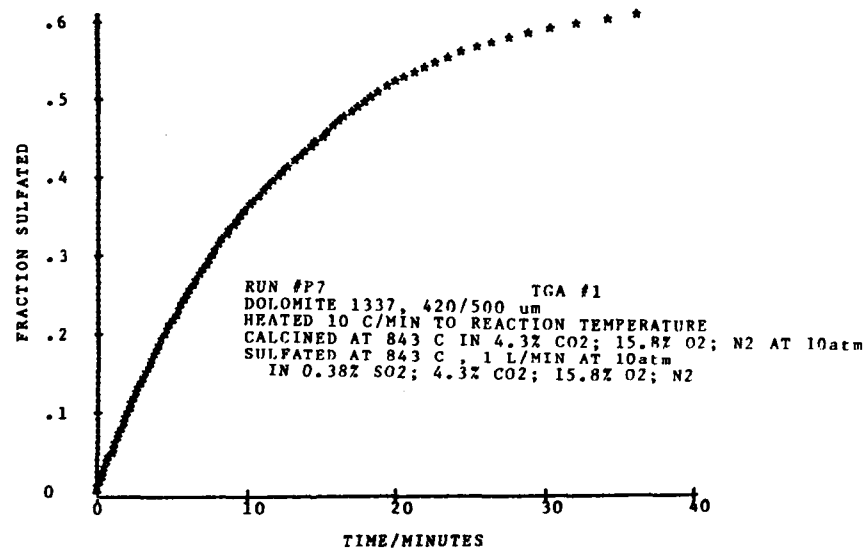


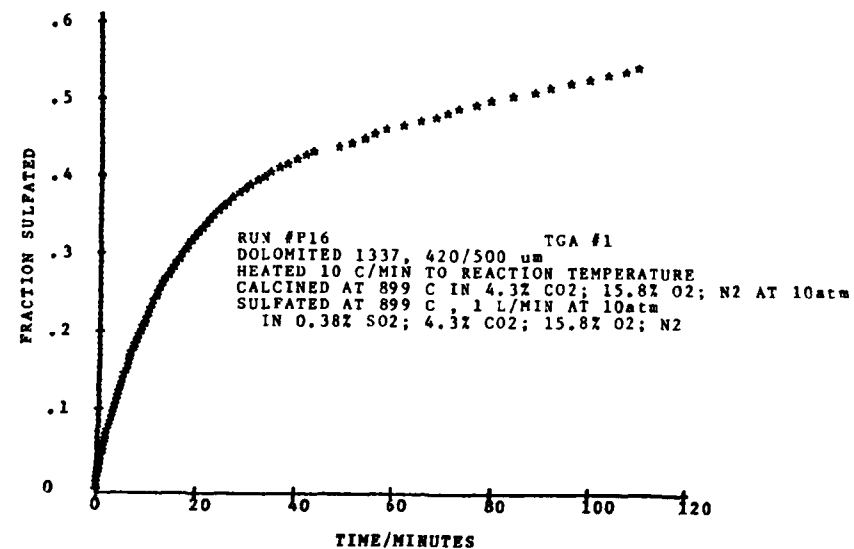
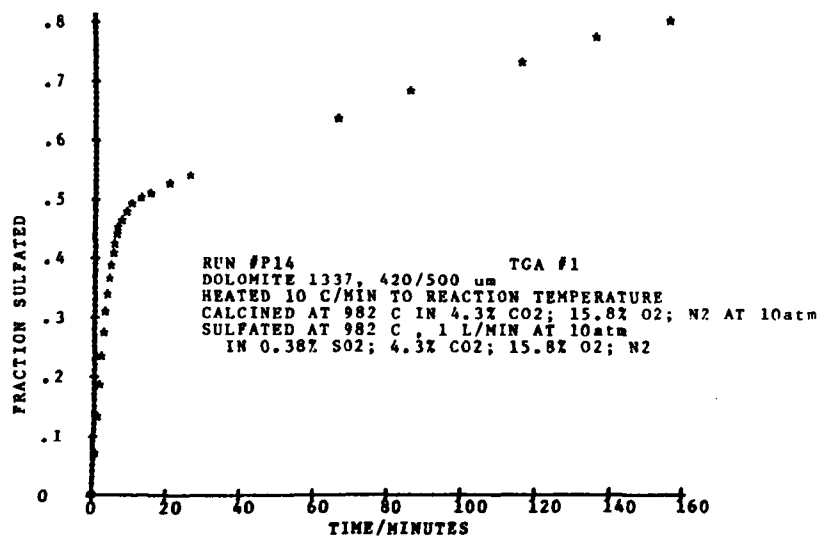
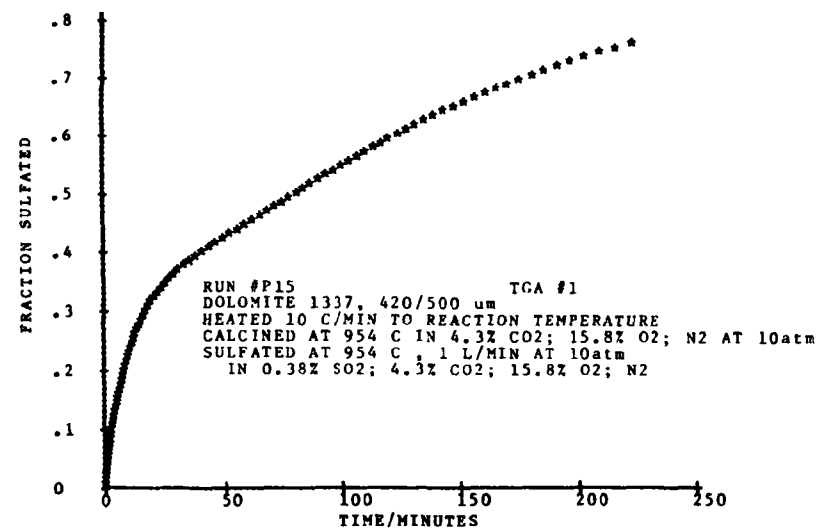
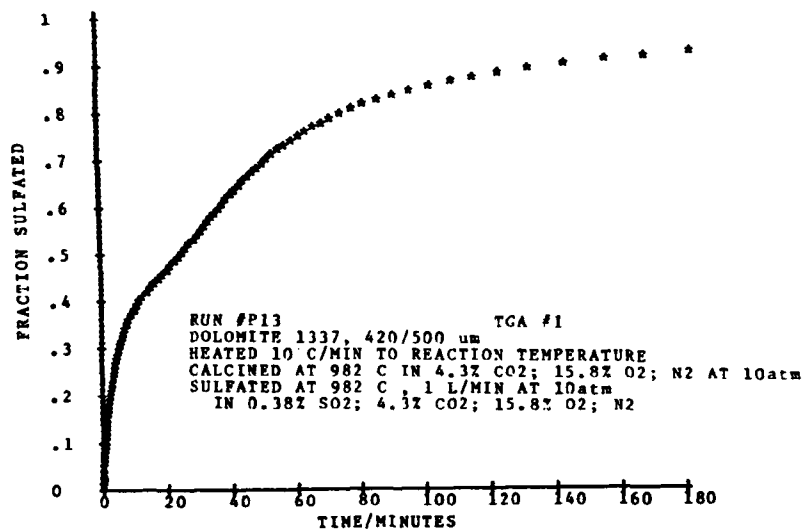


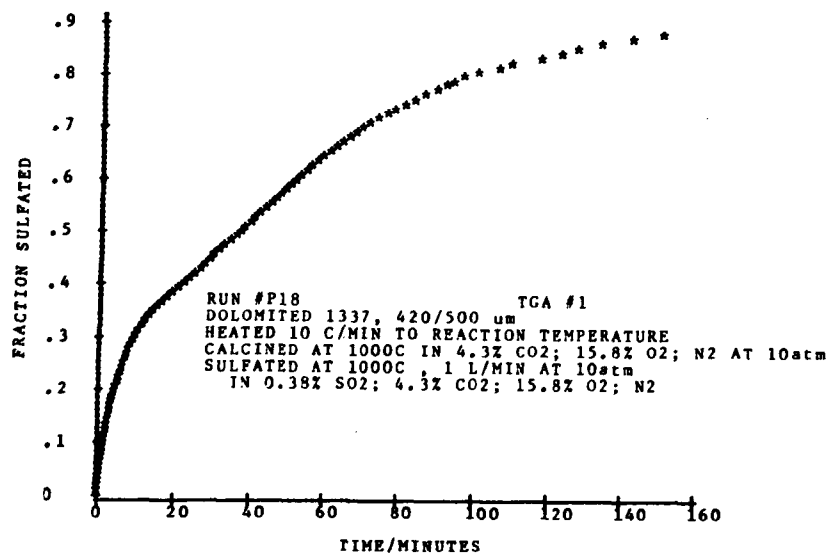
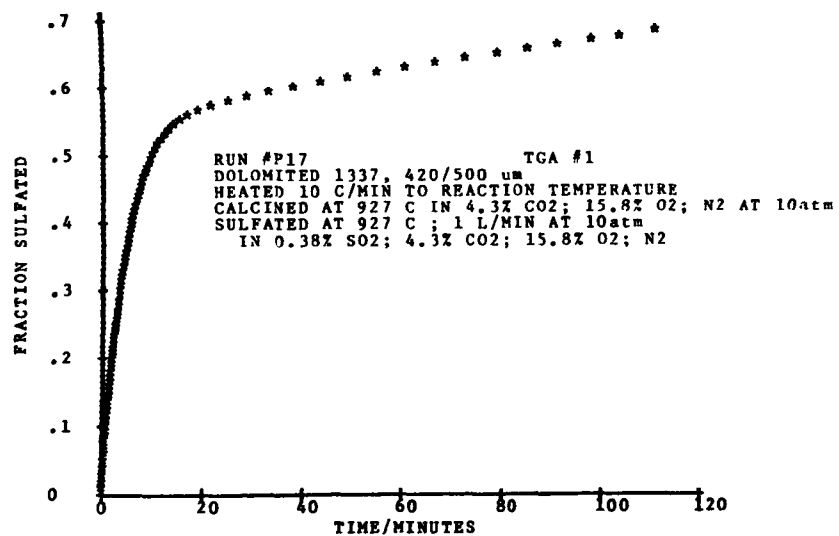


Set 2

The Effect of Temperature on Pressurized
Dolomite Sulfation

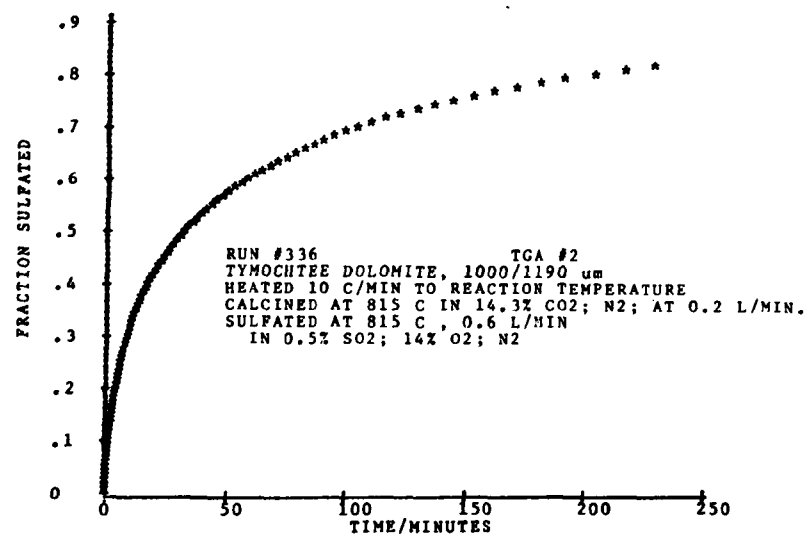
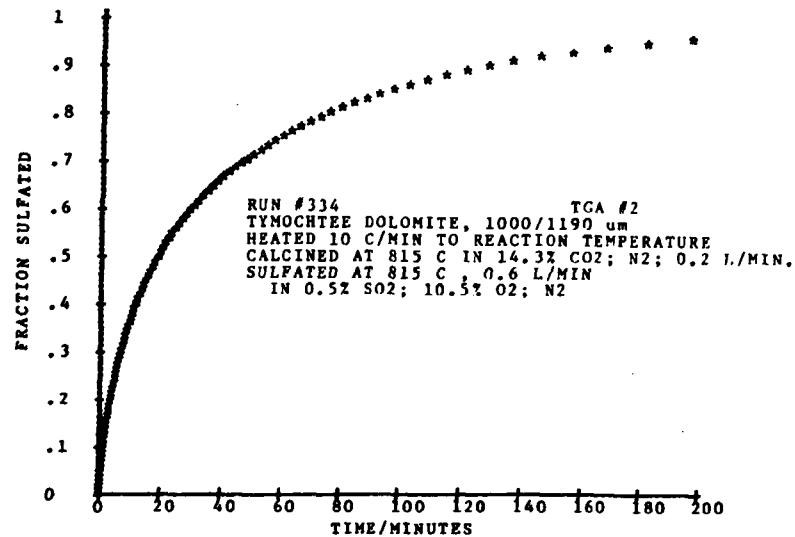
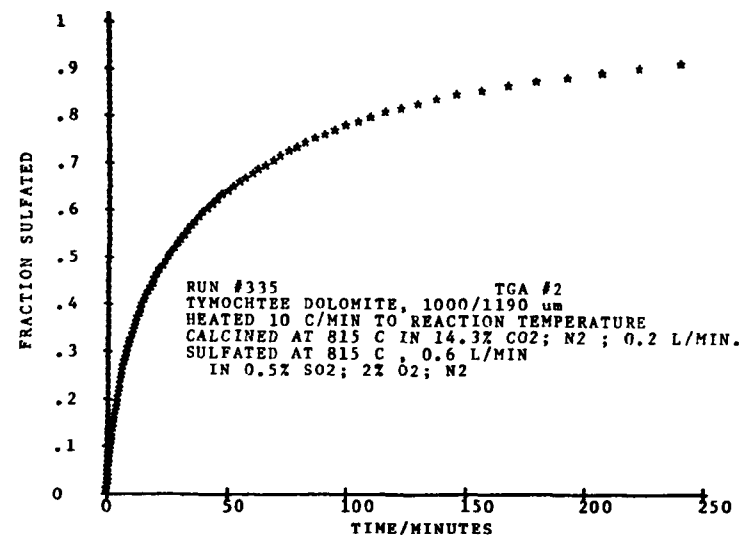
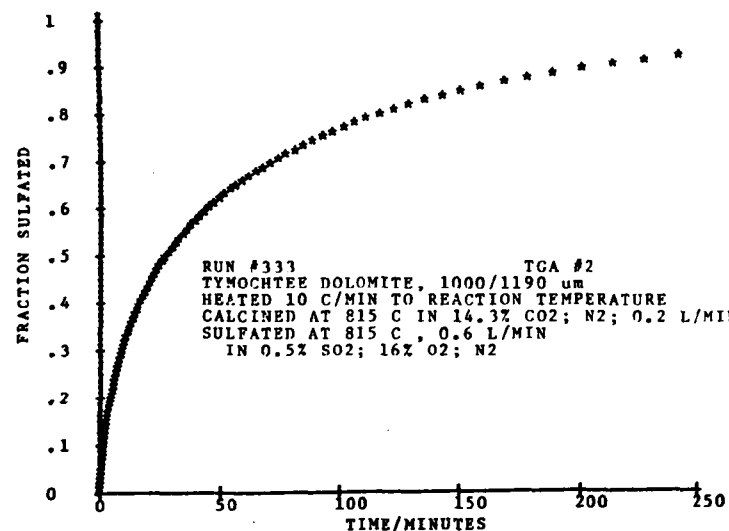


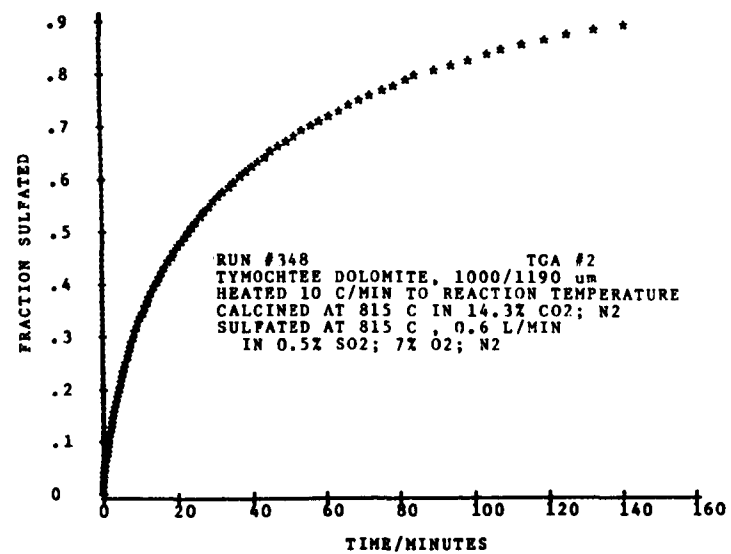




Set 3

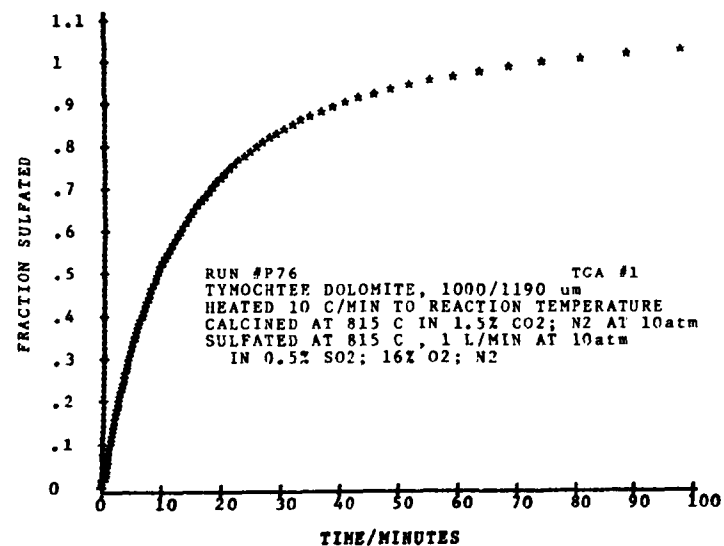
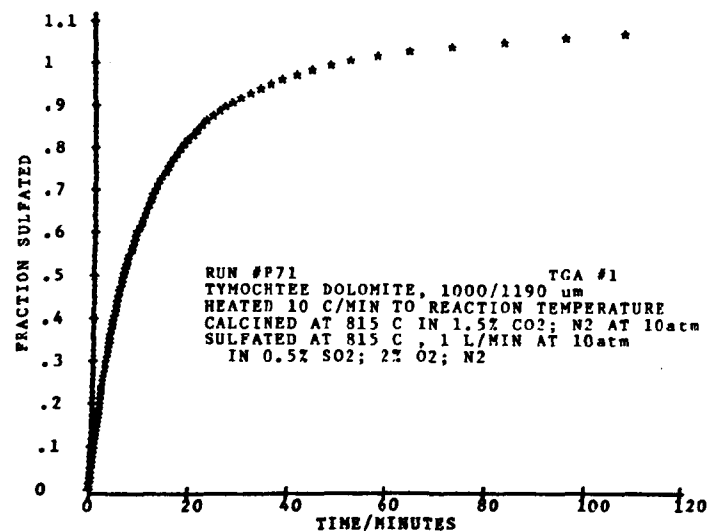
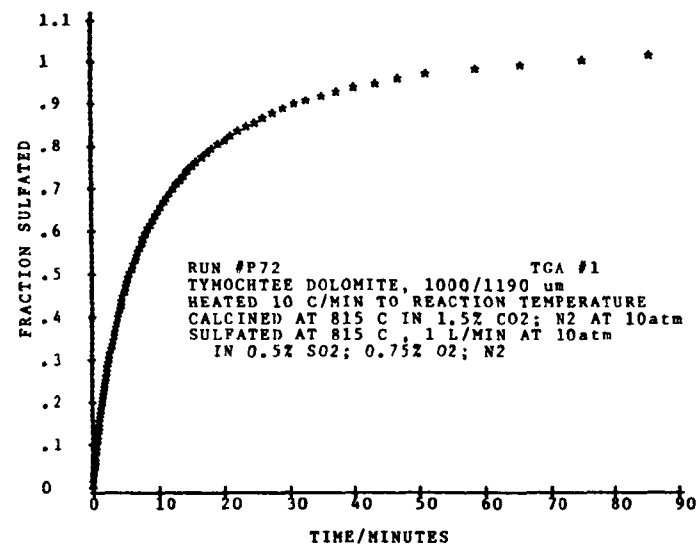
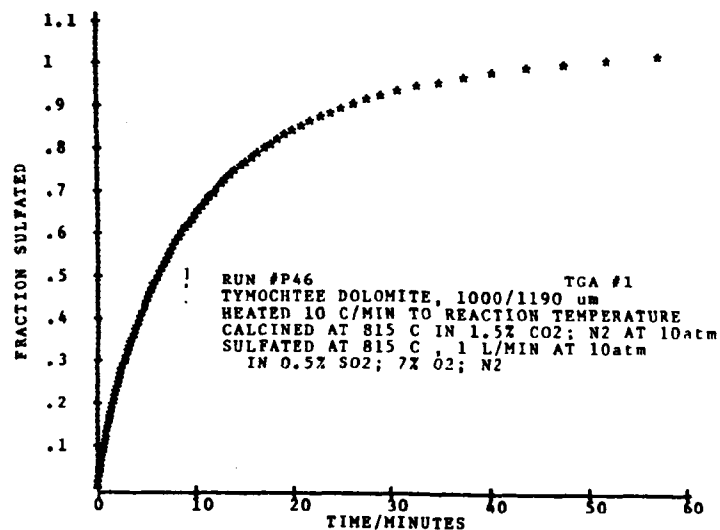
Effect of O_2 Concentration on
Atmospheric-Pressure Desulfurization of Dolomite

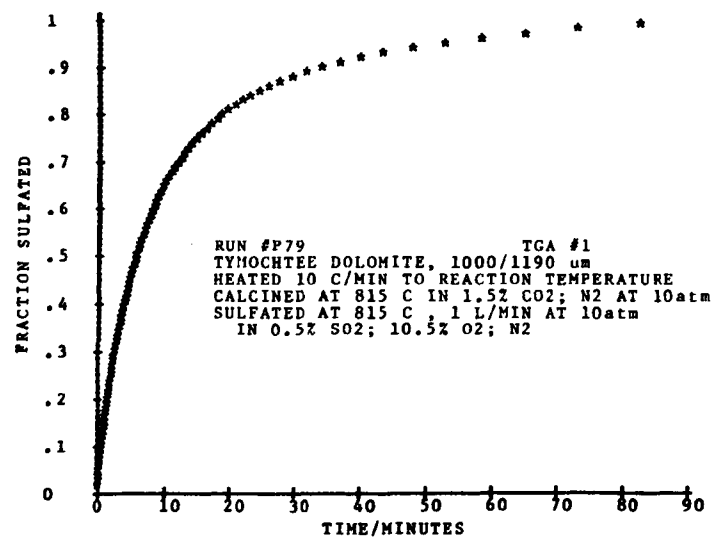




Set 4

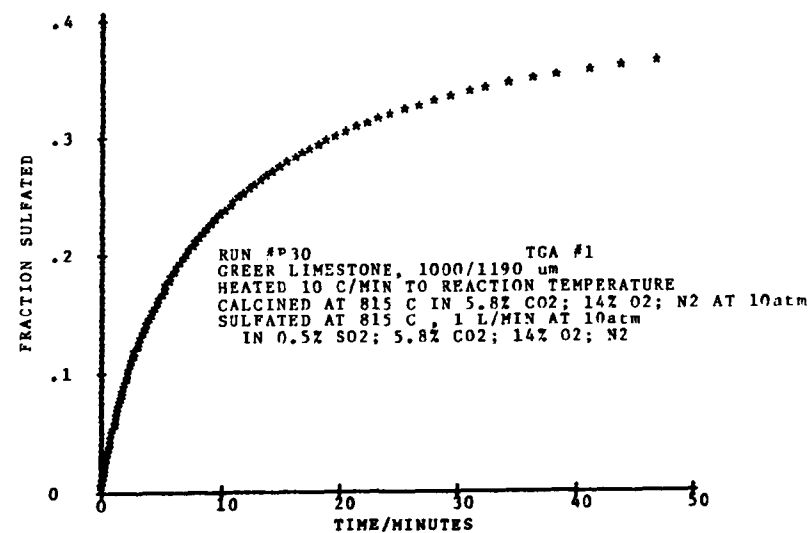
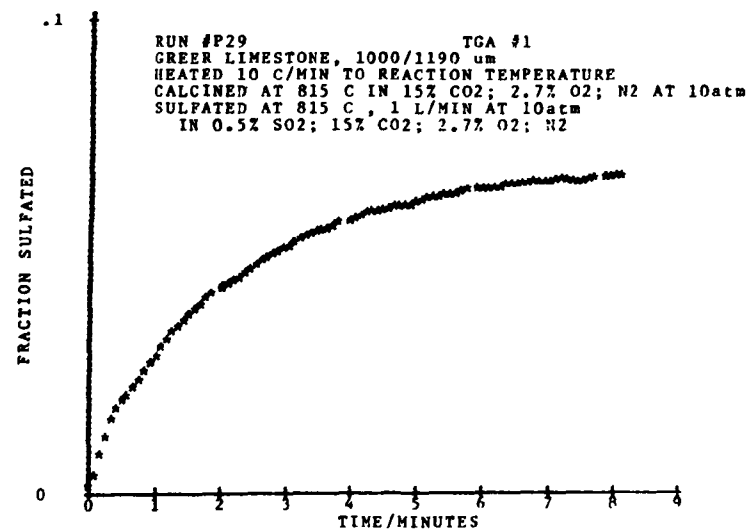
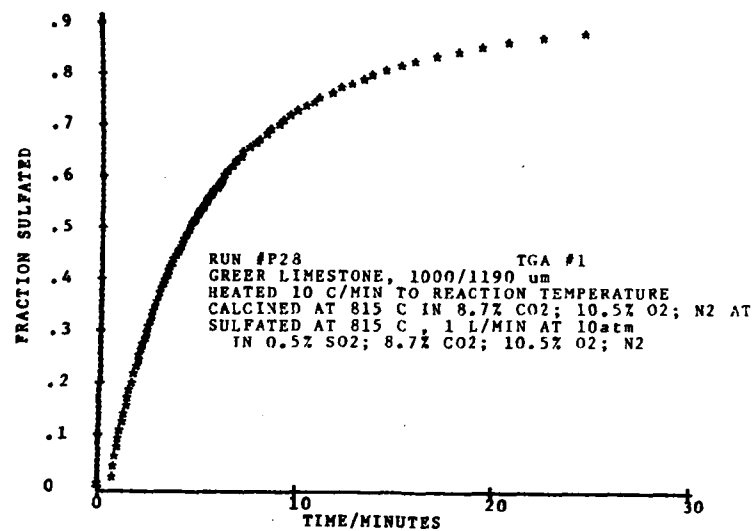
Effect of O_2 Concentration on
Pressurized Desulfurization of Dolomite





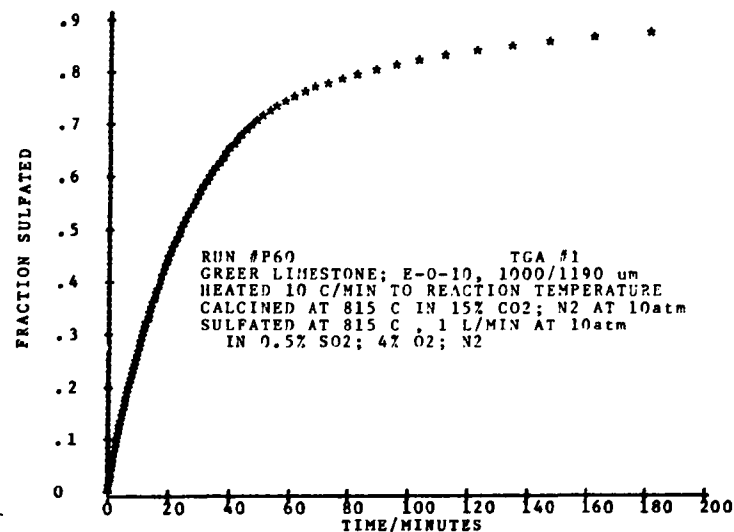
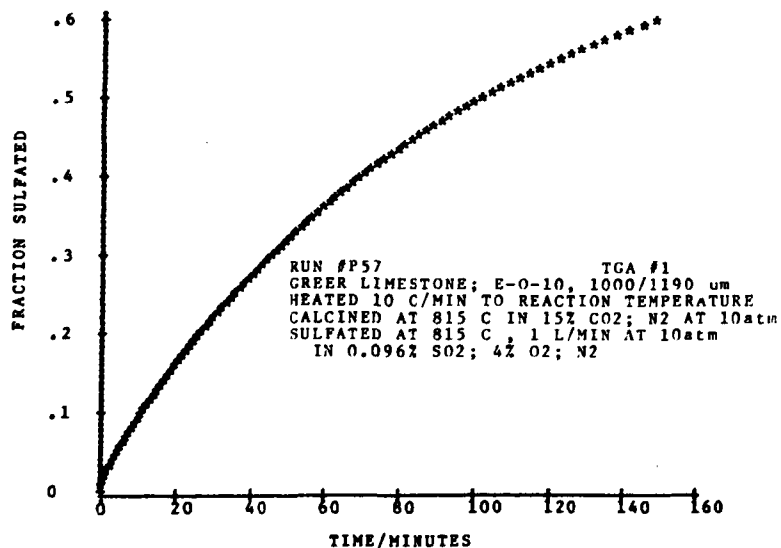
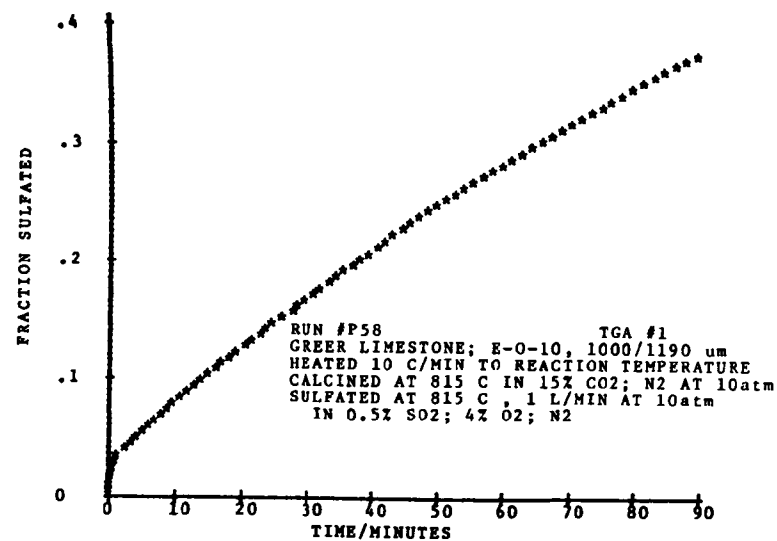
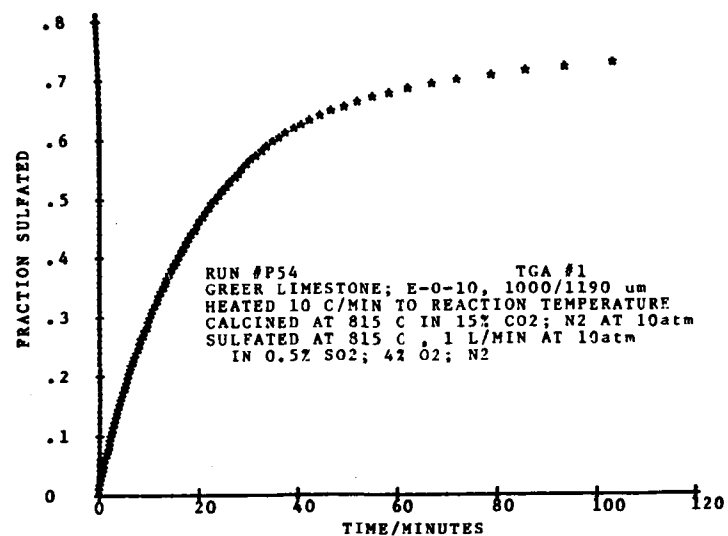
Set 5

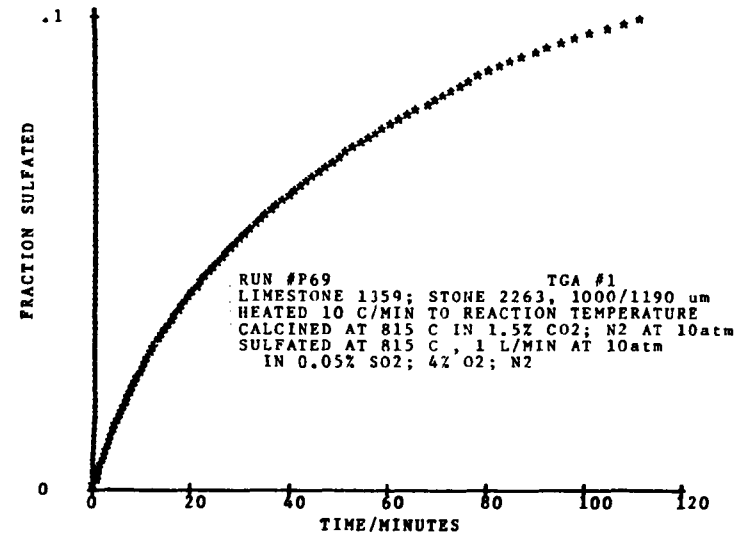
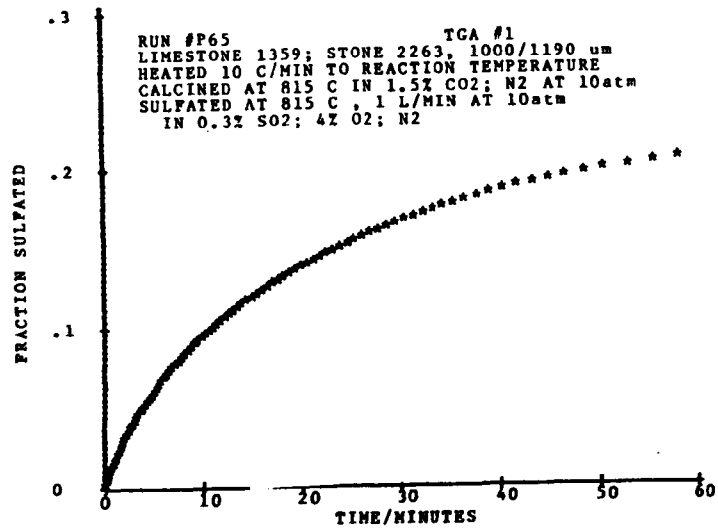
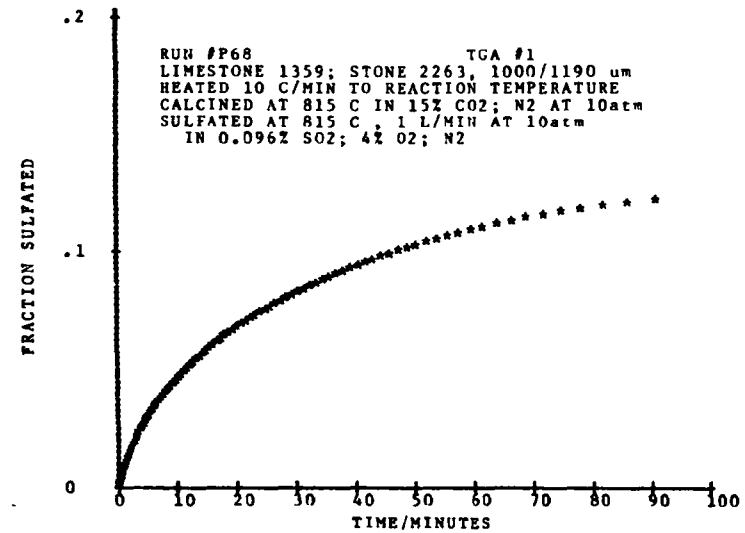
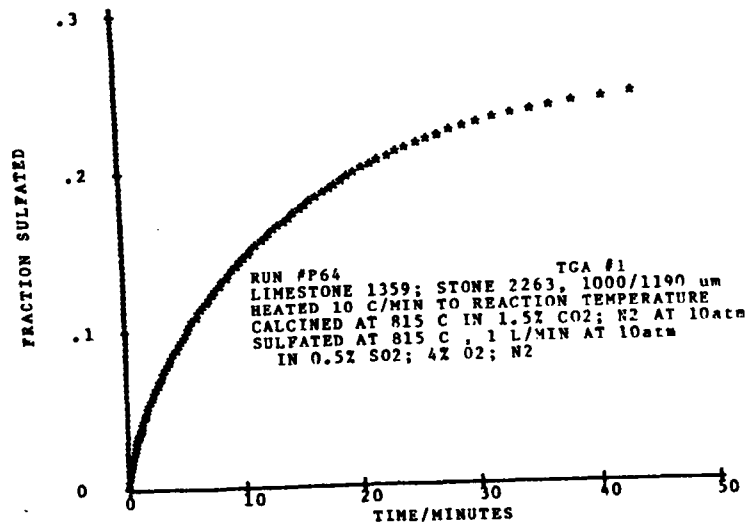
Effect of Excess Air on
Uncalcined Limestone Sulfation

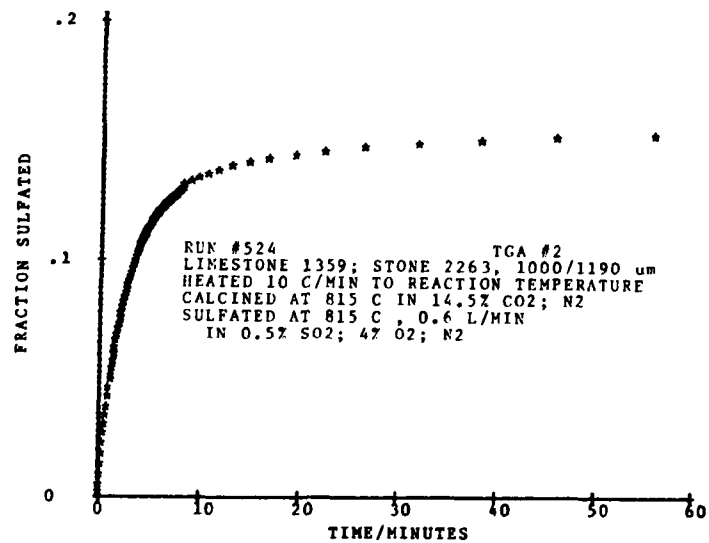
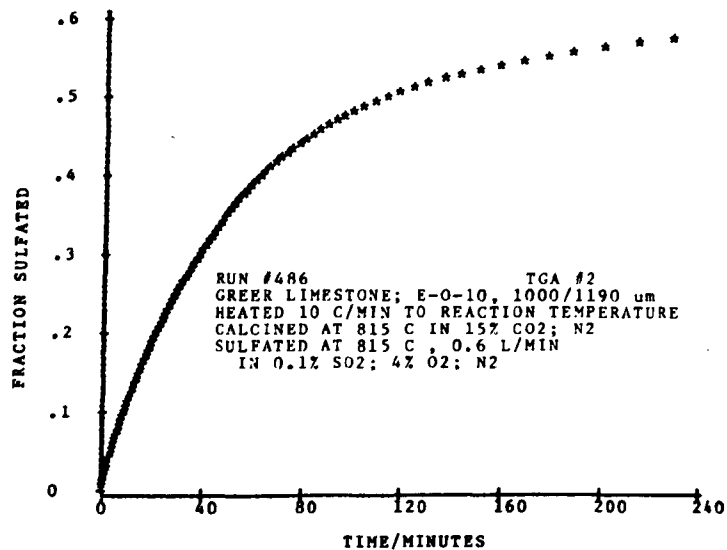
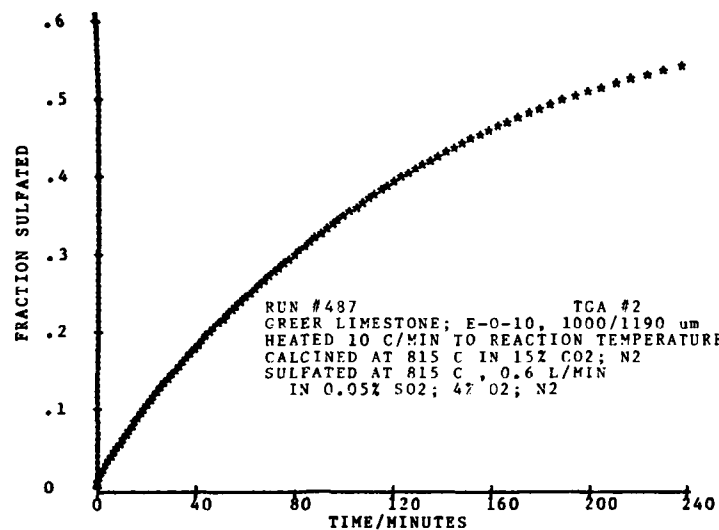
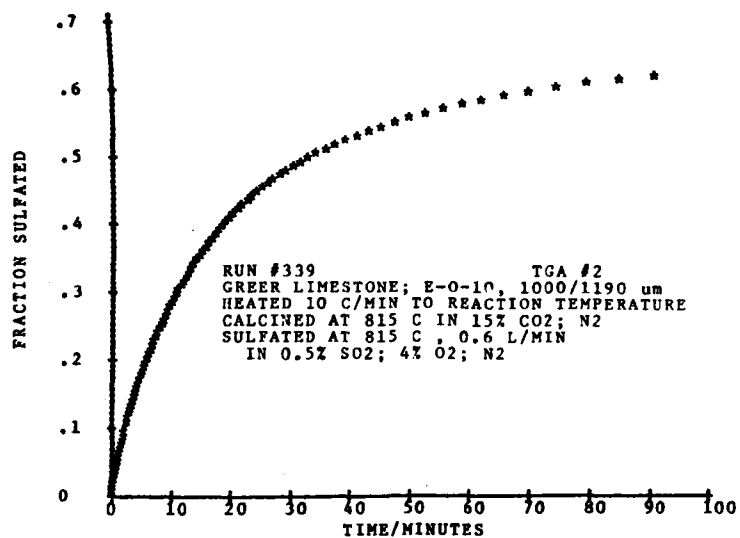


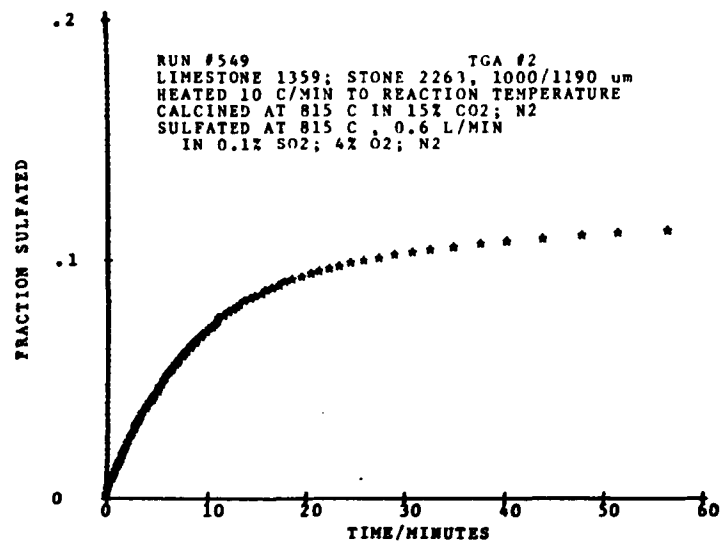
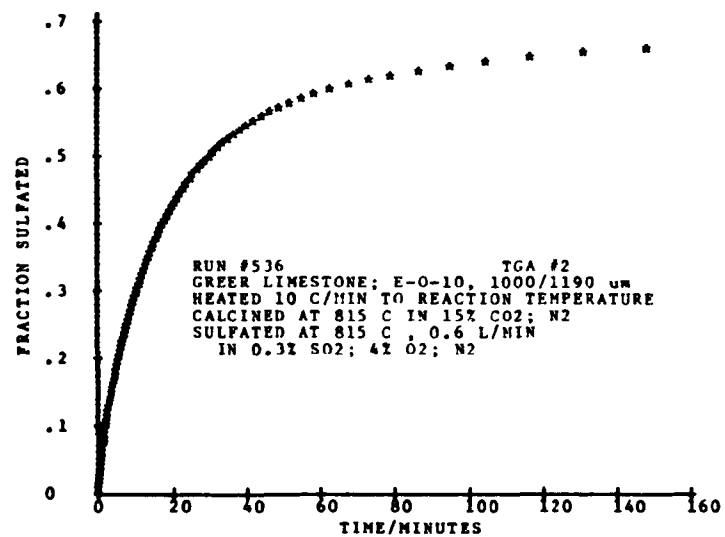
Set 6

Effect of Sorbent Residence Time on Desulfurization



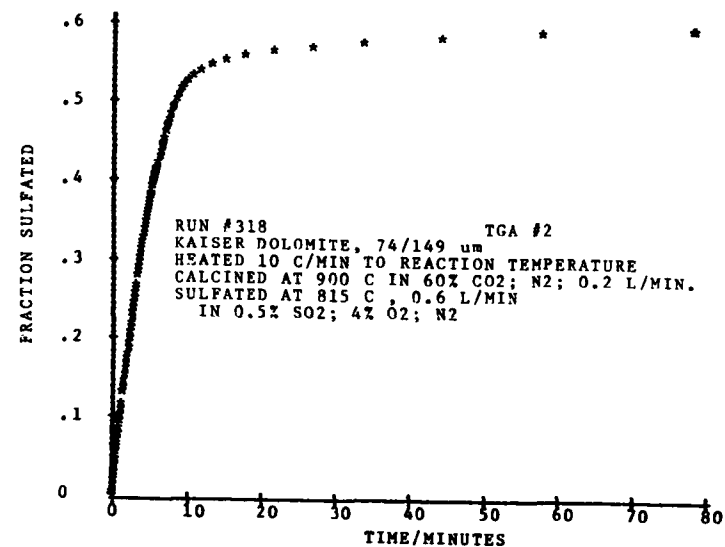
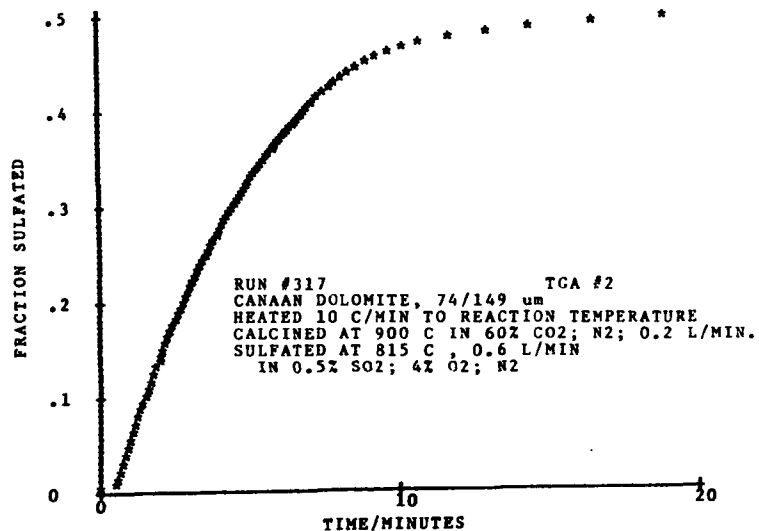
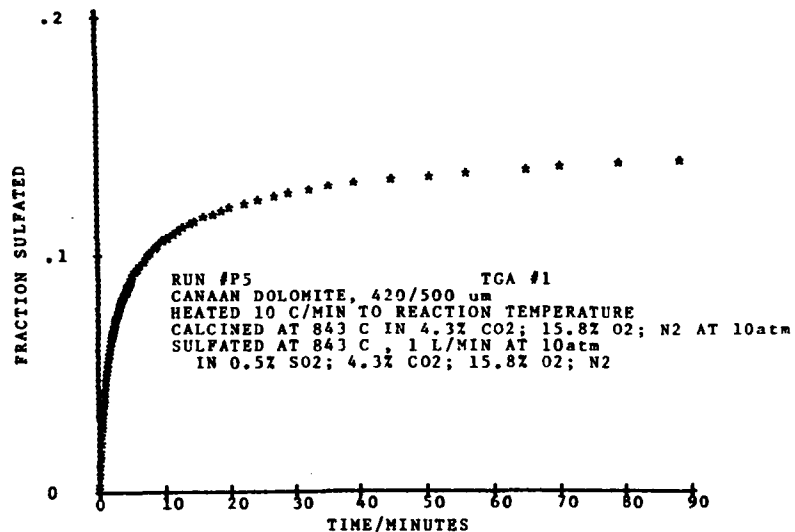






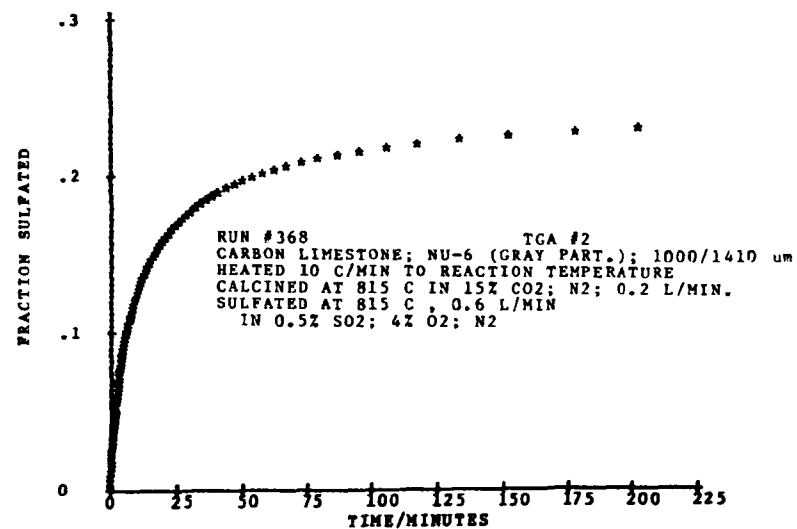
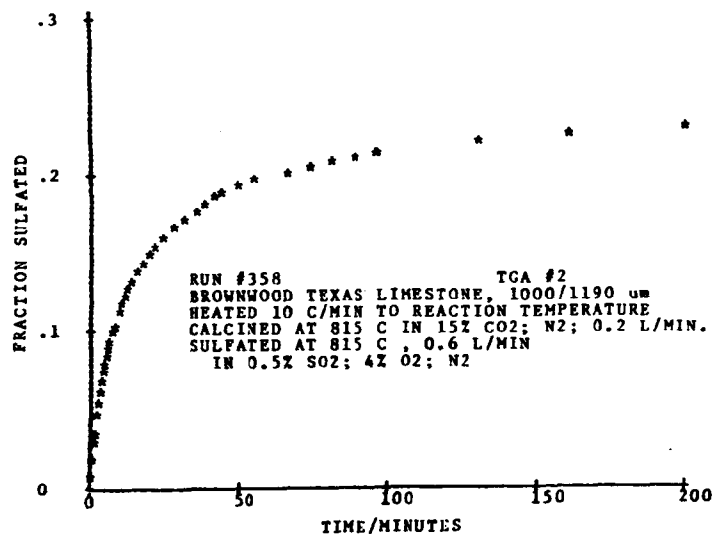
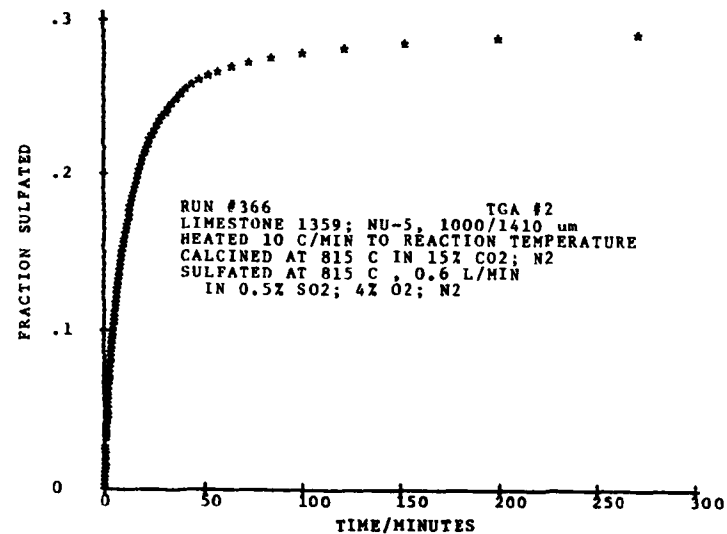
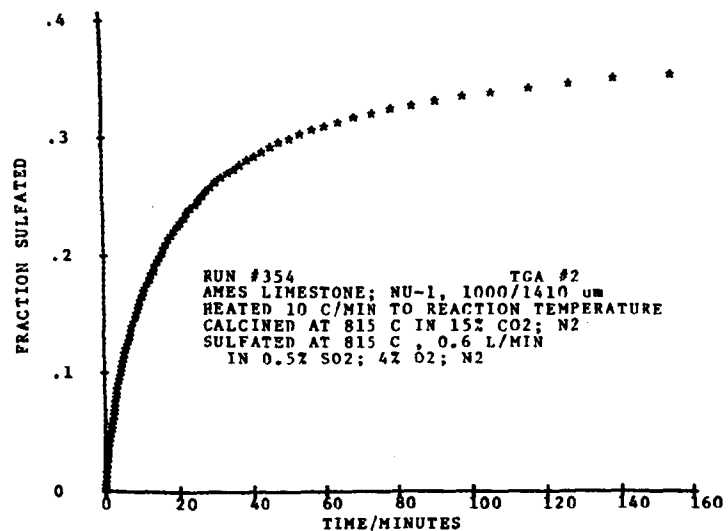
Set 7

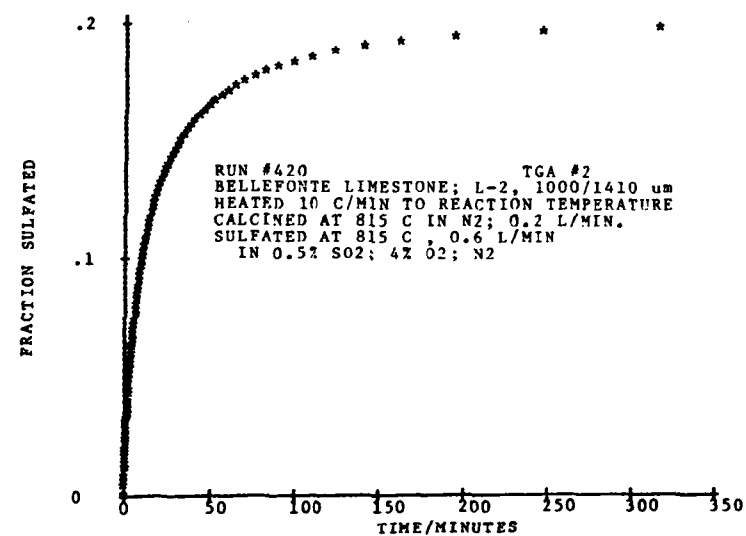
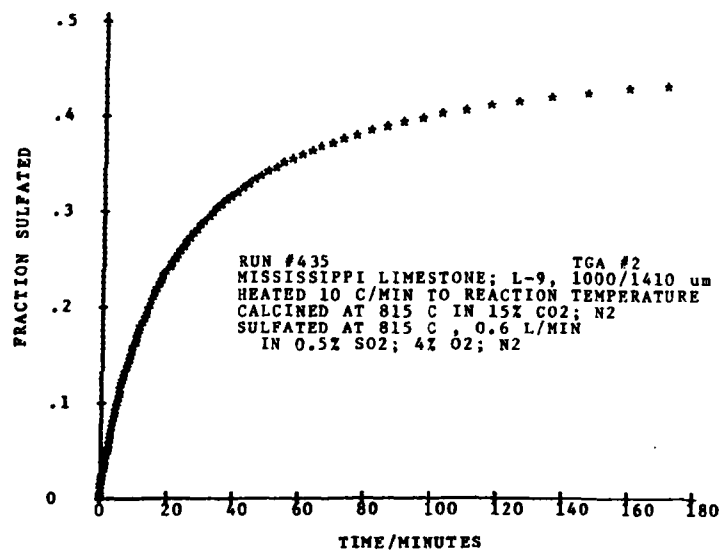
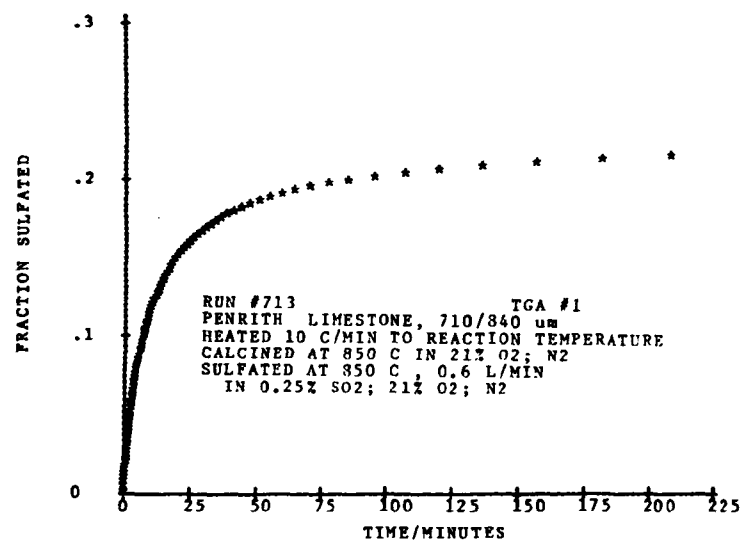
Large-Grained Dolomite Performance



Set 8

Data for Comparison with Batch Fluid-Bed Results





Set 9

Data for Projections of Pilot Plant Performance

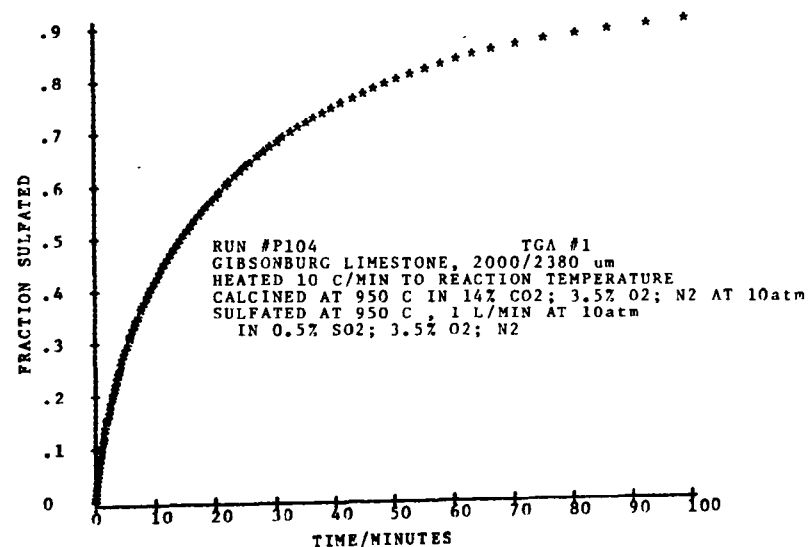
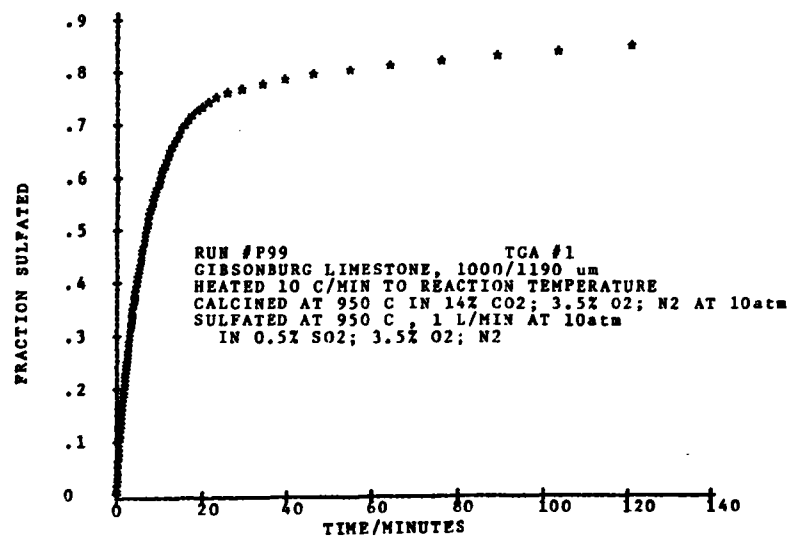
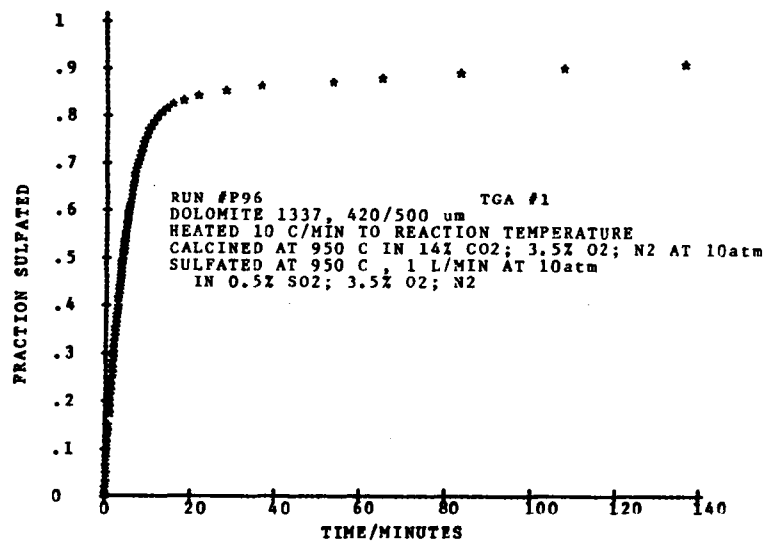


Table B1

Dwg. 8531028

SORBENT SUPPLIER INFORMATION

Sorbent	Quarry/Mine	Address	Comment
Ames Limestone	The Puskarich Quarry	Puskarich Limestone Co. 1258 Panda Road S. E. (Box 314) Carrollton, Ohio 44615 ct: Paul Tinlin 216-627-5915 216-799-3685 (Quarry)	Limestone, Marine, Shale & Siliceous Carroll County, Ohio Pennsylvanian System, Conemaugh Formation, Ames Member LA Abrasion Tests: Grading B = 17.1 % Grading C = 17.1 % Reserves : 48 Billion Ton Production: 200,000 Ton/Year
Belleville Limestone	Bell Mine	Warner Company Belleville, Pa. 16823 ct: Louis Yost Bob Greene 814-355-4761	Amorphous Stone Ordovician System Kambo/Bellefonte Ledge (formation) Chester County, Pennsylvania Deep Mined - 960' below the Surface Use - Kiln Feed
Brownwood Limestone	White Mines Inc. Quarry	White Mines Inc. P.O. Box 500 Brownwood, Texas 76801 ct: James Bitter 915-646-8526	Pennsylvania System Brown County, Texas Single Strata Mined "Pennsylvania Limestone"
Carbon Limestone	Lowellville Quarry	Carbon Limestone Co. Lowellville, Ohio 44436 ct: Mr. Reed Mr. W. S. Foster 216-536-6275	Limestone, Marine Mahoning County, Ohio Pennsylvania System, Allegheny Formation, Vanport Member LA Abrasion Tests: Grading B = 22 - 24 % Grading C = 22 % Production: 2 x 10 ⁶ Ton/Year Reserves: 30 Years 20 - 21 Ft. Strata With 100 Ft Overburden
Greer Limestone	Greer (Quarry) Mine	Greer Limestone Co. Greer Building Morgantown, W. Va. 26505 ct: Mr. Western 304-296-2549	Greenbrier Formation Near Dellslow W. Va. Monongalia County Deep Mined
Grove Limestone "Limestone 1359"	Stephens City Quarry	M. J. Grove Lime Co. Division of Flintkote Co. P.O. Box 656 Frederick, Md. 21701 ct: M. E. Barger 301-662-1181	Shenandoah County, Va. LA Abrasion Tests: Grading B = 21.6 % Grading C = 22.0 %
Mississippi Limestone	Alton Mine	Mississippi Lime Company 7 Alby Street Alton, Illinois 62002 ct: Jerry Lepchenske 618-465-7741	Mississippian System St. Louis Formation Madison County, Illinois Kiln Feed - Lime Co.
Penrith Limestone		Cambridge University Dept. of Engineering Pembroke Street Cambridge, England CB2 3RA ct: Blake Fields	
Canaan Dolomite		Pfizer Materials, Pigments and Metals Division Daisy Hill-Road P.O. Box 667 Canaan Conn. 06018 ct: G. M. Hicks 216-526-1293	Kiln Fed - Lime Co.
1337 Dolomite		Pfizer Minerals, Pigments and Metals Div. Gibsonburg, Ohio ct: Jim Garn 419-637-2186	Dolomite: light, massive and very pure Silurian System, Niagara Group, Guelph Formation at "NELCO" Sandusky County, Ohio
Kaiser Dolomite		Kaiser Refractories Div. of Kaiser Aluminum & Chem. Corp. Selinas, Calif. Gen. Off. 408-633-2413	Dolomite: Light; Very Pure Lime Plant: Natividad, Calif. Kiln Feed
Tymochtee Dolomite	Duff Quarry	C. E. Duff, Co. Huntsville, Ohio ct: Jim Duff 513-686-2488	Dolomite: thin to massive bedded, gray to brown Silurian System, Tymochtee Formation, Bass Island Group Production: 300,000 Ton/Year Reserves: 300 Years, 200 Acres - 410 Ft. Strata

Table B2
SORBENT ANALYSIS

Sorbent	Measured Grain Size (μm)	Chemical Analysis (% weight)						
		Ca as CaCO_3	Mg as MgCO_3	Al as Al_2O_3	Fe as Fe_2O_3	Si as SiO_2	Na as Na_2O	K as K_2O
Ames Limestone	29 ± 9	84.6	2.00	6.0	3.7	8.0	0.17	0.90
Bellefonte Limestone	330 ± 180 ; < 50	95.7	0.98	0.59	0.24	1.2	0.10	0.16
Brownwood Limestone	72 ± 31	95.1	1.11	0.94	0.97	1.8	0.026	0.17
Carbon Limestone	47 ± 11	90.1	1.42	2.6	2.0	3.4	0.046	0.42
Greer Limestone	11 ± 2	67.8	2.32	9.8	3.7	15.4	0.56	2.29
Limestone 1359	24 ± 7	96.4	1.5	< 0.4	1.0	< 0.1	0.008	0.10
Mississippi Limestone	~ 110 14-540 ooliths	98.1	0.46	0.12	0.10	0.47	0.030	0.039
Penrith Limestone	-	96.7	2.15	-	-	-	-	-
Canaan Dolomite	400 ± 75	55.7	40.9	0.19	2.7	0.49	0.024	0.48
Dolomite 1337	43 ± 11	53.2	46.0	0.076	0.17	0.41	0.043	0.053
Kaiser Dolomite	600 ± 180	55.5	43.7	0.011	0.17	0.043	< 0.002	< 0.004
Tymochtee Dolomite	15 ± 1	51.1	42.3	2.0	0.97	3.77	0.075	0.68

APPENDIX C
FLUIDIZED-BED DATA

Table C1

FLUIDIZED-BED CONDITIONS AND ASSUMPTIONS FOR CALCULATIONS

Sorbents Calcined at 815°C in 15% CO₂ for 4 hours
 Sulfated at 815°C in 0.5% SO₂, 4% O₂
 $\rho = 2.71$ g/cc assumed

Run	Limestone	Total Gas Flow, cc/s	Fraction SO ₂ in Feed Gas	Bed Charge, g	Mole Ca in Bed	FB Particle Radius, cm	TG Run	TG Particle Radius, cm
NU5	1359	905	0.0053	56.96	0.8461	0.05595	366	0.05595
NU6	Carbon	915	0.0053	64.0	0.7427	0.05265	231	0.05265
NU7	Brownwood	915	0.0053	54.29	0.8495	0.04715	358	0.0548
NU8	Ames	876	0.0053	100	0.8465	0.04585	354	0.0603
L-6	Bellefonte	983	0.0049	50	0.7313	0.0514	416	0.0514
L-11	Mississippi	925	0.0049	38.3	0.6373	0.0425	435	0.0425

RUN #NU5

SO₂ FRACTION OF EFFLUENT

TIME (MINUTES)

0.000000	0.000
0.000110	0.250
0.000210	0.500
0.000300	0.750
0.000790	1.000
0.000930	1.250
0.000300	1.500
0.000750	1.750
0.000190	2.000
0.000000	2.250
0.000000	13.000
0.000010	13.250
0.000050	13.500
0.000050	13.750
0.000020	14.000
0.000040	14.250
0.000030	14.500
0.000030	14.750
0.000050	15.000
0.000080	15.250
0.000030	15.500
0.000060	15.750
0.000070	16.000
0.000060	16.250
0.000030	16.500
0.000070	16.750
0.000070	17.000
0.000070	17.250
0.000070	17.500
0.000100	17.750
0.000090	18.000
0.000100	18.250
0.000130	18.500
0.000150	18.750
0.000140	19.000
0.000150	19.250
0.000120	19.500
0.000190	19.750
0.000190	20.000
0.000200	20.250
0.000210	20.500
0.000230	20.750
0.000230	21.000
0.000290	21.250
0.000280	21.500
0.000350	21.750
0.000290	22.000
0.000270	22.250
0.000300	22.500
0.000310	22.750
0.000310	23.000
0.000320	23.250
0.000390	23.500
0.000350	23.750
0.000350	24.000
0.000410	24.250
0.000420	24.500
0.000410	24.750
0.000440	25.000
0.000380	25.250
0.000510	25.500
0.000530	25.750
0.000560	26.000
0.000590	26.250
0.000520	26.500
0.000580	26.750
0.000600	27.000
0.000650	27.250
0.000620	27.500
0.000700	27.750
0.000710	28.000
0.000720	28.250
0.000780	28.500
0.000760	28.750
0.000850	29.000
0.000890	29.250
0.000950	29.500
0.000810	29.750
0.000950	30.000
0.000990	30.250
0.000910	30.500
0.000990	30.750
0.001000	31.000
0.001020	31.250
0.001100	31.500
0.001120	31.750
0.001050	32.000
0.001130	32.250
0.001090	32.500
0.001100	32.750
0.001100	33.000
0.000900	33.250
0.000150	33.500
0.000110	33.750
0.000050	34.000
0.000060	34.250
0.000020	34.500
0.000010	34.750
0.000020	35.000

RUN #NU6

SO₂ FRACTION OF EFFLUENT

TIME (MINUTES)

0.000000	0.000
0.000070	0.500
0.000300	0.750
0.000070	1.000
0.000040	1.250
0.000050	1.500
0.000030	1.750
0.000000	2.000
0.000000	13.000
0.000060	13.250
0.000060	13.500
0.000060	13.750
0.000060	14.000
0.000100	14.250
0.000060	14.500
0.000150	14.750
0.000110	15.000
0.000090	15.250
0.000090	15.500
0.000110	15.750
0.000130	16.000
0.000110	16.250
0.000140	16.500
0.000180	16.750
0.000120	17.000
0.000180	17.250
0.000270	17.500
0.000140	17.750
0.000200	18.000
0.000150	18.250
0.000180	18.500
0.000180	18.750
0.000190	19.000
0.000220	19.250
0.000210	19.500
0.000220	19.750
0.000210	20.000
0.000280	20.250
0.000260	20.500
0.000270	20.750
0.000270	21.000
0.000270	21.250
0.000300	21.500
0.000300	21.750
0.000310	22.000
0.000350	22.250
0.000350	22.500
0.000350	22.750
0.000390	23.000
0.000400	23.250
0.000410	23.500
0.000410	23.750
0.000450	24.000
0.000450	24.250
0.000500	24.500
0.000510	24.750
0.000530	25.000
0.000560	25.250
0.000590	25.500
0.000580	25.750
0.000630	26.000
0.000660	26.250
0.000660	26.500
0.000700	26.750
0.000710	27.000
0.000730	27.250
0.000750	27.500
0.000800	27.750
0.000820	28.000
0.000860	28.250
0.000900	28.500
0.000900	28.750
0.000910	29.000
0.000950	29.250
0.001010	29.500
0.000160	29.750
0.001000	30.000
0.001950	30.250
0.000470	30.500
0.000180	30.750
0.000390	31.000
0.000300	31.250
0.000100	31.500
0.000110	31.750
0.000080	32.000
0.000060	32.250
0.000050	32.500
0.000020	32.750
0.000000	0.000

RUN #NU7

SO₂ FRACTION OF EFFLUENT

TIME (MINUTES)

0.000000	0.000
0.000000	11.500
0.000080	13.500
0.000080	13.750
0.000090	14.000
0.000090	14.250
0.000110	14.500
0.000110	14.750
0.000110	15.000
0.000120	15.250
0.000145	15.500
0.000150	15.750
0.000160	16.000
0.000180	16.250
0.000200	16.500
0.000210	16.750
0.000230	17.000
0.000260	17.250
0.000280	17.500
0.000300	17.750
0.000320	18.000
0.000330	18.250
0.000350	18.500
0.000370	18.750
0.000390	19.000
0.000440	19.250
0.000470	19.500
0.000450	19.750
0.000540	20.000
0.000560	20.250
0.000570	20.500
0.000550	20.750
0.000630	21.000
0.000650	21.250
0.000680	21.500
0.000670	21.750
0.000710	22.000
0.000720	22.250
0.000770	22.500
0.000730	22.750
0.000770	23.000
0.000840	23.250
0.000820	23.500
0.000805	23.750
0.000910	24.000
0.000910	24.250
0.000930	24.500
0.000970	24.750
0.001000	25.000
0.001040	25.250
0.001080	25.375
0.001100	25.500
0.001110	25.750
0.001090	26.000
0.001070	26.250
0.001010	26.500
0.001000	26.000
0.000720	27.000
0.000200	27.250
0.000100	27.500
0.000080	27.750
0.000060	28.000
0.000050	28.250
0.000050	28.500
0.000020	29.000
0.000020	29.500
0.000010	30.500
0.000000	32.500

RUN #NU8

SO₂ FRACTION OF EFFLUENT

TIME (MINUTES)

0.000000	0.000
0.000000	14.750
0.000030	15.000
0.000060	16.000
0.000110	16.250
0.000040	16.500
0.000080	16.750
0.000100	17.000
0.000130	17.250
0.000120	17.500
0.000120	17.750
0.000150	18.000
0.000300	18.250
0.000150	18.500
0.000160	18.750
0.000300	19.000
0.000230	19.250
0.000290	19.500
0.000340	19.750
0.000310	20.000
0.000310	20.250
0.000400	20.500
0.000350	20.750
0.000350	21.000
0.000500	21.250
0.000480	21.500
0.000500	21.750
0.000520	22.000
0.000520	22.250
0.000560	22.500
0.000680	22.750
0.000680	23.000
0.000620	23.250
0.000590	23.500
0.000690	23.750
0.000640	24.000
0.000650	24.250
0.000640	24.500
0.000720	24.750
0.000630	25.000
0.000720	25.250
0.000730	25.500
0.000790	25.750
0.000810	26.000
0.000810	26.250
0.000790	26.500
0.000810	26.750
0.000900	27.000
0.000930	27.250
0.000920	27.500
0.000940	27.750
0.001070	28.000
0.001010	28.250
0.001050	28.375
0.001050	28.500
0.001170	28.750
0.001010	29.000
0.001040	29.250
0.000920	29.500
0.000980	29.750
0.000970	30.000
0.000990	30.250
0.000340	30.500
0.000130	30.750
0.000070	31.000
0.000000	32.000
0.000000	0.000

RUN #L6

SO₂ FRACTION OF EFFLUENT

TIME (MINUTES)

0.000000	0.000
0.000000	0.125
0.000010	2.000
0.000010	4.000
0.000010	6.000
0.000100	7.000
0.000500	8.000
0.000800	9.000
0.001100	10.000
0.001380	11.000
0.001560	12.000
0.001760	13.000
0.001900	14.000
0.002030	15.000
0.002200	16.000
0.002390	17.000
0.002520	18.000
0.002630	19.000
0.002770	20.000
0.002850	21.000
0.002920	22.000
0.003010	23.000
0.003110	24.000
0.003190	25.000
0.003280	26.000
0.003350	27.000
0.003400	28.000
0.003510	29.000
0.003570	30.000
0.003610	31.000
0.003680	32.000
0.003710	33.000
0.003780	34.000
0.003800	35.000
0.003830	36.000
0.003890	37.000
0.003910	38.000
0.003950	39.000
0.003990	40.000
0.004000	40.750
0.000050	41.000
0.000030	42.000
0.000019	43.000
0.000015	44.000
0.000013	45.000
0.000011	46.000
0.000010	47.000

RUN #L11

SO₂ FRACTION OF EFFLUENT

TIME (MINUTES)

0.000000	0.000
0.000000	0.075
0.000000	1.000
0.000000	3.000
0.000010	5.000
0.000050	7.000
0.000110	9.000
0.000190	11.000
0.000260	13.000
0.000370	15.000
0.000480	17.000
0.000630	19.000
0.000820	21.000
0.001100	23.000
0.001390	25.000
0.001680	27.000
0.001950	29.000
0.002240	31.000
0.002480	33.000
0.002670	35.000
0.002860	37.000
0.003000	39.000
0.003040	41.000
0.003170	43.000
0.003280	45.000
0.003340	47.000
0.003430	49.000
0.003410	51.000
0.003590	53.000
0.003630	55.000
0.003840	57.000
0.004000	59.000
0.001500	60.000
0.000310	61.000
0.000190	62.000
0.000110	63.000
0.000090	64.000
0.000050	65.000

APPENDIX D

A MODEL FOR PARTICLE ATTRITION BY ABRASION IN THE UPPER ZONE OF A FLUIDIZED BED

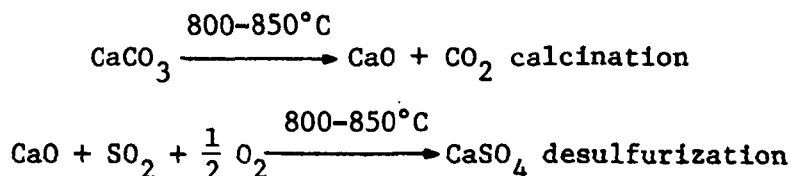
INTRODUCTION

This study of particle attrition in fluidized beds was carried out to aid in predicting makeup solids requirements and particle control in exhausts in fluidized-bed energy systems.

Fluidized-bed fossil fuel processing systems are now being commercialized. These systems provide for compact, nonpolluting combustion or gasification of coal and other solid or liquid fuels.^{1,2} Studies of fluidized-bed processes show that bed particles inevitably wear down into fine dust. This wearing down of particles, called attrition, is variable and not well understood.

If attrition rates are related to various properties of the particulate solids and fluidizing gas, and operating conditions, we should be able to develop an expression describing the rate of attrition in any given system. Several researchers have studied the effects of single variables under various conditions, but no general prediction equations have been formulated.

The examples used in this paper are generally related to fluidized-bed combustion of fossil fuels. A fluidized-bed combustor consists of 0.5-to-2-mm particles of calcined limestone that captures sulfur dioxide or dolomite (SO_2) as soon as it is formed



The specific objectives of this study were to

1. Identify the various causes or sources of attrition, focusing study on the cause of attrition occurring in fluidized-bed combustors and gasifiers
2. Develop an expression relating the attrition rate due to abrasion in the bubbling zone (one of the sources of attrition) to operating conditions and material properties
3. Test the proposed attrition formula in controlled laboratory experiments.

HYPOTHESES

What are the Sources of Attrition in a Fluidized Bed?

The frequently considered source of attrition in a fluidized bed is the obvious grinding and shattering collisions of particles. There are several causes of particle wear, however, which include:

1. Abrasion. In this process defects, edges, and corners are knocked from particles by low-energy collisions. Abrasion can occur during passage of a gas bubble through the bed of solids.
2. High-Energy Collisions. Particles may be accelerated to high velocity, for example when entrained in a jet at the distribution plate. The high-velocity particle can strike another particle or vessel wall and shatter into relatively large fragments.

Blinichev, Strel'tsov, and Lebedeva³ have distinguished two zones in a fluidized bed: the lower, which they call the "nozzle effect" zone in which gas jets accelerate large particles to energies sufficient for shattering; and the upper zone, characterized by intensive mixing and low-energy impacts which grind particle surfaces.

3. Thermal Shock. When cold particles are added suddenly to a bed of red-hot solids, there is severe thermal stress on the cold particles. One expects spalling at the particle surface and perhaps shattering into large fragments.⁴
4. Chemical Stress. Sorbent particles calcine, then react with SO_2 ; calcium oxide (CaO) forms calcium sulfate (CaSO_4), with subsequent changes in the lattice structure. This change in particle structure at its surface hardens particles in some cases, or in other cases causes internal stresses leading to spalling or weakened particle surfaces.⁴⁻⁶
5. Internal Gas Pressure. When cold limestone or dolomite makeup sorbent is added to a hot fluidized bed, the resulting calcination generates carbon dioxide (CO_2) within the particle. Esso Research Centre in Abingdon, UK, found that a slower calcination rate of fresh limestone results in lower production of fines.⁷ Similarly, water within particle cracks will flash when heated to bed temperatures. While CO_2 pressures are moderate (100.0 kPa equilibrium at 900°C), steam pressures are high and can explode particles.
6. Transfer Lines and Cyclones. These are not a part of the fluidization process but are generally included in a fluidized-bed system. This breakage rate is related to the circulation rate of the solids and is controlled by equipment-design effects on solids impact.

Kutyavina and Baskakov⁸ explain, "With fluidization, particles are ground by abrasion and splitting. ... Abrasion is evidently predominant even for brittle and insufficiently strong materials."

Similarly, Wei⁹ describes two mechanisms of particle attrition:

"grinding" or the abrasive removal of a layer of crystallites and matrix from the skin, and "shattering" of the deep disintegration of the matrix material.

The former mechanism leaves behind a large particle somewhat reduced in size and a pile of very fine particles; the latter mechanism leaves an assortment of fragments from the very small to the very large. The former is controlled by the hardness of the crystallites and the abrasion resistance of the matrix; the latter is controlled by the impact elasticity of the matrix and the imperfections in the structure.

Doheim, Ghaneya, and Rassoul¹⁰ observed with fluidized iron ores in a non-reacting system that the primary mechanism of attrition is by abrasion, not breakage. Jonke of Argonne National Laboratory (ANL), observed "that the mechanism for attrition is abrasion (the wearing away of surface material), in contrast to the break-up or splitting of particles due to particle or particle-wall collision."¹¹ Blinichev and others³ report that the wear of hard fluidized particles is by abrasion; soft materials split, then abrade. Forsythe and Hertwig,¹² Kut'yavina and Baskakov,⁸ and Zenz¹³ make the same observation.

In this appendix discussion is limited to only the first source of attrition: abrasion, or grinding caused by rising gas bubbles in a fluidized bed. In most fluidized beds several attrition mechanisms will act. In this study, grid (distribution-plate) jets were eliminated in the environmental work by using a porous, sintered-metal grid. Temperature and chemical effects were avoided by operating at room temperature.

Relation between Gas Velocity U and Minimum Fluidization Velocity in Attrition Testing

Meaningful measurement of attrition requires that tests be carried out under some specified conditions; that is to say, values of parameters (fixed variables) be specified.

Attrition testing is often carried out at some arbitrary gas velocity, U . In our earlier testing we measured attrition with the gas-velocity parameter held at a constant multiple of the minimum fluidization velocity U_{mf} . Exxon R&E¹⁴ has reported early testing at a constant gas velocity; some samples (low U_{mf}) fluidize vigorously at a given velocity, others (high U_{mf}) move only slowly. Exxon reports fluidizing all samples at a constant multiple of the minimum fluidizing velocity, $U = 1.6 U_{mf}$.

We propose that the rate of attrition for this mechanism of a fluidized solid is affected by the rate at which energy is supplied to the fluidized beds.

$$R = \phi \times [Q]^N$$

mass of fines formed per mass of bed solids per unit time	effects of all other variables	rate of energy influx to the bed per unit mass of bed solids	exponent N expected to be ≈ 1.0
--	--------------------------------------	--	---

This is a statement of Rittinger's law of grinding when $N = 1$.

The energy supplied by flowing gas to the bulk of a fluidized bed (in the abrasion attrition mechanism) is virtually all pressure energy that converts to kinetic energy of particles. In contrast, the energy at the grid jets is kinetic energy. In the current series of tests the grid is a sheet of sintered metal and grid jets are eliminated.

The specific* pressure energy causing attrition in the bulk of a fluidized bed is that fraction of the gas flow causing bubbling and particle collisions, namely the Pressure-Flow Rate energy per unit bed mass

$$\begin{aligned}
 \text{Energy} &= (U - U_{mf}) A \Delta P / M \\
 &= (U - U_{mf}) A \frac{g}{g_c} \rho_b Z / M \\
 &= (U - U_{mf}) A \frac{g}{g_c} \frac{M}{V} Z / M \\
 &\quad AZ = V \\
 &= \frac{g}{g_c} (U - U_{mf})
 \end{aligned}$$

U = superficial gas velocity
U_{mf} = min. fluidizing velocity
A = bed cross-sectional area
ΔP = bed pressure drop
M = bed mass
g = gravity acceleration
g_c = Newton's law factor
ρ_b = bed bulk density
V = bed volume
Z = bed depth

*Per unit mass of bed solids.

It is the energy potentially available for attrition that is held constant in these tests; if $U - U_{mf}$ is 30 cm/s, for example, this energy is

$$\begin{aligned}\frac{g}{g_c} (U - U_{mf}) &= \frac{980 \text{ cm/s}^2}{1 \text{ g cm/dyne s}^2} (30 \text{ cm/s}) \\ &= 29,400 \frac{\text{dyne-cm}}{\text{s}} / \text{g} \\ &= 0.00294 \text{ J/g}\end{aligned}$$

In conclusion, $U - U_{mf}$ is the velocity variable that is used in this study, rather than a multiple of U_{mf} . The difference $U - U_{mf}$ is held constant so that, as U_{mf} varies, U is varied accordingly.

The Westinghouse Model Relating the Rate of Particle Attrition by Abrasion to Particle Properties and Fluidizing Conditions

First, we need a definition of attrition. Because attrition in the upper zone of a fluidized bed is mainly erosion by removal of fine pieces, we define the attrition rate, R , as the rate of formation of fines per unit mass of the large bed particles. This is the same as defining R as the rate of loss of coarse particle mass per unit M of large particles (coarses)

$$R = - \frac{1}{M} \frac{dM}{dt} \quad * \quad (1)$$

*The extent of particle attrition A is defined as

$$A = \int_0^t R dt = - \int_{M_0}^{M_1} \frac{dM}{M} = \ln \frac{M_0}{M_1}$$

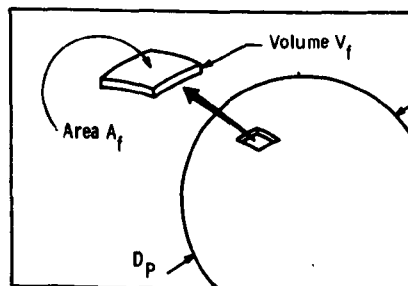
in which M_0 and M_1 are the masses of coarses before and after an interval of attrition.

The goal of the following development is to formulate an expression for the rate of particle attrition in the freely bubbling regime (upper zone) of a fluidized bed. We begin development of a formula for attrition rate by factoring the definition to include the rate of particle collision

$$R = \frac{\text{grams of fines formed}}{\text{sec x gram of coarses}} = \left[\frac{\text{grams of fines formed}}{\text{particle collision}} \right] \times \left[\frac{\text{collisions}}{\text{sec x gram of coarses}} \right] \quad (2)$$

The mass of fines formed per particle collision will depend upon particle shape and strength and the energy of the collision. For example, consider the spherical particle with volume $V_p = \frac{\pi}{6} D_p^3$ and mass $M_p = \frac{\pi}{6} \rho_s D_p^3$. The particle is traveling at some velocity U_p taken to be proportional to the bubble velocity, U_b , related to the bubble diameter, D_b , by the Davies-Taylor¹⁵ relation as

$$\left(\frac{\text{Particle Mass}}{\text{Unit Area Formed}} \right) = C_3 \cdot \rho_s$$



$$U_b = \frac{\sqrt{2}}{3} \sqrt{g D_b} \quad (3)$$

Figure D1 - Dimensions of a chip abraded from a bed particle

The constant of proportionality is $C_1 = \frac{U_p}{U_b}$ and the particle velocity is

$$U_p = C_1 \frac{\sqrt{2}}{3} \sqrt{g D_b} \quad (4)$$

During a collision, the particle's energy is transferred into creating new fracture surface area A_f with efficiency C_2 . The fracture energy of the solid is σ (=) erg/cm², and the new surface area formed is

$$A_f = C_2 \rho_s \frac{\pi}{6} D_p^3 C_1^2 D_p^2 / 2 g_c \sigma .$$

Combining this with the expression for U_p gives

$$A_f = \frac{\pi}{54} \frac{C_1^2 C_2 \rho_s g D_p^3 D_b}{g_c \sigma} \quad (5)$$

The chip volume and mass, and the fracture area, are related by

$$V_{\text{chip}} = C_3' A_f^n \quad (6)$$

$$M_{\text{chip}} = C_3' \rho_s A_f^n , \quad (7)$$

where $n = 1.5$ for knocking corners from a cube and $n = 1.0$ for chipping flat flakes from a rounded particle. We take $n = 1.0$ and interpret C_3' to be a measure of chip thickness

$$C_3' = \frac{V_{\text{chip}}}{A_f} (=) \text{ cm} .$$

For the remainder of the discussion, C_3' is taken to be constant for the quasi-steady-state interval, typically one-to-four hours for attrition in the bubbling regime. If we combine equations (5) and (7) and assume that two chips are formed in each collision.

$$\frac{\text{grams of fines formed}}{\text{particle collision}} = C_1^2 C_2 C_3' \frac{\pi}{27} \frac{\rho_s^2 g D_p^3 D_b}{g_c \sigma} . \quad (8)$$

This is the first factor needed in equation (2).

The second factor in equation (2) may be factored further into

$$\frac{\text{collisions}}{\text{sec} \times \text{gram of coarses}} = \frac{(\text{collisions/bubble}) (\text{bubble/sec})}{(\text{gram of coarses})} \quad (9)$$

Dwg. 6439A72

The number of collisions caused by a bubble rising up the bed of height Z is given by (Figure D2)

$$\begin{aligned} & C_4 \times \text{bubble area} \times \text{bed depth} \\ & \times \frac{\text{particle}}{\text{unit bed volume}} \\ & = C_4 \frac{\pi}{4} D_b^2 Z \frac{1-\epsilon}{\frac{\pi}{6} D_p^3} \\ & = C_4 (1-\epsilon) \frac{3}{2} \frac{Z D_b^2}{D_p^3}, \quad (10) \end{aligned}$$

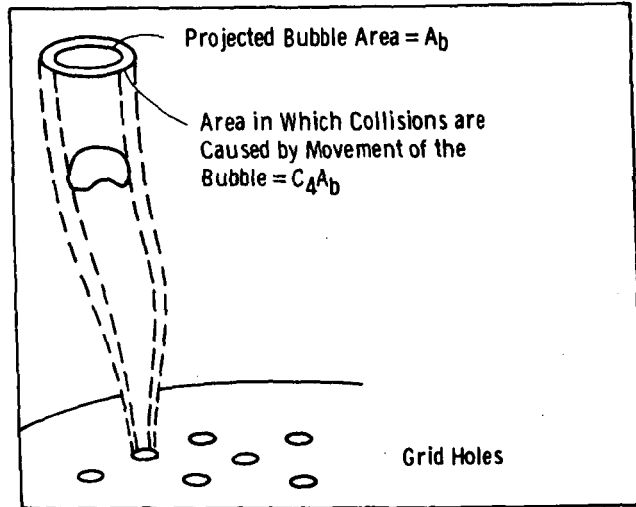


Figure D2 - Volume of particles disturbed by a rising bubble

where ϵ is bed porosity. The number of bubbles formed per second is

$$\frac{(U - U_{mf}) A}{V_b} \quad \text{where } V_b = \frac{\pi}{6} D_b^3 \text{ is bubble volume.}$$

Although not immediately evident, there are several circumstances that suggest the influence of another variable:

- The dimensional constant C_3' (=) length
- The dimensionless group C_3'/Z where Z is the bed depth
- Occurrence of the gravitational constant g, which implies something like hydrostatic pressure in the fluidized bed and, therefore, inclusion of the bed depth Z.

Consequently, in equation (8) the factors $C_3 Z$ replace C_3' ; rearrangement gives

$$\left[\frac{R Z}{U - U_{mf}} \right] = \frac{1}{3} C_1^2 C_2 C_3 C_4 \left[\frac{g Z^2 \rho_s}{g_c \sigma} \right] \quad (11)$$

Combining the constants in this expression gives

$$\left[\frac{R Z}{U - U_{mf}} \right] = C \times \left[\frac{g Z^2 \rho_s}{g_c \sigma} \right] \quad (12)$$

STROUHAL BOND
NUMBER NUMBER

It is physically consistent that the Bond number N_{Bo} should occur; it is the ratio of gravitational force to surface force. Gravitational force is necessary to press particles together, and the surface force is what resists attrition. The rate of attrition being proportional to $(U - U_{mf})$ is realistic: no attrition should occur for $U < U_{mf}$ as the bed is static; $(U - U_{mf})$ is proportional to the rate of energy input to the fluidized bed.

There is no universal agreement on the rate of attrition being proportional to the excess bubbling velocity $U - U_{mf}$; Gonzales and Otero¹⁶ assume the relation $dD_p/dt = -C_s D_p^m$ in which D is particle diameter and C and m are constants. They take $C \propto U^e$ where U is gas velocity in the bed and conclude from experimentation that the constant $e = 0$; that is, attrition rate is independent of U and, in turn, independent of $U - U_{mf}$. Merrick and Highley,¹⁷ on the other hand, invoke Rittinger's law of size reduction by abrasion, assume the rate of input of energy to the bed to be proportional to $(U - U_{mf})$, and deduce that $R = -\frac{1}{M} \frac{dM}{dt} = K (U - U_{mf})$, which agrees with the proposed model, equation (12).

A possible pitfall lies in interpreting the Merrick and Highley equation for particle diameter D_p , $dD_p/dt = -\frac{1}{3} K (U - U_{mf}) D_p$ and concluding that the attrition rate decreases as particle diameter decreases. This equation is derived from the first-order law describing the mass of the bed M , $dM/dt = -K (U - U_{mf}) M$. This equation does not imply that attrition rate depends on particle size. By substituting $M = \rho \frac{\pi}{6} D_p^3$, one derives $dD_p/dt = -\frac{1}{3} K (U - U_{mf}) D_p$, which again does not suggest a rate dependence on particle size.

Data from Other Sources Indicate that Attrition Rate is Independent of Particle Size

Equation (12) indicates that the rate of attrition for fluidized abrasion of particles does not depend on particle size. Wei and others,⁹ in discussing the attrition in jet mills, note the absence of experimental data:

The strength of an impact of a catalyst on the steel wall or on another catalyst can be measured by its kinetic energy $(1/2)mv^2$. In the absence of conclusive experimental data, one may theorize several alternatives: that the rate of attrition should be proportional to the impact energy, or that there should be a threshold energy, or that the attrition rate should increase faster than the impact energy. This point is neglected in the literature. Since particles of all sizes travel at nearly the same speed in the fluidized bed, the major variable in kinetic energy is the particle mass, roughly the cube of the particle diameter. On the other hand, the energy required to break a particle is proportional to the amount of new surface area formed; if the fracturing pattern is geometrically similar, the energy varies as the square of the diameter. In this case, the ratio of impact energy to fracturing energy requirement is proportional to particle diameter. Therefore, the larger the particle diameter, the greater is its rate of attrition. The mass fragmentation rate and pattern of catalyst cracking in a jet mill experiment yield useful information about the attrition mechanism, but this could be significantly different from what is actually happening in a commercial F.C.C. Thus, one should be extremely careful in the interpretation of the laboratory data.

It is important to notice that Wei is discussing the high-energy collisions of particles in a jet where particles shatter, not the low-energy abrasion in which chips are worn from a particle's surface.

Others interpret their data to suggest an effect of particle diameter on the rate of attrition, but scrutiny of those findings indicates no particle-size effect on attrition rate. Tarman and Punwami¹⁸ of IGT provide useful data. In studying the attrition of siderite at room

temperature, they observed that attrition rate varies inversely with initial particle size at a superficial gas velocity of 52 cm/s. Note that the superficial gas velocity U , not excess bubbling velocity $(U - U_{mf})$, was held constant. If we apply the IGT-developed expression for U_{mf} (Babu and others¹⁹),

$$U_{mf} = \frac{\mu}{\rho_g} \frac{D_p}{D_p} \left\{ (25.25^2 + 0.0651 Ga)^{1/2} - 25.25 \right\}$$

$$Ga = D_p^3 \rho_g (\rho_s - \rho_g) g \div \mu^2 ,$$

where:

- μ = gas viscosity (g/cm·s)
- g = gravity acceleration (cm/s²)
- ρ_s = solid density (g/cm³)
- ρ_g = gas density (g/cm³)
- D_p = particle diameter (cm),

to Tarman and Punwami's conditions, we have the data listed in Table D1.

Table D1
ANALYSIS OF IGT DATA

Initial Particle Diameter, μm	U_{mf} , cm/s	$U - U_{mf}$, cm/s
133	3	49
173	5	47
205	7	45
246	10	42
352	20	32
436	30	22
$\left. \begin{array}{l} * \mu = 0.0017 \text{ g/cm-s} \\ \rho_s = 3.0 \text{ g/cm}^3 \\ \rho_g = 0.0013 \text{ g/cm}^3 \end{array} \right\} \text{ Assumed conditions}$		

These are plotted in Figure D3, which shows an inverse relation between $U - U_{mf}$ and particle size.

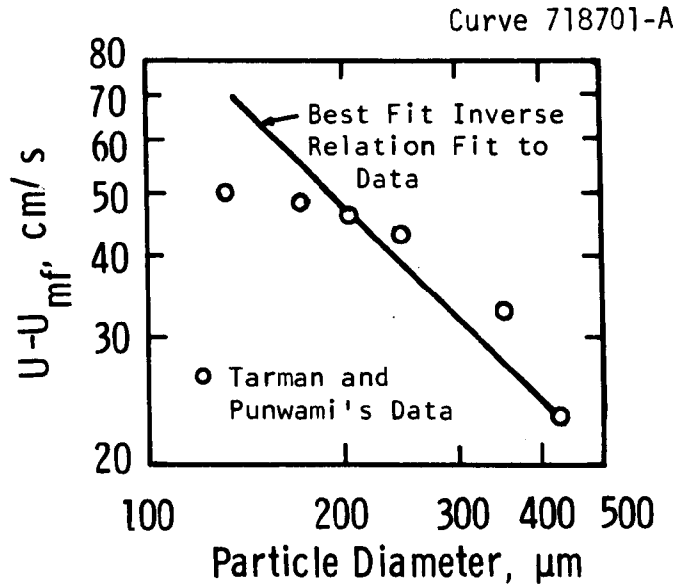


Figure D3 - Variation of $U - U_{mf}$ with particle diameter for siderite fluidized at $U = 52 \text{ cm/s}$ (1.7 ft/sec)

Applying the attrition equation developed in this study, equation (12),

$$R \propto (U - U_{mf}) ,$$

to the conclusion from Figure D3,

$$(U - U_{mf}) \propto D_p^{-1}$$

for constant U infers that

$$R \propto D_p^{-1}$$

for constant U within the range of Tarman and Punwami's data.

The above development shows that we expect Tarman and Punwami's result. The attrition rate R varies inversely with particle diameter D_p in this special case where $U-U_{mf}$ varies with D_p . The attrition rate R would not be expected to vary if $U-U_{mf}$ had been held constant.

Gas velocity is sometimes expressed in terms of the dimensionless and unfortunately chosen "fluidization number," U/U_{mf} .²⁰ Doheim, Ghaneya, and Rassoul¹⁰ studied attrition of iron ore fluidized with hydrogen above a woven-mesh grid. They conclude that "the amount of fines generated by attrition is larger for the coarse iron ore ... attrition increases with particle size." Their comparisons are made at constant $U/U_{mf} = 2$, not at constant power input to the bed for which $U-U_m$ is constant. Analysis of their data for attrition without chemical reaction gives the values of r for $R \propto (U-U_{mf})^r$ listed in Table D2.

Table D2

INTERPRETATION OF DOHEIM, GHANEYA, AND RASSOUL'S DATA

Temp., °C	D_p		R , mg/min	$(U-U_{mf})$	r [$R \propto (U-U_{mf})^r$]
	Range	Mean			
25	250-315	280	21.0	20.5	1.74
	315-400	355	30.7	25.5	
450	250-315	280	43.1	10.8*	0.89
	315-400	355	58.2	15.13*	

$$U-U_{mf} = 2U_{mf} - U_{mf} = U_{mf}.$$

*Calculated assuming fluidization with hydrogen.

As this analysis shows, the dependence of attrition rate R on $U-U_{mf}$ is variable, averaging $r = 1.3$. If we allow for variance in the data, this is interpreted to fit the model of $R \propto (U-U_{mf})^{1.0}$. We conclude that particle size does not influence attrition rate directly but indirectly as it affects U_{mf} , which in turn changes $U-U_{mf}$, a variable controlling R .

Data from Other Sources Indicate that Attrition Rate Is Proportional to Bed Depth, Z

Our model for attrition rate R at depth Z is the bubbling zone of a fluidized bed as given by equation (12). The model relates attrition rate R as proportional to bed depth Z as measured downward from the bed surface (Figure D4). Assuming that $(U - U_{mf})$ is independent of bed depth Z , we can calculate L , the total rate of mass loss from a bed containing mass M of solids by integrating equation (12) over the entire bed mass.

Dwg. 6439A73

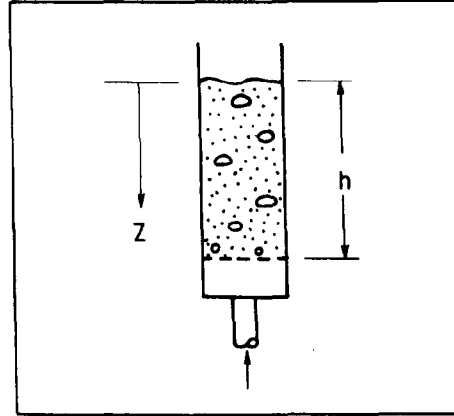


Figure D4 - Depth Units

$$L = \int_0^m R \, d(\text{mass of bed, } m) \quad (13)$$

$$= \int_0^v R (\text{bulk density of bed}) \, d(\text{volume of bed, } v) \quad (14)$$

$$= \int_0^h R \left(\frac{\text{particle density}}{1 - \text{bed porosity}} \right) (\text{bed cross-sectional area}) \, dz \quad (15)$$

$$= \int_0^h K' \frac{g}{g_c} \frac{\rho_s}{\sigma} (U - U_{mf}) \frac{\rho_s}{1 - \epsilon} A \, dz \quad (16)$$

$$L = \frac{K'}{2} \frac{g}{g_c} \frac{\rho_s^2}{\sigma} \frac{U - U_{mf}}{1 - \epsilon} A h^2 \quad (17)$$

Equation (17) states that the total rate of fines production by attrition (gram/second) is proportional to the square of bed depth h . This is substantiated by experimental results from the Esso Research Centre, Abingdon, UK.

Researchers at Esso⁷ reported:

The relative importance of all variables affecting bed loss rate of BCR 1691 is summarized in the equation below. This was derived from further analysis of the fresh bed test results.

$$L = \frac{223.31 \times h^{2.17}}{t^{0.44} \times (T-750)^{1.80} \times s^{0.41}}$$

L = total loss rate from bed (g/min) (= $R \times$ bed mass)

h = bed depth (inches)

t = bed age (hours)

T = bed temperature (deg. C) (750 deg. C is taken as CaCO_3 decomposition temperature)

S = bed sulphur content including inherent sulphur (% by weight)

This equation shows the approximately square relationship between losses and bed depth as observed previously. The loss rate of 3.1 g/min calculated from the above equation for cycle test conditions is in fair agreement with the measured rate of 4.5 g/min.

The Westinghouse model and the Esso data agree that the rate of solids loss (g/m) is proportional to the square of total bed depth, h ; this in turn substantiates that local attrition rate R is proportional to the depth in the bed, Z .

Equation (20) is further confirmed by ANL's²¹ tests in which bed-depth-to-bed-diameter ratio, h/D , was increased from 1.3 to 2.13, probably all within the bubbling, nonslugging regime (Table D3).

Table D3

ANL ATTRITION TESTS OF CALCINED TYMOCHTEE DOLOMITE

h/D	Fluidizing-Gas Velocity, ft/s	% Loss - $\hat{R}t = \hat{A}$					
		1/2 hr	1 hr	2 hr	5 hr	7 hr	10 hr
1.30	2	0.5	0.7	0.9	1.6	2.3	3.0
2.13	2	0.9	1.2	1.7	3.0	3.9	5.3

ANL's data give ratios of $\hat{R}t \Big|_{h/D=2.13} \div \hat{R}t \Big|_{h/D=1.30}$ of 1.80, 1.71, 1.89, 1.88, 1.70, 1.77, which average 1.79. These results fit closely with Esso's observation that the loss rate L (g/min) is proportional to (bed depth)^{2.17}

$$L \propto h^{2.17} . \quad (18)$$

In Table D3, \hat{R} is an overall bed attrition rate time averaged between 0 and time, t . We note that \hat{R} for a bed of depth h , $\hat{R}(h)$ is given by

$$\hat{R}(h) = \frac{L(h)}{V\rho_p(1-\epsilon)} = \frac{L(h)}{Ah\rho_p(1-\epsilon)} = K \frac{L(h)}{h} , \quad (19)$$

where K is some proportionality constant. For two different beds of depths h_1 and h_2

$$\frac{\hat{R}(h_2)t}{\hat{R}(h_1)t} = \frac{\hat{R}(h_2)}{\hat{R}(h_1)} = \frac{KL(h_2)/h_2}{KL(h_1)/h_1} = \frac{h_2^{2.17}/h_2}{h_1^{2.17}/h_1} = \left(\frac{h_2}{h_1}\right)^{1.17} . \quad (20)$$

Hence, from Esso's observation of $L \propto h^{2.17}$, we expect ANL's data to correlate by

$$\frac{\hat{R}(h_2)t}{\hat{R}(h_1)t} = \frac{\hat{R}(h_2/D)t}{\hat{R}(h_1/D)t} = \left(\frac{h_2}{h_1}\right)^{1.17} = \left(\frac{h_2/D}{h_1/D}\right)^{1.17} , \quad (21)$$

and, indeed, the mean \hat{Rt} ratio of 1.79 agrees well with

$$\left(\frac{h_2/D}{h_1/D}\right)^{1.17} = \left(\frac{2.13}{1.30}\right)^{1.17} = 1.78 . \quad (22)$$

We concluded that steady-state attrition in the freely bubbling zone of a fluidized bed (above the grid-jet region) is indeed described by equation (12)

$$\left[\frac{R Z}{U - U_{mf}} \right] \propto \left[\frac{g}{g_c} \frac{\rho_s}{\sigma} Z^2 \right]^m, \quad m \approx 1 . \quad (12)$$

STROUHAL	BOND
NUMBER	NUMBER

The Rate of Attrition Decreases with Time to a Steady State

The preceding expression for attrition applies to a steady-state condition in which the rate of attrition is constant. Several workers have reported that the rate of attrition decreases with time:

- Vaughan at Battelle Columbus Laboratories²² (2/7/77) reported, "there is an initial attrition period where the attrition loss is relatively high; this is perhaps due to the corner rounding or other stabilization effects."
- Curran at Conoco²³ observed a reduction in attrition rate when fluidizing sulfidized dolomite, described by $R - At^b$ with b ranging between -0.19 and -0.32. He attributed the rate decrease to sintering and densification of the stone.
- Merrick and Highley¹⁷ postulate that as attrition progresses finer particles will spend part of the time in voids between larger particles, and during this time no attrition will occur. Thus the attrition rate will change as time progresses.

- Mathur and Epstein²⁴ remark on spouted beds:

The grinding (attrition) rate tended to drop off with spouting time, as would be expected in any batch grinding operation.

- Stanley and others²⁵ report the equation form for specific surface in attrition milling using a mechanical mill:

$$S = S_{\text{ultimate}} \left[1 - e^{-a(t-t_0)} \right]$$

in which a and t are constants, S_{ultimate} is the limiting specific surface.

We can rearrange this equation to

$$\frac{d}{dt} (S_{\text{ultimate}} - S) = -a (S_{\text{ultimate}} - S) ,$$

which implies decreasing attrition rate with time.

- Kuttyavina and Baskakov⁸ report the equation for total fines formed ($M_0 - M$) as

$$M_0 - M = k t^m$$

in which k and m are constants. This equation form reflects a falling attrition rate. They explain, "The rate of abrasion decreased over the course of time, with rubbing off of the uneven parts and a decrease in the number of defects of the particles."

- Forsythe and Hertwig¹² explain the decrease in attrition rate with time as being caused by smoothing of rough edges, elimination of rough particles, and cushioning by the increasing fraction of fines.
- Tarman and Punwami¹⁸ propose that fines fluidize between larger particles, thus lubricating and reducing abrasion.

It seems well established that the attrition rate for initially angular particles decreases with time. The mathematical description of

this decrease is uncertain in the literature, and it seems improbable that it could be predicted. Exponential and power models seem reasonable, yet they are guesses. In a fluidized bed in the bubbling upper zone, the proposed attrition model is such that the rate of attrition decreases monotonically to the steady-state rate of equation (12). Defining the decreasing function $F(t)$ by

$$\begin{aligned} F(t) &\longrightarrow 0, \quad t \longrightarrow \infty \\ \frac{dF(t)}{dt} &< 0, \quad 0 < t \leq \infty \\ F(t) &> 0, \quad 0 < t \leq \infty, \end{aligned}$$

the model for transient and steady-state attrition is

$$\left[\frac{R Z}{U - U_{mf}} \right] = [F(t) + 1] \left[\frac{g}{g_c} \frac{\rho_s}{\sigma} Z^2 \right]^{m'}, \quad m' \approx 1. \quad (23)$$

This model then predicts the form of the attrition rate curve and the extent of attrition curve to be those shown in Figure D5. This is the final current form of the model proposed to describe attrition by abrasion in a FBC.

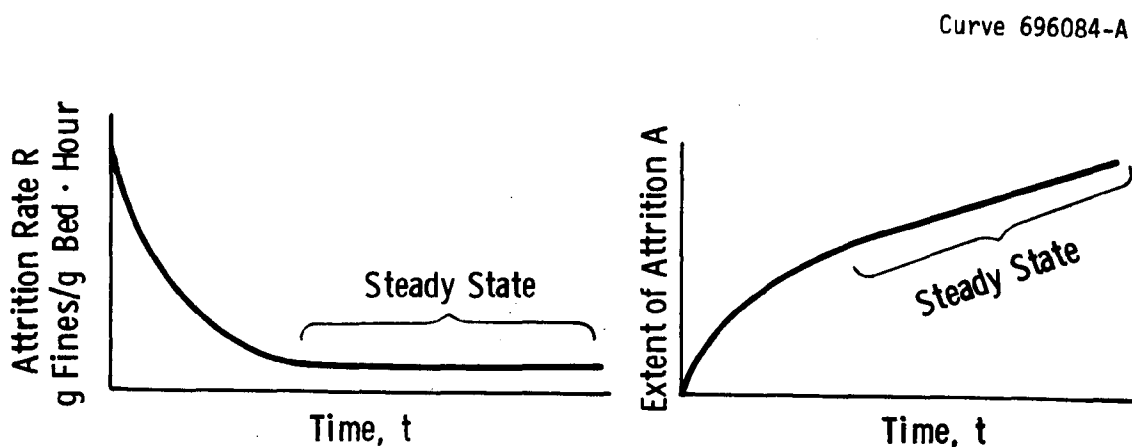


Figure D5 - Forms of the attrition rate curve $R(t)$ and its integral, the extent of attrition $A(t) = \int_0^t R(t)dt$.

Experimental Results Agree with the Attrition Rate Model

The model defined by equation (23) and pictured in Figure D5 is based on a variety of observations from different researchers. The observations have been unified into a single statement [equation (23)] under the conditions of consistency in dimensions and physical reality. Equation (23), however, is at this point a theory, unproved.

This experimental program tested two hypotheses of the attrition theory; first, that the attrition rate decreases steadily to a constant rate; and second, that attrition rate is proportional to $U - U_{mf}$. We did not test other hypotheses.

Figure D6 shows the apparatus for these experiments. The sintered-metal distribution plate eliminates jets and the attendant attrition from high-velocity collisions. The manometer allows measurement of a pressure drop across the bed of granular solids and, in turn, the minimum fluidization velocity U_{mf} at which bubbling in the bed of solids first begins.

The test procedure was to charge the apparatus with Grove limestone about 7 cm deep, then measure the minimum fluidization velocity U_{mf} .^{*} The bed was then fluidized in air at room temperature for time intervals after which gas flow was stopped and the bed solids were sieved into size fractions and weighed.

Test Results Substantiate the Idea that Attrition Rate Decreases to Constant Rate

The purpose of the first series of experiments was to test the hypothesis that attrition rate decreases to a constant value as indicated in the theoretical development [equation (23)] and depicted in Figure D5. The experimental approach was to fluidize a mass of stone over an interval of time long enough to determine the shape of the rate curve.

^{*}The value of U_{mf} is found by increasing superficial gas velocity U through the solids and recording pressured drop through the solids. At U_{mf} the bed weight equals the pressure force supporting the bed and Δp remains constant with increasing U .

We used the apparatus shown in Figure D6. A mass of 32 by 42 mesh limestone was first fluidized for 15 minutes, then wet sieved for measurement of the mass of coarse (>355 μm or 42 mesh) stone remaining. We repeated this procedure with increasing time intervals for a total fluidization time of 647 hours. Results are listed in Table D4.

The rate of attrition or rate of formation of fines is the first-order rate process defined by

$$R = - \frac{1}{M} \frac{dM}{dt}$$

where M is the mass of coarse granular solids in the bed. The percent of attrition is the mass of fines formed per unit mass of coarse bed solids (x100) or

$$A = \% \text{ extent of attrition} = 100 \times \int_0^t - \frac{1}{M} \frac{dM}{dt} dt ,$$

and with $M = M_0$ at $t = 0$, the above expression integrates to

$$A = \% \text{ extent of attrition} = 100 \ln \frac{M_0}{M_1} .$$

This is the value listed in the last row of Table D5 and is the measure of the extent of attrition.

Figure D7 is a graph of the extent-of-attrition data from Table D4; this graph of A against time looks like a logarithm graph so we chose a regression model for curve fitting:

$$A = K \ln (1 + k_1 x + k_2 x^2 + k_3 x^3 + k_4 x^4 + k_5 x^5)$$

Regression analyses gave the values

$K = 1.4688$	$k_3 = 1.99893 \text{ E} - 04$
$k_1 = 3.2658$	$k_4 = 4.83055 \text{ E} - 07$
$k_2 = -2.71103 \text{ E} - 02$	$k_5 = 3.78150 \text{ E} - 10$

Table D4

DATA FROM THE 647-HOUR ATTRITION OF GROVE 1359 LIMESTONE, NOVEMBER 1977, 25°C

Time Interval	Start	1	2	3	4	5	6	7	8	9	10	11	12	13
Length of Time	0	1/4	1/4	1/2	1	2	4	8	16	32	64	128	200	191
Total Time, hr	0	1/4	1/2	1	2	4	8	16	32	64	128	256	456	647
Wt > 42, M	316.1467	313.35	311.1658	309.0195	306.9038	304.8045	301.5885	298.9002	296.6960	294.4493	290.1494	287.15	284.238	280.8914
Wt < 42 F_b^*	0	2.4884	1.8614	1.7926	1.7081	1.6492	2.7149	2.1062	1.5707	1.5438	3.4671	2.0223	1.7891	2.1689
ΣF_b	0	2.4884	4.3498	6.1424	7.8505	9.4997	12.2146	14.3208	15.8915	17.4353	20.9024	22.9247	24.7222	26.8911
Filter Solids	Gross	4.2434	4.5517	4.5672	4.5971	4.6510	4.6935	4.7445	4.8255	4.8769	4.9463	5.0762	5.2205	5.3659
	Tare	4.2434	4.2434	4.2434	4.2434	4.2434	4.2434	4.2434	4.2434	4.2434	4.2434	4.2434	4.2434	4.2434
	ΣF_T Accumulated	0	0.3083	0.3228	0.3537	0.4076	0.4501	0.5011	0.5821	0.6335	0.7029	0.8320	0.9771	1.1781
$\Sigma F_b + \Sigma F_T$ Total Fines	0	2.7967	4.6726	6.4961	8.2581	9.9498	12.7157	14.9029	16.5250	18.1382	21.7352	23.9018	25.8447	28.0692
$\Sigma F_b + \Sigma F_T + M$ Total Solids	316.1467	316.1467	315.8384	315.5156	315.1619	314.7543	314.3042	313.8031	313.2210	312.5876	311.8846	311.0518	310.0747	308.9606
Possible Total Fines	0	2.7967	4.9809	7.1272	9.2429	11.3422	14.5582	17.2465	19.4507	21.6974	25.9973	28.9967	31.9083	35.2553
$100 \ln \frac{M^0}{M}$	0	0.79	1.59	2.28	2.97	3.65	4.71	5.61	6.35	7.11	8.58	9.62	10.64	11.82

* Calculated Estimate, Not Measured

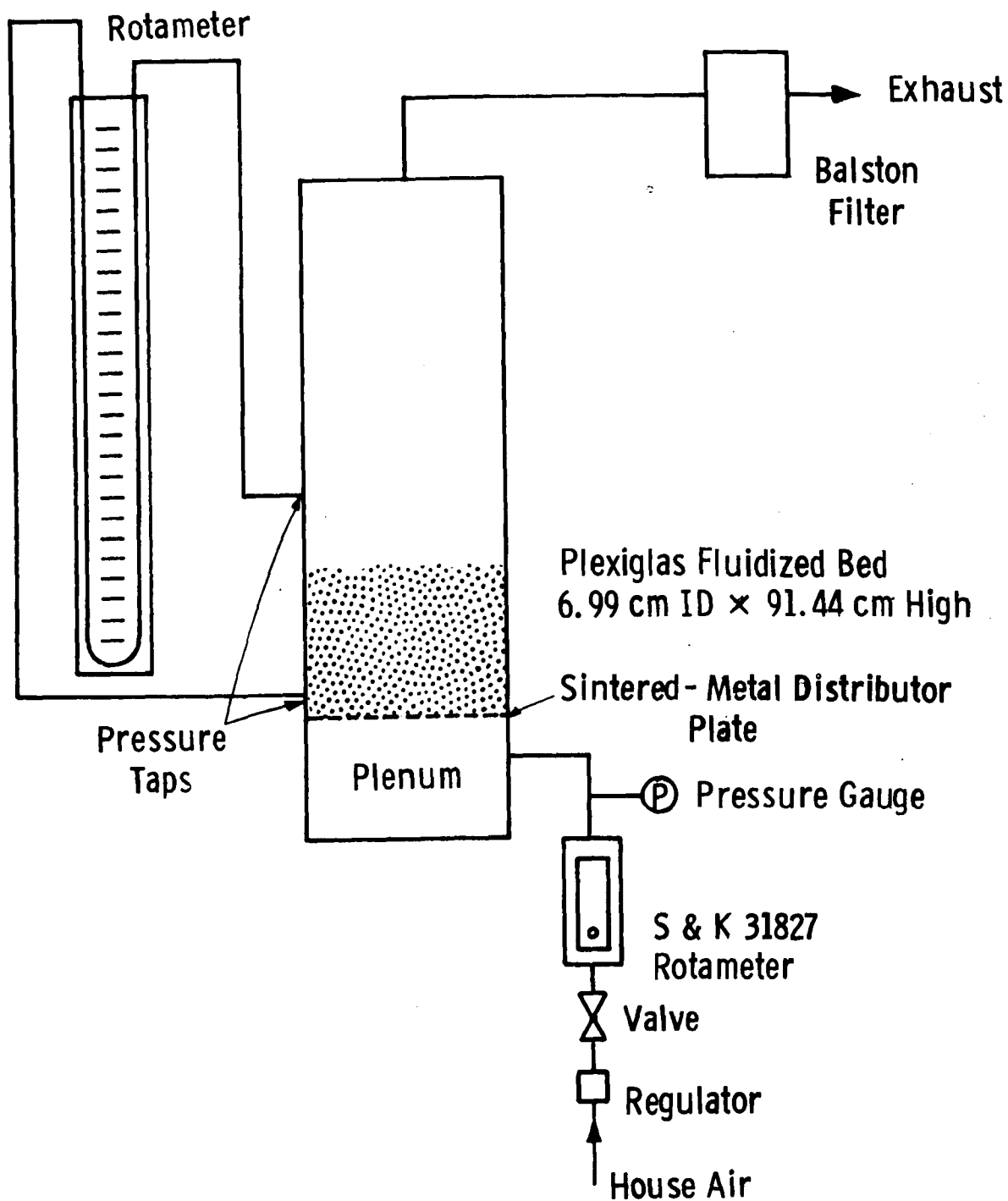


Figure D6 - Flow diagram for room-temperature fluidized bed

Table D5

SUMMARY OF DATA COLLECTED AND CALCULATED
VALUES FOR BED-SOLIDS MASS HAD SAMPLES
NOT BEEN REMOVED. CO₂-FREE BASIS

Hours Fluidized	Measured Mass g	% CO ₂ ()=meas'd []=est'd.	Mass CO ₂ -Free Stone, g	Mass CO ₂ -Free Stone, Corrected as if Sample Was Not Taken	% Attrition 100 ln (481.08/M)
Start	483.3	(0.5)	481.08	481.08	0
1	468.3	[0.4]	466.43	466.43	3.09
3	456.5	(0.35)	454.90	454.90	5.60
	455.3	[0.4]	453.48	--	
10	448.3	(0.42)	446.40	447.80	7.17
	447.6	[0.42]	445.72	--	
30	444.4	(0.20)	443.51	445.58	7.67
	443.6	[0.25]	442.49	--	
100	434.4	(1.47)	428.01	431.00	10.99
	437.4	[2.35]	[427.1]	--	
200	414.5	(0.59)	412.05	415.81	14.58

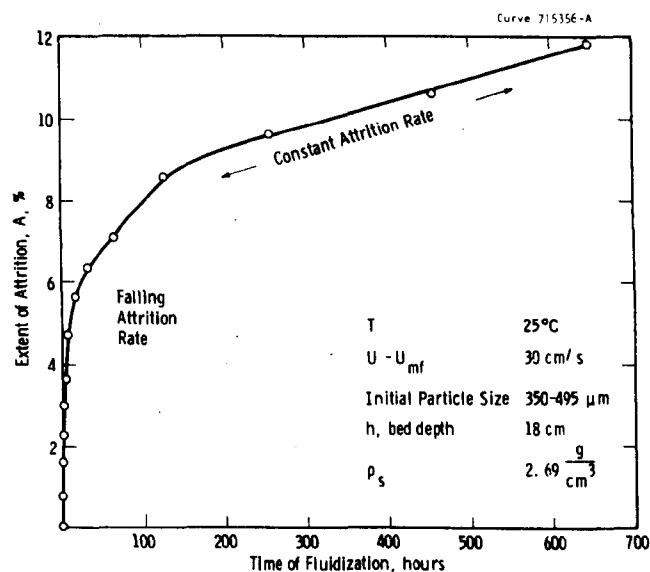


Figure D7 - Change of Extent of Attrition with Time
in Bubbling Fluidization

Figure D8 shows its derivative (% rate of attrition). These results, spanning 647 hours of vigorous fluidization, demonstrate that the rate of attrition does indeed decrease continually to a constant steady state. Notice how the rate R falls precipitously from its initial value of 4.80 %/hr at $t=0$ to 1.81 %/hr at $t = 0.5$. The rate approaches its final value of $R = 0.0055$ %/hr asymptotically. The rate reaches 99 percent of its final value ($4.80 - 0.99 \{4.80 - 0.0055\} = 0.0534$) after 25 hours of fluidization.

These results, more than ever, underscore the necessity for reporting attrition results on a consistent basis. Individual researchers need to keep the time interval of fluidization constant where possible or otherwise account for the effect of time.

Hot Attrition Testing Further Confirms that Attrition Rate Decreases to a Constant Rate

The previous tests at room temperature showed that attrition rate decreases with time until a constant rate is reached. We extended these experiments at combustor temperature to confirm that the rate decreases to a steady state under process conditions also.

Our apparatus consisted of a 8.57 cm-id attrition test cell fitted with a sintered-Inconel grid. We calcined 500-to-710 μm Grove limestone to $<0.5\%$ CO_2 , then fluidized it vigorously at 815°C and $U=U_{mf} + 20 \frac{\text{cm}}{\text{s}}$. After one hour of fluidization we removed the solids, sieved out fines smaller than 500 μm , weighed the coarse solids larger than 500 μm , and returned them for continued fluidization. This process was repeated several times with increasing intervals of fluidization time. Samples were removed for CO_2 assay. Figure D8 and Table D5 summarize results and calculations. The spots in Figure D8 (●) are measured masses of solids all other masses shown were calculated on the assumption that the curves are proportional.

The percent extent of attrition is calculated by

$$\% \text{ attrition, } A = 100 \ln \frac{M^0}{M}$$

where M^0 is the starting mass of solids. Calculated data from Figure D8 give these values of A plotted in Figure D9. Differentiation of this curve provides values of A, the percent attrition rate, plotted in the same figure. Values of A and R measured in these tests are listed in Table D6.

The effect of temperature on attrition rate is revealed by comparing results of both hot and cold attrition testing. Earlier cold tests were carried out with uncalcined 355-to-500 μm Grove 1359 limestone at a velocity of $U_{mf} + 200$ cm/s and a temperature of 25°C. The hot tests were performed with calcined 355 to 500 μm Grove 1359 limestone at a lower velocity of $U_{mf} + 20$ cm/s and at 810°C. In the hot tests the resistance to attrition, particle strength, was apparently much less, and the solids attrited notably faster. The characteristic values for the two tests are shown in Table D7.

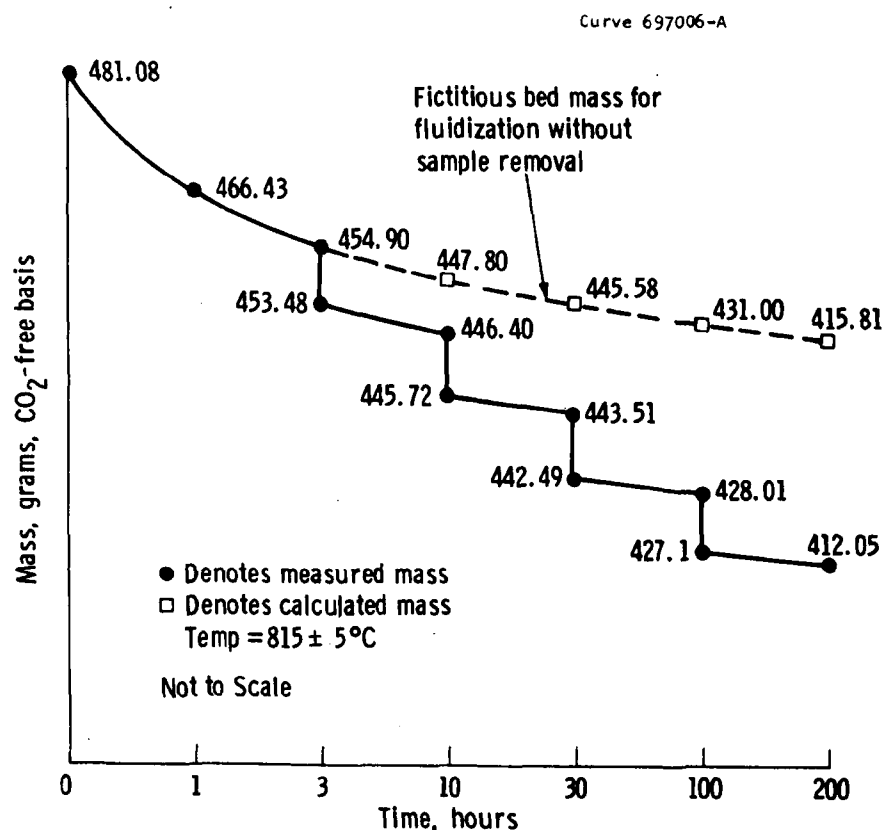


Figure D8 - Summary of Data Collected and Calculated Values for Bed Solids Mass Had Samples Not Been Removed. See Table D5.

Table D6

VALUES AT ATTRITION EXTENT AND RATE MEASURED FOR
24-32 MESH CALCINED GROVE LIMESTONE FLUIDIZED AT
810°C WITH $U = U_{mf} + 20 \text{ cm/s}$

Hours Fluidized	Extent of Attrition, A %	Rate of Attrition, R %/hour
0	0	3.86
1	3.09	2.18
3	5.60	0.71
10	7.17	0.052
30	7.67	0.0407
100	10.99	0.0407
200	14.58	

Curve 697005-A

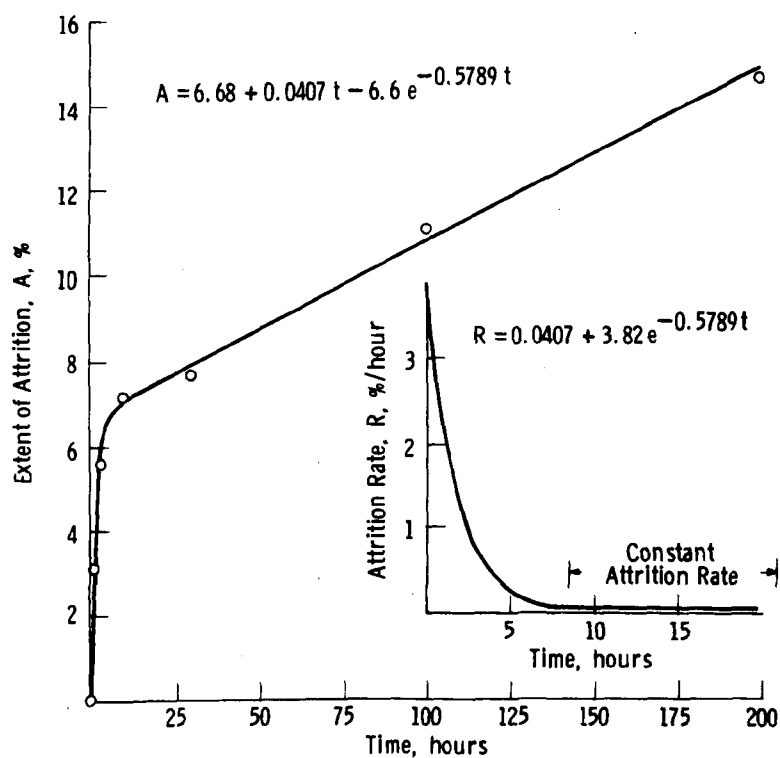


Figure D9 - Extent of Attrition and Attrition Rate for Grove 1359
Limestone Fluidized at $U = U_{mf} + 20 \text{ cm/s}$ and 875°C

Table D7

COMPARISON OF ATTRITION RATES AND TIME INTERVALS
REQUIRED TO REACH STEADY STATE

Test Temperature, °C	Transient Interval Required to Approach within 99% of Steady State, hr	Steady-state Rate of Attrition, %/hr
25	211	0.0056
810	7.95	0.0407

It is evident that attrition proceeds much faster at the higher temperature, presumably because hot calcined stone is weaker than cold uncalcined stone. At the high temperature the transient is much briefer.

These results suggest the caution needed in inferring attrition rates in a hot system from cold attrition rate data.

Test Results Substantiate Idean that Attrition Rate is Proportional to the Excess Bubbling Velocity $U-U_{mf}$

The development of an attrition equation was based on the hypothesis that the rate of formation of new particle surface, and in turn the rate of attrition (grams attrited/grams of coarse solid/hour), is proportional to the excess fluidizing velocity $U-U_{mf}$. We have tested this by measuring the specific surface of bed solids as a function of time at two different values of $U-U_{mf}$.

The experimental apparatus was that shown in Figure D6. We measured the size distribution of 330 g of crushed Grove limestone, then determined its minimum fluidization velocity from a velocity - ΔP curve. The stone was then fluidized in air at room temperature at $U = U_{mf} + 25$ cm/s for increasing time intervals up to a total time of eight hours. After each interval of fluidization we measured the size distribution of bed solids. Then we repeated the entire test, but at $U - U_{mf} = 12\text{-}1/2$ cm/s. Table D8 lists results from this test.

Table D8

Dwg.1692B53

DEPENDENCE OF SOLIDS SPECIFIC SURFACE ON TIME OF FLUIDIZATION

U - U _{mf} = 25 cm/s								
Time Interval, hr		Start	1/4	1/4	1/2	1	2	4
Total Fluidization Time, hr		0	1/4	1/2	1	2	4	8
Sieve Mesh	D _i , Mean Diameter, cm	Mass of Solids on Sieve, g						
42	0.042	330	316.188	315.815	311.631	309.081	303.903	300.957
60	0.030	0	10.857	10.366	12.516	12.869	15.849	16.621
115	0.018	0	0.429	0.328	0.510	0.599	0.723	0.906
250	0.009	0	0.418	0.148	0.181	0.122	0.186	0.136
325	0.0052	0	0.048	0.010	0.013	0.012	0.025	0.019
Pan	0.0036	0	0.016	0.009	0.009	0.009	0.009	0.014
Filter	0.0003	0	1.336	2.487	3.984	5.691	7.643	9.002
Lost ^a	0.0003	0	0.709	0.837	1.156	1.617	1.662	2.345
Specific Surface, cm ² /g ^a		53.91	101.46	130.25	171.69	220.92	266.54	312.97
% Increase in Specific Surface		0	88.2	141.6	218.5	309.8	394.4	480.5
U - U _{mf} = 12.5 cm/s								
Time Interval, hr		Start	1/4	1/4	1/2	1	2	4
Total Fluidization Time, hr		0	1/4	1/2	1	2	4	8
Sieve Mesh	D _i , Mean Diameter, cm	Mass of Solids on Sieve, g						
42	0.042	330	296.667	294.024	293.343	289.512	281.286	278.797
60	0.030	0	31.001	33.047	32.904	35.423	42.124	40.065
115	0.018	0	1.266	1.451	1.563	1.972	1.817	2.163
250	0.009	0	0.468	0.552	0.617	0.703	0.696	3.022
325	0.0052	0	0.024	0.036	0.095	0.118	0.222	0.287
Pan		0	0.009	0.033	0.039	0.036	0.030 ^b	0.023
Filter		0	0.032	0.129	0.441	0.967	1.573	3.102
Lost ^a		0	0.533	0.728	0.998	1.269	2.252	2.541
Specific Surface, cm ² /g ^a		53.91	69.36	76.27	89.62	108.05	144.64	187.31
Increase in Specific Surface		0	26.7	41.5	66.2	100.4	168.3	247.5

^a Sp. surf = $6 \sum (M_i \div D_i) / Mo \rho$ ^b Recorded datum of 0.128 rejected and replaced with 0.030 by interpolation.

The rate of increase in specific surface* was calculated by fitting a regression curve to the percent increase in specific surface vs. time data and differentiating. Results of this procedure are listed in Table D9. Specific surface was calculated from the particle size distribution.

Table D9

CALCULATION OF RATE OF INCREASE IN SPECIFIC SURFACE

$U-U_{mf}$, cm/s	Regression Line $S(t)$	$\frac{dS}{dt} = S'$	$S'_{25}/S'_{12.5}$
25	$106.01t^{0.490}$	$51.94t^{-0.510}$	$2.29t^{-0.128}$
12.5	$35.86t^{0.632}$	$22.7t^{-0.638}$	

The mean value of this ratio function $S'_{25}/S'_{12.5}$ is 2.003 over the interval $0 \leq t \leq 8h$.

The hypothesis being tested is that the rate of increase in specific surface is proportional to the excess fluidization velocity; that is,

$$dS/dt = S' \propto (U - U_{mf})^p$$

where $p \approx 1$. The average value of p calculated from Table D9 data is

$$\frac{S'_2}{S'_1} = \left[\frac{(U-U_{mf})_2}{(U-U_{mf})_1} \right]^p; 2.003 = \left(\frac{25}{12.5} \right)^p; p = 1.002.$$

This estimate of p is based on two data points ($U-U_{mf} = 25$ and 12.5) and does not have an error estimate. The calculated 1.002 is close to the hypothesized exponent of 1.0, and we conclude that the rate of generation of specific surface is proportional to $U-U_{mf}$. This is, in turn, related to the rate of attrition.

*Specific surface, denoted by S , is defined as the total particle surface area per unit volume of particulate solids. It has the units of cm^2/cm^3 or cm^{-1} .

The tests described in this section demonstrate that $(U-U_{mf}) \propto \frac{dS}{dt}$, the rate of formation of new particle surface area. Rittinger's law used in developing the Westinghouse model states that $\frac{dS}{dt} \propto$ input power by means of gas flow. For attrition in the bubbling bed input power $\propto (U-U_{mf})$. It follows that

$$R \propto \frac{dS}{dt} ; \frac{dS}{dt} \propto \text{input power}; \text{input power} \propto (U-U_{mf}) .$$

It follows then that $R \propto (U-U_{mf})$: the attrition rate in the bubbling regime of a fluidized bed is proportional to the energy velocity above the minimum, $U-U_{mf}$.

Discussion

The expression developed to describe the rate of attrition, R , in the bubbling zone of a fluidized bed is

$$\left[\frac{R Z}{U-U_{mf}} \right] = \left[F(t) + 1 \right] \left[\frac{g}{g_s} \frac{\rho_s}{\sigma} Z^2 \right]^m ; m \approx 1 . \quad (23)$$

Experiments described in this appendix demonstrate that

first: $R \propto (U-U_{mf})$ and

second: $R \propto [F(t) + 1]$; $F \rightarrow 0$ and $F' \rightarrow 0$ as $t \rightarrow \infty$

$F' < 0$ for $0 \leq t < \infty$;

and other experimental data, as described earlier in this paper, demonstrated that

third: $R \propto Z$.

The remainder of the theory, inferred by analogy and induction from other systems, proposes that

fourth: $R \propto 1/\sigma$ (soft materials attrite more easily than hard materials)

fifth: $R \propto \rho_s g/g_c$ (attrition rate is proportional to the gravity force on the bed of solids)

The transient decrease in attrition rate, described by $F(t)$, points out the need for caution in describing attrition rates. The average attrition rates, as reported in the literature, will vary with the time interval for averaging.

The attrition rates indicated by short-term tests may indicate a much higher rate than will be encountered in a commercial system. After hundreds or thousands of hours of fluidization, particles should attrite at the lower steady-state rate, and the rate of solids loss should be much less.

The increase in attrition rate with bed depth suggests design of deeper or shallower beds for control of fines production. Similarly, the effect of $U-U_{mf}$ on attrition rate suggests control of U_{mf} where U , the superficial gas velocity, is fixed. The minimum fluidization velocity, U_{mf} , can be controlled by selection of particle size.

Most effort in controlling (usually minimizing) attrition in fluidized-bed sulfur sorbent systems has been an extensive search for the ideal stone that attrites slowly because it is strong. The results of this study show that we can also control attrition rate in the bubbling zone by judicious specification of equipment and operating conditions.

REFERENCES

1. Keairns, D. L., ed., Fluidization Technology, Washington, D.C.: Hemisphere Publishing Company; 1976.
2. National Research Council, Committee on Processing and Utilization of Fossil Fuels, Reports on Assessment of Low- and Intermediate-Btu Gasification of Coal and Assessment of Advanced Technology for Direct Combustion of Coal, Washington, D.C.: National Academy of Sciences; 1977.
3. Blinichev, V. N., V. V. Strel'Tsov, E. S. Lebedeva, An Investigation into the Size Reduction of Granular Materials during their Processing in Fluidized Beds, Int'l Chemical Engrg. 8(4): 615-618; October 1969.

4. Snyder, R., et al., Annual report on a Development Program on Pressurized Fluidized-Bed Combustion, Argonne National Laboratory, Argonne, IL, July 1976, ANL/ES-CEN-1016, p. 189.
5. Paige, J. I., J. W. Town, J. H. Russell, H. J. Kelly, Sorption of SO_2 and Regeneration of Alkalized Alumina in Fluidized-Bed Reactors, Bureau of Mines Report of Investigations 7414, August 1970, p. 32.
6. Chemically Active Fluidized Bed Process, Monthly Technical Narrative No. 20, January 24-February 20, 1977, Foster Wheeler Energy Corporation, Livingston, NJ, Prepared March 14, 1977.
7. Craig, J. W. T., et al., Chemically Active Fluidized Bed Process for Sulphur Removal during Gasification of Heavy Fuel Oil, Second Phase, Report to EPA, Esso Research Centre, Abingdon, UK, November 1973, EPA-650/2-73-039.
8. Kutyavina, T. A., and A. P. Baskakov, Grinding of Fine Granular Material with Fluidization, Chemistry and Technology of Fuel Oils, 8(3): 210-13; March-April 1972.
9. Wei, J., L. Wooyoung, and F. J. Krambeck, Catalyst Attrition and Deactivation in Fluid Catalytic Cracking, Chemical Engineering Science, 32(10): 1211-18; 1977.
10. Doheim, M. A., A. A. Ghaneya, and S. A. Rassoul, The Attrition Behavior of Iron Ores in Fluidized-Bed Reactors, La Chimia E L'Industria, 58(12): 836-40; December 1976.
11. Jonke, A. A., A Development Program on Pressurized Fluidized-Bed Combustion, Monthly Progress Report, Argonne National Laboratory, Argonne, IL, June 1976, ANL/ES-CEN-F092, pp 29-35.
12. Forsythe, W. L., Jr., and W. R. Hertwig, Attrition Characteristics of Fluid Cracking Catalysts, I&EC, 41(6): 1200-06; June 1949.
13. Zenz, F. A., Fluid Attrition in Fluid Beds, Hydrocarbon Processing, pp 103-5, February 1971.

14. Regenerable Sorbents for Fluidized Bed Combustion, Quarterly Progress Report to EPA, No. 5, Exxon Research & Engineering Company, Linden, NJ, January 1-March 31, 1977.
15. Davidson, J. F., and D. Harrison, Fluidization, New York: Academic Press; 1971, p. 18.
16. Gonzales, V., and A. R. Otero, Formation of VO_3 Particles in a Fluidized Bed, Powder Technology, 7(3): 137-43.
17. Merrick, D., and J. Highley, The Effect of Particle Size Reduction on Elutriation from a Fluidized Bed with Feed from a Wide Size Distribution, AIChE Symposium Series No. 137, V. 40: 366-78.
18. Tarman, P. B., and D. V. Punwami, Development of the Steam-Iron System for Production of Hydrogen for the Hygas Process, Interim Report No. 2 to ERDA, IGT, Chicago, IL, July 1, 1974-June 30, 1975, FE-1518-34.
19. Babu, S., B. Shah, and A. Talwalker, Fluidization Characteristics of Coal Gasification Materials, AIChE 69th Annual Meeting, Chicago, IL, November 28-December 2, 1976, p. 33.
20. Catchpole, J. P., and G. Fulford, Dimensionless Groups, I&EC: 46-60; March 1966.
21. Jonke, A. A., A Development Program on Pressurized Fluidized-Bed Combustion, Monthly Progress Report, Argonne National Laboratories, Argonne, IL: 29-35; June 1976, ANL/ES-CEN-F092.
22. Vaughn, D. A., et al., Fluidized Bed Combustion Industrial Application Demonstration Project, Special technical report to ERDA on Battelle's Multi-Solids Fluidized-Bed Combustion Process, Battelle Laboratories, Columbus, OH, February 7, 1977, ERDA Contract E(49-18)-2472, p. 20.

23. Curran, G. P., et al., High-Temperature Desulfurization of Low-Btu Gas, Formal report to EPA, No. 5, Project 550, Consolidation Coal Company, Pittsburgh, PA, Series Period July 1, 1973-January 31, 1976. EPA 600/7-77-031, April 1977.
24. Mathur, K. B., and N. Epstein, Developments on Spouted Bed Technology, Canadian Journal of Chem. Engrg., 52(2): 129-45; April 1974.
25. Stanley, D. A., L. Y. Sadler, III, D. R. Brooks, and M. A. Schmarty, Production of Submicron Silicon Carbide Powders by Attrition Milling, 2nd International Conference on Fine Particles, Boston, MA, October 7-11, 1973, pp 331-36.

LIST OF SYMBOLS

- A_f = area of new fracture surface (cm^2)
 b = exponent in Curran formula
 C_1 = ratio of particle velocity to bubble velocity
 C_2 = efficiency of changing kinetic energy to surface energy
 C_3 = ratio of chip thickness to bed depth
 C'_3 = coefficient in equation (6), a measure of chip thickness (cm)
 C_4 = ratio of disturbed bed cross-section area to bubble cross-section area
 C_5 = coefficient in Gonzales and Otero equation (cm^{1-m}/s)
 $C = \frac{1}{3} C_1^2 C_2 C_3 C_4$ [equation (12)]
 D = fluidized-bed diameter (cm)
 D_b = diameter of a spherical bubble (cm)
 D_p = diameter of a bed particle
 F_f = function or "function of" or "the function"
 g = gravity acceleration (980 cm/s^2)
 g_c = Newton's law conversion factor ($1\text{g}\cdot\text{cm}/\text{dyne}\cdot\text{s}^2$)
 G_a = Gallileo number = $D_p^3 \rho_g (\rho_s - \rho_g) g \div \mu^2$
 h = total bed depth (cm)
 $K, k_1, k_2, k_3, k_4, k_5$ = coefficients in regression model (varied)
 L = total loss rate from bed by attrition [equation (18)] (g/min)
 = $R \times \text{bed mass}$

m'' = exponent in Kuttyavina and Baskakov equation
 m = exponent in Gonzales and Otero equation
 m' = exponent in equation (24)
 M = mass of coarse bed solids (g)
 M_o, M_l = value of M at the beginning and end of a time interval (g)
 N_{Bo} = Bond number = $g Z^2 \rho_s \div g_c \sigma$
 N_{st} = Strouhal number = $RZ \div (U - U_{mf})$
 n = exponent in equation (6)
 r = exponent in Table D2
 R = attrition rate per unit mass of bed (g/g.s) = $L \div$ bed mass
 S = specific surface of granular solids (cm²/g)
 t = time (s)
 U = superficial gas velocity (cm/s)
 U_b = bubble rise velocity (cm/s)
 U_{mf} = minimum fluidizing velocity (cm/s)
 U_p = particle velocity (cm/s)
 Z = distance measured downward from the bed surface (cm)
 ϵ = porosity of fluidized-bed dense phase
 μ = gas viscosity (g/cm.s)
 ρ_s = density of solid (g/cm³)
 ρ_g = density of gas (g/cm³)
 σ = solid fracture energy (erg/cm²) or (dyne/cm)

APPENDIX E
3.5-cm FLUIDIZED-BED TEST SYSTEM

3.5-cm FLUIDIZED-BED TEST SYSTEM

Purpose: To study attrition and sorption properties of fluidized-bed solids

- Extent of attrition, or attrition rates of sorbents at narrow temperatures, pressures, gas flow rates, and gas compositions; comparison of attrition tendencies of different sorbents
- Sorption kinetics of sorbents in SO_2 or H_2S atmospheres

Test Facility:

Flow diagram	Figure 1
Reactor assembly and grid	Figure 2
Pressure containment	Figure 3
Reactor assembly	Figure 4

Design Parameters:

Test cell:	35 cm id 42 cm total depth
Available grids:	Perforated, sintered
Maximum pressure:	1000 kPa, absolute
Maximum temperature:	1000°C
Gases:	N_2 , Air, CO_2 , CO, H_2 , SO_2 , H_2S
Gas flow:	
Bed materials:	Limestone, dolomite, sand, char

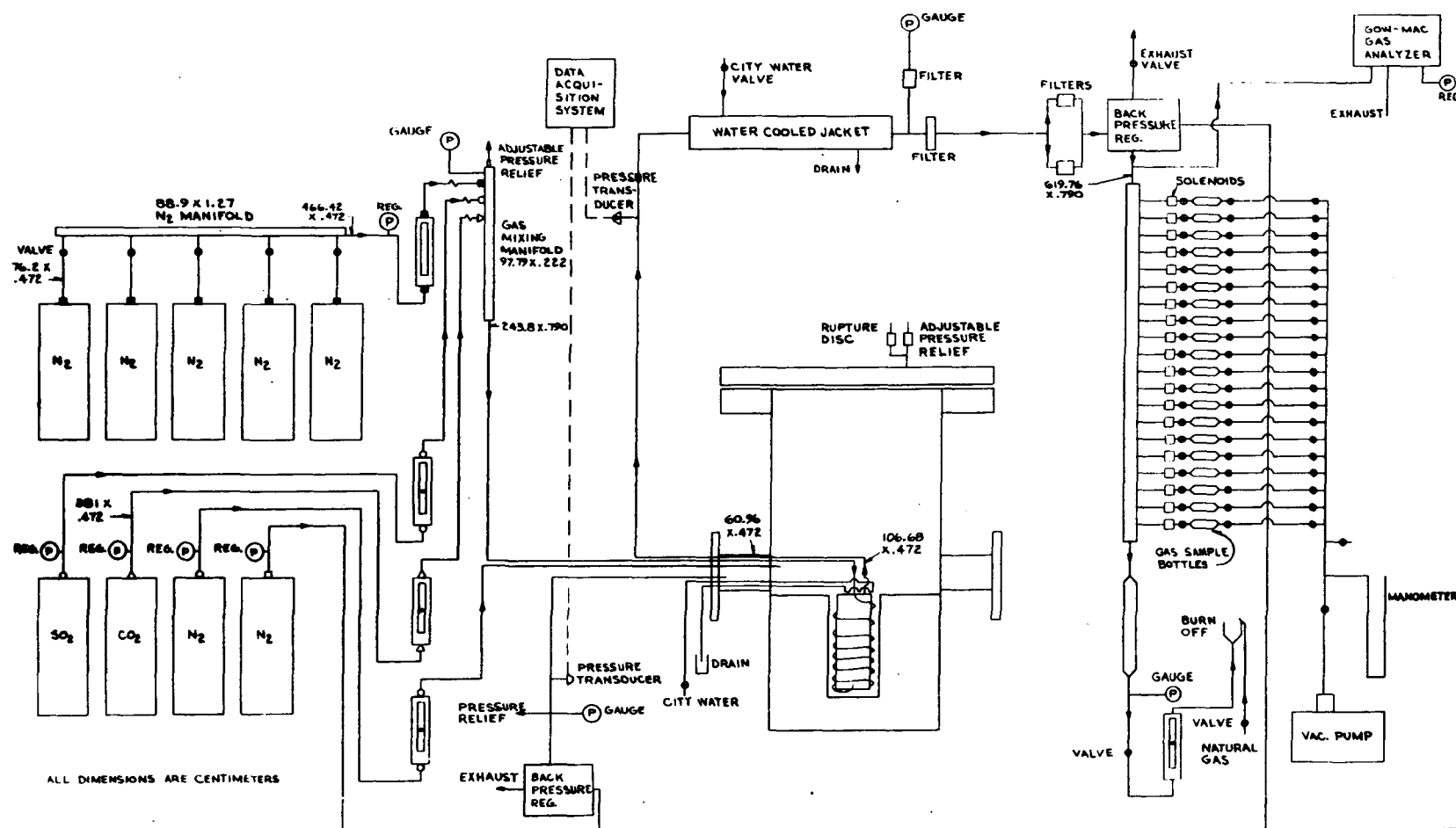


Figure E1 - Flow Diagram for the Attrition Reactor System

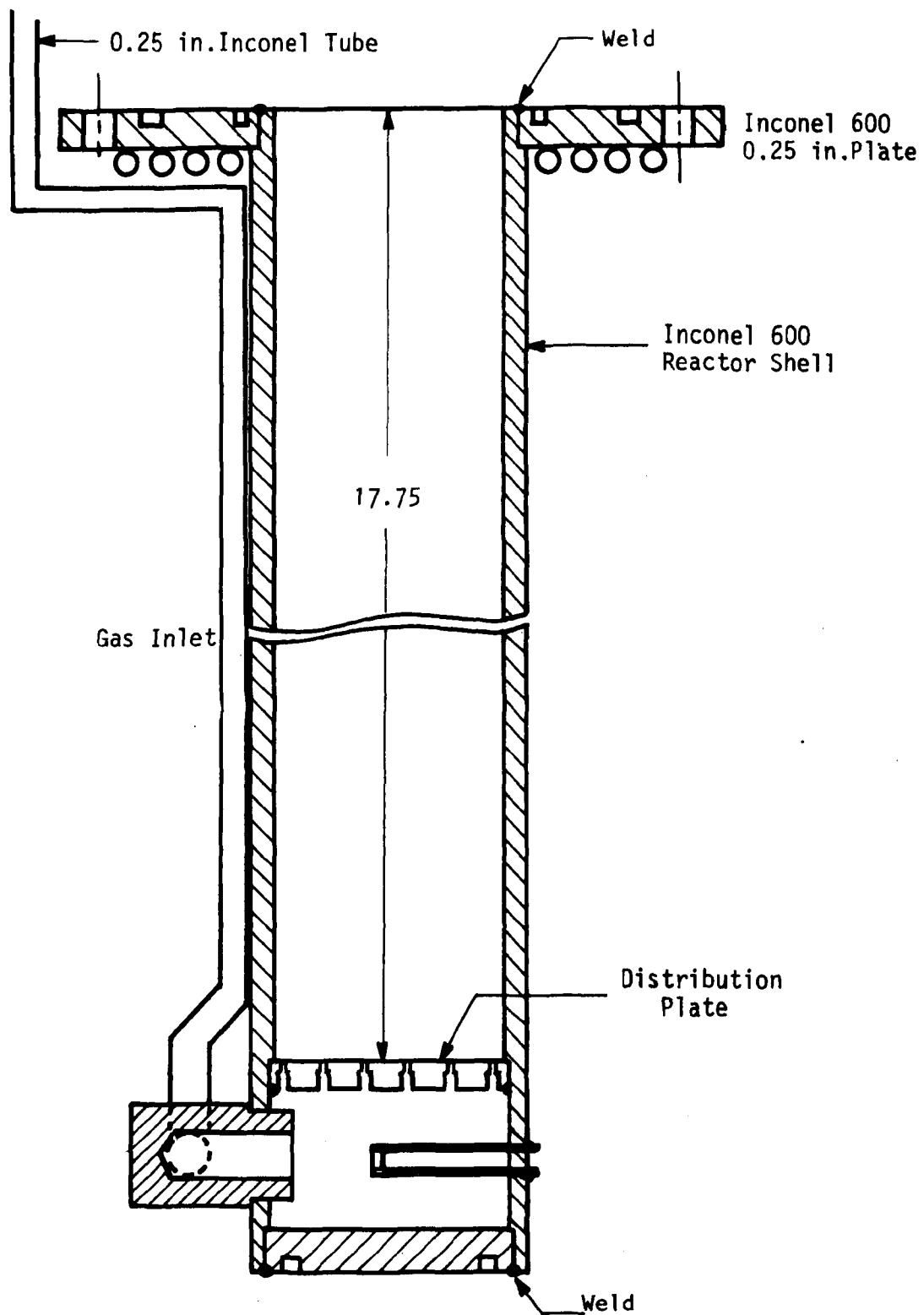


Figure E2 - Reactor Assembly and Grid

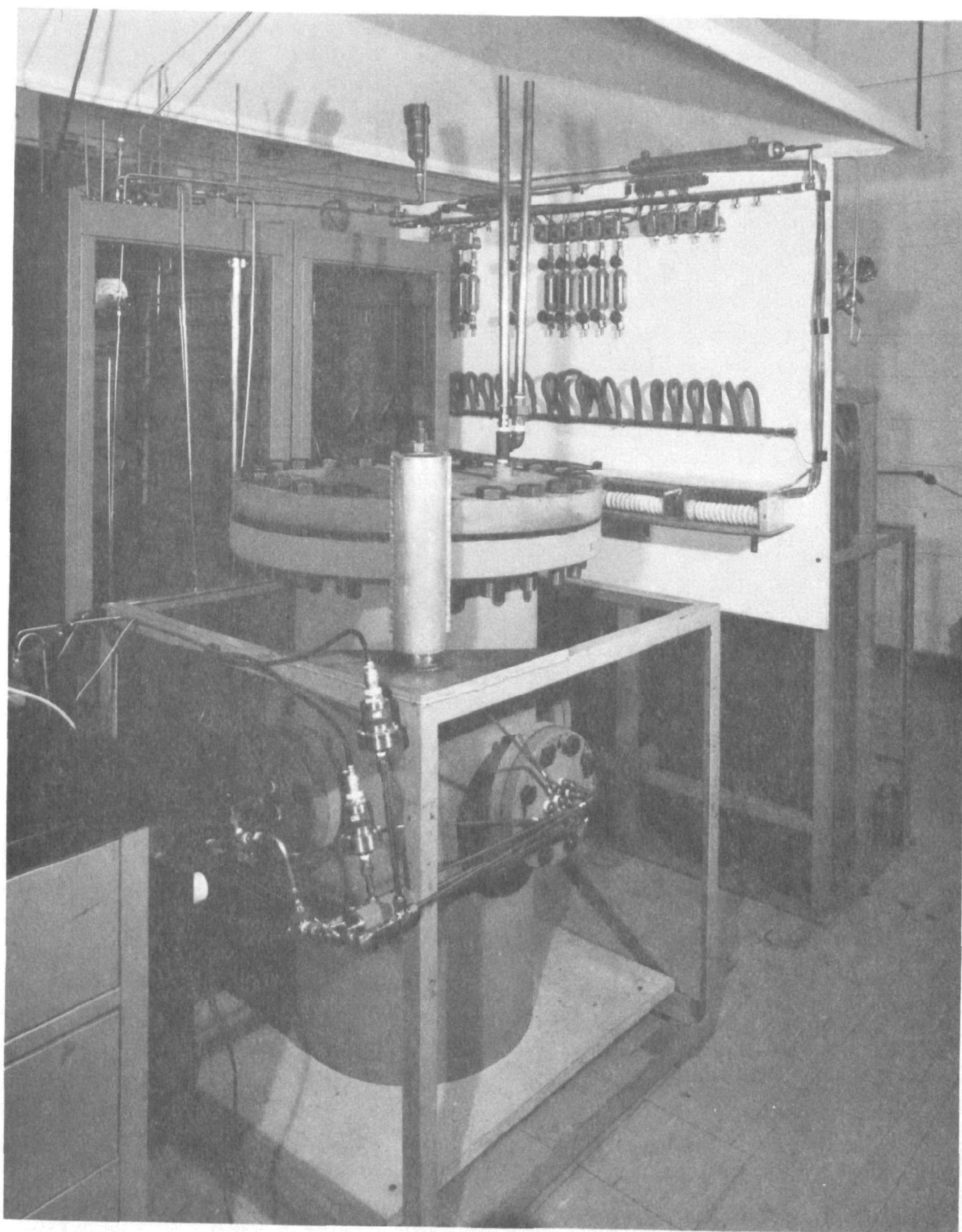


Figure E3 - Pressure Containment

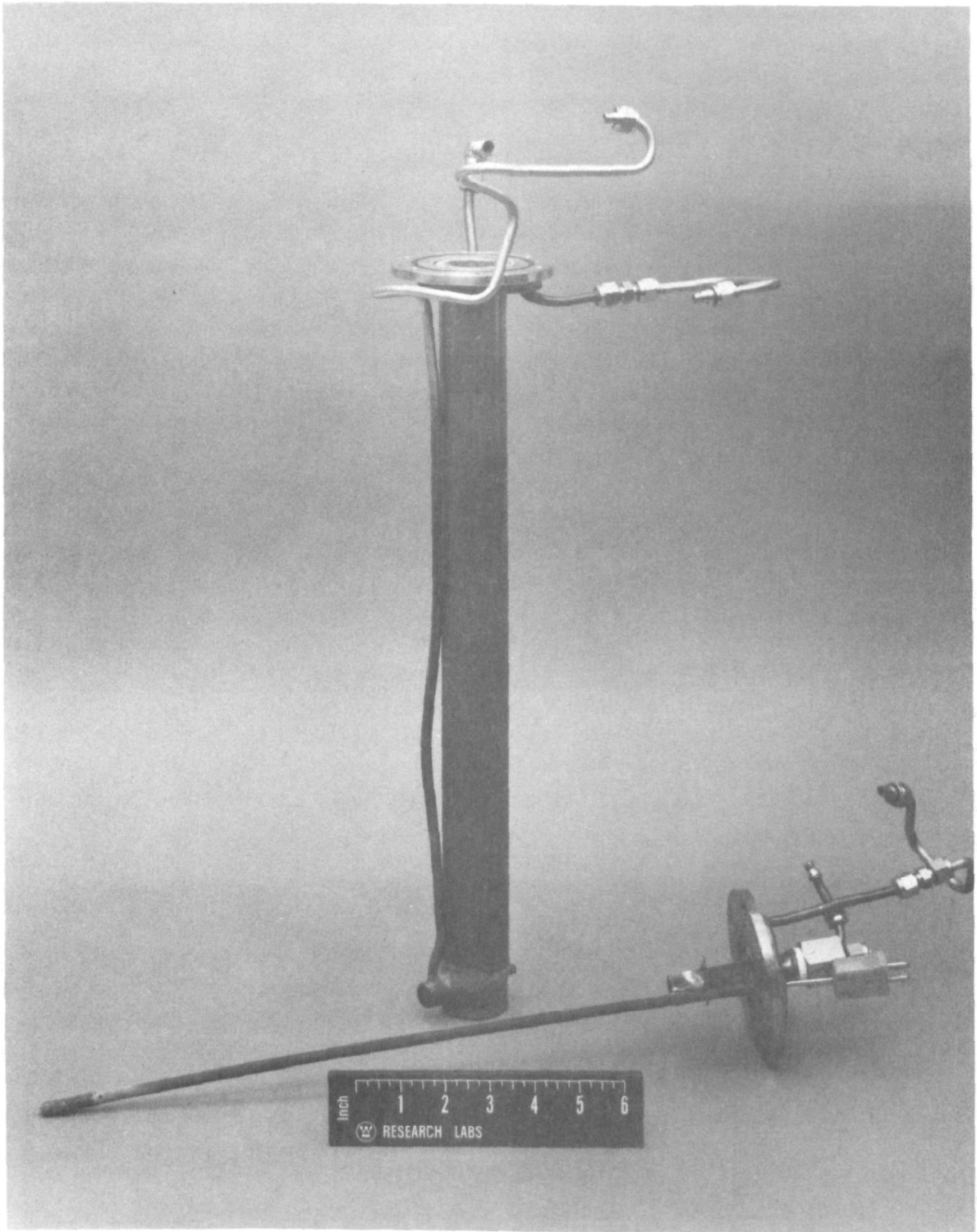


Figure E4 - Reactor Assembly

TECHNICAL REPORT DATA (Please read instructions on the reverse before completing)			
1. REPORT NO. EPA-600/7-80-015a		3. RECIPIENT'S ACCESSION NO.	
4. TITLE AND SUBTITLE Experimental/Engineering Support for EPA's FBC Program: Final Report Volume 1. Sulfur Oxide Control		5. REPORT DATE January 1980	
7. AUTHOR(S) N. H. Ulerich, W. G. Vaux, R. A. Newby, and D. L. Keairns		6. PERFORMING ORGANIZATION CODE	
9. PERFORMING ORGANIZATION NAME AND ADDRESS Westinghouse Research and Development Center 1310 Beulah Road Pittsburgh, Pennsylvania 15235		8. PERFORMING ORGANIZATION REPORT NO.	
12. SPONSORING AGENCY NAME AND ADDRESS EPA, Office of Research and Development Industrial Environmental Research Laboratory Research Triangle Park, NC 27711		10. PROGRAM ELEMENT NO. INE825	
		11. CONTRACT/GRANT NO. 68-02-2132	
		13. TYPE OF REPORT AND PERIOD COVERED Final; 12/75 - 12/78	
		14. SPONSORING AGENCY CODE EPA/600/13	
15. SUPPLEMENTARY NOTES IERL-RTP project officer is D. Bruce Henschel, Mail Drop 61, 919/541-2825. EPA-600/7-78-005, -039, and -163 also relate to this work.			
16. ABSTRACT The report gives results of an investigation of the desulfurization performance and attrition behavior of limestone and dolomite sorbents for atmospheric and pressurized fluidized-bed combustion (FBC) systems used with coal. It gives results of experimental thermogravimetric analyses (TGAs) of the kinetics of SO₂ capture by sorbents, and discusses the further development and application of a kinetic model for desulfurization, based on TGA results. It also gives results of a basic assessment of sorbent attrition mechanisms in FBC, including some laboratory experimental tests. Some conclusions from this work are: (1) pressurized FBC systems can achieve effective SO₂ removal at high temperatures (1000 C) or high excess air (300%) without an increase in sorbent requirements over lower temperature/excess air cases; (2) the agreement between actual FBC data and the TGA-based desulfurization model has been further demonstrated, using data from both atmospheric and pressurized FBCs; and (3) sorbent attrition screening tests indicate that sorbent type and FBC operating parameters will affect particle attrition. The report presents an experimental-data-supported sorbent attrition model for the bubbling bed regime in an FBC.			
17. KEY WORDS AND DOCUMENT ANALYSIS			
a. DESCRIPTORS		b. IDENTIFIERS/OPEN ENDED TERMS	c. COSATI Field/Group
Pollution Dolomite		Pollution Control	13B
Combustion Sorbents		Stationary Sources	21B 11G
Fluidized Bed Processing			13H, 07A
Coal Sulfur Dioxide			21D 07B
Desulfurization Kinetics			07D 20K
Limestone Mathematical Models			08G 12A
18. DISTRIBUTION STATEMENT Release to Public		19. SECURITY CLASS (This Report) Unclassified	21. NO. OF PAGES 247
		20. SECURITY CLASS (This page) Unclassified	22. PRICE